Osmotic and metabolic effects of hyperglycaemia on glycolysis, mitochondrial function and fibrosis-related microRNA expression in immortalised human proximal tubule cells

Fahad Alsehli

A thesis submitted in partial fulfilment of the requirements of the Manchester Metropolitan University for the degree of Doctor of Philosophy

**Department of Life Sciences,
Manchester Metropolitan University.
2019**

Abstract

The incidence of chronic kidney disease (CKD) is increasing and CKD can progress to end-stage renal disease (ESRD) which requires costly renal replacement therapies. Diabetes is one of the major factors for CKD and ESRD. Around 40% of the diabetic patients develop kidney damage known as diabetic nephropathy. Renal tubulointerstitial fibrosis (TIF) is irreversible and leads to the excessive deposition of extracellular matrix, disruption of cell-to-cell interactions and loss of tissue elasticity, thus leading to the destruction of the renal tubules. However, at present there are no successful therapies that can block or reverse TIF. Therefore, new approaches are required to identify suitable therapeutic targets for the prevention or reversal of TIF.

This thesis evaluated the metabolic and osmotic effects of hyperglycaemia on the glycolytic and mitochondrial function, the expression of fibrosis-related cytokines, markers of inflammation, ECM accumulation, and the expression of a panel of fibrosis-related miRNA in immortalised human proximal tubule (HK-2) cells.

The work demonstrated impairment of the two energy pathways, oxidative phosphorylation and glycolysis, in response to 30mM D-glucose, and that was linked to the osmotic effect of hyperglycaemia. In contrast, the reductions of cell viability and glucose consumption, and impaired wound healing were linked to its metabolic effect.

The study also showed that the osmolarity component of hyperglycaemia activated Smad3 and upregulated proximal tubular injury and inflammation markers (e.g. IL-6, KIM-1, MCP-1 and endostatin), suggesting a role of osmolarity in the pathogenesis of DN.

Finally, the thesis evaluated the expression of 84 fibrosis-related miRNAs in HK-2 cells exposed to different concentrations of glucose. The study showed that 16 miRNAs were dysregulated over a 72h exposure to hyperglycaemia. Furthermore, the pro-fibrotic miR-216a-5p was downregulated in response to hyperglycaemia. As one of the potential targets of miR-216a-5p is the TGF-β1 Receptor 2, hyperglycaemia may exacerbate fibrosis by facilitating the signalling of the pro-fibrotic cytokine TGF-β1.

Future work will investigate which of the 16 dysregulated miRNAs is a suitable target for treating TIF in diabetic nephropathy.

Acknowledgments

Table of Contents

List of Figures

List of Tables

Outputs generated by the work presented in this thesis

<u>**Conference Proceedings:**</u>

Alsehli, F., Ahmed, N. and Shalamanova, L (2018). Hyperglycaemia and tubulointerstitial fibrosis in renal proximal tubular epithelial cells. Centre for Biomedicine, School of Healthcare Science, Manchester Metropolitan University, Manchester, UK.

Alsehli, F., Lightfoot, A., Ahmed, N. and Shalamanova, L (2018). Fibrosis-related miRNAs are dysregulated by hyperglycaemia in human proximal tubular epithelial cells. Presented at Harrogate Convention Centre in the UK Kidney Week 2018 hosted by: *The British Renal Society*. Harrogate, UK.

Alsehli, F., Lightfoot, A., Ahmed, N. and Shalamanova, L (2018). Fibrosis-related miRNA are dysregulated by hyperglycaemia in human proximal tubular epithelila cells*.* Vol. 33. Oxford University Press, Great Clarendon St, Oxford, OX2 6DP, England.

Alsehli, F., Ahmed, N. and Shalamanova, L (2017). Mechanisms of renal proximal tubular cell injury and fibrosis induced by hyperglycaemia. Presented at ACC Liverpool in the UK Kidney Week 2017 hosted by: *The British Renal Society*. Liverpool, UK.

Alsehli, F., Ahmed, N. and Shalamanova, L (2017). Mechanisms of renal tubular fibrosis induced by hyperglycaemia. Presented at Manchester Central Centre at the Diabeties UK Professional Conference hosted by: *Diabetes UK*. Manchester, UK.

Manuscripts:

Mitsides, N., Alsehli, F. M. S., Mc Hough, D., Shalamanova, L., Wilkinson, F., Alderdice, J., Mitra, R., Swiecicka, A., Brenchley, P., Parker, G., Alexander, Y. and Mitra, S. (2019) 'Salt and Water Retention Is Associated with Microinflammation and Endothelial Injury in Chronic Kidney Disease.' *Nephron*, 143(4) pp. 234-242.

List of Abbreviations

Abbreviation	Stands for
ACR	Albumin:Creatinine (ACR)
AGEs	Advanced glycation end products
AKI	Acute kidney injury
AODM	Adult onset diabetes mellitus
Ang II	Angiotensin II
AP-1	Activator protein
AR	Aldose reductase
ARF	Acute renal failure
ATN	Acute tubular necrosis
ATP	Adenosine triphosphate
α-SMA	α-smooth muscle actin
Azin1	Antizyme inhibitor1
BCA	Bicinchoninic acid
BMP	Bone morphogenetic proteins
BSA	Bovine serum albumin
CCK-8	Cell Counting Kit-8
CCL2	Chemokine (C-C motif) ligand 2
CCR2	Receptor CC-chemokine receptor-2
CDKs	Cyclin-depended kinases
CKD	Chronic kidney disease
Co-Smad	Common Smad4
CRF	Chronic renal failure
CVD	Cardiovascular disease
CTGF	Connective tissue growth factor
$CuSO_4$	Copper sulphate
DAG	Diacylglycerol
2-DG	2-deoxy-D-glucose
DGRC8	DiGeorge syndrome critical region gene 8
DMEM	Dulbecco's modified Eagle medium
DN	Diabetic nephropathy
ECAR	Extracellular flux analysis
ECM	Extracellular matrix
EDTA	Ethylenediaminetetraacetic acid
EMT	Epithelial to mesenchymal transition
ERK/MAPK	Extracellular signal-regulated kinase/mitogen-activated protein kinase

ESRD	End-stage renal disease
ETC	Electron transport chain
FADH$_2$	Flavin adenine dinucleotide
FCCP	Carbonyl cyanide-4 (trifluoromethoxy) phenylhydrazone
FSP1	Fibroblast-specific protein-1
GAPDH	Glyceraldehyde-3-phosphate dehydrogenase
GBM	Glomerular basement membrane
GFR	Glomerular filtration rate
GLUTs	Glucose transporters
glycoPER	Glycolytic proton efflux rate
GOPOD	Glucose oxidase/peroxidase
GPCRs	G protein-coupled receptors
HAVCR-1	Hepatitis A cellular receptor-1
HCl	Hydrochloric acid
HCO^{-3}	Bicarbonate
HEPES	4-(2-hydroxyethyl)-1-piperazineethanesulfonic acid
H$_2$O$_2$	Hydrogen peroxide
HK-2	Immortalised human proximal tubule cells
HMCs	Human primary mesangial
HSE	Health Survey for England
IkBa	Inhibitor of NF-kB
IL-1	Iterleukin-1
IL-6	Iterleukin-6
IL-8	Iterleukin-8
ILK	Integrin-linked kinase
IL-6R	IL-6 receptor
IRS-1&2	Insulin receptor substrate-1&2
LAP	Latency-associated peptide
LPP3	Lipid phosphate phosphatase 3
LTBP	Latent TGF β-binding protein
Kim-1	Kidney injury molecule
MAPK	Mitogen-activated protein kinases
MCP-1	Monocyte Chemoattractant Protein-1
MIOX	*Myo*-inositol oxygenase
miRNA	MicroRNA
MMPs	Metalloproteases
MPT	Mitochondrial permeability transition
MPTP	Mitochondrial permeability transition pore
mtDNA	Mitochondrial DNA

NaCl	Sodium chloride
NADH	Nicotinamide adenine dinucleotide
NADPH	Nicotinamide adenine dinucleotide phosphate
NaOH	Sodium hydroxide
Na^+/K^+ ATPase	Sodium/potassium ATPase
NF-kB	Nuclear factor kappa B
NHS	National Health Service
NP-40	Nonyl phenoxypolyethoxylethanol
OCR	Oxygen consumption rates
OLETF	Otsuka Long-Evans Tokushima Fatty
OXPHOS	Oxidative phosphorylation system
PAI-1	Plasminogen activator inhibitor-1
PBS	Phosphate-buffered saline
PBST	Phosphate-buffered saline with Tween-20
PER	Proton efflux rate
PKC	Protein kinase C
PKD	Polycystic kidney disease
PPAR-γ	Peroxisome proliferator-activated receptor-γ
PPS	Pentosan polysulfate
pSmad3L/C	Linker phosphorylated Smad3C
PTC	Proximal tubule cells
PTEN	Phosphatase and tensin homologue
PINK1	PTEN-induced putative kinase 1
pri-miRNA	Primary miRNA
qPCR	Quantitative real-time PCR
RAGE	Receptor of AGE
RAS	Renin-angiotensin system
RISC	RNA-induced silencing complex
ROS	Reactive oxygen species
Rot/AA	Rotenone/antimycin A
RPTEC	Renal proximal epithelial tubule cell
R-Smads	Receptor-regulated
RT-PCR	Reverse transcriptase PCR
SGLT	Sodium-dependent glucose co-transporter
SDH	Sorbitol dehydrogenase
SDS	Sodium dodecyl sulphate
SFM	Serum-free medium
SIP1	Smad-interacting protein 1
Snail	Snail transcriptional factors

STZ	Streptozotocin
TCA	Tricarboxylic acid cycle
TGF-β1	Transforming Growth Factor β-1
TGFBR1	Transforming Growth Factor β receptor II
TGFBR2	Transforming Growth Factor β receptor II
TIF	Tubulointerstitial fibrosis
TIM-1	T cell-immunoglobulin-mucin
TIMPs	Tissue inhibitors of metalloproteinases
TNF-α	Tumour necrosis factor alpha
t-PA	Tissue-type plasminogen activator
TRPC1	Transient receptor potential cation channel, subfamily C, member 1
Tris HCL	Tris hydrochloride
u-PA	Urokinase-type plasminogen activator
uPAR	Urokinase receptor
3'UTR	3' Untranslated region
UUO	Unilateral ureteral obstruction
Ybx1	Y Box binding protein 1
ZEB	Zinc finger E-box-binding homeobox
ZO-1	Zonula occludens-1

Chapter 1: Introduction

1.1 The physiology of kidney function

The kidneys are important regulators of systemic blood pressure, acid-base and osmolarity homeostasis. As an endocrine organ, the kidney secretes a number of hormones (e.g. erythropoietin, renin and calcitriol) and also contributes to the degradation of certain hormones such as parathyroid hormone and insulin (Beto and Bansal, 2004; Pietilä and Vainio, 2014). However, one of the key functions of the kidney is the regulation of extracellular fluid volume and excretion of waste and toxins (Pietilä and Vainio, 2014).

In humans, the kidneys are a pair of bean-shaped organs situated in the lower back, just below the rib cage (Figure 1.1). Each kidney contains over one million structural and functional units called nephrons that filter metabolic waste from the blood to the urine.
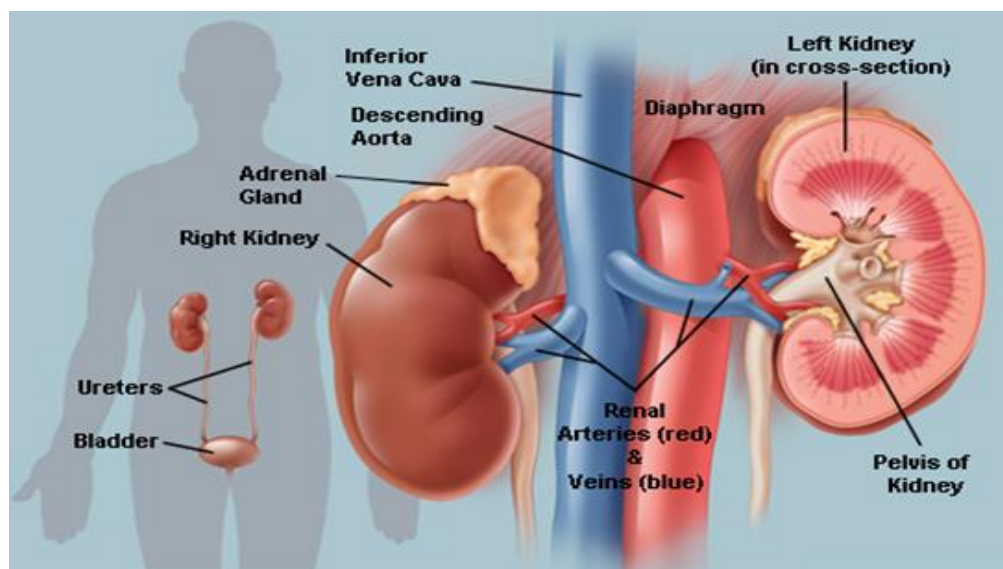
Figure 1. 1. The location and anatomy of the human kidneys, from (Hoffman, 2009)

Each nephron comprises a renal corpuscle and a renal tubule, which merges with the collecting duct that opens and releases urine in the renal pelvis (Figure 1.2). The renal corpuscle is responsible for the filtration of primary urine and is composed of the glomerulus (a network of capillaries) encapsulated by the Bowman's capsule. The glomerular capillaries are structurally supported and surrounding by intraglomerular mesangial cells (Scott and Quaggin, 2015; McMahon, 2016). The capillary wall is composed of three layers: the first layer of the glomerular filter is a fenestrated endothelium with a central lumen. The endothelial cells have numerous pores called fenestrae about 70–100 nm in diameter, allowing water, proteins and large molecules to pass through, but not blood cells (Pollak et al., 2014). The second layer of the glomerular filter is the glomerular basement membrane (GBM) that surrounds the endothelium and is a complex of extracellular matrix proteins such as collagen type IV, fibronectins, proteoglycans and lamina. GBM act as a filtration barrier, preventing large molecules (> 15 kDa) such as albumin from being filtered out of the bloodstream (Suh and Miner, 2013). The third layer of the glomerular filter is composed of the visceral epithelial cells, termed podocytes. The podocytes are attached to the GBM by podocyte foot processes. They form tight filtration slits (slit diaphragms) between each other with pores of around 40 nm in diameter, thus restricting large molecules from crossing to the glomerular space (Figure 1.3) (Grahammer et al., 2013; McMahon, 2016). The podocyte layer works as a final filtration barrier allowing only small molecules such as glucose, amino acids and mineral ions to enter the glomerular space and reach the proximal convoluted tubules (Grahammer et al., 2013; McMahon, 2016).

The renal tubule consists of proximal tubule cells, the loop of Henle, the distal tubule and the collecting duct. The proximal convoluted tubules lie in the cortex of the kidney and have a simple cuboidal epithelium with microvilli, which increase the luminal surface area of the cells and thus reabsorption (Figure 1.2) (Pietilä and Vainio, 2014; Scott and Quaggin, 2015; McMahon, 2016). The renal tubules are enriched in mitochondria, which provide a sufficient supply of energy for the active transport across the epithelial cells and for the maintenance of ion gradients across their cellular membrane (Soltoff, 1986; Bhargava and Schnellmann, 2017). The proximal tubules cells reabsorb 80% of the primary filtrate and therefore they contain more mitochondria than any other renal cell type, in order to help mediate this active transport (Bhargava and Schnellmann, 2017), and hence tubular mitochondria will be part of the focus of this study.

The proximal convoluted tubules normally reabsorb 100% of the filtered glucose, amino acids, and small peptides, and 65-70% of the sodium chloride (Carroll, 2007). Therefore, glucosuria (presence of glucose in the urine) is a sign of renal proximal tubular cell dysfunction where the tubules fail to reabsorb the filtered glucose (Santer and Calado, 2010).

The fluid then passes through into the loop of Henle, where the urine is concentrated, and then into the distal convoluted tubules, which regulate sodium, potassium and calcium homeostasis, pH balance and water uptake. The urine then passes through the collecting duct and reaches the bladder (Subramanya and Ellison, 2014).
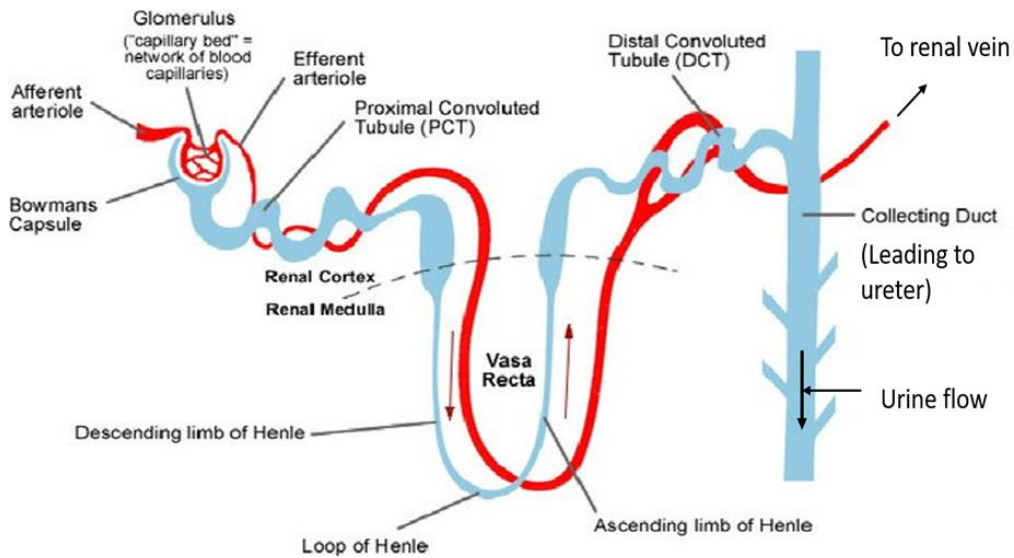
Figure 1. 2. Anatomy of a nephron. PTEC are located immediately after the glomerulus in the kidney nephron and are responsible for the reabsorption of different nutrients, adapted from www.ivy-rose.co.uk, (2018) and NIDDK, 2018.
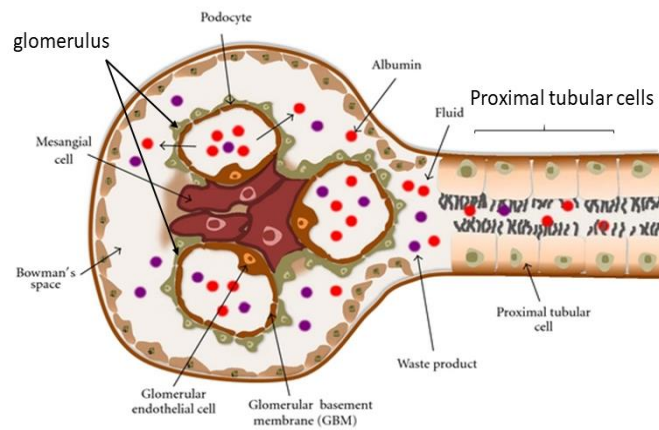
Figure 1. 3. Anatomy of the glomerulus. The glomerulus contains mesangial cells and a capillary wall with endothelial cells, glomerular basement membrane, and podocytes. Adapted from Tanaka et al., 2011.

1.2 Kidney disease

The ability of the kidney to excrete metabolic waste and reabsorb nutrients from the urine can be affected by a number of factors, including genetic mutations (e.g. polycystic kidney disease (PKD) caused by mutations in the *PKD1* or *PKD2* genes) (Bergmann et al., 2018), and kidney injury (e.g. acute renal failure and chronic kidney disease) (Peter et al., 2003; Patel et al., 2009; López-Novoa et al., 2010).

Acute renal failure (ARF) represents the sudden loss of kidney function over a few hours or days (increase in serum creatinine ≥0.3 mg/dL within 48 hours; or increase in serum creatinine ≥1.5 times baseline within 7 days; or urine volume <0.5 mL/kg/h for 6 hours), which results in a temporary inability to eliminate metabolic waste, concentrated urine, and to maintain fluid balance and electrolyte levels (Schrier et al., 2004; Makris and Spanou, 2016). ARF has a mortality rate of 50–80% and its incidence is higher in elderly people who are critically ill, and in intensive care patients (Schrier et al., 2004). There are three common causes of ARF: 1) an abrupt drop in blood flow, which may be caused by low blood pressure, heart attack, injury sepsis or dehydration; 2) urinary tract obstruction caused by a kidney stone, tumour, or a blood clot in the urinary tract; and 3) direct damage to the kidney as a result of infection, multiple myeloma, medication, kidney blockage or acute tubular necrosis (ATN) (Lameire et al., 2005). Management of ARF requires treatment of the underlying causes, by increasing the water intake if the patient is dehydrated, prescribing antibiotics in the case of infection or stopping the intake of medication that may be causing kidney damage (Rahman et al., 2012; Makris and Spanou, 2016). With the right treatment, the kidney function of the ARF patient can be recovered fully. However, these

patients become more prone to develop chronic kidney disease in the future (Rahman et al., 2012; Makris and Spanou, 2016).

Chronic kidney disease (CKD) is the gradual loss of the kidney function over time, leading to increased retention of body fluid, build-up of electrolytes and waste in the blood (Dedkova, 2015). Often, patients in the early stages of chronic kidney disease (CKD) are asymptomatic until their kidney function is significantly impaired (more than 85-90% loss of renal function) (Webster et al., 2017). Patients with CKD can be classified into 15 groups based on five GFR (G1-G5) and three albumin:creatinine ratios (ACR A1-A3), ACR being a marker of kidney damage. The stages of CKD are depicted in Table 1.1.

Table 1. 1: Classification of chronic kidney disease stages by the GFR and ACR.
Colours represent the progression of CKD; green: no CKD or low risk; yellow: moderate-risk CKD; orange: high risk; red: very high risk; deep red: highest risk. (Adapted from Levey and Coresh, 2012).

		ACR stages		
Stage	**GFR (ml/min/1.73 m2)**	**A1** Normal to mildly increased (<30 mg/g or <3 mg/mmol)	**A2** Moderately increased (30-299 mg/g or 3-29 mg/mmol)	**A3** Severely increased (≥ 300 mg/g or ≥ 30 mg/mmol)
G1	≥ 90 Normal or increased			
G2	60-90 Slight decrease			
G3a	45-59 Mildly to moderately decreased			
G3b	30-44 Moderately to severely decreased			
G4	15-20 Severely decreased			
G5	<15 Established renal failure			

In England, it is estimated that 2.6 million people aged 16 years and older have CKD stage 3-5 (see Table 1.1 for CKD stages); accounting for 6.1% of the population of this age group. The prevalence of CKD stage 3-5 is higher in women than in men (7.4% vs. 4.7%) as demonstrated by data from the Health Survey for England (HSE) 2009 and 2010, and the 2011 Census. The prognosis is that the prevalence of CKD stage 3-5 for those aged 16 years and older is expected to increase to 3.2 million people in 2021 and to 4.2 million in 2036, which accounts around 8.3% of population (Public Health England, 2015).

A number of factors cause CKD, such as diabetes, hypertension, cardiovascular disease (CVD), glomerulonephritis, interstitial nephritis (inflammation of the glomeruli and the renal tubules, respectively), polycystic kidney disease, and obstruction of the urinary tract by kidney stones or certain types of cancer (Rahman and Smith, 1998; Pyram et al., 2012). The progression of CKD is also associated with a number of complications, including the increased incidence of cardiovascular disease, anaemia, metabolic bone disease and hyperlipidaemia (Thomas et al., 2008).

Cardiovascular disease (CVD) accounts for more than 50% of deaths in patients with CKD, mostly due to blood vessel disease (Steigerwalt, 2008; Briasoulis and Bakris, 2013; Hill et al., 2016; Romagnani et al., 2017). Furthermore, the prevalence of cardiovascular complications increases with the decline of kidney function. For example, CVD increased the risk of mortality by 8.1-fold in CKD patients (stage G5 A3, eGFR < 15 ml/min/1.73 m^2 and urinary albumin-creatinine ratio > 300 mg/g) than in a reference population without CKD (Levey et al., 2011). Furthermore, in the general population, sudden cardiac death accounts approximately one death per 1000 person-years, which is 6–13% of all deaths.

In contrast, in individuals with kidney failure, sudden cardiac death accounts for approximately 59 deaths per 1000 persons/year (Green et al., 2011). However, CKD, even in its early stages, can cause hypertension and increase the risk for CVD leading to increased patient morbidity and mortality (Said and Hernandez, 2014). Thus, therapeutic approaches targeting CKD are required to prevent or slow down CKD and its complications to reduce the morbidity and mortality in patients with CKD.

Diabetes and high blood pressure are responsible for up to two-thirds of CKD cases (Okura, 2010). Both conditions directly damage the kidneys' small blood vessels due to filtration of high levels of glucose in the blood, and dilation of the blood vessels as a result of hypertension (Van Buren and Toto, 2011; Nazar, 2014). The consequent damage increases albumin leaking into the renal tubules and urine, which can be detrimental in kidney disease (Okura, 2010).

Although the progression of kidney disease is often slow following the initial injury, it may subsequently lead to end-stage renal disease (ESRD) which is characterised by the decrease of glomerular filtration rate (GFR) to less than 15 mL/min/1.73 m^2 for at least 3 months (Haynes and Winearls, 2010). Proteinuria (the excessive loss of protein in the urine) can accelerate the decline of GFR especially when it exceeds 3g/day (Lim et al., 2019).

As CKD progresses and the kidney function declines, uraemia (metabolic waste products in the blood) increases, causing a number of symptoms like oedema, fatigue, hypertension and weight loss (Foris and Bashir, 2019). Uraemia is life-threatening and when the GFR falls below 15 mL/min/1.73 m^2, renal replacement

therapy (dialysis or kidney transplant) is the only treatment option (Foris and Bashir, 2019).

In the UK, around 40,000 patients are under dialysis or have functioning kidney transplants (Kerr et al., 2012). Dialysis is costly for the National Health Service (NHS): the mean annual cost of dialysis is £27,000 per patient per year, which accounts for approximately 1.3% of the NHS budget (Kerr et al., 2012). Moreover, the two types of dialysis: haemodialysis and peritoneal dialysis, are associated with a number of complications, including infection (Dalal et al., 2011; Zazzeroni et al., 2017). It is estimated that approximately 18% of infection-related mortality in peritoneal dialysis patients is due to peritonitis (Li et al., 2010). Although less than 5% of peritonitis episodes result in death, peritonitis is the main contributing cause of death in 16% of peritoneal dialysis patients (Li et al., 2010; 2016), and patients on haemodialysis are prone to sepsis (Abou Dagher et al., 2015).

A kidney transplant is the preferred treatment option in ESRD due to the positive effects on patients' wellbeing and reduced costs (around £17,000 in the first year and £5,000 for every subsequent year after transplantation) (NHS-England, 2013). However, there is a shortage of organ donors in the UK, which leads to a long waiting list for kidney transplants. For example, in 2017–2018 there were about 2,573 kidney transplantations; however, over 5,033 patients remained still on the UK kidney transplant waiting list (NHS, 2018).

From a clinical point of view, the best strategy for treatment of ESRD is the prevention or the delay of CKD progression to ESRD. Treatment of the underlying disease, life-style management, anti-hypertensive therapy, tight glycaemic control, and anti-proteinuric therapy can slow down the progression of CKD to ESRD (Riegersperger and Sunder-Plassmann, 2007). Furthermore, other

strategies may prevent the incidence of CKD including increased awareness of CKD and screening programs for kidney function (Chen and Harris, 2015). However, currently, one of the main challenges in treating patients with CKD, regardless of the underlying cause for their condition, is the prevention or slowing down of renal fibrosis, a pathological process which can lead to ESRD (Sharaf El Din et al., 2016), and hence is the focus of this study.

1.3 Complication of diabetes and hyperglycaemia in kidney patients

Diabetes is a group of chronic metabolic disorders diagnosed by persistent hyperglycaemia caused either by insulin deficiency (Type 1) or insulin resistance (Type 2 diabetes). Diabetes is associated with high glucose levels in the blood (hyperglycaemia) and decreased body weight (Baron, 2001; Eknoyan and Nagy, 2005). Hyperglycaemia often leads to polyuria (urine output exceeding 3 L/24h in adults) which is a result of increased glucose excretion in the urine (McFarlane et al., 2013).

Worldwide, 285 million people between the ages of 20 and 79 currently have diabetes and this number is expected to increase by more than 50% over the next 20 years if preventive programmes are not implemented (Pecoits-Filho et al., 2016). In the UK approximately 3.8 million people (9% of the population) have been diagnosed with diabetes with a further 1,000,000 people going undiagnosed (Diabetes-UK, 2018). Type 1, or juvenile onset diabetes, is an autoimmune disease which results in the destruction of the insulin-producing β-cells in the pancreas (Rowe et al., 2011).

Approximately 90% of patients with diabetes in the United Kingdom have type 2 diabetes, especially patients over the age of 45 (Bermudez, 2004). Type 2, or adult onset diabetes mellitus (AODM), is characterised by either insulin resistance, insulin deficiency or a combination of both (Kuzuya et al., 2002). In patients with type 2 diabetes, the pancreatic β-cells often produce sufficient insulin amounts, but the body's cells are unable to use it effectively due to impaired insulin signalling (also known as 'insulin resistance'). However, over time the insulin production may eventually decrease (Cantley and Ashcroft, 2015).

At present, Type 1 diabetes cannot be cured but can be controlled by the administration of insulin. In contrast, patients with type 2 diabetes have a number of treatment options, for example dietary modifications, exercise and drugs that improve insulin sensitivity (e.g. metformin). However, in the advanced stages of type 2 diabetes, insulin therapy may be required (Dasari et al., 2008).

1.4 Diabetes and cardiovascular disease

Cardiovascular disease is the major cause of morbidity and mortality in diabetic patients (Matheus et al., 2013). Diabetes is a critical risk factor for cardiovascular disease, and is associated with many micro- and macrovascular complications such as retinopathy, nephropathy, and neuropathy (Beckman and Creager, 2016). Hyperglycaemia is the primary aetiology for microvascular disease (leading to nephropathy), which induces pathognomonic alterations in the microvasculature, resulting in increased extracellular matrix (ECM) protein synthesis and increase thickness of the capillary basement membrane of

arterioles in the glomeruli, skin, retina, muscle and myocardium (Orasanu and Plutzky, 2009; Chawla et al., 2016). The thickening of the capillary basement membrane leads to abnormal vessel function and causes multiple clinical problems, including hypertension, tissue hypoxia and delayed wound healing (Orasanu and Plutzky, 2009; Chawla et al., 2016).

Hyperglycaemia can induce vascular complications by several mechanisms, including the formation of advanced glycation end products (AGEs), increased oxidative stress, protein kinase C (PKC) and low-grade inflammation, which eventually contribute to both macrovascular and microvascular complications (Aronson and Rayfield, 2002; Chawla et al., 2016).

1.5 Diabetic nephropathy

Diabetes is a risk factor for kidney disease and is the leading cause of ESRD with approximately 40% of diabetic patients developing nephropathy (Alicic et al., 2017). Clinically, DN is characterised by albuminuria and a decline in the estimated GFR. In addition, DN leads to glomerulosclerosis, tubulointerstitial fibrosis (TIF) and tubular atrophy (Slyne et al., 2015). Glomerulosclerosis is characterised by the thickening of the basement membrane, increased matrix formation and expansion of mesangial cells (Slyne et al., 2015). Similarly, TIF correlates with increased interstitial matrix deposition, loss of tubule cells, accumulation of inflammatory cells (such as macrophages) and the activation of fibroblasts (Zeisberg and Neilson, 2010).

Although research has focused on the glomerulus in DN, there is increasing evidence for the pivotal role of the tubules in the development and progression of the disease (Slyne et al., 2015).

TIF plays a central role in the final common pathway of the progression of DN, and is a better indicator of disease progression than glomerular damage. A number of factors such as hyperglycaemia, inflammation, proteinuria and hypoxia cause damage of renal proximal tubules in DN, and this occurs through the activation of several mechanisms including TGF-β signalling, activation of protein kinase C and the renin-angiotensin system, AGEs, and oxidative stress (Kanwar et al., 2008).

Hyperglycaemia has been implicated in the damage of the renal proximal tubule cells in DN (Vallon, 2010). The high glucose concentration in these cells in diabetes is caused either by the elevated plasma glucose or by increased glucose filtration by the glomeruli (Slyne et al., 2015). The excessive glucose load increases the production of nicotinamide adenine dinucleotide (NADH) and flavin adenine dinucleotide (FADH$_2$) by the tricarboxylic acid cycle (TCA) cycle, which increases the production of ATP and the generation of superoxide from complexes I and III in the mitochondrial electron transport chains (Bhargava and Schnellmann, 2017). The abnormal generation of free radicals and peroxides can lead to the increased production of inflammatory cytokines and ECM proteins through activation of redox-sensitive signalling pathways involving the transcription factors nuclear factor kappa B (NF-kB) and activator protein (AP-1) (Elmarakby and Sullivan, 2012; Bhattacharyya et al., 2014). In turn, particular cytokines and growth factors may stimulate the production of free radicals, leading to cellular damage, and may modify ECM proteins, thus contributing to

the pathogenesis of diabetic nephropathy and its progression to ESRD (Kanwar et al., 2008; Elmarakby and Sullivan, 2012). It has been shown that diabetes increases the reactive oxygen species (ROS) generation in PTECs, suggested an important role for ROS in the pathogenesis of diabetic nephropathy (Liu et al., 2007). According to Rhyu et al. (2012), ROS mediate the TGF-β1- induced PAI-1 expression in the glomeruli and tubulointerstitium (including renal tubule epithelial cells) via the activation of mitogen-activated protein kinase (MAPK).

AGEs are proteins or lipids that become glycated in non-enzymatic reactions in the presence of sugars (Kim et al., 2017). Diabetes leads to an increase in AGEs as a result of a high level of blood glucose in the body (Goh and Cooper, 2008). AGEs have detrimental effects on the structure and function of blood vessels and other tissues (Ramasamy et al., 2005; Goldin et al., 2006). They exert their biological effects directly, by changing the structure and function of the ECM, or by interacting with the receptor for advanced glycation end products (RAGE) (Masola et al., 2011; Slyne et al., 2015). RAGE plays an important role in the induction of the expression of TGF-β and cytokines that mediate the EMT to the accumulation of ECM in fibrotic disease (Oldfield et al., 2001).

According to Ahmed (2005), AGEs and hyperglycaemia together increase the release of TGF-β and the deposition of ECM in the glomerulus. The proximal tubule cells are a key target for AGEs, as the PTCs are a primary site for the reabsorption of filtered AGEs (Slyne et al., 2015). Morcos et al, (2002) demonstrated an increased secretion of the proinflammatory IL-6 by human renal proximal tubule epithelial cells in response to NF-κB activation following an exposure to AGE-albumin. AGEs can also activate the Smad2/3 signalling pathway to induce tubular EMT and fibrosis independently of TGF-β via ERK/p38-

Smad signalling crosstalk pathways (Li et al., 2004). Collectively, these data suggest that AGEs cause activation and increased expression of various of disease mediators that have been implicated in DN including NF-κB and TGF-β (Morcos et al., 2002; Chung et al., 2010).

Another metabolic pathway which is activated by hyperglycaemia and which may cause damage to the proximal tubule epithelial cells in diabetes is the polyol pathway. This metabolic pathway uses the cofactor nicotinamide adenine dinucleotide phosphate (NADPH) to convert glucose to fructose (Yan, 2018). The resulting NADPH depletion in hyperglycaemia may induce ROS generation which can cause modifications to ECM proteins and resistance to proteolysis (Slyne et al., 2015). For example, an accumulation and modulation of fibronectin was observed in the porcine LLC-PK1 proximal tubule cell line in response to hyperglycaemia following the activation of the polyol pathway, demonstrating the role of polyol pathway in the renal fibrosis and pathogenesis of DN (Morrisey et al., 1999).

Protein kinase C (PKC) belongs to a family of serine/threonine-related protein kinases and affects several signal transduction pathways, including some involved in the pathogenesis of DN (Soetikno et al., 2012). PKC can be activated by both diacylglycerol (DAG), which is produced from excess glyceraldehyde-3-phosphate in hyperglycaemia, and by the polyol pathway (Evcimen and King, 2007). The activation of PKC has been implicated in renal fibrosis through the overexpression of ECM and TGF-β (Ha and Lee, 2005). The activation of PKC can induce plasminogen activator inhibitor-1 (PAI-1) overexpression and can activate the NF-κB signalling, as well as participating in the inflammatory response and renal fibrosis in DN (Ha and Lee, 2005; Slyne et al., 2015).

1.6 Role of human renal proximal tubule epithelial cells (RPTEC) in glucose reabsorption

Up to 90% of the parenchymal mass of the kidney comprises the tubulointerstitial compartment (Mauer et al., 1984; Nath, 1992). The reduction of the parenchymal mass due to renal injury may lead to the destruction of renal tubule cells, which leads to the progression of CKD, thus indicating the importance of the tubule cells in kidney disease (Mauer et al., 1984; Nath, 1992).

The proximal tubule cells (PTC) play a central role in the reabsorption of useful nutrition from the primary urine, including vitamins, glucose, minerals and protein (Alelign and Petros, 2018). The glomeruli filter approximately 180 g/day of glucose from the plasma, and almost 100% of it is subsequently reabsorbed in the proximal convoluted tubule (Mather and Pollock, 2011; Ghezzi et al., 2018).

There are two types of the glucose transporters in the proximal tubule cells that maintain glucose reabsorption from the urine and its secretion into the circulation: the sodium-dependent glucose transporters 1 and 2 (SGLT 1/2) that are situated on the apical side of the proximal tubule cells, and glucose transporters (GLUTs) situated on the basolateral side. Up to 90% (some sources mention 97%) of the filtered glucose is reabsorbed by the low-affinity, high-flux SGLT2 and its efflux is mediated by GLUT2 in the early proximal tubule segments S1 and S2 (Vallon, 2011; Szablewski, 2017). The remaining glucose is reabsorbed from the primary urine by the high-affinity, low-flux SGLT1 and excreted by GLUT1 in the late proximal tubule segment S3 (Mather and Pollock, 2010; Vallon, 2011).

Through active transport, SGLT1/2 absorb glucose from the primary urine against the concentration gradient (Mather and Pollock, 2011; Ghezzi et al., 2018). The

cotransport of glucose and sodium into the proximal tubule cells depends on the sodium/potassium (Na^+/K^+) ATPase, located on the basolateral membrane. The (Na^+/K^+) ATPase transports sodium ions out of the cell and potassium ions into the cell, which maintains a sodium concentration gradient in the proximal tubule lining (Figure 1.4) (Mather and Pollock, 2011; Triplitt, 2012). This allows the glucose concentration to become higher in the epithelial cell than in the interstitial space. As a result, the glucose then moves passively through the GLUTs across the basolateral membrane of the epithelial cells into the interstitium and the circulation (Bakris et al., 2009; Komala et al., 2013).

Hyperglycaemia increases the ability of the proximal tubule to reabsorb the glucose by increasing the capacity for glucose transport. For example, primary human proximal tubule cells obtained from fresh urine of patients with diabetes have shown elevated expression of SGLT2 (Rahmoune et al., 2005). Another study of the animal model of Zucker rats has demonstrated that diabetes may increase RNA expression of both SGLT2 and SGLT1 in the kidney (Tabatabai et al., 2009). Furthermore, the increased expression of GLUT2 has been reported in diabetic rats, which is translocated to the luminal surface of the proximal tubule cell, playing a role in increased glucose reabsorption (Marks et al., 2003). However, the reduction of glucose transport via the proximal tubule cells may decrease the proximal tubule cell-induced inflammation and fibrosis in diabetic nephropathy. It has been reported that the inhibition of SGLT2 in HK-2 cells decreases high glucose-induced Toll-like receptor 2 and 4, NFκB and activator protein 1 expression, the key mediators of inflammation and fibrosis in diabetic nephropathy (Mather et al., 2011). However, a different result was obtained by

other investigations, and this will be discussed with the glucose intake results (chapter 3).

Overall, it appears that the exposure of proximal tubule cells to elevated glucose can lead to progression of diabetic nephropathy (Mather and Pollock, 2010).
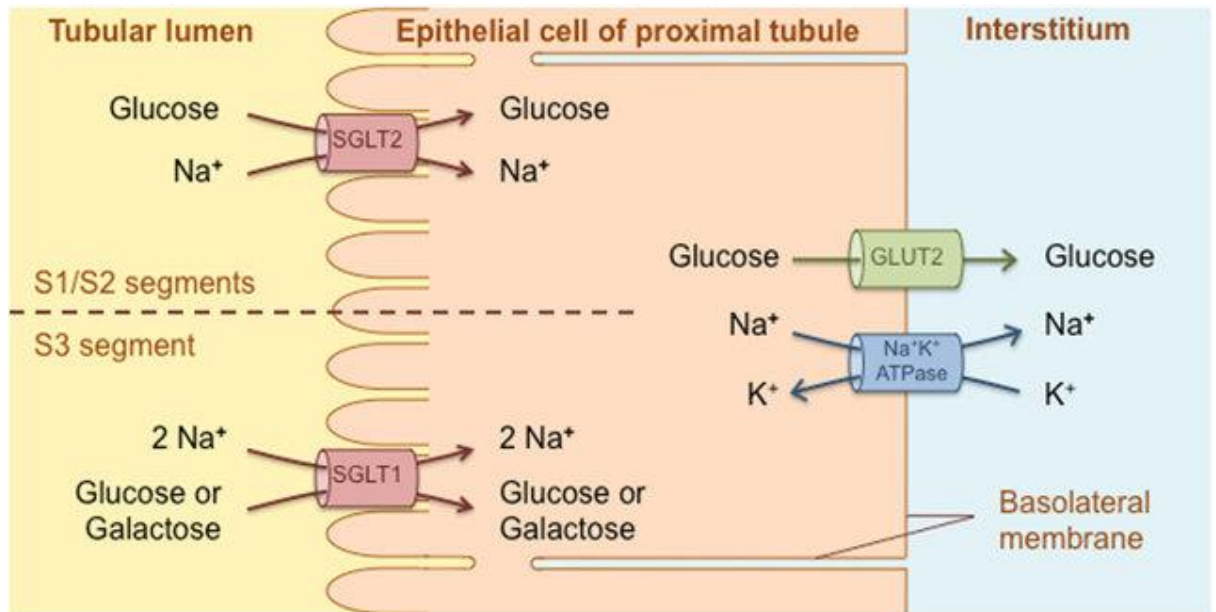
Figure 1. 4: Glucose reabsorption from the proximal tubule. The cotransport of glucose and sodium into the proximal tubule cell is dependent on a sodium gradient produced by sodium/potassium (Na+/K+) ATPase pumps located on the basolateral membrane (Faillie, 2017).

1.7   Renal fibrosis and tubulointerstitial fibrosis (TIF)

Renal fibrosis is the hallmark of CKD and can lead to ESRD. Renal fibrosis can affect the glomerulus and/or the tubule causing glomerulosclerosis and tubulointerstitial fibrosis (TIF) (Boor et al., 2007). TIF is considered irreversible and is characterised by the excessive deposition of extracellular matrix (ECM) in the renal tubules (Zeisberg and Neilson, 2010). TIF causes a thickening of the glomerular basement membrane, increased numbers of inflammatory cells and fibroblasts, rarefaction of peritubular capillaries, disruption of normal cell-to-cell interactions and loss of tissue elasticity, which lead to the gradual destruction of

nephrons (Zeisberg and Neilson, 2010). Studies using a mouse model of renal fibrosis, and renal human tissue from CKD patients with diabetes have demonstrated that the process of epithelial-to-mesenchymal transition (EMT) can be triggered by hyperglycaemia/diabetes, proteinuria and hypoxia through the action of transforming growth factor beta-1 (TGF-β1) (Haase, 2006; Higgins et al., 2007; 2008; Efstratiadis et al., 2009b). Furthermore, various factors, including inflammatory cytokines (such as Tumour necrosis factor alpha (TNF-α)) and reactive oxygen species (ROS), have been shown to induce EMT and the activation of mesangial cells, tubule epithelial cells, and fibroblasts to increase the production of ECM proteins (Hills and Squires, 2010; Jha et al., 2016).

Tubulointerstitial fibrosis is the final common pathway for all kidney diseases. It is characterised by the progressive detrimental connective tissue deposition on the kidney parenchyma, leading to chronic renal failure (Efstratiadis et al., 2009). The widened interstitial spaces in fibrotic kidneys fill with fibrillar material of collagens type I and III and fibronectin and fragments of collagen type IV, which is normally found in basement membranes, and this may result in the abnormal deposition of the extracellular matrix (Zeisberg and Neilson, 2010; Hewitson et al., 2017).

The tubule epithelial cells spark the progression of fibrogenesis (a mechanism of wound healing and repair) in response to their own injury. Damage to the tubule cells may result in dysregulation of their proliferation and survival, or the expression of cytokines and proinflammatory chemokines (e.g. IL-1, IL-6, MCP-1 and TGF-β1) that stimulate mononuclear inflammation (e.g. attraction and activation of macrophages, dendritic cells, and T lymphocytes) and the formation of fibroblasts (Zeisberg and Neilson, 2010). EMT is a key mechanism leading to

TIF, through the loss of phenotypical characteristics of the tubule epithelial cells and their transformation to mesenchymal fibroblasts (Docherty et al., 2006; Yang et al., 2010; Zeisberg and Neilson, 2010). TGFβ/Smad signalling is central to EMT as it affects several EMT-related genes such as connective tissue growth factor, integrin-linked kinase (ILK), PINCH-1, β1-integrin, Snail, α-smooth muscle actin (α-SMA), collagen IA2, and MMP-2, leading eventually to tubulointerstitial fibrosis (Li et al., 2003; Phanish et al., 2006; Li et al., 2007a; Li et al., 2007b; Liu, 2010). Several *in vitro* studies have demonstrated that TGF-β1 induces the transition of tubule epithelial cells to fibroblasts through the loss of epithelial proteins including E-cadherin, cytokeratin and zonula occludens-1 (ZO-1) and the acquisition of mesenchymal markers including fibroblast-specific protein-1 (FSP1), vimentin, α-SMA, interstitial matrix components type I collagen, and fibronectin (Liu, 2004; Strutz, 2009; Liu, 2010). *In vivo* studies with tagged proximal tubule epithelial cells, found that after unilateral ureteral obstruction up to 36% of all fibroblasts in the interstitial space came from renal proximal tubule cells. These data suggest that there is a significant role for EMT contributing to the pathogenesis of renal fibrosis (Iwano et al., 2002).

Increased blood glucose concentration increases the glomerular filtration rate (GFR) above normal, which strains the filtration ability of the glomeruli and raises blood pressure. Consequently, the glomerular basement membrane begins to thicken and expand, taking up the space originally occupied by the glomerular capillaries. In response to the initial injury, macrophages and T cells begin to accumulate, and these scarred and inflamed capillaries lose their ability to filter blood as effectively as they should (Gerich, 2010; Palatini, 2012; McFarlane et al., 2013). Similarly, in the tubulointerstitium, tubular hypertrophy and associated

basement membrane alteration predate tubulointerstitial fibrosis, which accompanies progressive renal fibrosis (Phillips and Steadman, 2002).

1.8 The extracellular matrix (ECM)

Renal fibrosis is caused by excessive deposition of extracellular matrix (ECM). Collagen is one of the most abundant proteins in the human body; it accounts for approximately 30% of the total protein in the body and is the main protein of the ECM. Various collagens in the ECM provide tensile strength, regulate cell adhesion, support chemotaxis and migration, and direct tissue development (Frantz et al., 2010). The collagens are categorised into 28 different types with I, III, IV with collagen IV being the most prominent (Batzios et al., 2013). Collagens I, II and III are important for forming fibrils of similar structures, while collagen IV supports the basal lamina. However, the overproduction and/or decreased degradation of collagen are associated with the progression of kidney disease and tubulointerstitial fibrosis (Liu et al., 2012).

ECM proteins, such as collagen, elastin, fibronectin and laminin, form an intricate network of macromolecules that serve as a relatively inert scaffold to stabilise the physical structure of tissues (Alberts et al., 2002). The ECM regulates the behaviour of the cells in contact with it and also has a metabolic function that influences the proliferation and migration of the cells, and their shape and survival (Davies, 2001; Davis and Senger, 2005; Frantz et al., 2010). It is of note that the abnormal accumulation of ECM components is a key pathogenic feature of chronic fibrotic kidney disease (Jung et al., 2009; Zeisberg and Neilson, 2010), and hence the regulation of this process will be addressed in this study.

1.8.1 Matrix metalloproteinases (MMPs) and tissue inhibitors of matrix metalloproteinases (TIMPs)

MMPs are a group of proteolytic enzymes that belong to large a family of zinc-dependent endopeptidases. They are key factors which regulate the degradation and remodelling of the ECM (Klein and Bischoff, 2011). The ECM turnover is fundamental for embryonic development, cell migration, reproduction, morphogenesis and remodelling of tissues under normal and pathologic states (Klein and Bischoff, 2011). MMPs play a role in various renal diseases that include glomerulonephritis and tubular diseases. The accumulation of ECM is the hallmark of diabetic nephropathy, which is linked not only to the excessive synthesis of the ECM component, but also to a decrease in the degradation of ECM by the MMPs (Xu et al., 2014).

Tissue inhibitors of metalloproteinases (TIMPs) are the main inhibitors of MMPs, and cause the accumulation of ECM and renal fibrosis by suppressing the degradation of matrix proteins (Eddy et al., 2000). There are at least four secreted TIMPs (TIMP1, 2, 3 and 4), and patients with any stage of CKD display increased expression of TIMP1 and 2 (especially in CKD stages 4 and 5) (Musiał and Zwolińska, 2011).

1.8.2 Plasminogen activator inhibitor-1 (PAI-1)

Plasminogen activator inhibitor-1 (PAI-1) is a member of the serine proteinase inhibitors (serpin) superfamily and plays a pivotal role in ECM remodelling and fibrinolysis (Ghosh and Vaughan, 2012). In a healthy kidney, PAI-1 is produced in trace amounts, but its expression is upregulated in acute and chronic kidney

disease. It has been shown that PAI-1 plays a central role in glomerulosclerosis and tubulointerstitial fibrosis and, therefore, in the progression of renal disease (Eddy, 2002; Rhyu et al., 2012; Malgorzewicz et al., 2013).

PAI-1 is the major inhibitor of plasminogen activators, such as tissue-type plasminogen activator (t-PA) and urokinase-type plasminogen activator (u-PA) (Yasar et al., 2014). These activators convert not only plasminogen to plasmin (an MMP activator and ECM protease) (Lee and Huang, 2005), but also catalyse the conversion of the latent form of TGF-β to its active form, and of the pro-MMPs to MMPs. By inhibiting uPA/tPA, PAI-1 prevents the activation TGF-β and protects ECM proteins from proteolytic degradation (Hertig et al., 2003; Lackie, 2008; Ghosh and Vaughan, 2012). In fibrosis, PAI-1 inhibits the degradation of collagen and thus leads to the abnormal accumulation of ECM proteins, which exacerbate tissue fibrosis (Hertig et al., 2003; Lackie, 2008; Ghosh and Vaughan, 2012).

The expression of PAI-1 is increased in response to lipopolysaccharide, growth factors, cytokines and ROS (Hagiwara et al., 2003; Lee and Huang, 2005). TGF-β1 is a key factor of fibrosis which stimulates the expression of the *PAI-1* gene and the deposition of interstitial collagen in TGF-β1 transgenic mice. In addition, the absence of PAI-1 demonstrates the synergetic action of PAI-1 and TGF-β1, as it prevents TGF-β1-induced collagen deposition and kidney fibrosis (Krag et al., 2005; Ghosh and Vaughan, 2012).

The key role of PAI-1 in diabetes is demonstrated in PAI-1-deficient mice with streptozotocin (STZ) -induced insulin deficiency. After 1 month of diabetes, PAI-$1^{-/-}$ mice displayed a reduction in albuminuria, TGF-β and fibronectin levels in

the renal cortex compared to wild type mice (Nicholas et al., 2005). Furthermore, Hagiwara et al. (2003) reported overexpression of PAI-1 mRNA in intraglomerular cells and tubule epithelial cells in STZ-induced diabetic rats and Otsuka Long-Evans Tokushima Fatty (OLETF) rodents. In addition, tPA and uPA mRNA levels were significantly decreased in OLETF rodents. Collectively, these data suggest that PAI-1 is a key factor in DN (Hagiwara et al., 2003; Nicholas et al., 2005).

1.8.3 Key factors in extracellular matrix remodelling, inflammation and kidney injury

1.8.3.1 Cytokines and chemokines

Cytokines are a large family of proteins and peptides, with molecular weights of less than 30 kDa, that promote autocrine, paracrine, and juxtacrine signalling in response to infections and changes in the environment (Pérez-Morales et al., 2018). A main immune function of the cytokines is to regulate the inflammatory process. Cytokines act via a range of specific receptors, and several cytokines may act synergistically by either interacting with the same receptor or by activating the same intracellular signalling pathways (García-García et al., 2014).

The collective renal cells, including glomerular, tubular, mesangial and endothelial cells, produce inflammatory cytokines in response to hyperglycaemia, and the level of these cytokines rises as DN progresses (Chow et al., 2005; Vestra et al., 2005; Pérez-Morales et al., 2018).

The chemokines are a family of chemoattractant cytokines that play an important role in cell movement. Chemokines are classified into four main subfamilies; C,

CC, CXC, and CX3C based on the number and location of the cysteine residues near the amino terminus. The chemokines act by activating G protein-coupled receptors (GPCRs) called chemokine receptors, located on the surfaces of their target cells (Deshmane et al., 2009; Gupta et al., 2013).

Several factors related to diabetes, such as hyperglycaemia, AGEs, ROS, Ang II, haemodynamic alteration and hyperinsulinemia, activate the nuclear transcription factor (NF-κB) which upregulates the expression of cytokines and chemokines in the kidney (Wada and Makino, 2013; Barutta et al., 2015), but for the purpose of this study, the response of proximal tubule cells to hyperglycaemia will be investigated. In an autocrine or paracrine mode of action they interact with renal cells (epithelial, endothelial, mesangial, tubule cells and podocytes) and/or recruit and activate inflammatory cells (monocytes, lymphocytes and neutrophils) (Navarro-González et al., 2011; Barutta et al., 2015).

1.8.3.2 Transforming growth factor-β1 (TGF-β1)

Transforming growth factor β is a multifunctional cytokine that plays a vital role in controlling proliferation, differentiation, motility and apoptosis in a wide range of cells (Chang et al., 2016). TGFβ is expressed as three isoforms (TGF-β1, TGFβ-2 and TGFβ-3), and all mammalian cells express specific receptors for TGFβ (TGF-β receptor types I, II, and III), which mediate the intracellular signalling of the TGFβ isoforms (Huang and Huang, 2005). In the healthy human adult kidney, TGF-β2 and TGF-β3 are expressed in the glomerulus (mainly in podocytes), while TGF-β1 is detected in the tubules (Ito et al., 2010). However, in kidney biopsies from patients with proliferative glomerulonephritis, diabetic nephropathy or IgA nephropathy, TGF-β1 is co-expressed with TGF-β2 and TGF-β3 in

podocytes and in mesangial cells, and this is correlated with severe glomerulonephritis and glomerulosclerosis (Ito et al., 2010).

TGF-β1 is secreted as a latent precursor (latent TGF-β1), which binds to the latent TGF β-binding protein (LTBP). TGF-β1 is released from the latency-associated peptide (LAP) and the LTBP in response to several factors including ROS and MMPs to form activated TGF-β1 (Lyons et al., 1990; Munger et al., 1999; Meng et al., 2013). The activated TGF-β1 binds to TGFβ-receptor 2 (TGFβR2), which activates TGFβR1 to phosphorylate signalling proteins of the Smad pathway (Yu et al., 2003; Sureshbabu et al., 2016). The Smad family comprises: 1) receptor-activated (R-) Smads (Smad2 and 3 are phosphorylated by TGF-β and activin receptors, and Smad1, 5 and 8 by bone morphogenetic proteins (BMP) receptors); 2) a single common-mediator Co-Smad (Smad4); 3) the inhibitory I-Smads (Smad6 and Smad7) (Dijke and Heldin, 2007; Heldin et al., 2009).

The activation of TGFβR1 leads to phosphorylation of Smad2/3 proteins, which then form an oligomeric complex with Smad4 that translocates into the nucleus. In the nucleus, the complex regulates the transcription of TGF-β1 target genes including ECM proteins such as collagen I, IV and PAI-1 (Lan, 2012; Conserva et al., 2013). Diabetes induces the expression of TGF-β1, which then plays a central role in renal hypertrophy and the deposition ECM proteins, which eventually leads to kidney fibrosis and the progression of DN (Sharma and Sharma, 2013). It has been shown that hyperglycaemia upregulates the production of TGF-β1 in mesangial and proximal tubule cells, which in turn increases cell proliferation, the expression of collagen, stimulates autophagy and thus can lead to epithelial cell tubular atrophy (Koesters et al., 2010; Bonventre, 2012).

1.8.3.3 Interleukin-6 (IL-6)

Interleukin-6 (IL-6) is a pleiotropic cytokine involved not only in the immune and inflammatory responses, but also in the regulation of numerous biological processes including metabolism, haematopoiesis and organ development (Su et al., 2017). IL-6 signals through a cell surface receptor that consists of the ligand-binding IL-6 receptor (IL-6R)-α chain (CD126) and the signal-transducing component CD130 (García-García et al., 2014). In kidney disease patients with DN, IL-6 is involved in the tubulointerstitial neutrophil infiltration, alteration of the renal structure with changes in the extracellular matrix, and promotion of thickening in the glomerular basement membrane, kidney and podocyte hypertrophy and in the interruption of the normal cell cycle (Suzuki et al., 1995; Vestra et al., 2005; Pérez-Morales et al., 2018). IL-6 mRNA was detected in mesangial, tubular, interstitial and infiltrating cells by the immunohistochemical analysis for a renal biopsy from patients with diabetic nephropathy (Suzuki et al., 1995; Navarro-González et al., 2011).

1.8.3.4 Monocyte chemoattractant protein-1 (MCP-1)

Monocyte Chemoattractant Protein-1 (MCP-1), also known as chemokine (C-C motif) ligand 2 (CCL2), consists of 76 amino acids and has a molecular weight of 13 kDa. MCP-1 regulates migration, initiation and mobilisation as well as the recruitment of monocytes to sites of inflammation produced by either tissue injury or infection (Deshmane et al., 2009).

MCP-1 is excreted by mononuclear cells as well as by a diversity of mesenchymal cells including renal resident cells (mesangial cells and tubule epithelial cells)

(Wada et al., 2000). MCP-1 plays a central role in regulating the recruitment and activation of monocytes, by binding to its receptor CC-chemokine receptor-2 (CCR2) (Barutta et al., 2015). In response to cytokine overexpression and increased urinary protein excretion, MCP-1 regulates the recruitment of monocytes to the renal tubules and also their activation (Prodjosudjadi et al., 1995; Wang et al., 1999; Viedt and Orth, 2002). The infiltration of the inflammatory cells, monocytes and macrophages in kidney disease is the hallmark of the progression of DN. Patient biopsies and animal models demonstrate that MCP-1 mRNA and protein are upregulated in podocytes, mesangial cells, and tubules in diabetic kidneys, and this is associated with the accumulation of macrophages (Wada et al., 2000; Chow et al., 2004; Chow et al., 2006). Furthermore, elevated expression of MCP-1 in renal tubule cells was reported in both experimental diabetes and human DN (Mezzano et al., 2003; Chow et al., 2006; Barutta et al., 2015).

1.8.4 Markers of PTC injury

1.8.4.1 Kidney injury molecule (KIM-1)

T cell-immunoglobulin-mucin (TIM-1) is a type I trans-membrane receptor known as kidney injury molecule (KIM-1) or hepatitis A virus cellular receptor-1 (HAVCR) (Bonventre, 2014). KIM-1 is recognised as the most highly upregulated proximal tubule cell protein following a kidney injury in both humans and animals (Brooks and Bonventre, 2015). KIM-1 plays a vital role as an apoptotic cell phosphatidylserine and scavenger receptor by inducing the binding and uptake of dead cells from the renal tubule lumen in acute kidney injury (AKI) (Ichimura et

al., 2008). The expression of KIM-1 can transform the renal proximal tubule cells into semi-professional phagocytes (Ichimura et al., 2012). KIM-1 is usually undetectable in a healthy kidney, but its expression is increased dramatically in AKI, and its synthesis is localised to the proximal tubule cells (Ichimura et al., 2008).

1.8.4.2 Endostatin

Endostatin is a C-terminal fragment of type XVIII collagen produced by cleavage by proteases or metalloproteases (MMPs). *In vivo* endostatin is an inhibitor of angiogenesis. *In vitro*, it plays an important role in the inhibition of endothelial and epithelial proliferation, migration and tubule formation. It may also have an anti-tumour effect in animal models (Bellini et al., 2007; Kinnunen et al., 2011).

Proteolytic MMPs and other proteases produce endostatin by generating the fragment from collagen XVIII. Endostatin can then remain immobilised to the basement membrane or be released into the bloodstream (soluble form). Immobilised endostatin helps endothelial cells survive and migrate, while soluble endostatin triggers endothelial cell apoptosis, migration, proliferation and invasion (Cichy et al., 2009; Cichy et al., 2015).

1.9 Potential cellular mechanism underpinning renal pathogenesis

The mitochondria are one of the main sources of energy in most eukaryotic cells. They consist of an outer membrane, an inner membrane, which forms cristae, and intermembrane space (Khoshjou and Dadras, 2014). Although the main function of the mitochondria is to supply the cells with energy, they also play a

key role in controlled cell death (apoptosis), regulation of cell metabolism, control of cell growth, cell cycling and cellular differentiation (McBride et al., 2006). Damage or dysfunction of mitochondria has been associated with several renal diseases, including acute kidney injury, chronic kidney disease, renal tumours, and transplant nephropathy (Eirin et al., 2017).

The kidneys, together with the brain and heart, utilise a significant part of the body's energy in the form of adenosine triphosphate (ATP) which is generated through cellular respiration. Although the kidneys are around 0.5% of the total body mass, they use almost 10% of the body's oxygen for cellular respiration to generate energy for active transport related to the reabsorption and secretion of nutrients and metabolites in the formation of urine (Berg et al., 2002; Czajka and Malik, 2016; Perico et al., 2016). The mitochondria generate ATP through the oxidative phosphorylation system (OXPHOS) (Che et al., 2013; Czajka et al., 2015). Electrons produced from cellular metabolism in the cytosol and mitochondrial matrix are transported to the OXPHOS by the coenzymes nicotinamide adenine dinucleotide (NADH) and flavin adenine dinucleotide (FADH$_2$). The electrons then pass through the electron transport chain (ETC) that consists of five protein complexes situated in the inner membrane of the mitochondrial matrix, which is associated with proton transport from the mitochondrial matrix into the intramembrane space. The generated proton gradient drives ATP production by ATP synthase and leads to the formation of water in the mitochondrial matrix from protons, oxygen and electrons from the ETC (Figure 1.5) (Cooper and Hausman, 2000; Granata et al., 2015).

However, two side processes may interfere with the optimal ATP-generating capacity of the mitochondria: the leakage of electrons from the respiratory chain

and the leak of protons from the intermembrane space through the inner membrane into the mitochondrial matrix (Brand et al., 2004). The diversion of protons away from ATP synthase reduces the ATP output and increases heat production (uncoupling), whereas electrons leaking from the ETC complexes may react with oxygen to form reactive oxygen species (ROS) such as superoxide, which can cause cellular oxidative damage and trigger pathological processes in the kidney, including TIF. The mitochondria are considered to be a primary source of ROS, through the generation of superoxide at complexes I and III (Granata et al., 2015). Moreover, increased mitochondrial ROS generation has been associated with increased glucose levels (Shenouda et al., 2011).

Several studies have shown an association between mitochondrial dysfunction and the pathogenesis of DN (Sharma et al., 2013; Czajka and Malik, 2016), however, little is known about mitochondrial dysfunction in kidney disease and hence this is the focus of this study. Hyperglycaemia is a main factor in the development of DN and is associated with mitochondrial dysfunction (Sifuentes-Franco et al., 2018). Hyperglycaemia has been shown to induce oxidative stress as a result of the overproduction of mitochondrial ROS (superoxide). This is combined with decreased mitochondrial antioxidant defence mechanisms, which leads to cell damage through damage to DNA, proteins and lipids
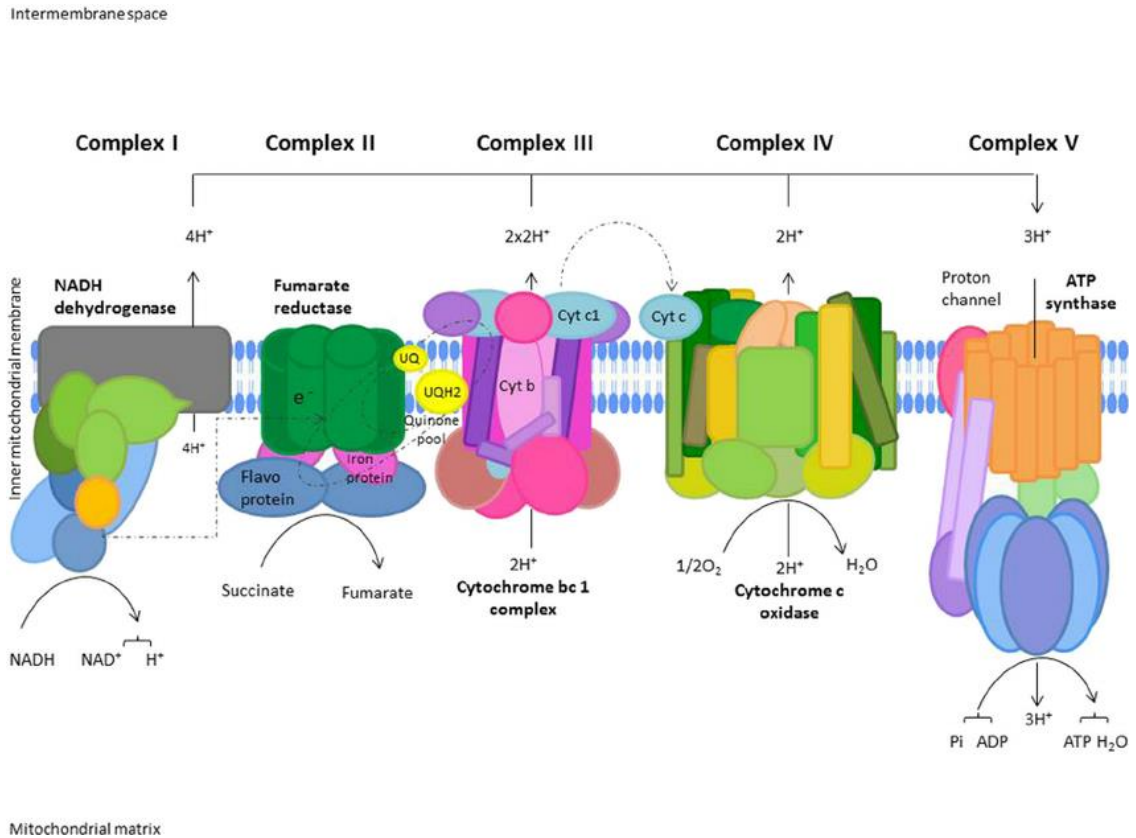
Figure 1. 5: Oxidative Phosphorylation System (OXPHOS). Electrons produced from cellular metabolism in the cytosol and mitochondrial matrix are transported to the OXPHOS by the coenzymes NADH and $FADH_2$. These electrons are then transferred to coenzyme Q (ubiquinone), an electrons transporter from complex I or II, to III. Then, particles are shifted form cytochrome b to cytochrome c with a consequent transfer to Complex IV (cytochrome oxidase) where they reduce O2. This electrons transport through mitochondrial complexes is coupled to shipment of protons in the intermembrane space. The generated proton gradient drives the ATP production by the ATP synthase and leads to the formation of water in the mitochondrial matrix from protons, oxygen and electrons from the ETC (in complex V) (Granata et al., 2015).

(Higgins and Coughlan, 2014). An upregulation of the tubule-specific enzyme *Myo*-inositol oxygenase (MIOX) (MIOX modulates redox imbalance and apoptosis in tubule cells in diabetes) has been observed in human and porcine renal proximal tubule epithelial cell lines (HK-2 and LLC-PK1, respectively) exposed to hyperglycaemia (Zhan et al., 2015). The upregulation of MIOX was accompanied by mitochondrial fragmentation and depolarisation, a decrease in mitophagy-related proteins such as PTEN-induced putative kinase 1 (PINK1) and Parkin (E3 ubiquitin ligase), and inhibition of autophagy/mitophagy. Furthermore,

48

this correlates with increased ROS generation, activation of Bax, the release of cytochrome C, and apoptosis (Zhan et al., 2015). Furthermore, mitochondrial fragmentation has been also observed in diabetic rat proximal tubules in the early stages of diabetes in rat kidneys at 4, 8 and 16 weeks of diabetes (Coughlan et al., 2016). This study showed a reduction in the ATP generation accompanied by the fragmentation of mitochondria, and mitochondrial fragmentation was also associated an increase of ROS generation in proximal tubule epithelial cells in the early stage after 4 weeks of diabetes (Coughlan et al., 2016). At 8 weeks of diabetes, the capacity of the mitochondrial permeability transition pore (MPTP) was increased, which correlated with a generation of mitochondrial hydrogen peroxide (H_2O_2) and contributed to glomerular damage (Coughlan et al., 2016). After 16 weeks of diabetes, tubule damage was observed with increased the expression of urinary KIM-1, where an increase in the complex I-linked oxygen consumption rate (OCR), in the context of a decrease in kidney ATP, indicated mitochondrial uncoupling. Taken together, the study suggested that mitochondrial dysfunction maybe a primary cause of DN (Coughlan et al., 2016). However, as the control animals were non-diabetic, these *in vivo* results do not distinguish between metabolic and osmotic effects of hyperglycaemia on mitochondrial function. *In vitro* experiments could address this question with greater precision. However, the limited number of published studies either do not report on findings related to effects of an osmotic control, or make use of mannitol, a known antioxidant, as an osmotic control (Liu et al., 2010; André and Villain, 2017).

For example, it has been demonstrated that hyperglycaemia (25mM D-glucose) increased the production of mitochondrial superoxide and the loss of cell viability

in cultured rat renal proximal tubule cells (Munusamy and MacMillan-Crow, 2009). However, no osmotic control was been used in that study.

Although an osmotic control was included in a study on the effect of hyperglycaemia (25mM D glucose) on the mitochondrial respiration of primary human mesangial cells and HK-2 cells, it was composed of 5mM D-glucose and 20mM mannitol (Czajka and Malik, 2016). Therefore, one of the aims of the present study was to examine whether hyperglycaemia affects mitochondrial function as a metabolic or osmotic factor, or a combination of both.

1.10 MicroRNA (miRNA)

In recent years, studies have demonstrated that diabetes causes dysregulation of miRNA expression in the kidney and *in vitro* models of renal cells exposed to hyperglycaemia, suggesting a key role in DN (Du et al., 2010; Slyne et al., 2015).

The miRNAs are small non-coding RNA molecules of around 19-25 nucleotides that are involved in the post-transcriptional regulation of gene expression (Dewanjee and Bhattacharjee, 2018). Approximately 2,000 human miRNAs have been identified so far, and the protein expression of around 60% of the human protein-coding genes are regulated by miRNAs. miRNAs play an important role in various cellular and physiological processes, including metabolism, cell cycle regulation, growth, apoptosis and proliferation (Kato and Natarajan, 2015).

The biogenesis of miRNAs consists of multiple steps. The primary miRNA transcripts (pri-miRNA) are transcribed in the nucleus by either RNA polymerase II or RNA polymerase III to long stem loop pri-miRNA. This stem loop is then cleaved into a double-strand shorter precursor miRNA (pre-miRNA) by Drosha

(an RNase III enzyme) and its cofactor DiGeorge syndrome critical region gene 8 (DGRC8). Next, the pre-miRNAs are exported to the cytoplasm by Exportin 5. In the cytoplasm, the pre-miRNAs are cleaved into a mature 20-22 base pair (bp) double-stranded miRNA by Dicer (an RNase III enzyme). The mature miRNA duplex is then unwound and the mature guide single-stranded miRNAs are then loaded into the RNA-induced silencing complex (RISC). The RISC complex binds to the 3' untranslated region (3'UTR) of the target mRNA, which ultimately results in post-transcriptional gene silencing, as the target mRNA is degraded (Figure 1.6) (Jiang et al., 2010; Schena et al., 2013; Chung and Lan, 2015). By inhibiting the expression of a target protein, the miRNA contributes to the epigenetic regulation of its function or downstream targets. Therefore, the miRNAs can be key regulators of the pathogenesis of several diseases, including renal fibrosis, which makes them an attractive therapeutic target in DN.
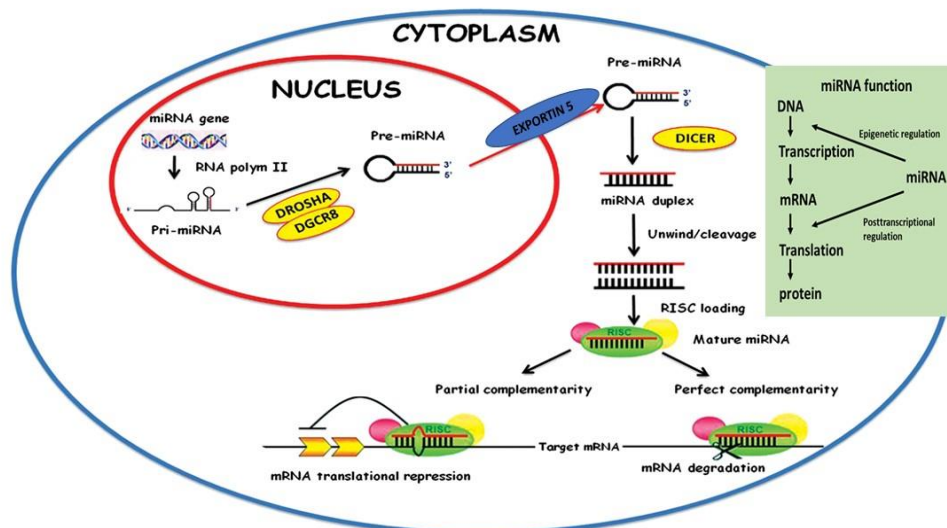
Figure 1. 6: The process of miRNA biogenesis and function in the cell. Adapted from (Schena et al., 2013; Ichii and Horino, 2018)

1.10.1 Fibrotic PTC miRNA in diabetes/hyperglycaemia

Several studies have reported that miRNAs play a role in renal fibrosis and DN.

Table 1.2 represents a summary of literature evidencing miRNA involvement in

fibrosis in response to hyperglycaemia (cell models) or diabetes (animal models),

in relation to PTC.

Table 1. 2: Summary of the miRNAs involved in fibrosis in response to hyperglycaemia (cell models) and diabetes (animal models), in relation to PTC.

First author, year	miRNA	Expre-ssion	Tissue	Type	Predicted target	Results
Bai et al. (2016)	miR-130b	down	PTC, biopsy	Human Rat	Snail	↑ Snail,↑ Col IV ↑ vimentin ↑ α-SMA; ↑ TIF
Du et al. (2010)	miR-29a	down	HK-2 cells	Human	Col IV	↑ Col IV
He et al. (2014)	miR-135a	up	PTC, mesangial cells, serum	Human, mice	TRPC1	microalbuminuria and renal fibrosis
Hou et al. (2016)	miR-27a	up	PTC, biopsy, serum	Rat and Human	PPARγ	↑ TGF-β1;↑ Smad3 ↑ CTGF; ↑ Col I ↑ Fibronectin
Krupa et al. (2010a)	miR-192	down	PTC, biopsy	Human	ZEB1/2	tubulointerstitial fibrosis and low eGFR
Li et al. (2013)	miR-433	up	PTC	Rat	Azin1	↑ TGF-β1 ↑ P-SMAD3
Tang et al. (2018)	miR-302a-3p	up	HK-2 cells plasma	Human	ZEB1	↓ E-cadherin ↑ vimentin ↑ TGF-β1;↑ EMT
Wang et al. (2010)	miR-215	down	PTC, mesangial cells, podocytes	Rat and Human	ZEB1/2	↑ EMT
Zanchi et al. (2017)	miR-184	up	PTC, Blood, urine	Rat	LPP3	↑ Col 3; ↑ PAI-1 ↑ MCP-1; ↑ fibrosis ↑ NF-κB; ↑CTGF ↑ albuminuria
Zhang et al. (2018)	miR-22	up	PTC	Rat	PTEN	↑ α-SMA, ↑ COL4; ↑fibrosis ↓ autophagy

ZEB: zinc finger E-box-binding homeobox, PTEN: phosphatase and tensin homologue, PPAR-γ: peroxisome proliferator-activated receptor-γ, LPP3: lipid phosphate phosphatase 3, Azin1: antizyme inhibitor1, Snail: Snail transcriptional factors, TRPC1: Transient receptor potential cation channel, subfamily C, member 1, Col: collagen.

Evidence has demonstrated that miRNAs play a role in the development of fibrosis (Wang et al., 2012). Several studies indicate that TGF-β may regulate several miRNAs, which exacerbate the progression of renal fibrosis in DN. According to Wang et al (2011), in DN, TGF-β1 induces EMT and renal fibrosis through the downregulation of miR-200a in rat proximal-tubule epithelial cells. Furthermore, the overexpression of miR-200a inhibited the Smad3 activation and suppressed the TGF-β1-induced fibrosis. Hyperglycaemia and TGF-β1 have reported to upregulate miR-377 in animal models of Type 1 diabetes and in mesangial cells, leading to increased fibronectin expression, suggesting a possible role for miR-377 in DN (Wang et al., 2008). However, evidence on the differential metabolic and osmotic effects of hyperglycaemia on the regulation of fibrosis-related miRNA is lacking. Therefore, one of the key aims of the current project was to study the expression of fibrosis-related miRNAs in response to hyperglycaemia in HK-2 cells and to identify potential diagnostic and therapeutic targets involved in DN-induced TIF.

1.11 Hypothesis and aims of the thesis

Multiple mechanisms lead to DN, and many of them are triggered by hyperglycaemia. Hyperglycaemia has two effects: metabolic and osmotic. Although there is a significant number of *in vitro* studies which have investigated the role of hyperglycaemia in renal disease, these two effects are rarely distinguished from one another due to two factors: i) failure to use an osmotic control; or ii) use of an inappropriate osmotic control (e.g. the antioxidant mannitol).

It may appear that the delineation of the metabolic and osmotic effects of hyperglycaemia is not crucial in the investigation of DN. However, it may provide an insight into new pathological mechanisms and treatment targets in diabetes.

1.11.1 Hypothesis

The osmotic and metabolic components of hyperglycaemia have differential detrimental effects on the human proximal tubule epithelial cells (HK-2 cells) in terms of mitochondrial function, the expression of markers of injury, inflammation and fibrosis-related miRNAs.

1.11.2 Overarching aim

To establish the metabolic and osmotic effects of hyperglycaemia on the energy generation and the regulation of the expression of markers of fibrosis and fibrosis-related miRNAs in immortalised human proximal tubule (HK-2) cells.

This will be addressed in the following objectives:

1. To determine whether differences exist in the glycolytic and mitochondrial function of HK-2 cells in response to high D-glucose concentrations or to a metabolically inactive osmotic control (L-glucose).

2. To elucidate the metabolic and osmotic effects of hyperglycaemia on the expression of key fibrosis-related cytokines, and markers of inflammation and ECM accumulation in HK-2 cells.

3. To identify the effect of the metabolic and osmotic components of hyperglycaemia on the miRNA expression of a panel of fibrosis-related miRNAs in HK-2 cells, and to identify potential diagnostic and treatment targets for DN.

Chapter 2: Materials and Methods

2.1 Cell culture

Cell culture techniques were used to study the effect of different concentrations of D-glucose (5, 25 and 30 mM) or osmotic control (5 mM D+ 25 mM L-glucose) (D-glucose, SIGMA #080M0182V; L-glucose, Alfa Aesar #10127841) on human renal proximal tubule epithelial cells (HK-2 cells, ATCC, UK). HK-2 cells were grown in growth medium (50:50 DMEM:Ham's F-12 (Life Technologies; #11966 and Lonza #BE12-61F)) containing 5 mM glucose, 2.5 mM glutamine, 10% foetal calf serum, 50 U/ml penicillin, and 50 µg/ml streptomycin. The cells were grown in 5% CO_2 at 37°C in a cell culture incubator.

Upon reaching 80-90% confluence, the cells were detached with trypsin-EDTA, counted and seeded onto six-well plates at a density of $4x10^4$ cells/well. The growth medium was refreshed every other day and the cells were cultured to 70-75% confluence. The cells were then rinsed twice with sterile phosphate-buffered saline (PBS) (Lonza #BE17-517Q) and growth-arrested in serum-free medium (SFM) containing 50:50 DMEM:Ham's F-12 medium, 5 mM glucose, 2.5 mM glutamine, 50 U/ml penicillin and 50 µg/ml streptomycin.

The cells were then exposed for 24h, 48h and 72h to SFM with 5 mM D-glucose (control), or SFM supplemented with 25 mM, 30 mM D-glucose (hyperglycaemia), or 5 mM D-glucose+25 mM L-glucose (osmotic control). The media were refreshed daily.

2.2 Harvesting of conditioned media and cells for chemokine and cytokine analyses

The medium was collected from each well and was centrifuged at 4°C for 10 min at 1,000 g to remove cell debris. Aliquots of the supernatant were stored at −80°C prior to analysis.

The cells were washed once with 2 ml of PBS and were harvested in 0.2 M NaOH using a rubber policeman. The samples were then incubated for 2 h at 37°C and stored at −20°C prior to the analysis of total protein content.

2.2.1 Harvesting of cells for Western blotting

The medium was removed from the wells of 6-well plates and the cells were rinsed with 2 ml of ice-cold PBS. Then, 80 µl of lysis buffer (20 mM Tris HCl pH 7.5, 150 mM NaCl, 1% NP-40), supplemented with phosphatase (Sigma: # 076M4056V) and protease (Thermo Scientific: # 1862209) inhibitors, were added to each well. The cells were scraped off and transferred into an Eppendorf tube, and another 80 µl of lysis buffer were added into the same well. The remaining cell lysate was collected and the suspension was transferred into the same tube.

A probe sonicator (Vibra cell; Sonics & Materials) was used to break down the cell membrane in an ice/water bath at an amplitude of 20 for 10 seconds. The samples were then centrifuged at 4°C for 10 minutes at 17,200 g. Aliquots of the supernatants were then transferred into Eppendorf tubes and were stored at -80°C prior to Western blotting experiments.

2.3 Protein estimation by the bicinchoninic acid (BCA) method

A BCA kit (Novagen: #71285-3) was used for the protein estimation as per manufacturer's protocol. Briefly, BSA standards with the following concentrations were used: 0, 0.05, 0.1, 0.2, 0.25 and 0.4 mg/ml.

Samples of cells harvested in 0.2 M NaOH were centrifuged at 4°C for 10 min at 17,200 g. For cytokine experiments, the supernatants were diluted 1:5 with dH_2O and the same dilution of 0.2 M NaOH was used as a blank. Cell lysates for Western blot were diluted 1:10 with dH_2O prior to analysis, and the same dilution of lysis buffer, supplemented with protease and phosphatase inhibitors, was used as a blank.

For total protein estimation, 20 µl of samples or standards were mixed with 200 µl of a working BCA reagent containing one part of $CuSO_4$ and fifty parts of BCA in a 96-well plate. After an incubation for 30 min at 37°C, the absorbance was measured at 562 nm in a plate reader (Multiskan Go, Thermo Scientific, UK).

2.4 Scratch wound healing test

Cells were grown as described in section 2. Cells were growth-arrested when 80-90% confluence was reached and the SFM was removed. Sterile yellow tips were used to scratch the cell monolayer in each well. The cells were rinsed once with 2 ml of PBS and were exposed to different concentrations of glucose in SFM. The media were refreshed daily. A Primo Vert microscope (Carl Zeiss, Germany, # 02171), AxioVision software (ZEISS microscope, UK) and Image J software (LOCI, University of Wisconsin) were used to take photographic images of each well at 0, 4, 8, 24, 48 and 72 h.

2.5   Glucose intake analysis

A D-glucose kit (glucose oxidase/peroxidase; GOPOD; Magazyme: # K-GLUC 09/14) containing GOPOD reagent buffer, GOPOD reagent enzymes and D-glucose standard solution was used to measure the glucose intake by HK-2 cells. Standards with the following concentrations were used: 0, 1, 3, 5,10 and 15mM.

Cells growth-arrested to confluence of 80-90% were rinsed twice with 2 ml of PBS and were then exposed to different concentrations of glucose for 72h, as described above. 150 µl of medium was collected from each well at 0, 24, 48, and 72h. The media were centrifuged at 1,000 g for 5 min at 4°C to remove cell debris, and aliquots of the supernatant were stored at −20°C prior to analysis. The cells were harvested at 24, 48 or 72h for total protein estimation by the BCA assay (2.3).

A 96-well plate was used to measure the glucose concentration in 10 µl of medium according to the manufacturer's recommendations. Briefly, 300 µl of GOPOD reagent were added to each well containing medium or a standard, and the plate was incubated for 20 min at 45°C. The absorbance was then measured at 510 nm using a Multiskan Go plate reader (ThermoScientific, UK).

2.6   Cell Viability and Proliferation

A Cell Counting Kit-8 (Dojindo Molecular Technologies, Inc, USA: # CK04: Cell Counting Kit-8) was used to determine the viability of HK-2 cells in 96-well cell culture plates. The Cell Counting Kit-8 (CCK-8) is a sensitive colorimetric assay to determine the metabolic activity of cells and thus their viability in cell proliferation and cytotoxicity assays. The test is based on the reduction of the

water-soluble tetrazolium salt (WST-8) by NAD(P)H in cells to an orange-coloured product (formazan), which is soluble in the tissue culture medium (Figure 2.1). The amount of formazan dye generated by dehydrogenases in cells is directly proportional to the viability of cells and their metabolic activity.
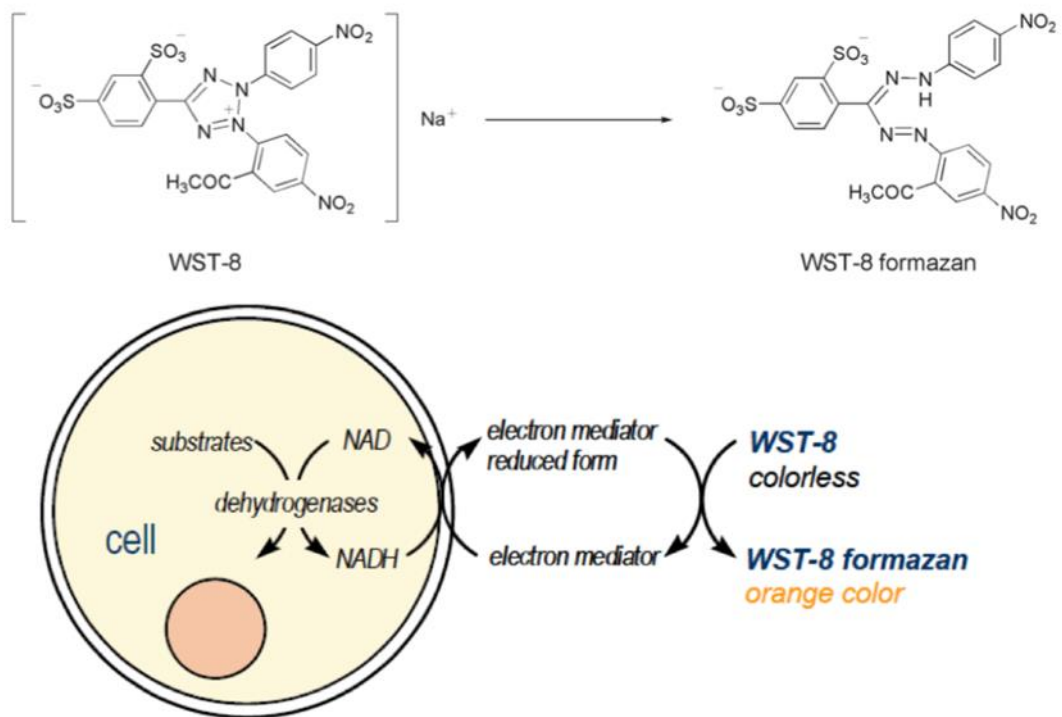
Figure 2. 2: Principle of the cell viability detection with Cell Counting Kit-8. From CCK-8 manual sheet, (Dojindo Molecular Technologies, Inc, USA: # CK04: Cell Counting Kit-8).

For the cell viability experiments, 9,000 cells were seeded per well with 200 µl of growth medium and the plate was incubated for 24h in a humidified incubator at 37°C and 5% CO_2. The cells were rinsed once with 150 µl of PBS and then exposed for 24h to 200 µl of SFM for growth arrest. The cells were then washed with 150 µl of PBS and then exposed to 200 µl of SFM supplemented with different concentrations of glucose. Nine µl of CCK-8 solution were added to each well and then the plate was incubated for 3h at 37°C and 5% CO_2 prior to being

read. The absorbance was then measured at 450 nm using the Multiskan Go plate reader (Thermo Scientific, UK).

2.7 Cell Mitochondrial Stress Test

Mitochondrial stress was measured in HK-2 cells using the Agilent Seahorse XF Cell Mito Stress Test Kit (Agilent Technologies: # 103015-100) and the Seahorse XFp platform.

Agilent seahorse XFp FluxPak miniplates (Agilent Technologies: # 103022-100) were used to culture 8,000 cells per well in growth medium for 24h. When the cells reached 80% confluence, they were growth-arrested in SFM for 24h. The cells were then exposed to different concentrations of glucose for up to 72h. On the day prior to the assay, Agilent seahorse XFp extracellular FluxPak sensor cartridges (Agilent Technologies: # 103022-100) were hydrated overnight in 200 µl of Seahorse XF Calibrant (Agilent Technologies: # 103022-100) at 37°C in a non-CO_2 incubator. On the day of the assay, 20 ml of Agilent seahorse XF Base Medium (Agilent Technologies: # 103022-100) supplemented with 1 mM pyruvate and 2 mM glutamine were warmed to 37°C, and the pH was adjusted to 7.4 with 0.1 NaOH. The cells were washed with SFM by removing all but 20 µl of the culture medium and replacing it with assay medium supplemented with different concentrations of glucose to a final volume of 180 µl per well. The miniplates were then placed into a 37°C non-CO_2 incubator for 1 hour prior to the assay. Oligomycin, FCCP and rotenone/antimycin A compounds were loaded into the appropriate ports of a hydrated sensor cartridge as the following: 20 µl of 1 µM oligomycin, 22 µl of 2 µM FCCP and 25 µl of 0.5 µM rotenone/antimycin A. The

mito stress was then assessed immediately by Agilent Seahorse XFp Analyzers (S7802A). The data were analysed as the following: **non-mitochondrial oxygen consumption** representing the minimum rate measurement after rotenone/antimycin A injection. **Basal respiration** is the non-mitochondrial respiration rate subtracted from the last rate measurement before oligomycin injection. **Maximal respiration** represents non-mitochondrial respiration subtracted from the maximum rate measurement after FCCP injection. **H+ (Proton) Leak** is non-mitochondrial respiration subtracted from the minimum rate measurement after Oligomycin injection. **ATP production** is minimum rate measurement after Oligomycin injection subtracted from the last rate measurement before Oligomycin injection. **Spare respiratory capacity** is basal respiration subtracted from maximal respiration. **Coupling efficiency** is (ATP production rate divided by basal respiration rate) × 100 (Figure 2.2).
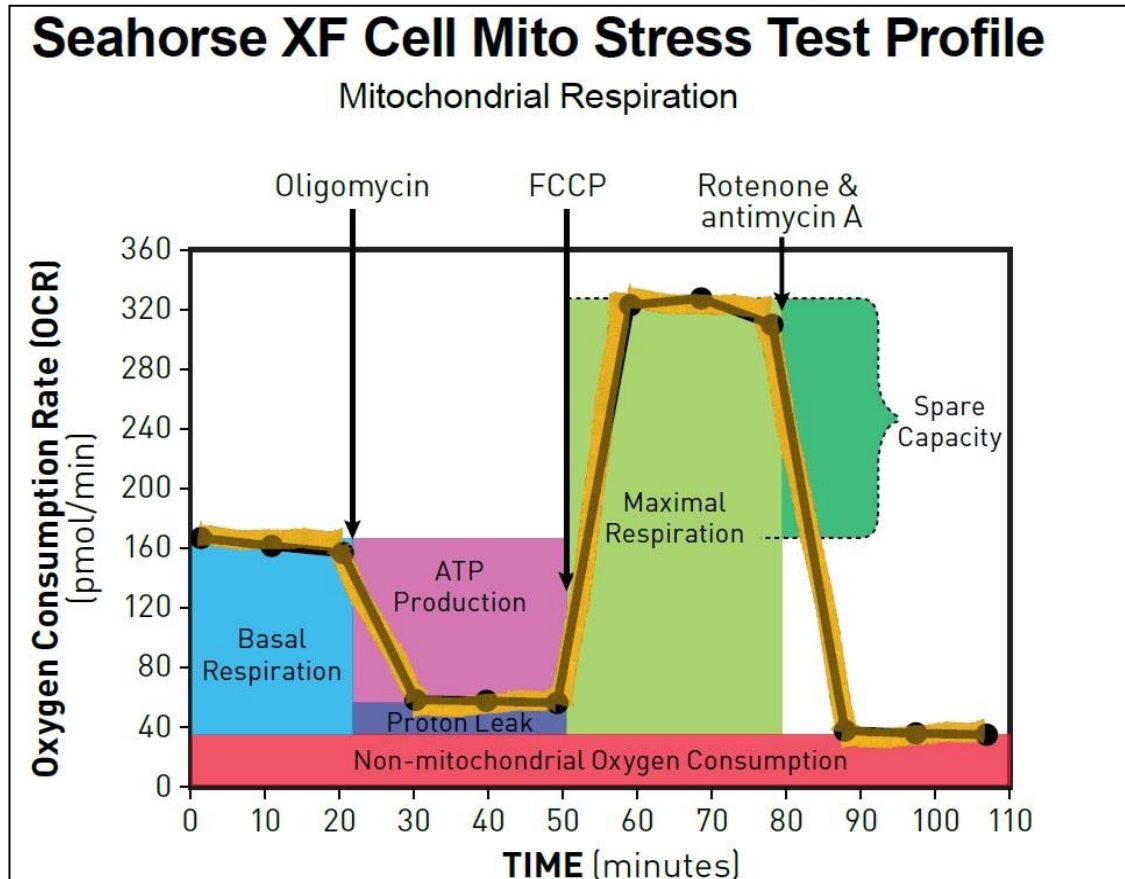
Figure 2. 2: Seahorse XF Cell Mitochondrial stress profile. From Agilent Seahorse XFp Cell Mitochondrial Stress Test Kit, User Guide Kit #103010-100.

2.8 Glycolytic Rate Assay

An Agilent Seahorse XF Glycolytic Rate Assay Kit (Agilent Technologies: # 103344-100) and the Seahorse XFp platform were used to assess the glycolytic rate in HK-2 cells.

Similar to the mitochondrial stress test, the cells were grown in miniplates. After the growth arrest step, when the cells had reached 80% confluence, they were then treated with different concentrations of glucose as mentioned above for up to 72h. The day prior to the assay, 200 μl of Seahorse XF Calibrant was used to hydrate the sensor cartridges in at 37°C in a non-CO_2 incubator overnight. On the

day of the assay, 20 ml of Agilent Seahorse XF base medium without phenol red (Agilent Technologies: # 103335-100) supplemented with 1 mM pyruvate, 2 mM glutamine and 5.0 mM HEPES (Agilent Seahorse XF: # 103337-100) was warmed to 37°C and the pH was then adjusted to 7.4 with 0.1 NaOH. SFM was used to rinse the cells by removing all except 20 µl of the culture medium and was replaced with assay medium supplemented with different concentrations of glucose to a final volume of 180 µl per well. The miniplates were incubated with assay medium at 37°C in a non-CO_2 incubator for 45-60 minutes prior to the assay. Rotenone/antimycin A and 2-deoxy-D-glucose compounds were loaded into the appropriate ports of a hydrated sensor cartridge as the following: 20 µl of 0.5 rotenone/antimycin A, and 22 µl of 50 µM 2-deoxy-D-glucose. The glycolytic rate was then assessed immediately by Agilent Seahorse XFp Analyzers (S7802A). The data were analysed as follows: **basal glycolysis**, which is the last glycolytic proton efflux rate (glycoPER) measurement before rot/AA injection. **Basal proton efflux rate (PER)** which is the last PER measurement before first injection. **% PER from glycolysis (basal)** is (basal glycolysis divided by basal PER) x 100%. **Compensatory glycolysis** is the maximum glycoPER measurement after Rot/AA injection. **mitoOCR/glycoPER (basal)** is (minimum OCR after Rot/AA injection subtracted from the last OCR measurement before Rot/AA injection) divided by basal glycolysis. **Post 2-DG acidification** is the minimum glycoPER measurement after 2-DG injection (Figure 2.3).
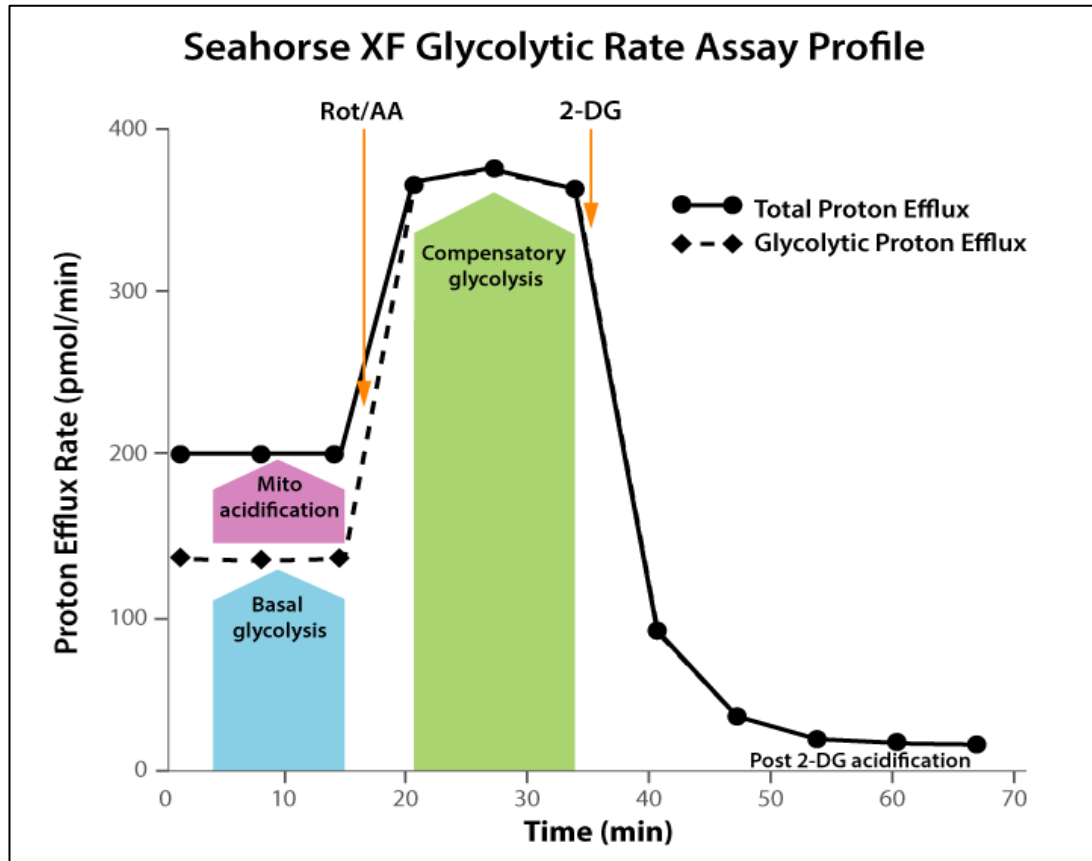
Figure 2. 3: Seahorse XF Glycolytic Rate profile. From Agilent Seahorse XF Glycolytic Rate Assay Kit, User Guide Kit #103344-100.

2.9 Luminex® Multiplex Assays

A Human Premixed Multi-Analyte Kit (R&D systems: #LXSAHM) was used to determine the concentrations of MCP-1, IL-6, KIM-1 and Endostatin in media from HK-2 cells exposed to different concentrations of glucose as described in section 2, according to the manufacturer's recommendations.

The principle of the Luminex assay is based on mixing the samples or the standards with colour-coded beads, pre-coated with analyte-specific capture antibodies (Figure 2.4). The immobilised antibodies bind to the analytes of interest. Biotinylated detection antibodies specific to the analytes of interest are added, forming an antibody-antigen sandwich. Phycoerythrin (PE)-conjugated

65

streptavidin, which binds to the biotinylated detection antibodies is then added. Beads are read on a dual-laser flow-based detection instrument (Luminex 200). The first laser classifies the bead dyes and determines the analyte that is being detected. The second laser determines the magnitude of the PE-derived signal, which is in direct proportion to the amount of analyte bound.
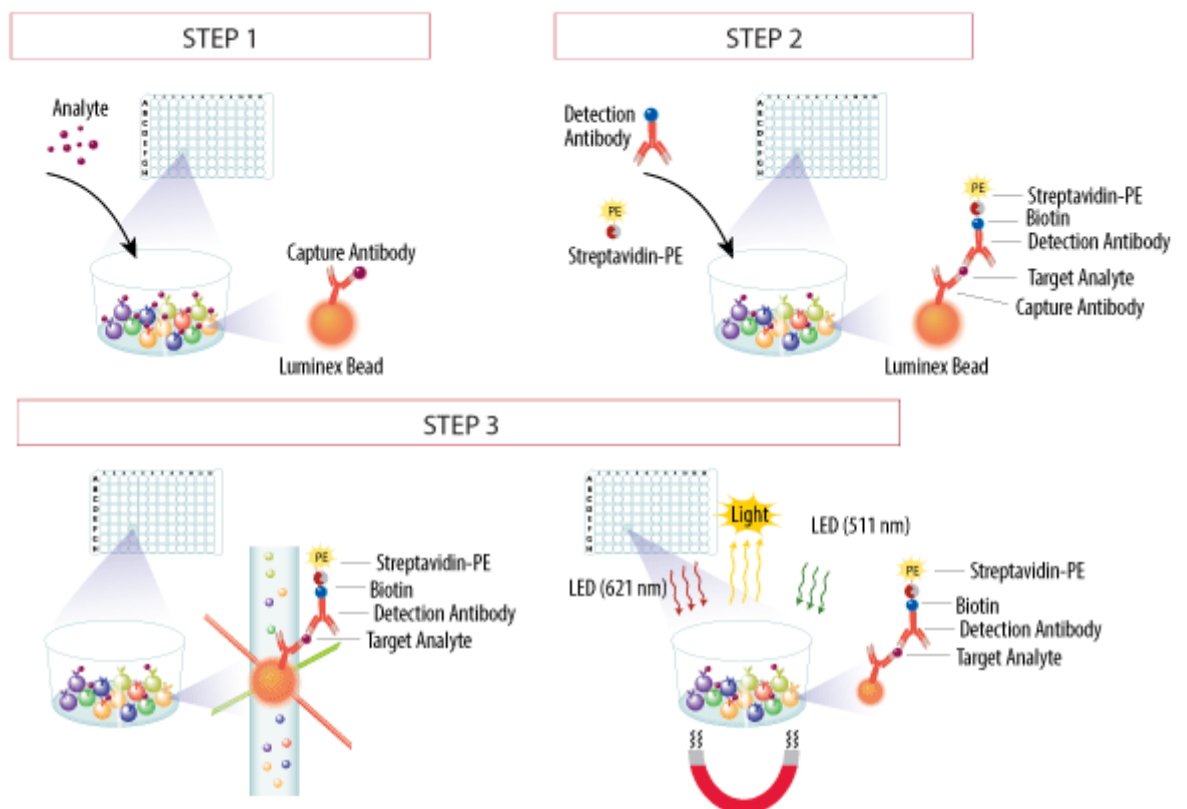
Figure 2. 4: Luminex assay principle (From R&D Systems, 2019).

For the purpose of this work, the concentration of soluble targets was measured in cell-cultured supernatants of control cells or cells exposed to high glucose. Briefly, samples and standards were analysed in duplicate, and the samples were diluted 1:1 with calibrator diluent RD6-52. Fifty µl of standard or sample were

mixed with 50 µl of the magnetic microparticle bead cocktail in a 96-well plate. The plate was then incubated for 2h at room temperature on a horizontal orbital microplate shaker. All incubation steps on the shaker were performed at 800 ± 50 rpm. Wash buffer (100 µl) was used to wash the plate and 1 minute on a magnetic device was allowed before removing the buffer. The wash procedure was performed four times in total. Fifty µl of diluted biotin-antibody cocktail was added to each well and the plate was incubated for 1 hour at room temperature on the shaker. The plate was washed again as described above, followed by adding 50 µl of diluted streptavidin-PE per well and incubated for 30 minutes at room temperature on the shaker. The plate was washed again as described above. One hundred microlitres of wash buffer per well was used to resuspend the microparticles, and the plate was incubated for 2 minutes on the shaker. The biomarker levels were then assessed by a Luminex 200 Multiplex analyser (Luminex xMAP Technology, 0135027).

The raw fluorescence signals of the samples were used to calculate the coefficients of variation (CV) between duplicates where $CV=\sigma/\mu$ (σ = standard deviation; μ = mean optical density of replicates). The intra-assay CV representing the average CV of all samples for a particular test target was less than 10% in all experimental plates (data not shown).

In order to accommodate all cell supernatant samples from a single day (e.g. 24h, 48h or 72h) on one Luminex plate, no plate control samples could be used to calculate the inter-assay CVs due to the lack of space.

2.10 TGF-β1 ELISA test

Media from HK-2 cells exposed to different glucose concentrations 24h, 48h or 72h were generated as described in section 2.

A TGF-β1 kit (R&D Systems: # DY240-05) was used to measure the concentration of TGF-β1 in media from HK-2 cells.

Prior to the analysis, the media samples were activated by acidification, as per manufacturer's protocol. Briefly, 80 µl of 1 N HCl were added to 400 µl of medium, and then the samples were incubated for 10 min at room temperature. The acidified samples were neutralised by the addition of 63.3 µl of 1.2 N NaOH/0.5 M HEPES.

The wells of 96-well plates were coated with 100 µl of the diluted capture antibody overnight at room temperature. The wells were then rinsed with 400 µl of washing buffer 3 times in total, and 300 µl of blocking buffer was added per well. The plates were incubated for 1h at room temperature and washed again as mentioned above. A hundred µl of standards or 250 µl of activated samples were added per well and the plates were incubated for 2h at room temperature. They were washed and 100 µl of diluted detection antibody were added to each well. The plates were then incubated for 2h at room temperature and washed 3 times. Then, 100 µl of streptavidin-HRP was added to each well and the plate was incubated for 20 min at room temperature in the dark. The wells were rinsed again with wash buffer, and 100 µl of substrate solution were added per well before the plate was incubated for 20 min at room temperature in the dark. Finally, 50 µl of the stop solution was added to each well and the optical density was determined from each well within 30 min at 450, 540 and 570 nm.

The raw optical densities of the samples were used to calculate the coefficients of variation (CV) between duplicates where $CV = \sigma/\mu$ (σ = standard deviation; μ = mean optical density of replicates). The intra-assay CV representing the average CV of all samples was less than 10% in all experimental plates (data not shown).

In order to accommodate all cell supernatant samples from a single day (e.g. 24h, 48h or 72h) on one ELISA plate, no plate control samples could be used to calculate the inter-assay CVs due to the lack of space.

2.11 SDS-PAGE and Western Blotting

Cell lysates containing 25 µg of total protein were mixed with 4x non-reducing Laemmli loading buffer (0.5 M Tris/HCl, pH 6.8, 4% SDS, 40% glycerol and traces of bromophenol blue dye) and were denatured by heating for 5 minutes at 95°C. The samples were loaded on precast gels Mini-PROTEAN TGX 4%-15% gradient gels (BioRad, UK: Cat#456-1083) alongside a molecular weight protein marker (BioRad; #161-0305) which was used to determine the molecular weight of the detected proteins. The gels were subjected to electrophoresis in a BioRad gel tank (BioRad, Mini-PROTEAN3 Cell, # 28512) using SDS-PAGE running buffer containing 0.025 M Tris/HCl, 0.1% SDS and 0.192 M Glycine, at 20 mA/gel while the samples were in the stacking gel. Subsequently, the current was increased to 30 mA/gel until the samples reached the end of the resolving gel.

When the bromophenol blue dye reached the bottom of the gels, the current was stopped and the proteins in the gels were transferred onto nitrocellulose membrane by electroblotting.

2.11.1 Electroblotting

Two pieces of extra-thick filter paper (8.5 × 7.5 cm) (BIO RAD: #1703969) and one piece of nitrocellulose membrane (8.5 × 7.5 cm) (GE Life Science, Amersham, # 10600012, Germany) were used per gel. The nitrocellulose membrane, filter paper and ready gels were equilibrated in transfer buffer (48 mM Tris pH 9.2, 39 mM glycine and 20% methanol) and were arranged in the following order in the Trans-Blot SD machine (BIO RAD; #170-3940): filter paper–nitrocellulose membrane–gel–filter paper. The protein transfer took place at 45 mA/membrane for 90 minutes. The membranes were air dried and stored at -20°C prior to further analysis.

2.11.2 Protein detection

The membranes were blocked with 1% bovine serum albumin (BSA) in PBST (0.05% Tween 20 in PBS) at room temperature for at least 30 minutes. Subsequently, a specific primary antibody against one of the following proteins was added in 1% BSA/PBST buffer: phospho-Smad3 (1:1000 rabbit mAb; Cell Signaling: # 9520), total Smad3 (1:1000 rabbit mAb; Cell Signaling: #9523). The membranes were incubated on a shaker for 2 hours at room temperature and subsequently washed five times with PBST for 5 minutes. Fresh 1% BSA/PBST was added with secondary horse-radish peroxidase (HRP)-labelled antibodies (anti-rabbit IgG HRP, #A0545; Sigma-Aldrich; 1:10,000) and the membrane was incubated for 60 minutes. The membrane was rinsed five times with PBST for 5 minutes, then incubated for 1 minute with a chemiluminescent substrate (Thermo Scientific: #QD214271A) according to the manufacturer's protocol. The

chemiluminescence signal was analysed by a G: Box imaging system (Syngene, UK). The membranes were washed for five minutes with 10 ml of PBST on the shaker, and then dried and stored at -20°C.The images were then analysed using Image J lab software (LOCI, University of Wisconsin).

2.12 Molecular biology methods

2.12.1 Quantitative real-time PCR (qPCR)

2.12.1.1   RNA isolation

HK-2 cells were grown in 6 well plates and exposed for 24, 48 or 72h to SFM supplemented with different concentrations of glucose. To isolate RNA for quantitative PCR (qPCR), the media were aspirated, the cells were washed once with 2 ml of ice-cold PBS, and any residual PBS was removed. The cells were harvested according to the manufacturer's recommendations in 700 μl of QIAzol lysis reagent (Qiagen, # 55709615). The cells were scraped using a rubber policeman and the lysates were transferred to a test tube. The cells were homogenised by vortexing for 1 minute and the lysates were then stored at –80°C prior to further analysis.

A miRNeasy Mini Kit (Qiagen, UK: #217004) containing buffer RWT, buffer RPE, RNase-free water and RNeasy mini column were used to isolate and purify the total RNA.

The cell lysates were defrosted and incubated for 5 minutes at room temperature to dissociate the nucleoprotein complex. Then, 140 μl of chloroform was added, followed by vigorous shaking for 15 seconds. The mixtures were then incubated

at room temperature for 2-3 minutes, and centrifuged at 12,000 g for 15 minutes at 4°C. The upper aqueous phase (350 μl) was transferred to a new collection tube, 525 μl of 100% ethanol were added, and the samples were then mixed thoroughly by pipetting. Up to 700 μl of the samples were pipetted, including any precipitate, into the RNeasy mini columns in a 2 ml collection tube, the columns were centrifuged at 8,000 g for 15 seconds at room temperature, and then the flow-through was discarded. After 2 more washes of the columns, 500 μl of RPE buffer was added onto the RNeasy mini columns, which were then centrifuged at 8,000 g for 2 minutes at room temperature. The columns were placed into a new 1.5 ml collection tube, followed by adding 40 μl of RNase-free water into the RNeasy mini column. To elute the RNA, the columns were centrifuged at 8,000 g for 1 minute and the RNA concentration of the eluent was measured using a Nanodrop (Thermo Fisher Scientific, USA, 02611). Aliquots of the RNA samples were then stored at – 80°C for further analysis.

2.12.1.2   Reverse transcriptase PCR (RT-PCR)

A Tetro cDNA Synthesis Kit (Bioline: # 65042) was used to convert the mRNA to cDNA, according to the manufacturer's recommendations. Briefly, total RNA samples were defrosted on ice and the mRNA in 1 μg of total RNA was transcribed to cDNA using master mix containing primer oligo (dT)18, 1 dNTP mix, RT Buffer, riboSafe RNase Inhibitor and tetro reverse transcriptase. The samples were then incubated in a thermocycler (Q Cycler II, Biotron Healthcare, India), 45°C for 30 minutes. The reaction was terminated at 85°C for 5 minutes.

The samples were then chilled on ice and the cDNA samples were then stored at –20°C for further analysis.

2.12.1.3   Quantitative real-time PCR (qPCR)

A QuantiNova SYBR Green PCR Kit (Qiagen: # 208056) was used to measure relative mRNA expression levels, according to the manufacturer's recommendations. Briefly, the cDNA samples were diluted 1:10 with RNase-free water and 2 µl were used for analysis per well. Eighteen µl of the master mix (10 µl of 2xSYBR Green PCR Master Mix, 2 µl of QN ROX Reference Dye, 0.14 µl of forward primer (0.7 µM), 0.14 µl of reverse primer (0.7 µM) and 5.72 µl of nuclease free water) was dispensed per well in 96-well plates.

The relative mRNA expression of the ECM proteins collagen I α1, PAI-1, MMP-9 and TIMP-1 was analysed using GAPDH as a housekeeping gene. The primers (Invitrogen, UK) were designed to anneal to different exons that were at least one intron apart (Table 2.1).

Table 2. 1: Primer sequences and size of amplified target cDNA.

Human Genes	Primer Sequences	Molecular size (bp)
Col Iα1	Forward 5' GTCGAGGGCCAAGACGAAGA 3' Reverse 5' GTTGTCGCAGACGCAGATCC 3'	114
PAI-1	Forward 5' CGAGGTGAACGAGAGTGGCA 3' Reverse 5' CCCAGGGTCAGGGTTCCATC 3'	170
MMP-9	Forward 5' TTCGACGTGAAGGCGCAGAT 3' Reverse 5' GGAACTCACGCGCCAGTAGA 3'	150
TIMP-1	Forward 5' CGCAGCGAGGAGTTTCTCAT 3' Reverse 5' CTCTGCAGTTTGCAGGGGATG 3'	188
GAPDH	Forward 5' GTGAGGACGGGCGGAGAGAAA 3' Reverse 5' GGTGACCAGGCGCCCAATA 3'	175

RNase-free water instead of cDNA template was used as a negative qPCR control with each primer pair, and all samples were analysed in triplicate. The qPCR plates were sealed tightly with an optical film and centrifuged at 1,400 g for 3 minutes at room temperature. The qPCR was performed using an AB StepOne Plus real time thermocycler (Applied Biosystems; California, US) with the following steps: PCR initial heat activation at 95°C for 2 minutes, followed of 40 cycles of 2-step cycling: denaturation at 95°C for 5 seconds and combined annealing/extension at 60°C for 10 seconds. The melting curve was generated according to the instrument's melting curve programme.

StepOne software (Applied Biosystems; California, US) was used to obtain the Ct values for target and housekeeping genes. The mean values of triplicate Ct of each sample was calculated. The Ct values for each target gene were then normalised to Ct values of the respective housekeeping gene (GAPDH) using the $\Delta\Delta$Ct method to assess the relative difference in gene expression. The ΔCt value presented the difference between the sample average and the housekeeping average, followed by the calculation of $2^{-\Delta Ct}$, as well as its mean for each condition. Finally, the values of $\Delta\Delta$Ct were calculated by dividing the $2^{-\Delta Ct}$ mean of the treated samples to the $2^{-\Delta Ct}$ mean of the control. Fold change (mean $\Delta\Delta$Ct expression) of the control was expressed as 1 and the treated samples were assessed relative to that.

The raw SYBR Green fluorescence densities of the samples were used to calculate the coefficients of variation (CV) between triplicates of each sample where $CV = \sigma/\mu$ (σ = standard deviation; μ = mean optical density of replicates). The intra-assay CV representing the average CV of all samples was less than 10% in all experimental plates (data not shown).

In order to accommodate all cDNA samples from a single day (e.g. 24h, 48h or 72h) on one qPCR plate, no plate control samples could be used to calculate the inter-assay CVs due to the lack of space.

2.13 Human fibrosis-related miRNA PCR array

2.13.1 Reverse transcriptase PCR for human fibrosis miRNA PCR array analysis

Total RNA was isolated as described in the RNA isolation section (2.12.1.1). A miScript II RT Kit (Qiagen: #218160) was used to convert the miRNA to cDNA, according to the manufacturer's recommendations. For each sample, 1 µg of total RNA was transcribed to cDNA, with a total volume of samples and RNase-free water up to 12 µl being added to the PCR tube. Eight µl of the master mix containing 4 µl of 5x miScript hiSpec buffer, 2 µl of 10x miScript nucleics mix and 2 µl of miScript reverse transcriptase mix were added per PCR tube. The mixture was mixed by pipetting and the tubes were centrifuged briefly. The samples were transcribed in a thermocycler (Q Cycler II, Biotron Healthcare, India) at 37°C for 60 minutes, and the reaction was terminated at 95°C for 5 minutes. The samples were then stored at – 20°C prior further analysis.

2.13.2 Quantitative human fibrosis-related miRNA PCR arrays

A miScript SYBR green PCR kit (Qiagen: # 218073) was used to analyse the miRNA PCR arrays, according to the manufacturer's recommendations. Briefly, the cDNA samples from cells exposed to (5 mM D-glucose (control), 25 mM, 30

mM D-glucose (hyperglycaemia) or 5 mM D-glucose+25 mM L-glucose (osmotic control) and individual reagents were defrosted, mixed and centrifuged briefly. For each treatment condition, 4 independent cDNA samples were pooled together in equal amounts (2.5 µl of each cDNA sample). The pooled samples (10 µl) were diluted with 200 µl of RNase-free water. A reaction mix was prepared containing the following: QuantiTect SYBR Green PCR Master Mix, miScript Universal Primer, RNase-free water and 100 µl of the diluted cDNA template as per manufacturer's protocol. The mixture was mixed by pipetting and 25 µl from the reaction mix were added per well in 96-well miScript miRNA PCR array plate. The array plate was sealed tightly with an optical film and centrifuged at 1,400 g for 3 minutes at room temperature. The plates were then analysed using AB StepOne Plus real time thermocycler (Applied Biosystems; California, US).

The cycler conditions consisted of the following steps: initial heat activation at 95°C for 15 minutes, followed by 40 cycles of 3-step cycling: denaturation at 94°C for 15 seconds, annealing at 55°C for 30 seconds and extension at 70°C for 30 seconds. Melting curve was performed according to the instrument melting curve programme (95°C for 15 seconds and 60°C for 60 seconds). StepOne software was used to obtain the Ct values for each array (Applied Biosystems; California, US). Both the baseline and the threshold values were defined manually in the stepOne software to obtain the Ct values. The Ct values were uploaded onto the free data analysis tools on the QIAGEN website (https://www.qiagen.com/gb/shop/genes-and-pathways/data-analysis-center-overview-page/) using the $\Delta\Delta CT$ method of relative quantification and interpretation of the control wells. $\Delta\Delta CT$ for each miRNA across 2 samples was calculated using the formula: $\Delta\Delta CT = \Delta CT$ (sample 2) $- \Delta CT$ (sample 1) where

sample 1 is the control sample and sample 2 is the experimental sample. Fold-change for each gene from sample 1 to sample 2 is calculated as $2^{(-\Delta\Delta CT)}$.

2.13.3 Quantitative real-time PCR for miR-216 and snoRNA/snRNA (SNORD95)

A miScript SYBR green PCR kit (Qiagen: # 218073) was used to measure the relative expression levels of miR-216a-5p or the references snoRNA/snRNA (SNORD95), according to the manufacturer's recommendations. Briefly, the cDNA samples were diluted 1:60 with RNase-free water. Fourteen µl of the master mix containing QuantiTect SYBR Green PCR master mix, miScript universal primer, miScript primers (miR-216a-5p and the references SNORD95) were dispensed in 96-well plates and mixed with 6 µl of diluted cDNA samples. RNase-free water instead of cDNA template was used as a negative qPCR control with each primer, and all samples were analysed in duplicate. The plate was sealed tightly with an optical film and centrifuged at 1,400 g for 3 minutes at room temperature. The plates were then analysed using AB StepOne Plus real time thermocycler (Applied Biosystems; California, US) with initial heat activation at 95°C for 15 minutes, followed by 40 cycles of 3-step cycling: denaturation at 94°C for 15 seconds, annealing at 55°C for 30 seconds and extension at 70°C for 30 seconds. The melting curve was performed according to the instrument melting curve programme (95°C for 15 seconds and 60°C for 60 seconds). StepOne software was used to obtain the Ct values for target miR-216a-5p and reference (SNORD95) miRNAs and calculate their mean values (Applied Biosystems; California, US). The Ct values of the target miRNA miR-

216a-5p were then normalised to the respective reference miRNA (SNORD95) using the $\Delta\Delta$Ct method to assess the relative difference in gene expression. ΔCt value presented the difference between the sample average and the housekeeping average, followed by the calculation of 2^-ΔCt, as well as its mean for each condition. Finally, the values of $\Delta\Delta$Ct were calculated by dividing the 2^-ΔCt mean of the treated samples to the 2^-ΔCt mean of the control. Fold change (mean $\Delta\Delta$Ct expression) of the control was expressed as 1 and the treated samples were assessed relative to that. This target was normalized to the two references (miR-192 and SNORD95) and both results were equally stable and showed similar patterns.

2.13.4 Reporter Plasmid-Cloning

The 3'UTR of TGFBR2 was amplified using DNA isolated from HK-2 cells (DNeasy blood and tissue kit; Qiagen, UK) and Q5 high-fidelity PCR kit (#0121606, New England BioLab) according to the manufacturers' recommendations in order to clone the UTR into a luciferase reporter vector. Briefly, for 50 µl reaction the following was added in a PCR tube: 25 µl of Q5 high-fidelity 2X master mix, 2.5 µl of 10 µM forward and reverse primers (Invitrogen, UK) (Table 2.2).

Table 2. 2: Primer sequences and size of amplified target TGFBR2.

Amplification Primer Sequence		Molecular size (bp)
5'GAGAAGATTCCTGAAGACGG 3'	Forward	
5' GGAGATTATTTACTTGGTGACG 3	Reverse 1	2,649
5'CTGTCAGTTGAGAAAGACAG 3'	Reverse 2	2,681
Gateway Primer Sequence		
5' **ACAAGTTTGTACAAAAAAGCAGGCTTC** GAGAAGATTCCTGAAGACGG 3'	GW Forward	
5' **GACCCAGCTTTCTTGTACAAAGTGGT** GGAGATTATTTACTTGGTGACG 3'	GW Reverse 1	2,755
5' **GACCCAGCTTTCTTGTACAAAGTGGT** CTGTCAGTTGAGAAAGACAG 3'	GW Reverse 2	2,787

100 ng of HK-2 genomic DNA (168 ng/µl) and nuclease-free water was used. PCR was performed using a thermocycler (Q Cycler II, Biotron Healthcare, India) with following steps: PCR initial denaturation at 98°C for 30 second, followed by 35 cycles: at 98°C for 10 seconds, 60°C for 30 seconds, 72°C for 30 seconds and the final extension at 72°C for 2 minutes.

The size of the amplified products was verified using electrophoresis with 1% agarose gel.

A mixture of 25 µl of sample and 5 µl of Gel loading dye (6x) (#B7021A, BioLabs) was loaded on the gel. A hyperLadder (1kb, #H1-618106A, Bioline, UK) was used

as a molecular weight marker. The gels were subjected to electrophoresis at 80 V, and the DNA bands were visualised under UV illumination in the G: Box imaging system (Syngene, UK).

A QIAquick Gel Extraction Kit (Qiagen, #28704) was used to extract the amplified DNA from the agarose gel. Briefly, DNA fragments of expected size were excised using a scalpel. In an Eppendorf tube, 3 volumes of buffer QG were added to 1 volume of gel (100 mg gel ~100 µl QG buffer) and incubated at 50°C for 10 minutes with intermittent vortexing. One gel volume of isopropanol was then added, the sample was loaded onto the QIAquick column and centrifuged at 17,200 g for 1 minute. The flow-through was discarded and 500 µl of QG buffer were added to the QIAquick column. The column was centrifuged at 17,200 g for 1 minute and the flow-through was discarded and then the QIAquick column was placed back into the same tube. The column was washed with 750 µl of buffer PE with centrifugation at 17,200g for 1 minute and the column was then placed into a clean 1.5 ml Eppendorf tube. Then, 50 µl of buffer EB (10 mM TrisCl, pH 8.5) were added to the centre of the QIAquick membrane and the column was centrifuged at 17,200 for 1 minute. The DNA concentration of the eluent was measured using a Nanodrop machine (Thermo Fisher Scientific, USA, 02611).

In a 1.5 Eppendorf tube, a 10 µl of BP reaction was prepared by mixing 66 ng of PCR product, 130 ng of pDONR 221 vector, 2 µl of BP Clonase II enzyme (#19072287, Invitrogen) and Tris-EDTA (TE) buffer (pH 8). The reaction was mixed and incubated overnight at 25°C. Then, 2 µl of 150 ng/µl destination vector and 3 µl of LR Clonase II enzyme (#1824455, Invitrogen) were added and incubated at 25°C for up to 18 h. Next, 2 µl of proteinase K solution (#1733731, Invitrogen) was added to the mixture and incubated at 37°C for 10 minutes.

In a new Eppendorf tube, 50 µl of competent *E. coli DH5α* (subcloning efficiency DH5α, #1608535, Invitrogen) were transformed with 1 µl of the reaction sample. The tube was incubated on ice for 30 minutes, and then it was shock-heated for 30 second at 42°C. The tube was immediately transferred onto ice for 5 minutes and 450 µl of a room temperature S.O.C medium (#1746996, Invitrogen) was added. The sample was incubated on a horizontal shaker (200 rpm) at 37°C for 1 h. Then, 20 and 100 µl of *E. coli* suspension was spread on a pre-warmed selective plate (40 g/L of LB agar (#7095862, BD and BD, US), pH 7.5, and ampicillin (100 µg/ml) (#16402, Fisher Scientific)) and incubated overnight at 37°C.

Five ml of LB medium (10 g/L of Tryptone, 5 g/L of yeast extract, 10 g/L of NaCl, 40 g/L LB agar, pH 7.5, #6258870, BD and BD, US) were aliquoted in 5 tubes of 50 ml, followed by 5 µl of ampicillin (50 mg/ml) in each tube. Individual clones were picked up and transferred into tubes with selective LB medium. The tubes were then incubated on a shaker (200 rpm) at 37°C overnight.

2.14 Statistical analysis

The results were presented graphically using Graph Pad Prism 5 software. IBM SPSS version 25 software was utilised in the statistical analysis of the data. One-way ANOVA was used to compare the treatment groups and Tukey's HSD post-hoc test was carried out when significant p-values (*$p \leq 0.05$) were detected.

With the exception of the fibrosis-related miRNA array experiment (Chapter 5), most experiments in this project were repeated 2 or 3 times, each with biological repeats of n=3, 4 or 6 (the respective number is stated in the figure legends). The

numbers of biological repeats in this study are in line with those reported in other studies, that observed significant effects. Furthermore, a review of the confidence intervals and mean differences was carried out to identify cases where a larger sample size may have potentially resulted in a statistically significant mean difference between contrasted conditions. The mean differences and confidence intervals obtained as a result of the statistical analyses are presented in Appendix 1A (experiments in Chapter 3), Appendix 1B (experiments in Chapter 4) and Appendix 1C (experiments in Chapter 5), and the comparisons potentially to be influenced by a larger sample size are highlighted.

Chapter 3: Metabolic and osmotic effects of hyperglycaemia on glycolysis and mitochondrial function in HK-2 cells

3.1 Introduction

Diabetes is the major cause of ESRD worldwide, with around 40% of diabetic patients likely to progress to DN (Slyne et al., 2015). Hyperglycaemia is a key pathogenesis factor in DN and can lead to mitochondrial dysfunction, increased ROS generation and the expression of pro-inflammatory factors, which can cause cell damage and activate a series of pathways leading to diabetic complications (Higgins and Coughlan, 2014; Czajka and Malik, 2016).

Renal tubule epithelial cells have a large number of mitochondria that sustain the high energy demand for the reabsorption and secretion of substances. Therefore, impairment of PTC mitochondrial function can lead to the gradual decline of renal function (Higgins and Coughlan, 2014; Tran and Parikh, 2014). In response to hyperglycaemia, a reduction in ATP generation, mitochondrial fragmentation, apoptosis, ROS generation and tubule damage have been observed in animal and human proximal tubule cells (Tan et al., 2009; Zhan et al., 2015; Coughlan et al., 2016). This body of evidence suggests that mitochondrial dysfunction is a key factor in the progression of kidney disease (Tran and Parikh, 2014).

The majority of studies in proximal tubule cells in DN have focused on mitochondrial fragmentation, ATP production and the generation of ROS (Yu et al., 2008; Sun et al., 2010). In contrast, studies on glycolysis and mitochondrial bioenergetic profiles in hyperglycaemia are limited. Furthermore, they either do

not report on the inclusion of an osmotic control or use mannitol, which is a known antioxidant (Liu et al., 2010; André and Villain, 2017). Therefore, for the first time, this study assessed the metabolic and osmotic effects of hyperglycaemia on mitochondrial stress and glycolytic rate (glycolysis) in proximal tubule cells in response to hyperglycaemia by the use of L-glucose as an osmotic control.

3.2 Methods

3.2.1 Cell culture

In order to study the metabolic and osmotic effects of hyperglycaemia on the cellular energetics of PTC, a suitable cell culture model using immortalised human HK-2 cells was used. The cells were grown to approximately 80% confluence, and then they were growth-arrested for 24h in serum-free medium. The cells were then exposed for 24h, 48h and 72h to SFM supplemented with 5 mM D-glucose (control), 25 mM or 30 mM D-glucose (hyperglycaemia), or 5 mM D-glucose+25 mM L-glucose (osmotic control) section 2.1.

3.2.2 Harvesting of cells and protein estimation by the bicinchoninic acid (BCA) method

The HK-2 cells were harvested in 0.2 M NaOH, then incubated for 2 h at 37°C and stored at −20°C prior the analysis of total protein content, as described in section 2.2. A BCA kit (Novagen, #71285-3) was used for the protein estimation as per manufacturer's protocol as described in section 2.3.

3.2.3 Scratch wound healing test

Cells were growth-arrested to 80-90% confluence and sterile yellow tips were used to scratch the cell monolayer in each well. The cells were then exposed to different concentrations of glucose in SFM and a Primo Vert microscope (Carl Zeiss, Germany, # 02171), AxioVision software (ZEISS microscope) and Image J were used to take photographic images of each well at 0, 4, 8, 24, 48, and 72

h to assess the scratch wound healing of the HK-2 cell exposed to different concentrations of glucose, as described in section 2.4.

3.2.4 Glucose intake analysis

As described in section 2.5, a kit for the estimation of D-glucose concentration was purchased from the Magazyme company (# K-GLUC 09/14) and was used to measure the glucose intake by the HK-2 cells under different concentrations of glucose at 24h, 48h and 72h.

3.2.5 Cell Viability and Proliferation

A Cell Counting Kit-8 (Dojindo Molecular Technologies, Inc, USA: # CK04) was used to determine the viability of HK-2 cells exposed to different concentrations of glucose for up to 72h, as described in section 2.6.

3.2.6 Glycolytic Rate Assay

An Agilent Seahorse XF Glycolytic Rate Assay Kit (Agilent Technologies, #103344-100) was used to assess the glycolytic rate of HK-2 cells incubated for up to 72h with different concentrations of glucose as described in section 2.8. The glycolytic rate was analysed using an Agilent Seahorse XFp Analyzer (S7802A).

3.2.7 Cell Mitochondrial Stress Test

An Agilent Seahorse XF Cell Mito Stress Test Kit purchased from Agilent Technologies (# 103015-100) was used to assess the mitochondrial stress of HK-2 cells exposed to different concentrations of glucose at 24h, 48h and 72h, as described in section 2.7. The mitochondrial stress was then analysed using an Agilent Seahorse XFp Analyzer (S7802A).

3.2.8 Statistical analysis

Graph Pad Prism 5 software and IBM SPSS statistics version 25 software were used to analyse the data. One-way ANOVA was used to compare the treatment groups. Tukey's HSD post-hoc test was carried out when significant p-values (*$p \leq 0.05$) were detected.

3.3 Results

3.3.1 Cell viability

Cell viability was evaluated in HK-2 cells incubated with different concentrations of glucose: control (5mM D-glucose), hyperglycaemia (25mM D-glucose and 30mM D-glucose) and osmotic control (5mM D-glucose+25mM L-glucose) at 24h (Figure 3.1A), 48h (Figure 3.1B) and 72h (Figure 3.1C). As shown in Figure 3.1, cell viability was significantly decreased by 30mM D-glucose after 24h, 48h and 72h (74.7% ± 4%, 74.1% ± 3.8% and 74.0% ± 6.8% respectively), as compared to control. In contrast, although cell viability was reduced by 25mM D-glucose and the osmotic control after 24h, 48h and 72h (Figure 3.1A, B, C) as compared to the control, these effects were not significant.
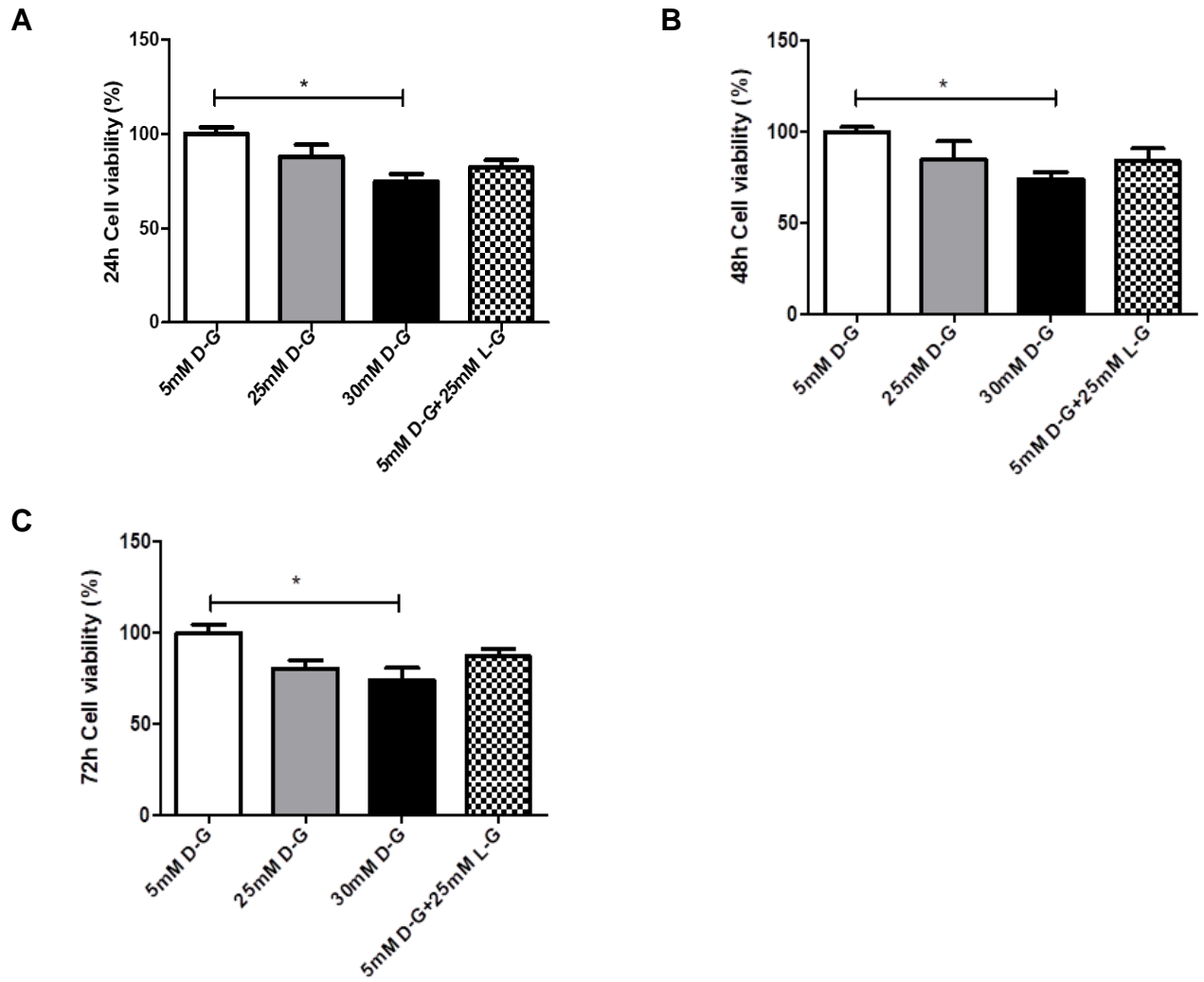
Figure 3. 1. Cell viability of HK-2 cells exposed to different concentrations of glucose: control (5mM D-glucose), hyperglycaemia (25mM D-glucose and 30mM D-glucose) and osmotic control (5mM D-glucose+25mM L-glucose) at 24h **(A),** 48h **(B),** and 72h **(C)**. Cell viability relative to control was determined using a Multiskan Go plate reader. Cell viability of HK-2 cells was significantly reduced by 30mM D-glucose compared to the control (*p≤0.05 5 mM D-glucose vs 30mM D-glucose). Data are presented as Mean ± SEM, n=6. One-way ANOVA was used to compare the treatment groups. Tukey's HSD post-hoc test was carried out when significant p-values (*p≤0.05) were detected.

3.3.2 Scratch wound healing test

Scratch wound healing tests were carried out to determine the effect of hyperglycaemia on the migration and proliferation of HK-2 cells over a 72h period with photographic images taken at 0h, 4h, 8h, 24h, 48h and 72h. Representative images of cells exposed to different glucose treatments demonstrated a complete wound healing at 72h, regardless of the glucose concentration (Figure 3.2A). Figure 3.2B shows that the rate of wound closure over a 48h period was fastest in cells exposed to 25 mM D-glucose. After 4h, 8h and 24h there was a significant increase of wound healing in response to 25 mM D-glucose (23.5% ± 0.85%, 35.6% ± 1.13%, 70.1% ± 5.30% wound closure) as compared to 30mM D-glucose. In contrast, the wound healing of cells exposed to 30mM D-glucose was significantly slower at these time points (10.5% ± 0.5%, 15.3% ± 0.4%, 28.4% ± 0.4% wound closure). At 48h, there was also a significant increase in the wound closure, (almost 95% ± 2.30%) with 25 mM D-glucose, as compared to control and 30 mM D-glucose (63.5% ± 9.7% and 47.1% ± 0.9% wound closure respectively).

Up to 24h the osmotic control had the same effect on wound healing as the control treatment. However, at 48h it significantly increased the wound recovery, with wound closure values approaching those of 25mM D-glucose.
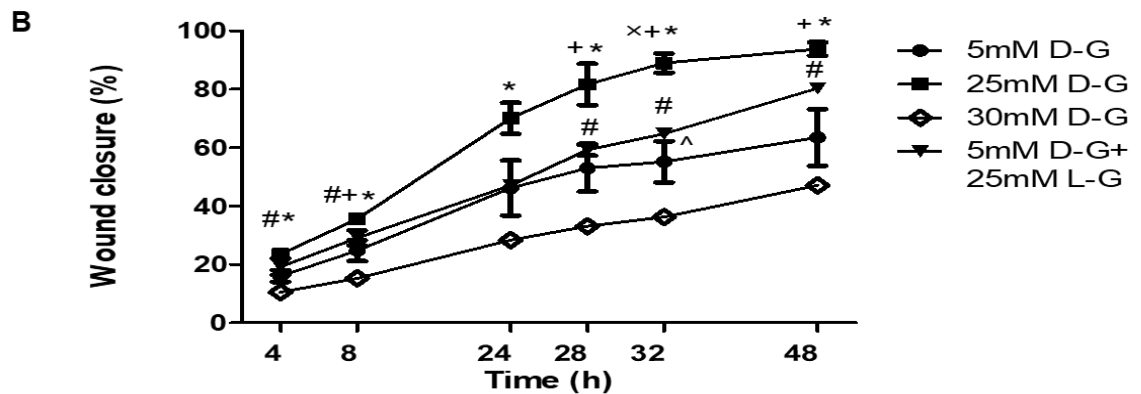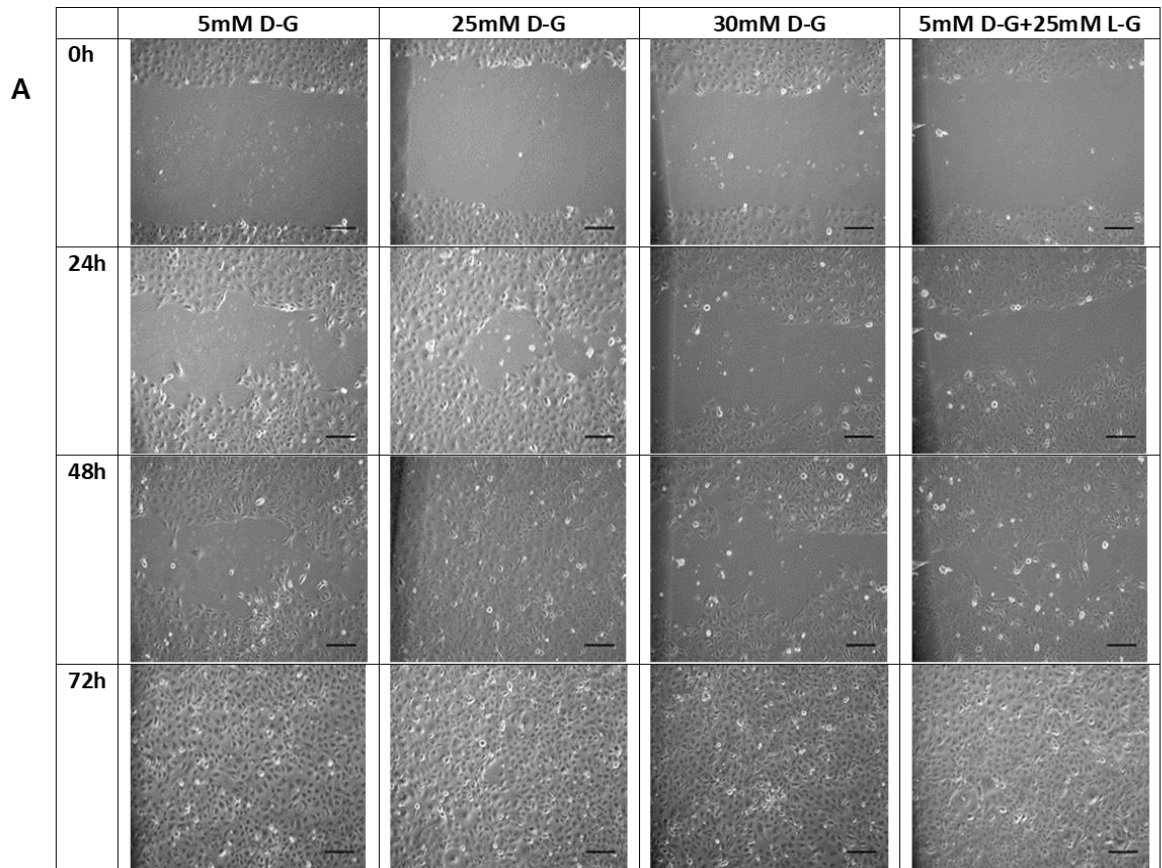
Figure 3. 2. Effects of hyperglycaemia on wound healing of HK-2 cells. **(A)** Representative images of HK-2 cells exposed to different glucose treatments at 0, 24, 48 and 72h, (Scale bar = 320 μm). **(B)** Rate of wound closure measured at 0h, 4h, 8h, 24h and 48h After 24h, 25mM D-glucose induced significant wound healing in HK-2 cells (*p≤0.05), as compared to 30mM D-glucose. After 48h 25mM D-glucose induced significant wound recovery compared to the control group and 30mM D-glucose (*p≤0.05). (*p≤0.05; 25mM D-G vs 30mM D-G, +p≤0.05; 25mM D-G vs 5mM D-G, ×p≤0.05; 25mM D-G vs 30mM L-G, #p≤0.05; 30mM D-G vs 30mM L-G, ^p≤0.05; 5mM D-G vs 30mM D-G). Data are presented as Mean ± SEM, n=3. One-way ANOVA was used to compare the treatment groups. Tukey's HSD post-hoc test was carried out when significant p-values were detected.

3.3.3 Glucose consumption

The glucose consumption of HK-2 cells exposed to control, 25mM D-glucose, 30mM D-glucose and osmotic control (5mM D-glucose+25mM L-glucose) was measured every 24h over a 72h period (Figure 3.3A, B and C). Of note, the media were refreshed daily and the amount of glucose consumed in the media was normalised to total cellular protein content. The results demonstrated that at 24h there was no significant difference between the amount of glucose consumed by cells exposed to control (3.91 ± 0.05 mg/mg protein), 25 mM D-glucose (3.93 ± 0.30 mg/mg protein) or the osmotic control (3.93 ± 0.07 mg/mg protein) (Figure 3.3A). In contrast, cells incubated with 30 mM D-glucose consumed significantly less glucose (2.88 ± 0.27 mg/mg protein) as compared to all other treatments.

At 48h, the glucose intake was significantly decreased in HK-2 cells exposed to 25 mM D-glucose: (2.63 ± 0.27 mg/mg protein) and 30mM D-glucose (2.57 ± 0.11 mg/mg protein), with a slight reduction in cells incubated with the osmotic control (3.23 ± 0.09 mg/mg protein), as compared to the control (3.49 ± 0.14mg/mg protein) (Figure 3.3B).

At 72h, hyperglycaemia and the osmotic control had no significant effect on the glucose intake, as compared to the control (Figure 3.3C).
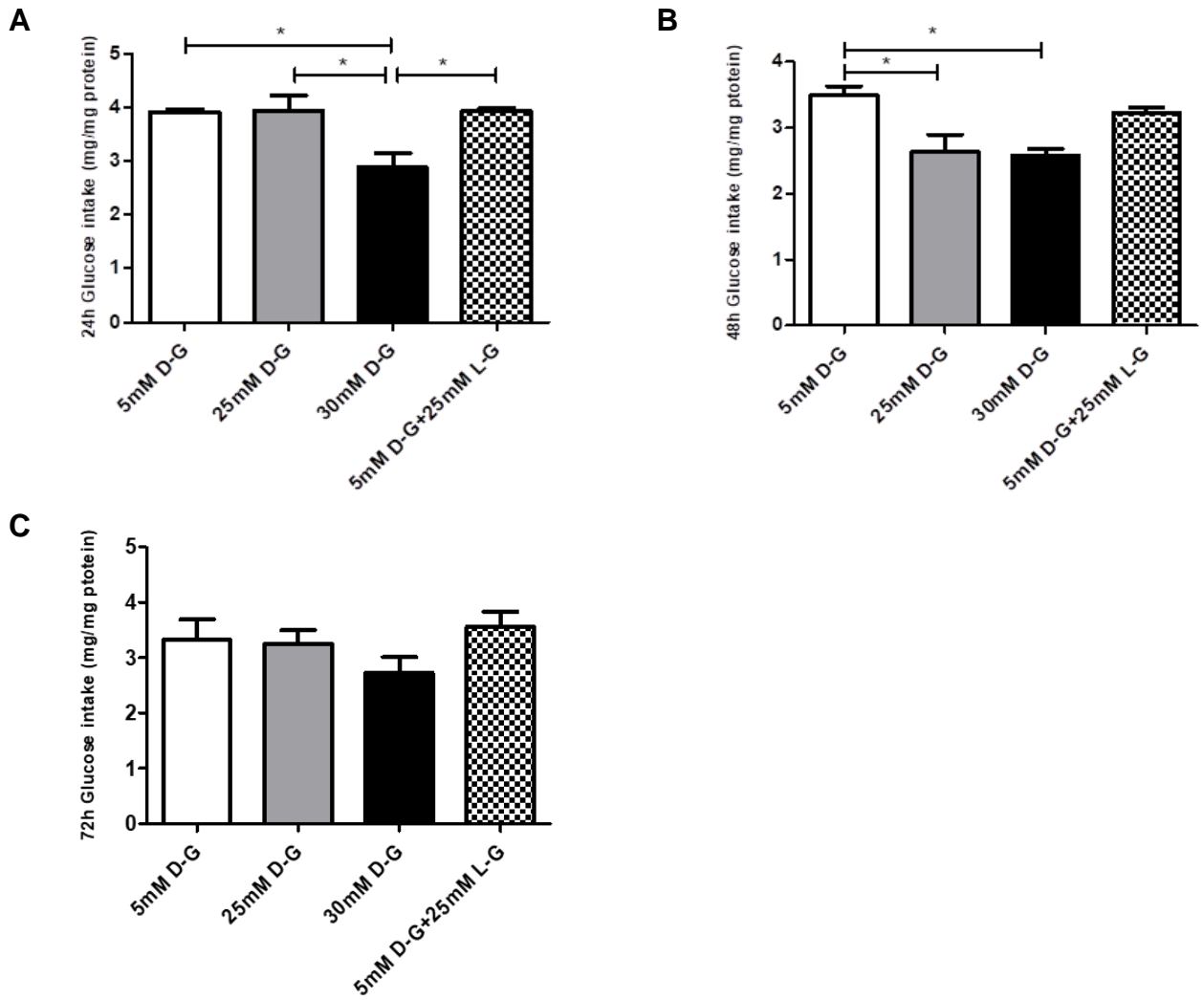
Figure 3. 3. Glucose consumption by HK-2 cells exposed to different glucose concentrations. The SFM supplemented with different concentrations of glucose was refreshed daily and the concentration of glucose was measured in control, hyperglycaemic (25 and 30mM D-glucose) and osmotic control media at 24h **(A),** 48h **(B)** and 72h **(C).** The glucose consumed (mg) was normalised to total cellular protein content (mg). Data are presented as Mean ± SEM, n=6. One-way ANOVA was used to compare the treatment groups. Tukey's HSD post-hoc test was carried out when significant p-values (*p≤0.05) were detected.

3.3.4 Glycolytic Rate of HK-2 cells exposed to hyperglycaemia

The effect of different concentrations of glucose on the glycolytic rate of HK-2 cells was examined every 24h over a 72h period using Seahorse analysis. The glycolytic profiles, including basal glycolysis, compensatory glycolysis (glycolysis rate in cells after the addition of mitochondrial inhibitors), basal proton efflux rate (basal PER) (protons exported by cells into the assay medium), % PER from glycolysis (basal), basal mitoOCR/glycoPER (mitochondrial oxygen consumption rate/ glycolysis proton efflux rate) and post 2-DG acidification were evaluated using specific inhibitors and activators of cellular respiration, and the results were normalised to total protein content (Figure 3.4A-F).

With the exception of mitoOCR/glycoPER (basal) and the osmotic control in post 2-DG acidification, all other glycolysis parameters (i.e. basal glycolysis, compensatory glycolysis, basal proton efflux rate (basal PER), % PER from glycolysis (basal), and post 2-DG acidification) decreased significantly over time with every glucose treatment, including control (Figure 3.4A-F: statistical significances not shown).

As shown in Figure 3.4A, at 24h, the basal glycolysis was reduced significantly in cells exposed to 30 mM D-glucose and osmotic control (5mM D-glucose+25mM L-glucose). At 48h, all hyperglycaemic treatments, including the osmotic control, significantly reduced the basal glycolytic rate of HK-2 cells, as compared to the control. In contrast, at 72h there was no significant difference between any of the treatments.

Similar patterns were observed for basal PER, % PER from glycolysis (basal), and compensatory glycolysis (Figures 3.4 B, C and D).

In contrast, over 72h the ratio of basal mitoOCR/glycoPER in cells exposed to control and 30 mM D-glucose consistently increased, whereas the ratio in cells exposed to 25 mM D-glucose and the osmotic control peaked at 48h and decreased at 72h (Figure 3.4E). Furthermore, at 24h and 48h the basal mitoOCR/glycoPER ratios of cells incubated with 30mM D-glucose were significantly lower, as compared to all other treatments, suggesting an increased glycolysis over mitochondrial respiration.

The contribution of glycolysis to the overall PER, and therefore to ATP synthesis, was evaluated by the administration of the glycolysis inhibitor 2-DG. The results demonstrated that 2-DG significantly reduced the PER in control cells, and those exposed osmotic control, over 24h, 48h and 72h, thus suggesting that the energy produced in these cells prior to the 2-DG injection is primarily due to glycolysis (Figure 3.4F). The significantly higher PER levels in HK-2 cells exposed to hyperglycaemia (25mM and 30mM D-glucose) suggest that mitochondrial respiration, other sources of extracellular acidification, or residual glycolysis, not fully inhibited by 2-DG are the main contributors to the extracellular proton efflux rate. Figure 3.5 shows an example of the trace graph produced in a glycolytic rate experiment.
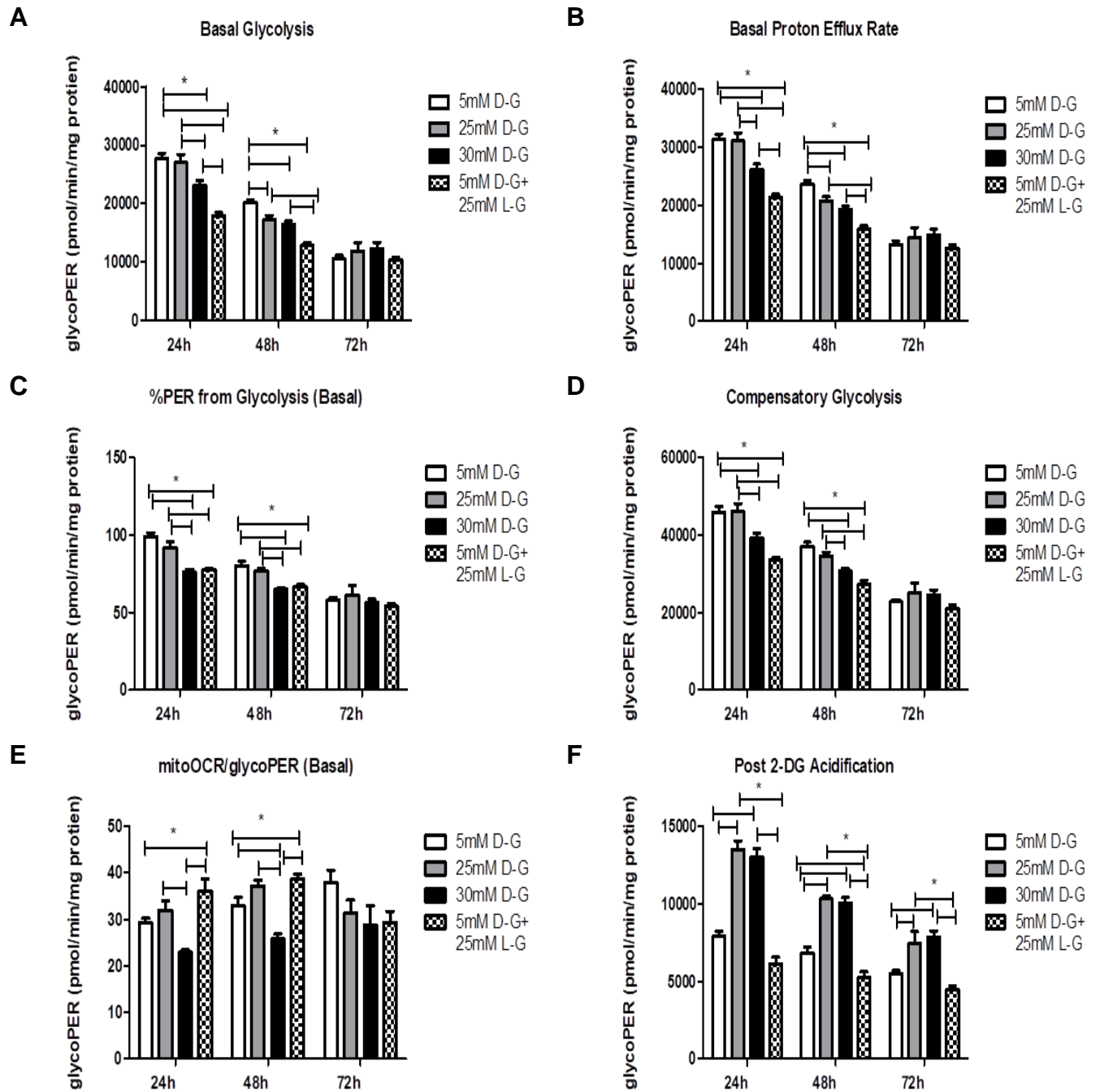
Figure 3. 4. Glycolytic profiles in HK-2 cells exposed to different concentrations of glucose (control-5mM D-glucose; hyperglycaemia - 25mM D-glucose and 30mM D-glucose; and osmotic control - 5mM D-glucose+25mM L-glucose) for 24h, 48h and 72h. The glycolytic profiles include **A)** basal glycolysis; **B)** basal proton efflux rate; **C)** % PER from glycolysis (basal); **D)** compensatory glycolysis; **E)** mitoOCR/glycoPER (basal); and **F)** post-2-DG acidification and were determined by a Seahorse analyser using specific inhibitors and activators of cellular respiration. The results were normalised to total protein content. Data are presented as Mean ± SEM, n=6. One-way ANOVA was used to compare the treatment groups. Tukey's HSD post-hoc test was carried out when significant p-values (*p≤0.05) were detected.
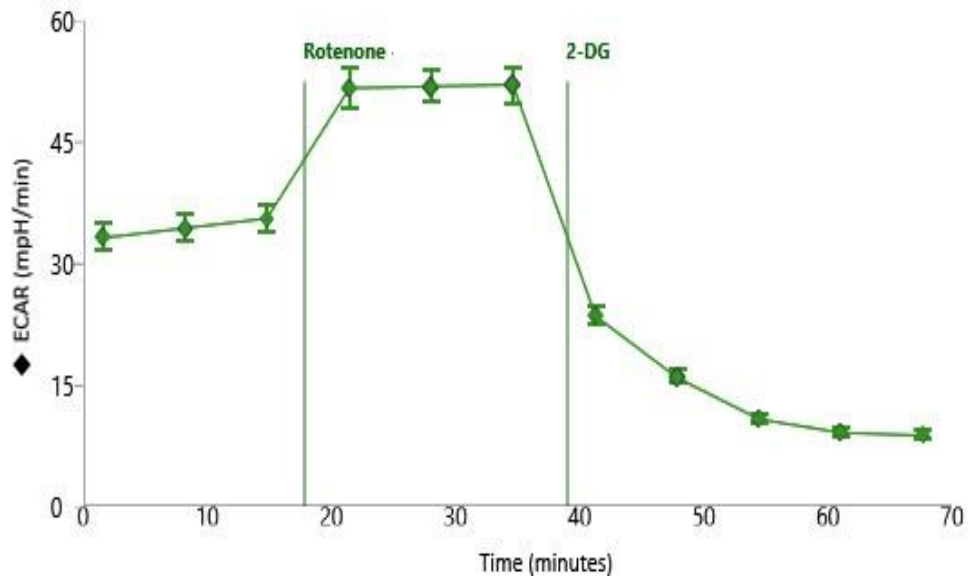
Figure 3. 5: A representative trace pattern of a typical glycolytic rate experiment using specific inhibitors and activators of cellular respiration and determined by Seahorse analysis.

3.3.5 Cell Mitochondrial Stress Test

The bioenergetic profiles of HK-2 cells exposed to different concentrations of glucose for 24h, 48h and 72h were evaluated using Seahorse analysis. The oxygen consumption rate (OCR) of the cells was measured before and after the addition of specific inhibitors and activators of cellular respiration to evaluate basal and maximal respiration, proton leak, ATP production, spare respiratory capacity, non-mitochondrial oxygen consumption and coupling efficiency. The results were normalised to total protein content and are shown in Figure 3.6A-G.

The maximal mitochondrial respiration was measured following the administration of FCCP (an ETC uncoupler), which disrupts the mitochondrial membrane potential thus leading to maximal use of oxygen by complex IV. Hyperglycaemia had no significant effect on the level of basal respiration (Figure 3.6A) or maximal respiration (Figure 3.6B) as compared to the effects of the control over 72h of incubation. However, the ability of the cells to respond to an increased energy demand, as measured by the spare respiratory capacity of the cells (the difference between maximal and basal respiration), increased over 72h in cells exposed to control and 25mM D-glucose (Figure 3.6C). The spare respiratory capacity peaked at 48h in response to 30mM D-glucose and the osmotic control. All hyperglycaemia treatments reduced the ability of the cells to respond to the increased energy demand, as compared to control cells at 48h, and this effect was statistically significant at 72h with the exception of 25mM D-glucose (Figure 3.6C).

The ATP production measured after the administration of oligomycin (an ATP synthase inhibitor) was reduced over 72h in all treatments but most profoundly in

cells exposed to hyperglycaemia (Figure 3.6D). Although in some instances (e.g. at 72h under all hyperglycaemic treatments) the mitochondrial ATP production was reduced by more than 20%, as compared to control, the decrease was not significant.

The proton leak marker represents the remaining basal respiration not coupled to ATP production. It can be either a sign of mitochondrial damage or it can be a physiological mechanism for regulation of mitochondrial ATP production. Mirroring the ATP production, the proton leak in control cells decreased over 72h (Figure 3.6E). In contrast, the proton leak in cells exposed to 25mM D-glucose peaked at 48h, and it increased in cells treated with 30mM D-glucose and osmotic control over 72h. At 72h the proton leak was significantly lower in control cells. As compared to cells treated with 25mM D-glucose, there was a significantly higher proton leak in cells exposed to 30 mM D glucose and osmotic control, suggesting the presence of mitochondrial damage due to the osmotic effect of these treatments.

Non-mitochondrial oxygen consumption was evaluated following the administration of rotenone (inhibitor of ETC complex I) and antimycin (inhibitor of ETC complex III) (Figure 3.6F). The non-mitochondrial oxygen consumption was significantly reduced in cells exposed to the control after 48h and 72h, as compared to 24h of exposure (significant differences not indicated in the graph). In contrast, there was no change in the non-mitochondrial oxygen consumption of cells exposed to 30mM D-glucose or osmotic control over a 72h period. At 24h only, there was a significant reduction in the non-mitochondrial oxygen consumption of cells treated with 30mM D-glucose or osmotic control, as compared to control cells. No such differences were observed at 48h and 72h.

The coupling efficiency represents the proportion of oxygen consumption which is used to generate ATP. The coupling efficiency of control cells or those exposed to 25mM D-glucose remained stable over a 72h period, and over a 48h period in cells exposed to 30mM D-glucose and osmotic control (Figure 3.6G). However, at 72h there was a significant reduction of coupling efficiency of these two treatments (statistical differences not shown). At 24h and 72h of treatment, 30mM D-glucose and the osmotic control had significantly reduced coupling efficiency, as compared to the control and 25mM D-glucose-treated cells, suggesting an osmotic effect. At 48h the coupling efficiency was reduced in all hyperglycaemia treatments, as compared to control. Figure 3. 7 shows an example of the trace graph produced in a mitochondrial stress experiment.
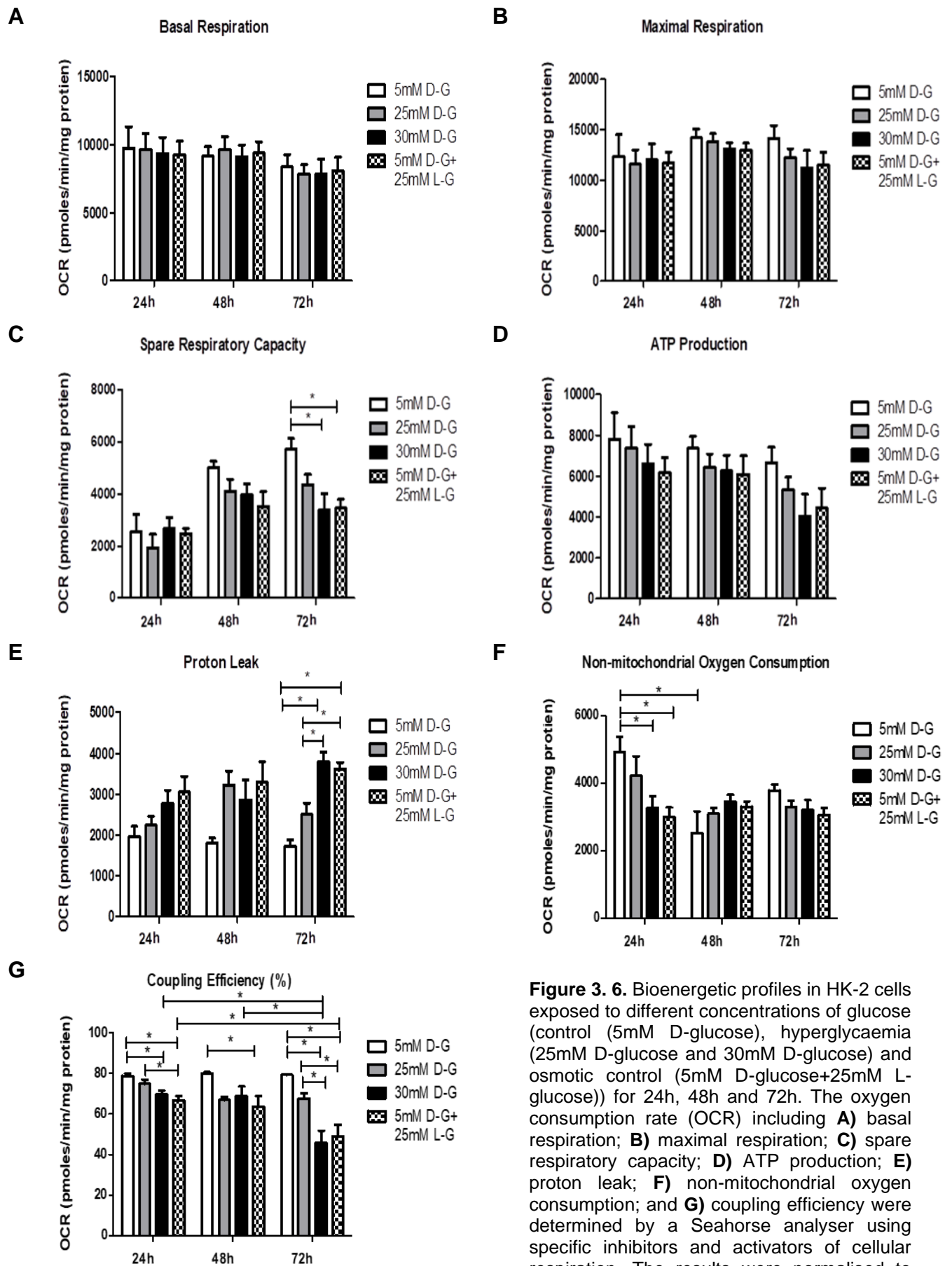
Figure 3. 6. Bioenergetic profiles in HK-2 cells exposed to different concentrations of glucose (control (5mM D-glucose), hyperglycaemia (25mM D-glucose and 30mM D-glucose) and osmotic control (5mM D-glucose+25mM L-glucose)) for 24h, 48h and 72h. The oxygen consumption rate (OCR) including **A)** basal respiration; **B)** maximal respiration; **C)** spare respiratory capacity; **D)** ATP production; **E)** proton leak; **F)** non-mitochondrial oxygen consumption; and **G)** coupling efficiency were determined by a Seahorse analyser using specific inhibitors and activators of cellular respiration. The results were normalised to total protein content. (continues on next page)

Figure 3. 6 Bioenergetic profiles in HK-2 cells exposed to different concentrations of glucose **(cont.)**

Data are presented as Mean ± SEM of 3 independent experiments, n=9. One-way ANOVA was used to compare the treatment groups. Tukey's HSD post-hoc test was carried out when significant p-values (*p≤0.05) were detected.
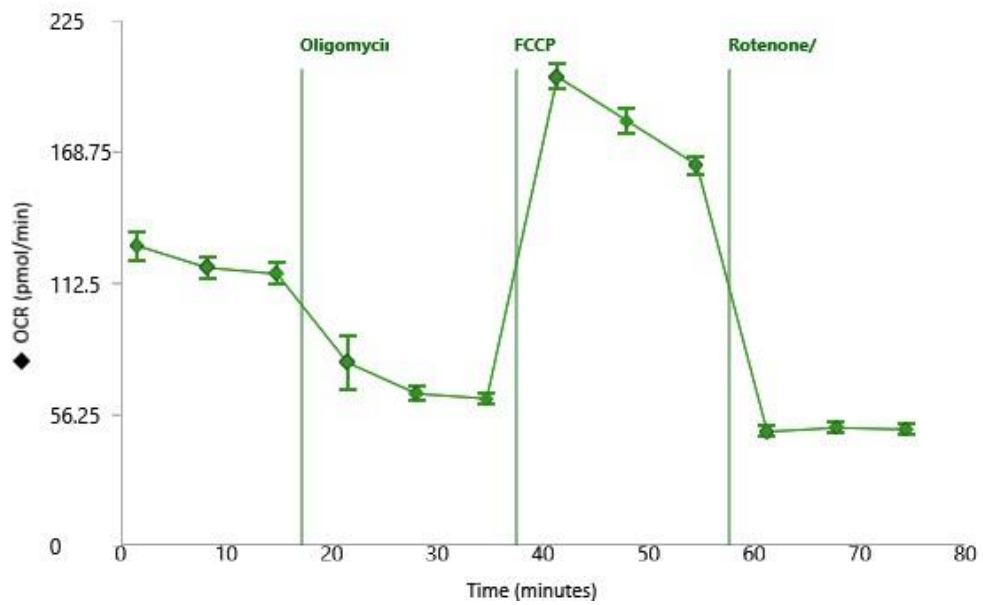
Figure 3. 7: A trace pattern of a representative mitochondrial stress experiment, using specific inhibitors and activators of cellular respiration.

3.4 Discussion

Renal fibrosis is caused by the excessive accumulation of ECM components, such as collagen and fibronectin, and is the final common pathway of progressive kidney disease leading to CKD and potentially, ESRD (Liu, 2011). Diabetic nephropathy is the most common cause of ESRD that is managed with haemodialysis, which is costly and is associated with the increased risk of cardiovascular mortality and morbidity (Kanasaki et al., 2013). The dysregulation of the normal wound healing process, in association with excessive deposition of ECM components, are considered to be the main causes of renal tubular fibrosis (Kanasaki et al., 2013). However, the renal proximal tubule cells depend on the mitochondria to generate energy in the form of ATP for tubular reabsorption, therefore mitochondrial dysfunction may play a central role in DN (Higgins and Coughlan, 2014). As evidence about the roles of the metabolic and osmotic effects of hyperglycaemia on glycolysis and mitochondrial function of proximal tubule epithelial cells is lacking, the aim of this part of the study was to investigate, *in vitro,* the effect of hyperglycaemia on the energy metabolism and mitochondria of renal proximal tubule cells and to delineate the role of the metabolic and osmotic effects of hyperglycaemia on viability, recovery from injury (cell migration), mitochondrial function and energy production.

3.4.1 Viability, migration and glucose utilisation of HK-2 cells in response to hyperglycaemia

Studies on the effect of hyperglycaemia on the viability of renal proximal tubule epithelial cells have provided conflicting evidence. For example, the exposure of primary human PTCs for 24h to 30mM D-glucose had no detrimental effect on cell viability (Zhang et al., 2016). Furthermore, 30mM D-glucose did not influence the viability of HK-2 cells either after 24h or 48h (Verzola et al., 2002). In contrast, HK-2 cells incubated with 30 mM D-glucose for 48h, displayed a significant reduction in cell viability compared to 5mM D-glucose control (Chen et al., 2018). However, the studies of Zhang et al. (2016) and Chen et al. (2018) did not include an osmotic control, whereas Verzola et al. (2002) used mannitol, which failed to induce apoptosis.

Mannitol is an antioxidant (Liu et al., 2010; André and Villain, 2017), therefore it is not a suitable control in hyperglycaemia experiments. The present study addressed the osmotic effect of hyperglycaemia on the viability of HK-2 cells by using L-glucose as an osmotic control. L-glucose is not metabolised by eukaryotic cells and has no known antioxidant effects. The results demonstrated that although both 25mM D-glucose and the osmotic control reduced the viability of HK-2 cells slightly, only 30mM D-glucose decreased it significantly over a 72h period. This suggests that the detrimental effect of hyperglycaemia on cell viability is metabolic, rather than osmotic.

Although tests such as CCK-8, MTT and MTS, which reduce tetrazolium dyes to formazan are widely used to evaluate cell viability, the results should be interpreted with caution, as metabolically active cells generate a stronger

formazan signal than quiescent cells, thus giving the impression of increased viability. Furthermore, increased formazan levels could also be observed when a treatment increases cell proliferation, as compared to a control. Therefore, based on this test alone, it cannot be definitely concluded that 30 mM D glucose decreases the viability of HK-2 cells, as it may also decrease their proliferation or metabolic activity (Quent et al., 2010).

The effect of hyperglycaemia on the proliferation/migration of HK-2 cells and the link between cell migration, extracellular matrix (ECM) and cell–cell interactions *in vitro* was studied using a wound healing assay (Liang et al., 2007). High glucose levels can alter PTC proliferation and induce hypertrophy, which are some of the early abnormalities in diabetic nephropathy. It has been shown that 25 mM glucose inhibits primary renal PTC proliferation in rabbits by increasing their metabolism, which subsequently leads to increased oxidative stress and the activation of protein kinase C (Park et al., 2001). The osmotic control mannitol (25 or 50 mM) had no effect on PTC proliferation in this study (Park et al., 2001). Furthermore, hyperglycaemia has been shown to delay wound healing. For example, after 48h 30mM D-glucose significantly inhibits the wound healing in immortalised rat kidney proximal tubule cells (RPTC) via the activation of PKC (Peng et al., 2017). In contrast, the 30mM mannitol had no effect on the wound healing (Peng et al., 2017). The lack of effect of mannitol on cell proliferation and migration in these studies suggests that hyperglycaemia suppresses the proliferation of PTC through its metabolic effect. This, however, is debatable as mannitol may neutralise ROS in these cells and thus prevent osmolarity-induced ROS upregulation TGF-β1. TGF-β1 induces cytostasis via a G_1 phase cell cycle

arrest through the expression of p27, a cyclin-dependent kinase inhibitor (Kamesaki et al., 1998).

To address the question about the osmotic effect of hyperglycaemia on proliferation/migration of proximal tubule cells, L-glucose was used in the present study as an osmotic control instead of mannitol. The results demonstrated that 25mM D-glucose was most beneficial for wound healing, whereas in comparison, 30mM D-glucose had an inhibitory effect over 48h. These results suggest that, there is a critical D-glucose concentration between 25mM D-glucose and 30mM D-glucose beyond which the wound healing is significantly impaired. This effect appears to be metabolic, as at 24h the osmotic control and the control had a similar effect, and although at 48h the osmotic control accelerated the wound healing, there was no significant difference to the control. The data indicate that the osmolarity of the osmotic control may play a slightly positive non-metabolic role in wound healing.

3.4.2 Glucose consumption

The proximal tubule cells are sensitive to the side effects of hyperglycaemia in diabetes, as glucose is transported into them by SGLT2 in an insulin-independent manner (Vallon, 2010). Studies demonstrating the effects of hyperglycaemia on glucose utilisation in proximal tubule cells are limited. Morais et al. (2005) have demonstrated that the glucose concentration in media from HK-2 cells exposed to 5mM, 17mM, 30mM or 47mM decreases gradually over 6 days of incubation (Morais et al., 2005). Furthermore, no significant differences in the amount of

glucose utilisation have been reported in this study, and no osmotic control has been tested.

The present study is the first to report on glucose consumption by HK-2 cells exposed to different concentrations of glucose and an osmotic control. The data demonstrated that cells exposed to 30 mM D-glucose use significantly less glucose than control cells, or those exposed to osmotic control for 24h or 48h. Similarly, the glucose intake was significantly reduced in cells exposed to 25mM for 48h, as compared to the control. The reduction of glucose intake by 30mM glucose may be due to the direct inhibition of glucose transporters to reduce the excessive glucose intake, or to an inhibition of pathways associated with glucose metabolism. The vast majority of research on glucose transporters in hyperglycaemia demonstrates that hyperglycaemia induces the expression of glucose transporters, thus increasing the ability of proximal tubule cells to reabsorb the glucose (Marks et al., 2003; Tabatabai et al., 2009). In agreement with our results, a rat model of streptozotocin-induced diabetes has demonstrated a reduction in the glucose uptake and reduced activity of SGLT2 after 3, 7 and 14 days (Borghese et al., 2009). Furthermore, the decreased activity of SGLT2 may be due to downregulated expression of SGLT2 at 3 and 7 days, and alteration in membrane lipid composition at day 14 as protective mechanisms to reduce the return of excessive glucose in the circulation. Therefore, it could be suggested that the inhibition of glucose intake at 30mM D-glucose in this study maybe due to a direct inhibition or downregulation of the glucose transporters' expression to regulate the excessive glucose intake and to protect the cells. However, further experiments are required to evaluate the

mRNA and protein levels of SGLT2 and their activity in HK-2 cells exposed to 30 mM glucose.

Regardless of the mechanism of glucose uptake inhibition, the results suggest that the suppressed migration and impaired viability of HK-2 cells exposed to 30mM D-glucose may be potentially linked with reduced ATP production.

3.4.3 Cellular respiration: glycolytic rate and mitochondrial function in hyperglycaemia

Pathological changes of PTC in response to diabetes play a significant role in the development and progression of DN, leading to tubulointerstitial fibrosis (Wolf, 2004; Francesco Schena and Gesualdo, 2005). The pathogenesis of TIF in DN is multifactorial, however the early effects of hyperglycaemia on cellular respiration and energy deficit in PTCs have been largely unaddressed and conflicting, especially with respect to glycolysis. Glycolysis is an intracellular biochemical pathway that converts glucose into pyruvate to extract energy for cellular metabolism (TeSlaa and Teitell, 2014). Seahorse analysis has demonstrated in human mesangial cells that glycolysis is unaffected after 8 days in 25mM D-glucose (Czajka and Malik, 2016), whereas it was inhibited in primary mouse mesangial cells exposed to hyperglycaemia (30mM D-glucose) for 14 days (Chacko et al., 2010). Czajka and Malik, (2016) reported an increase of glycolysis by Seahorse analysis after 8 days of exposure of immortalised human HK-2 cells to 25mM glucose. This is the only study to evaluate glycolysis in proximal tubule cells in hyperglycaemia. The studies of Czajka and Malik (2016) and Chacko et al. (2010) used mannitol (25mM and 30mM respectively) as an

osmotic control, and they have stated that osmolarity had no effect on the mitochondrial respiration and glycolysis.

The present study is the first to analyse specifically, and in more detail, the effect of hyperglycaemia/hyperosmolarity on glycolysis in HK-2 cells for up to 72h by using the advanced Seahorse analysis. The significant decrease of basal glycolysis and basal proton efflux rates over 72h, regardless of the treatment, suggests that the energy demand of the cells is decreasing over time. Unpublished data from our research group show that the HK-2 cells display contact inhibition but maintain proliferative ability even in serum-free conditions, reaching over-confluence. Therefore, the decreasing glycolysis over time may represent decreasing energy demand due to reduced proliferation and the establishment of the steady-state over-confluence equilibrium at 72h. This is in agreement with data reported by Czajka and Malik (2016), which show no difference in basal glycolysis rate between control and 25mM glucose at 4 days and 8 days.

Although at 72h there were no statistically significant differences in glycolysis between cells exposed to different concentrations of glucose, at 24h and 48h the basal glycolysis and the basal proton efflux rate were significantly lower in cells exposed to 30 mM D-glucose and especially in cells exposed to the osmotic control. These results suggest that above 25mM D-glucose, osmolarity has a significant negative effect on glycolysis. Interestingly, the patterns of basic glycolysis and proton efflux rate were very similar to the patterns of glucose consumption of cells exposed to the control, 25mM D-glucose or 30mM D-glucose. In contrast to the basal glycolysis results, HK-2 cells exposed to the osmotic control displayed glucose consumption similar to the control over 72h.

The inhibition of oxygen consumption rate (OCR) by Rot/AA drives compensatory changes in the HK-2 cells and stimulates them to use glycolysis instead of mitochondrial respiration to meet their energy demands. This study showed that the levels of both compensatory glycolysis and glycoPER were significantly decreased by the 30mM D-glucose and the osmotic control as compared to the control and 25mM D-glucose after 24h and 48h, suggesting that cells exposed to higher osmolarity have a lower glycolytic capacity. The ratios of basal mitoOCR/glycoPER of cells exposed to 30mM D-glucose were significantly lower as compared to all other treatments at 24h and 48h, suggesting an increased glycolysis over mitochondrial respiration.

Interestingly, the inhibition of glycolysis by 2-DG demonstrated that the proton efflux rate is significantly reduced only in control cells and in those exposed to osmotic control (both of which contain 5mM D-glucose) suggesting that these two conditions predispose to glycolysis (and thus mitochondrial respiration). In contrast, the post 2-DG acidification rates of cells exposed to 25mM D-glucose or 30mM D-glucose, were significantly higher during the 72h incubation period as compared to the control and osmotic control, which may indicate an extracellular acidification not related to either glycolysis or the TCA cycle (tricarboxylic acid cycle) or the incomplete inhibition of glycolysis by 2-DG. Interestingly, at 72h, compared to control, hyperglycaemia and hyperosmolarity had no effect on glycolytic rate parameters except on post 2-DG acidification. It seems that 30mM D-glucose and the osmotic control had a negative effect on the glycolytic pathway in the tubule cells, suggesting that these conditions can impair the effectiveness of the two major energy pathways (glycolysis and oxidative phosphorylation) and participate in renal injury in DN.

Several reports have focused on the effect of hyperglycaemia on mitochondrial dysfunction of kidney cells, and its contribution to the pathogenesis in diabetic nephropathy (Tan et al., 2009; Zhan et al., 2015; Coughlan et al., 2016). For example, Seahorse analysis was used to measure the effect of 30mM D-glucose and 30mM mannitol for 14 days in primary mouse mesangial cells (Chacko et al., 2010). The results demonstrated that 30mM D-glucose decreased the mitochondrial cellular respiration, basal oxygen consumption rate and mitochondrial reserve capacity, and inhibited of the glycolytic rate of the cells. In contrast, immortalised mouse podocytes exposed to 30mM D-glucose for 48h demonstrated an increase in the basal and the maximal respiration compared to 30 mM mannitol, suggesting a significant change in the mitochondrial energy metabolism in response to the metabolic effect of glucose (Stieger et al., 2012).

There is a single study that evaluates the mitochondrial bioenergetics of HK-2 in hyperglycaemia by Seahorse analysis. Czajka and Malik, (2016) have demonstrated that 4 and 8 days of exposure of HK-2 cells to 25mM D-glucose, resulted in the reduction of the respiratory parameters basal, ATP-linked, and maximal respiration, non-mitochondrial respiration and reserve capacity, as compared to the effects of 5mM glucose. In contrast, 25 mM glucose had no effect on the proton leak of these cells (Czajka and Malik, 2016). Furthermore, the authors have reported that the mitochondrial respiration was not affected by the osmotic control (20 mM mannitol + 5 mM glucose) (Czajka and Malik, 2016). These data suggest that the alteration of mitochondrial respiration in HK-2 cells was a direct consequence of the metabolic effect of hyperglycaemia. However, the use of the free radical scavenger mannitol as an osmotic control in this and

the previous studies does not allow the delineation of the metabolic from the osmotic effects of hyperglycaemia (André and Villain, 2017).

In the present study, L-glucose was used as an osmotic control to study the osmotic and metabolic effects of 30mM glucose. In contrast with the findings of Czajka and Malik, (2016), the results of the present study show that the oxygen consumption at basal respiration and maximal respiration in HK-2 cells was not affected by any of the treatments, over a 72h period. The ATP production was moderately reduced by 30mM glucose and osmotic control, especially at 72h. These results are similar to the observations of Czajka and Malik (2016), where the ATP production was significantly reduced in HK-2 cells after 4 and 8 days of exposure to 25 mM glucose. In contrast to the results of Czajka and Malik (2016) at 4 and 8 days, in this study, the gradual increase over time of the proton leak in HK-2 cells exposed to 25mM glucose, 30 mM glucose and osmotic control suggests that mitochondrial damage may be the cause for the reduction in ATP production. The significant increase of proton leak at 72h with 30mM D-glucose and osmotic control treatments suggests that the osmolarity is the driving factor of mitochondrial damage. For the first time, this study demonstrated that the increased proton leak across the mitochondrial membrane results in the significant lowering of the mitochondrial coupling efficiency, especially in response to 30mM D-glucose and osmotic control, at 72h.

The spare respiratory capacity increased over time in all treatments, including the control. However, the significant decrease in this parameter at 72h in HK-2 cells exposed to 30mM D-glucose, and osmotic control suggests that hyperglycaemia/hyperosmolarity impairs the cells' ability to adequately respond when an increased energy demand is required. These findings are similar to the

effect of 25mM glucose observed by Czajka and Malik (2016) at 4 and 8 days of exposure of HK-2 cells.

Hyperglycaemia (30mM D-glucose) and the osmotic control significantly decreased the non-mitochondrial oxygen consumption only after 24h, while there was no effect of the hyperglycaemia and hyperosmolarity on the non-mitochondrial oxygen consumption after 48 and 72h.

Our data demonstrate that hyperglycaemia, especially after a prolonged exposure to 30mM D-glucose and osmotic control, reduces the ATP production through an increase in the mitochondrial proton leak, which ultimately may contribute to PTC injury, and thus to renal tubular fibrosis in DN.

3.4.4 HK-2 cell phenotype in *in vitro* model of hyperglycaemia

The HK-2 *in vitro* model of hyperglycaemia is prolonged (the cells are cultured for 96h at confluence of 100% in serum-free medium), and therefore the possible alteration in the proximal tubule cell phenotype should be considered when the results are interpreted.

TIF is key feature of DN, in which EMT plays a crucial role. In EMT, tubule epithelial cells lose their characteristic of producing high levels of α-SMA, a marker of the myofibroblast phenotype (Lovisa et al., 2015; Hills et al., 2018). A study with rat renal proximal tubule epithelial cells demonstrated an increased expression of α-SMA in response to 25 mmol/L glucose for 24h and 48h, with no effect of mannitol (5.6 mmol/L D-glucose + 19.4 mmol/L D-mannitol) (Bao et al., 2019). This evidence suggests that high glucose may induce EMT and may lead to alteration in the tubular epithelial cell phenotype. Furthermore, a change in the

morphologic phenotype of the HK-2 cells into bipolar- or spindle-shaped cells with a myofibroblast-like phenotype was observed after 72h of exposure to 60 mM/L D-glucose, with overexpression of the myofibroblastic mesenchymal markers fibronectin and vimentin (Shin et al., 2019).

These data suggest that hyperglycaemia has the potential to alter the phenotype of proximal tubule cells, in particular at prolonged exposure of high glucose. However, in the present study no microscopic changes were observed in the appearance of HK-2 cells exposed for 72h to 30 mM of D-glucose Previous unpublished results from our research group have demonstrated no significant increase of α-SMA protein after 72h of exposure to 25 mM D-glucose (data not shown). However, further Western blot experiments are required to demonstrate whether 30 mM D-glucose can modify the HK-2 cell phenotype by upregulating the expression of α-SMA.

3.5   Conclusions

This study has shown that RPTECs appear to not only tolerate, but to thrive in hyperglycaemic conditions up to a certain threshold. In contrast to 30mM D-glucose, 25mM D-glucose seems to have beneficial effects on wound healing as compared to the 5mM D-glucose control. In terms of glycolysis, with the exception of post 2-DG acidification, 25mM D-glucose had a similar effect to that of the control. However, in terms of mitochondrial function, its effect was closer to the effect of 30mM D-glucose.

The mechanism by which 30mM D-glucose exerts its adverse effects are different, depending on the physiological process studied. For example, the

effects on mitochondrial function parameters, such as proton leak, spare respiratory capacity and coupling efficiency appear to be linked to the osmotic effects of glucose. However, other parameters (e.g. viability, wound healing and glycolysis) may be influenced by its metabolic effect, which may be linked to the reduced glucose uptake, the mechanism of which needs a further investigation.

Such a distinction of the mechanisms of action of hyperglycaemia can be achieved only through the use of an appropriate osmotic control (L-glucose), which does not have the antioxidant properties of mannitol. The use of L-glucose as an osmotic control without a metabolic function can also provide an insight into the damaging effects of artificial sweeteners on kidney function (Lin and Curhan, 2011).

In summary, in relation to the overall aim of this project, this chapter provides evidence that hyperglycaemia impairs the two main energy pathways (mitochondrial respiration and glycolysis) in the proximal tubule cells. However, the effect of hyperglycaemia on each pathway is underpinned by a different mechanism: its osmotic effect impedes the mitochondrial respiration, whereas glycolysis (and also cell viability, wound healing and glucose uptake) is impaired through the metabolic effect of hyperglycaemia.

These findings provide evidence that the osmotic and metabolic features of hyperglycaemia have differential effects, and thus provide the rationale for investigating their effect on the expression of key fibrosis-related cytokines, markers of inflammation and ECM components, in the next chapter.

Chapter 4: Effect of hyperglycaemia on markers of proximal tubular injury

4.1 Introduction

Although DN is classically considered a non-immune disease caused by interaction between hemodynamic and metabolic factors, accumulating evidence demonstrates that the immune response and inflammatory process play a crucial role (Navarro-Gonzalez and Mora-Fernandez, 2008).

TGF-β/Smad signalling is a key mediator of renal fibrosis in DN (Lan, 2012; Meng et al., 2015). In fibrogenesis, Smad3 is activated and the inhibitory Smad7 is downregulated, which results in the activation of myofibroblasts, the excessive deposition of ECM and/or the suppression of ECM turnover (Li et al., 2003; Meng et al., 2015). It has been reported that rat renal proximal tubule cells exposed to 35 mM D-glucose for 24h activated the TGF-β-Smad2/3 signalling pathway and induced the synthesis of collagen, while 35 mM mannitol had no effect on the phosphorylation of Smad2/3 (Li et al., 2003).

The excessive deposition of ECM proteins such as collagens and fibronectin play a central role in the progression of renal fibrosis in DN. The abnormal matrix deposition might be due to either increased synthesis or decreased degradation of ECM proteins. PAI-1 activates a number of MMPs and thus is a key regulator of ECM remodelling (Małgorzewicz et al., 2013). In health, there is a balance between the degradation of ECM proteins by MMPs and the inhibition of MMPs by TIMPs. Overproduction of TIMPs can increase the accumulation of ECM and renal fibrosis (Klein and Bischoff, 2011). The upregulation of both the MMPs and

TIMPs has been associated with glomerulonephritis and tubular diseases (Gonzalez-Avila et al., 1998; Liu 2006)

Cytokines, such as IL-6, play a crucial role in the regulation of the inflammatory process by promoting autocrine, paracrine, and juxtacrine signaling in response to innate immune system activation (Pérez-Morales et al., 2018). MCP-1 is a chemoattractant cytokine produced either by tissue injury or infection, and plays a central role in controlling cell trafficking and the recruitment of monocytes to sites of inflammation (Deshmane et al., 2009). It has been reported that hyperglycaemia upregulates the expression of both IL-6 and MCP-1 in cultured human renal proximal tubule epithelial cells (Tang et al., 2009).

The kidney injury molecule-1 (KIM-1) is the most highly upregulated proximal tubule cell protein following a kidney injury in both humans and animals (Brooks and Bonventre, 2015) and serves as an early clinical biomarker of kidney injury. Endostatin plays an important role in the inhibition of tubule formation, endothelial cell proliferation and migration, and the upregulation of endostatin is associated with renal injury (Cichy et al., 2009; Bellini et al., 2007).

Clear evidence of the osmotic effect of hyperglycaemia on markers of proximal tubular injury is lacking as mostly mannitol, which has antioxidant properties, is used as an osmotic control. Therefore, the aim of this next part of the study was to delineate the metabolic and the osmotic effects of hyperglycaemia in proximal tubule epithelial (HK-2) cells on markers of ECM accumulation, inflammation and injury that are associated with renal tubular fibrosis in DN.

4.2 Materials and Methods:

4.2.1 Cell culture

Cell culture techniques were used to study the effect of different concentrations of glucose (5, 25 and 30mM D-glucose or osmotic control (5 mM D+25mM L-glucose) on HK-2 cells at 24h, 48h and 72h as described in section 2.1.

4.2.2 Harvesting of cells and media for TGF-β1 and Luminex biomarker analyses

Media and cells were harvested for TGF-β1 ELISA and Luminex assays as described in section 2.2. Briefly, HK-2 cells were harvested for normalisation in 0.2 M of NaOH, the samples were incubated for 2 h at 37°C and stored at −20°C prior to analysis of total protein content.

4.2.3 Protein estimation by the bicinchoninic acid (BCA) method

A BCA kit purchased from Novagen (#71285-3) was used for the protein estimation as per manufacturer's protocol as described in section 2.3.

4.2.4 TGF-β1 levels in media from cells exposed to hyperglycaemia

TGF-β1 was measured in media from cells exposed to hyperglycaemia for 24h, 48h or 72h using an ELISA kit (R&D systems, # DY240-05) as described in section 2.10.

4.2.5 Activation of the Smad pathway in response to hyperglycaemia

SDS-PAGE and Western blotting techniques were used to determine the activation of the Smad pathway by detecting the relative amounts of phosphorylated Smad3, as described in section 2.11. The chemiluminescence signal was analysed by a G: Box imaging system (Syngene, UK). The images were then analysed by Image lab software.

4.2.6 RNA isolation and purification

Cells were harvested using QIAzol lysis regent (Qiagen, # 55709615), as described in section 2.12.1.1. The cells were then stored at – 80°C prior to further analysis.

A miRNeasy Mini Kit (Qiagen, #217004) was used to purify and isolate the total RNA as described in section 2.12.1.1. The RNA concentration was measured using a Nanodrop (Thermo Fisher Scientific, USA, 02611). The RNA samples were then stored at –80 °C for further procedures.

4.2.7 Reverse transcriptase PCR and quantitative real-time PCR (qPCR)

Total RNA was converted to cDNA using a Tetro cDNA Synthesis Kit (Bioline; # 65042) as described in section 2.12.1.2. A QuantiNova SYBR Green PCR Kit (Qiagen; # 208056) was used to quantify the mRNA expression of *Col Iα1*, *PAI-1*, *MMP-9*, *TIMP-1* using *GAPDH* as the housekeeping gene, as described in section 2.12.1.3.

4.2.8 Luminex biomarker analysis

A Human Premixed Multi-Analyte Kit (R&D systems, #LXSAHM) was used to measure the levels IL-6, MCP-1, KIM-1 and Endostatin in response to hyperglycaemia, as described in section 2.9.

4.2.9 Statistical analysis

Graph Pad Prism 5 software and IBM SPSS statistics version 25 software were used to analyse the data with a one-way ANOVA. Tukey's HSD post-hoc test was carried out when significant p-values (*p≤0.05) were detected.

4.3 Results

4.3.1 TGF-β1 levels in media of cells exposed to hyperglycaemia

ELISA tests were used to measure the concentrations of TGF-β1 in media from cells exposed to control (5mM D-glucose), hyperglycaemia (25mM D-glucose and 30mM D-glucose) or osmotic control (5mM D-glucose+25mM L-glucose) for up to 72h. At 24h TGF-β1 was increased in media from cells exposed to 30mM D-glucose and osmotic control, as compared to control, and this effect was significant in response to the osmotic control (Figure 4.1A). No significant differences in the levels of TGF-β1 were observed at 48h in response to any treatment condition (Figure 4.1B). In contrast, at 72h TGF-β1 was increased in media from cells exposed to 25mM or 30mM D-glucose, and the effect of 30mM D-glucose was significant, when compared to cells exposed to control or osmotic control (Figure 4.1C). The basal TGF-β1 level at 72h was increased 10 fold, as compared to 24h and 48h (Figures 4.1A, B and C).
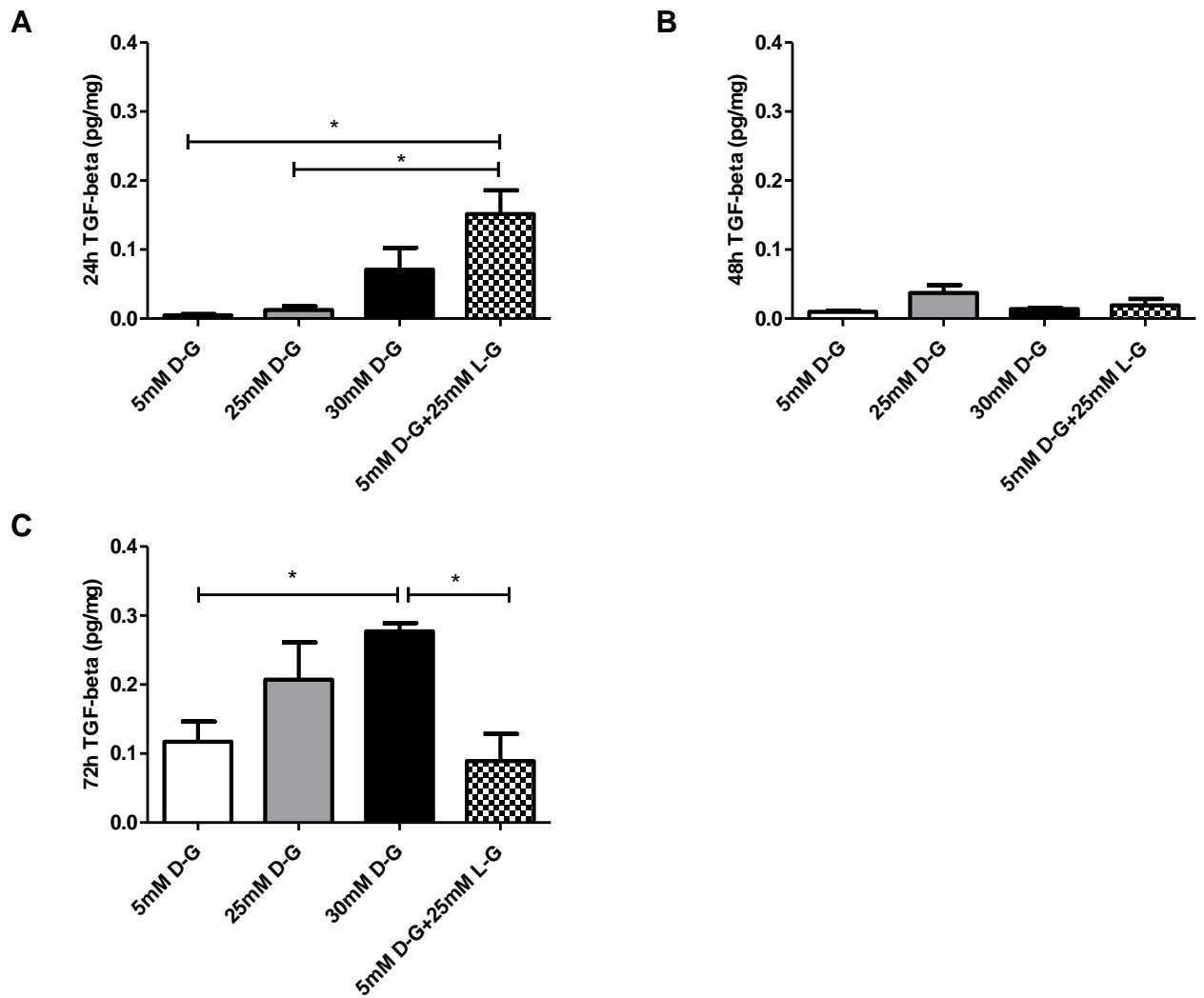
Figure 4. 1.TGF-β1 levels in media from HK-2 cells exposed to hyperglycaemia for up to 72h.

ELISA was used to measure the TGF-β1 levels in media from cells exposed to control, hyperglycaemia (25 or 30mM D-glucose) or osmotic control 24h **(A),** 48h **(B)**or 72h **(C)**. The TGF-β1 levels were normalised to total cellular protein content. Data are expressed as Mean±SEM, n=6. One-way ANOVA was used to compare the treatment groups. Tukey's HSD post-hoc test was carried out when significant p-values (*p≤0.05) were detected.

4.3.2 Activation of the Smad pathway

Western blotting was used to determine the activation of the Smad pathway in HK-2 cells in response to hyperglycaemia by detecting the relative expression of phosphorylated Smad3 (P-Smad3). An antibody, which specifically detected Smad3 phosphorylated at Ser423/425, was used to ensure the detection of P-Smad3C (C-terminus phosphorylated Smad3), which is phosphorylated in the canonical TGF-β1 pathway of activation by TGFBR1.

The cells were exposed to control (5mM D-glucose), hyperglycaemia (25mM D-glucose and 30mM D-glucose) and osmotic control (5mM D-glucose + 25mM L-glucose) for 24h, 48h and 72h and the expression of P-Smad3 was normalised to the levels of total Smad3 (T-Smad3). The results demonstrated that P-Smad3 was elevated by hyperglycaemia (25mM and 30mM D-glucose) and the osmotic control at 24h (Figure 4.2A), 48h (Figure 4.2B), and 72h (Figure 4.2C). However, this increase was significant only in response to 30mM D-glucose at 24h, 48h and 72h, and after an exposure to the osmotic control for 48h and 72h.
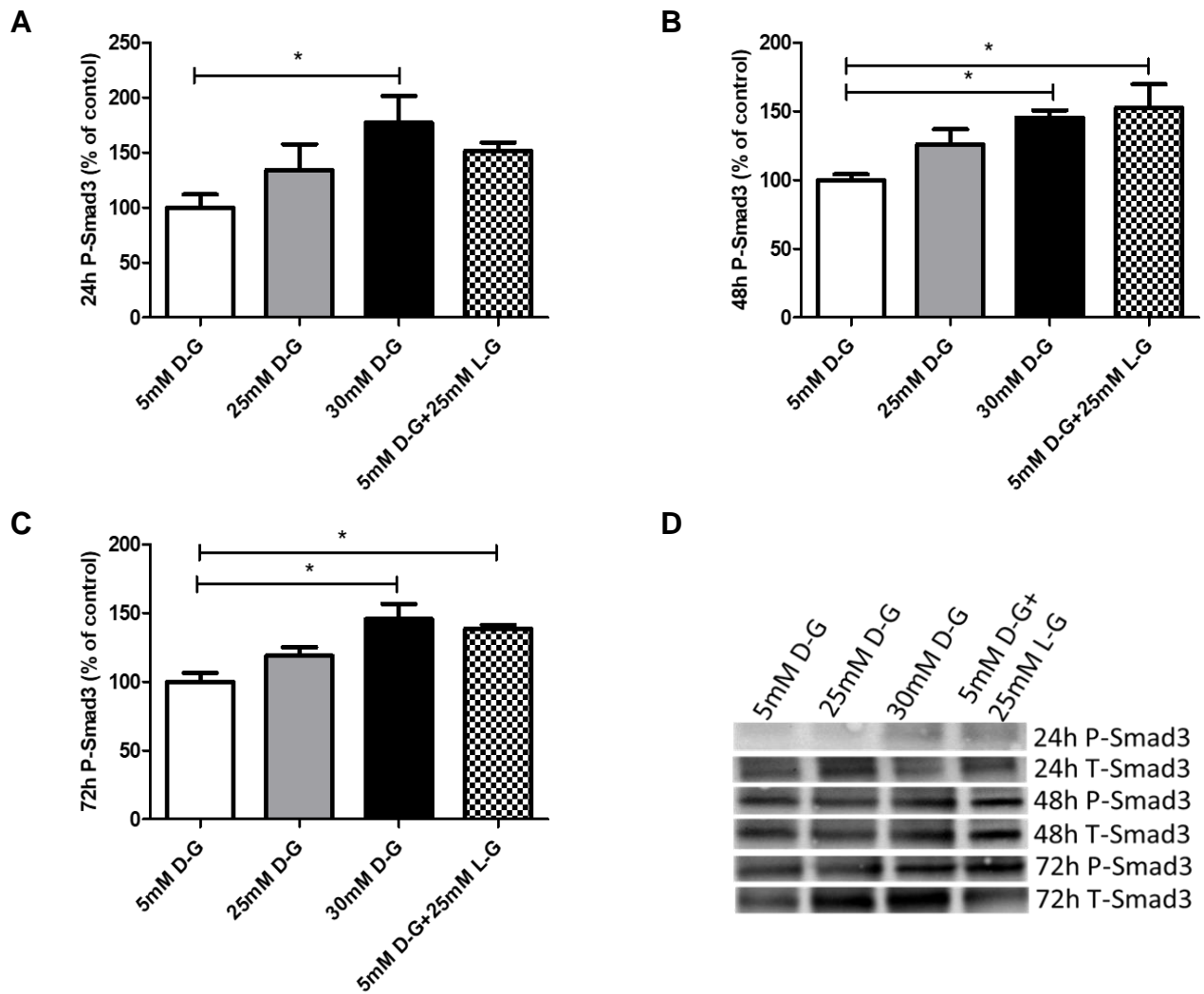
Figure 4. 2. Activation of the Smad signalling pathway in HK-2 cells in response to hyperglycaemia.

Quantitative scanning densitometry of relative P-Smad3 (molecular weight 52 kDa) expression in response to control, hyperglycaemia (25 and 30mM D-glucose) or osmotic control Smad3 for 24h (**A)**, 48h (**B)** and 72h (**C).** The relative P-Smad3 expression was normalised to T-Smad3 and expressed as % of P-Smad3 levels of cells exposed to control. **D)** Representative Western blot images of P-Smad and T-Smad showing the effect of hyperglycaemia at 24h, 48h and 72h. Data are presented as Mean±SEM, n= 4. One-way ANOVA was used to compare the treatment groups. Tukey's HSD post-hoc test was carried out when significant p-values (*p≤0.05) were detected.

4.3.3 mRNA expression of markers of renal fibrosis

The effect of hyperglycaemia on the mRNA expression of Col1α1, PAI-1, MMP-9 and TIMP-1 was evaluated by qPCR in HK-2 cells exposed to control (5mM D-glucose), hyperglycaemia (25mM D-glucose and 30mM D-glucose) or osmotic control (5mM D-glucose+25mM L-glucose) for 24h, 48h and 72h.

Although at 24h 30mM D-glucose and 25mM D-glucose decreased the expression of Col1α1 mRNA by 50% and 20%, respectively, and by 20% at 48h and 72h as compared to the respective controls, these effects were not significant (Figure 4.3A, B and C). The osmotic control had no significant effect on the expression of Col1α1 mRNA.

Hyperglycaemia had no significant effect on the mRNA expression of PAI-1 (Figure 4.3 D, E, F), MMP-9 (Figure 4.4 A, B and C), and TIMP-1 (Figure 4.4 D, E and F), as compared to the control. The mean of the triplicate Ct values for Col1α1, PAI-1, TIMP-1, MMP-9 and GAPDH are presented in Appendix 2.
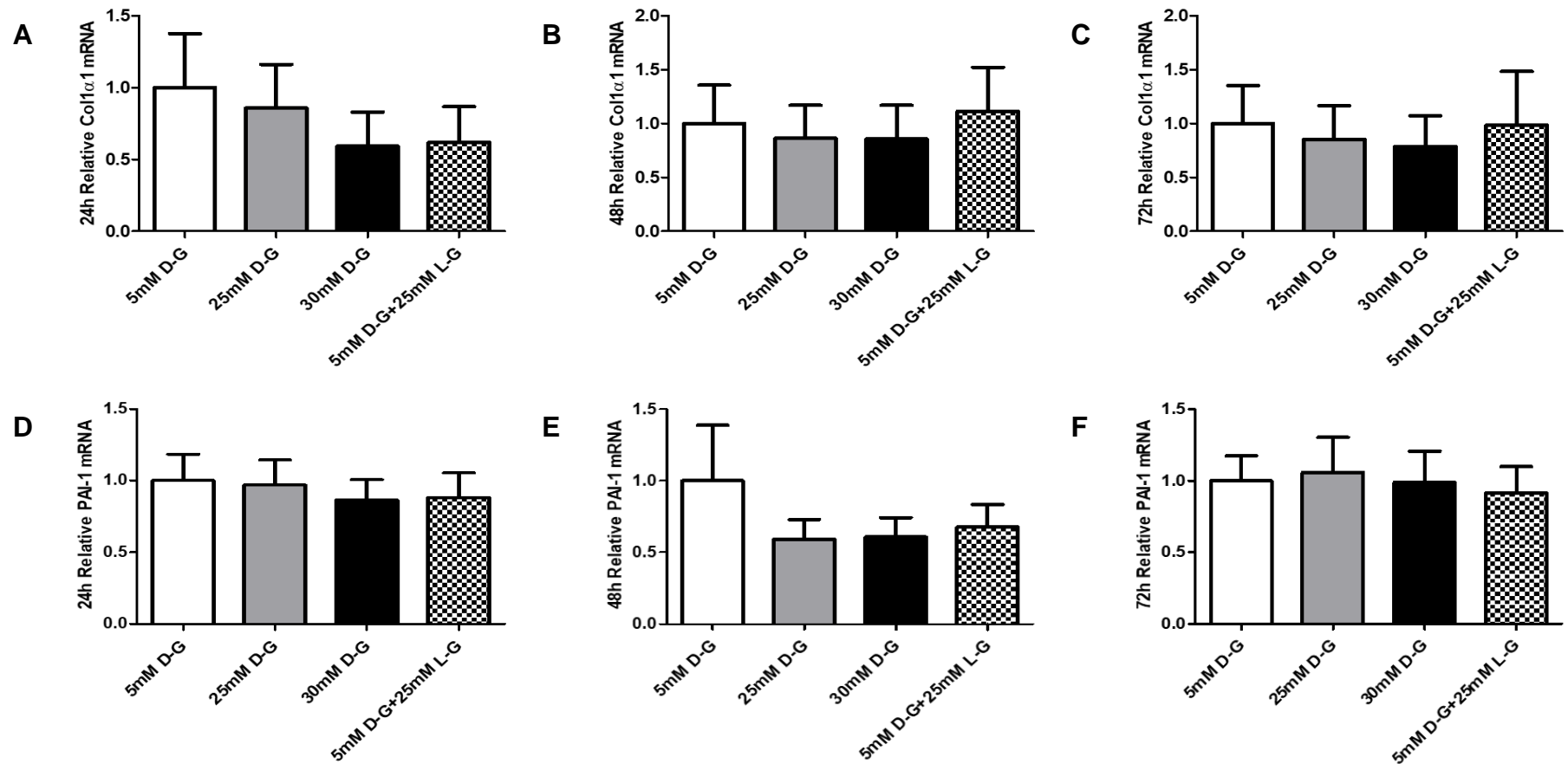
Figure 4. 3. Relative mRNA expression of collagen 1α1 and PAI-1 in response to hyperglycaemia for up to 72h.

The relative mRNA of the targets was evaluated in HK-2 cells exposed to different concentrations of glucose: control (5mM D-glucose), hyperglycaemia (25mM D-glucose and 30mM D-glucose) and osmotic control (5mM D-glucose+25mM L-glucose) for 24h, 48h and 72h. **A)** Col1α1 at 24h; **B)** Col1α1 at 48h; **C)** Col1α1 at 72h; **D)** PAI-1 at 24h; **E)** PAI-1 at 48h; **F)** PAI-1 at 72h. The results were normalised to GAPDH mRNA expression and presented as fold-change in relation to the respective controls. Representative data are expressed as Mean±SEM of 2 independent experiments (n=7). One-way ANOVA was used to compare the treatment groups. Tukey's HSD post-hoc test was carried out when significant p-values (*p≤0.05) were detected.
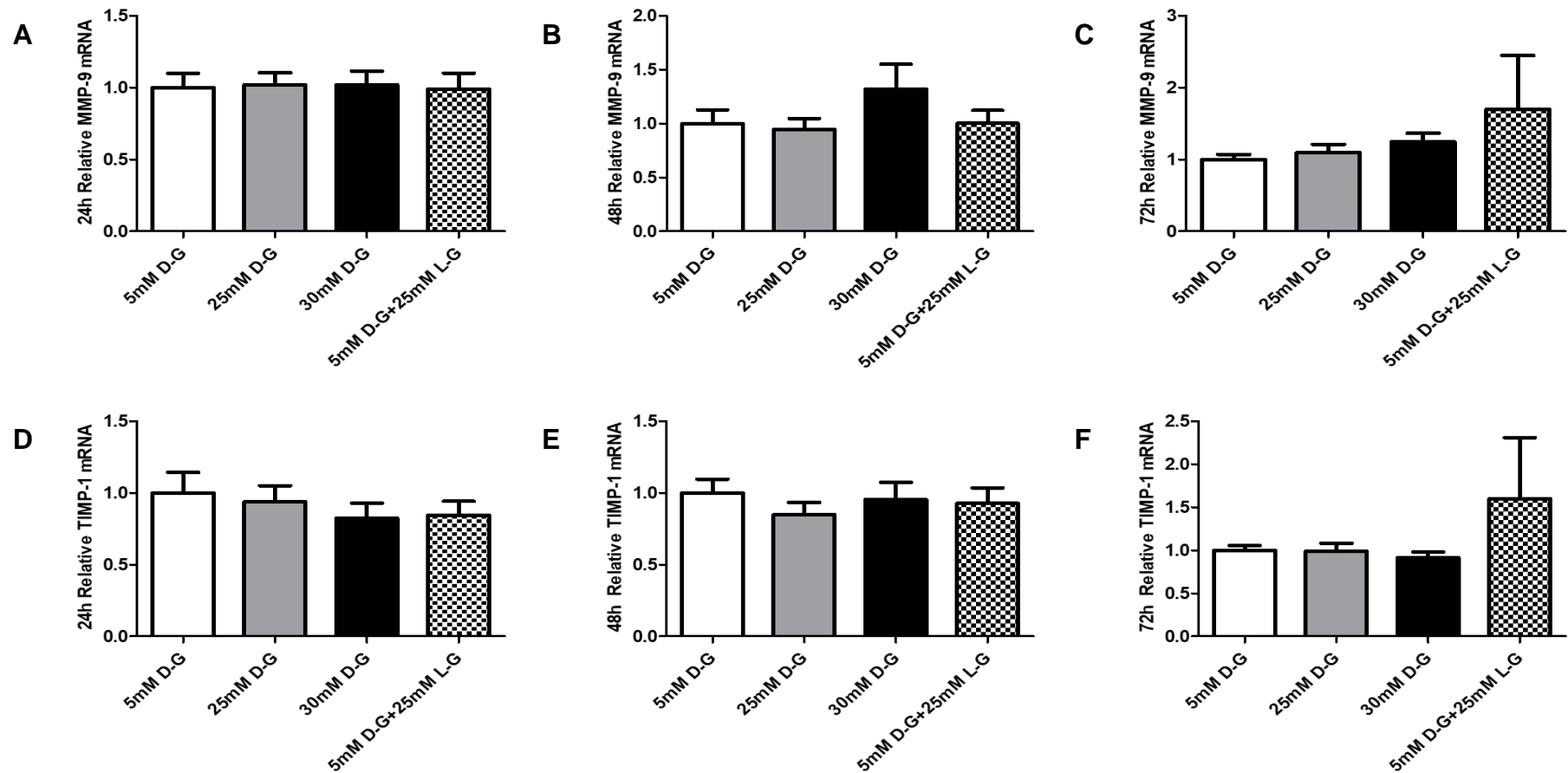
Figure 4. 4. Relative mRNA expression of MMP-9 and TIMP-1 in response to hyperglycaemia for up to 72h.

The relative mRNA of the targets expression was evaluated in HK-2 cells exposed to different concentrations of glucose: control (5mM D-glucose), hyperglycaemia (25mM D-glucose and 30mM D-glucose) and osmotic control (5mM D-glucose+25mM L-glucose) for 24h, 48h and 72h. **A)** MMP-9 at 24h; **B)** MMP-9 at 48h; **C)** MMP-9 at 72h; **D)** TIMP-1 at 24h; **E)** TIMP-1 at 48h; **F)** TIMP-1 at 72h. The results were normalised to GAPDH mRNA expression and presented as fold-change in relation to the respective controls. Representative data are expressed as Mean±SEM of 2 independent experiments (n=7). One-way ANOVA was used to compare the treatment groups. Tukey's HSD post-hoc test was carried out when significant p-values (*p≤0.05) were detected.

4.3.4 Biomarkers of inflammation and PTC injury: IL-6, MCP-1, KIM-1 and endostatin

The levels of the inflammatory cytokine IL-6, MCP-1, KIM-1 and endostatin were measured simultaneously using Luminex analysis in media from HK-2 cells exposed to control (5mM D-glucose), hyperglycaemia (25mM D-glucose or 30mM D-glucose), or osmotic control (5mM D-glucose+25mM L-glucose) for 24h, 48h or 72h.

The IL-6 levels were increased significantly in media from cells exposed to 30mM D-glucose or the osmotic control for 24h, as compared to control or 25mM D-glucose (Figure 4.5A). Compared to the control, 25mM or 30mM D-glucose had no effect on the IL-6 levels at 48h and 72h. In contrast, the osmotic control significantly increased the IL-6 concentration in media at 48h and 72h, as compared to control and hyperglycaemia (25mM D-glucose and 30mM D-glucose) (Figure 4.5B and C).

A slight increase in the baseline levels of IL-6 was observed over 72h (Figure 4.5A, B and C).
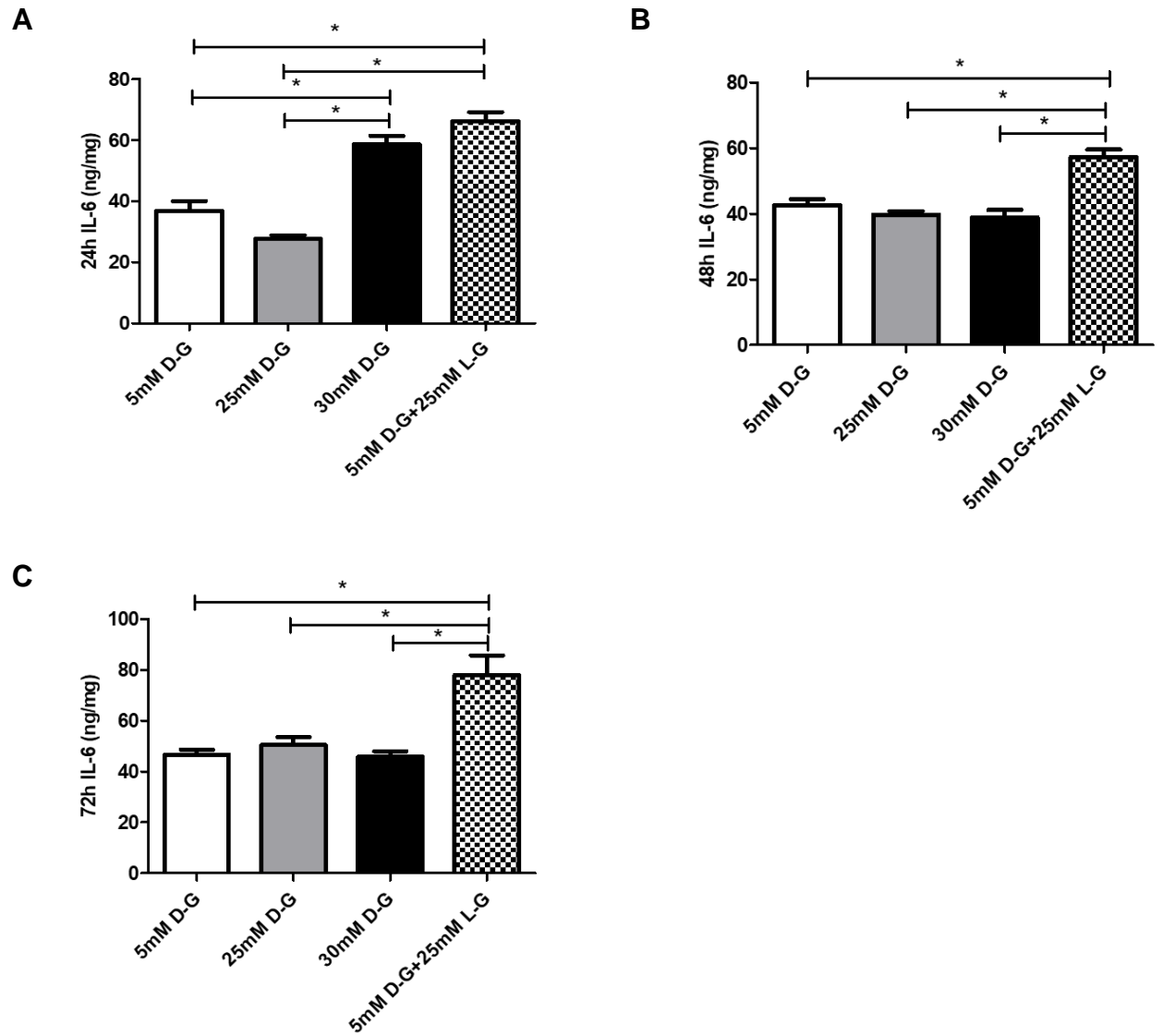
Figure 4. 5. IL-6 levels in media from HK-2 cells exposed to hyperglycaemia for up to 72h.

IL-6 levels were measured in media from HK-2 cells exposed to control, hyperglycaemia (25 or 30mM D-glucose) or osmotic control. for 24h **(A),** 48h **(B)** and 72h **(C)** using Luminex analysis. The IL-6 levels were normalised to total cellular protein. Data are expressed as Mean±SEM (n=6). One-way ANOVA was used to compare the treatment groups. Tukey's HSD post-hoc test was carried out when significant p-values (*p≤0.05) were detected.

At 24h, the levels of MCP-1 were significantly increased by 30mM D-glucose compared to the control and 25mM D-glucose (Figure 4.6A). The osmotic control significantly increased the expression of MCP-1 only in comparison with 25mM D-glucose. At 48h and 72h there was no change of MCP-1 levels in response to hyperglycaemia, as compared to control (Figure 4.6B and C).

A slight increase in the baseline levels of MCP-1 was observed over 72h (Figure 4.6A, B and C).
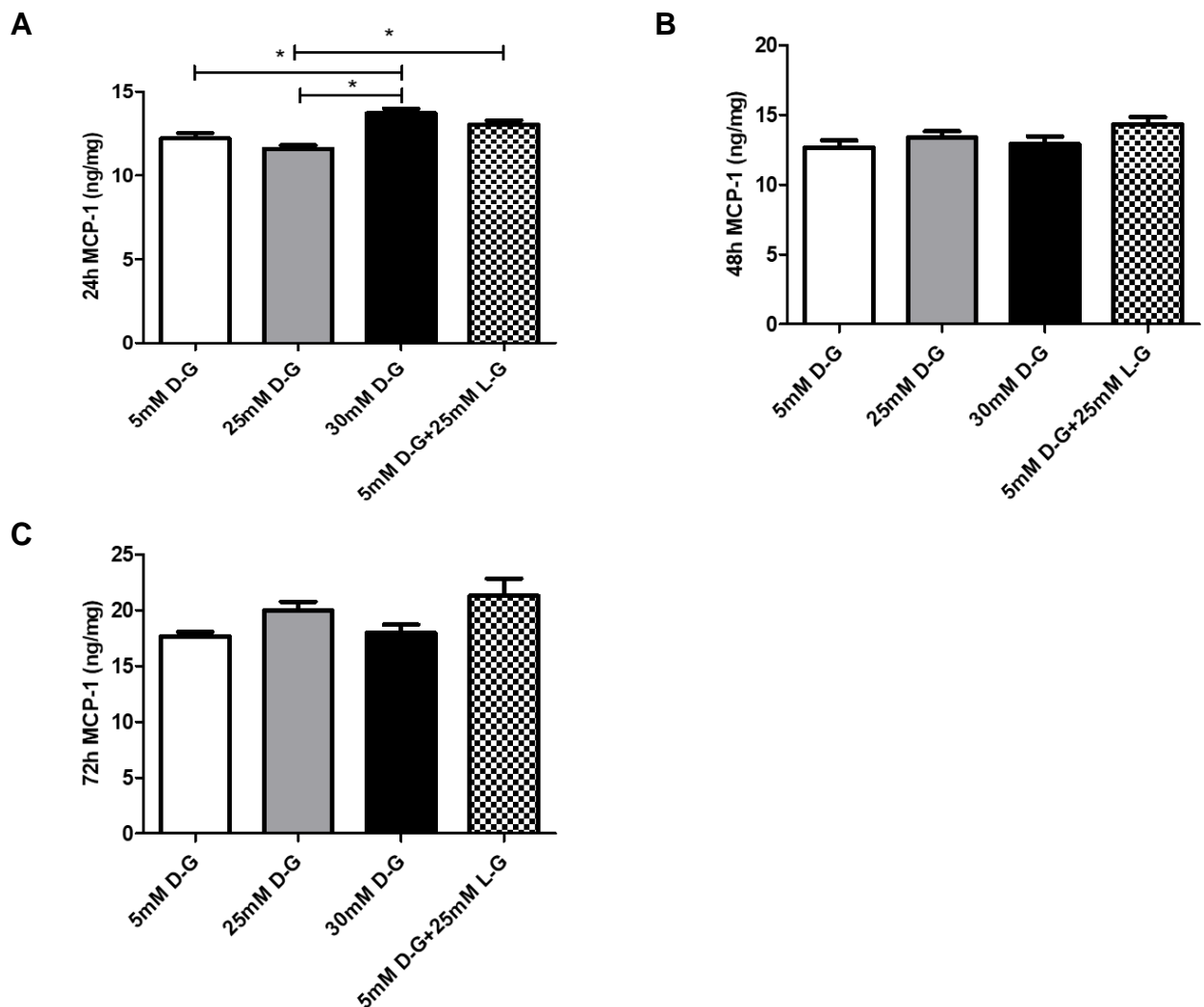
Figure 4. 6. MCP-1 levels in media from HK-2 cells exposed to hyperglycaemia for up to 72h.

MCP-1 levels were measured in media from HK-2 cells exposed to control, hyperglycaemia (25 or 30mM D-glucose) or osmotic control. for 24h **(A),** 48h **(B)** and 72h **(C)** using Luminex analysis. The MCP-1 levels were normalised to total cellular protein. Data are expressed as Mean±SEM (n=6). One-way ANOVA was used to compare the treatment groups. Tukey's HSD post-hoc test was carried out when significant p-values (*p≤0.05) were detected.

At 24h, the levels of KIM-1 were significantly increased by 30mM D-glucose and the osmotic control as compared to control and 25mM D-glucose (Figure 4.7A). However, at 48h and 72h, hyperglycaemia and the osmotic control had no effect on the expression of KIM-1 compared to control (Figure 4.7B and C).

A time-dependent significant increase was observed in the baseline levels of KIM-1 over 72h (Figure 4.7A, B and C).
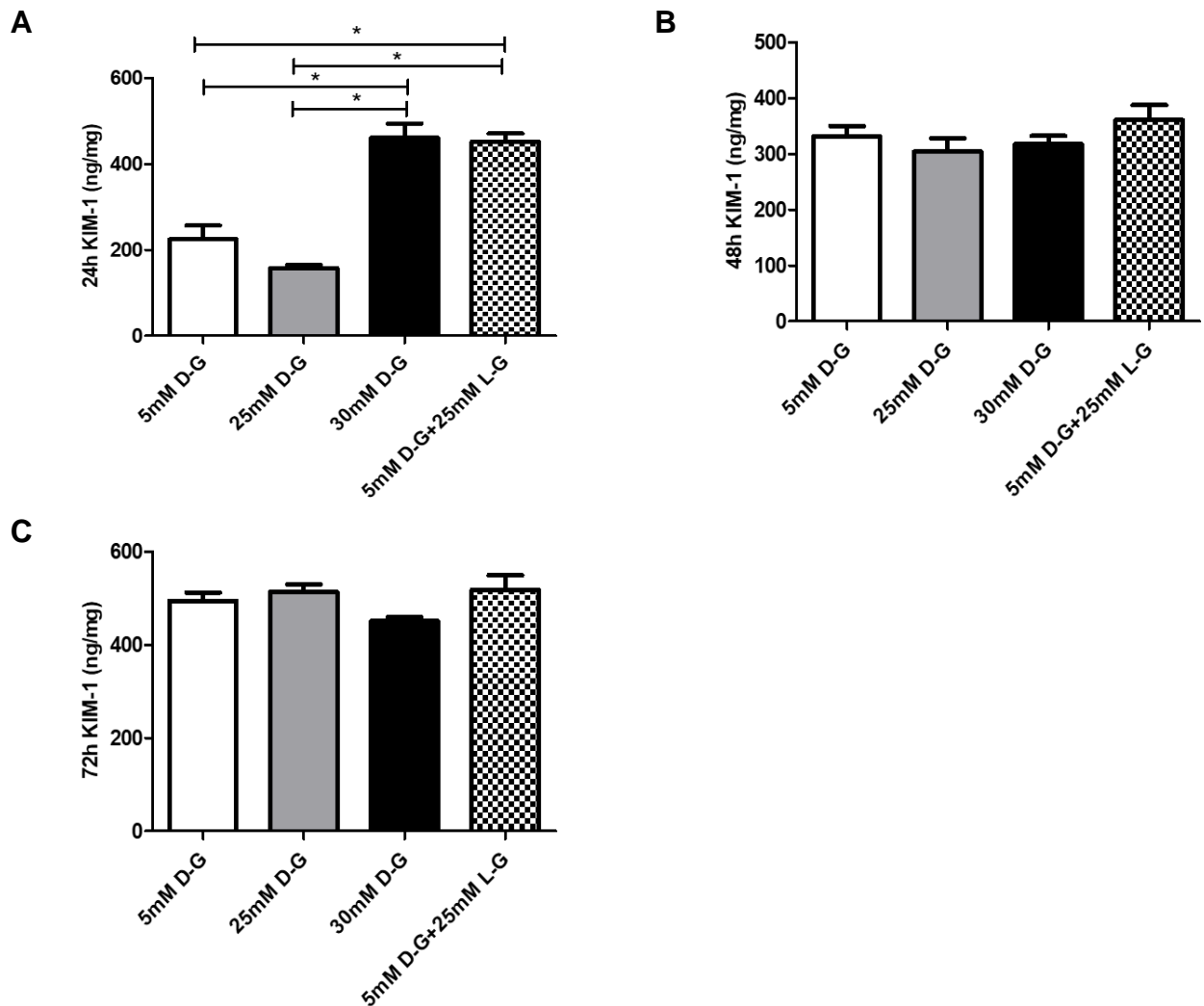
Figure 4. 7. KIM-1 levels in media from HK-2 cells exposed to hyperglycaemia for up to 72h.

KIM-1 levels in media from cells exposed to control, hyperglycaemia (25 and 30mM D-glucose) or osmotic control were measured at 24h **(A)**, 48h **(B)** and 72h **(C)** using Luminex analysis. The amount of KIM-1 was normalised to total protein content. Data are expressed as Mean±SEM (n=6). One-way ANOVA was used to compare the treatment groups. Tukey's HSD post-hoc test was carried out when significant p-values (*p≤0.05) were detected.

Similar to KIM-1, the levels of endostatin were significantly higher in media from cells exposed to 30mM D-glucose and the osmotic control at 24h, as compared to control and 25mM D-glucose (Figure 4.8A). Adaptation was observed at 48h and 72h, with no significant changes of endostatin levels between the different treatments (Figure 4.8B and C).

A significant increase in the baseline levels of endostatin was observed at 48h, as compared to 24h. The baseline levels of endostatin decreased at 72h, as compared to 48h (Figure 4.8A, B and C).
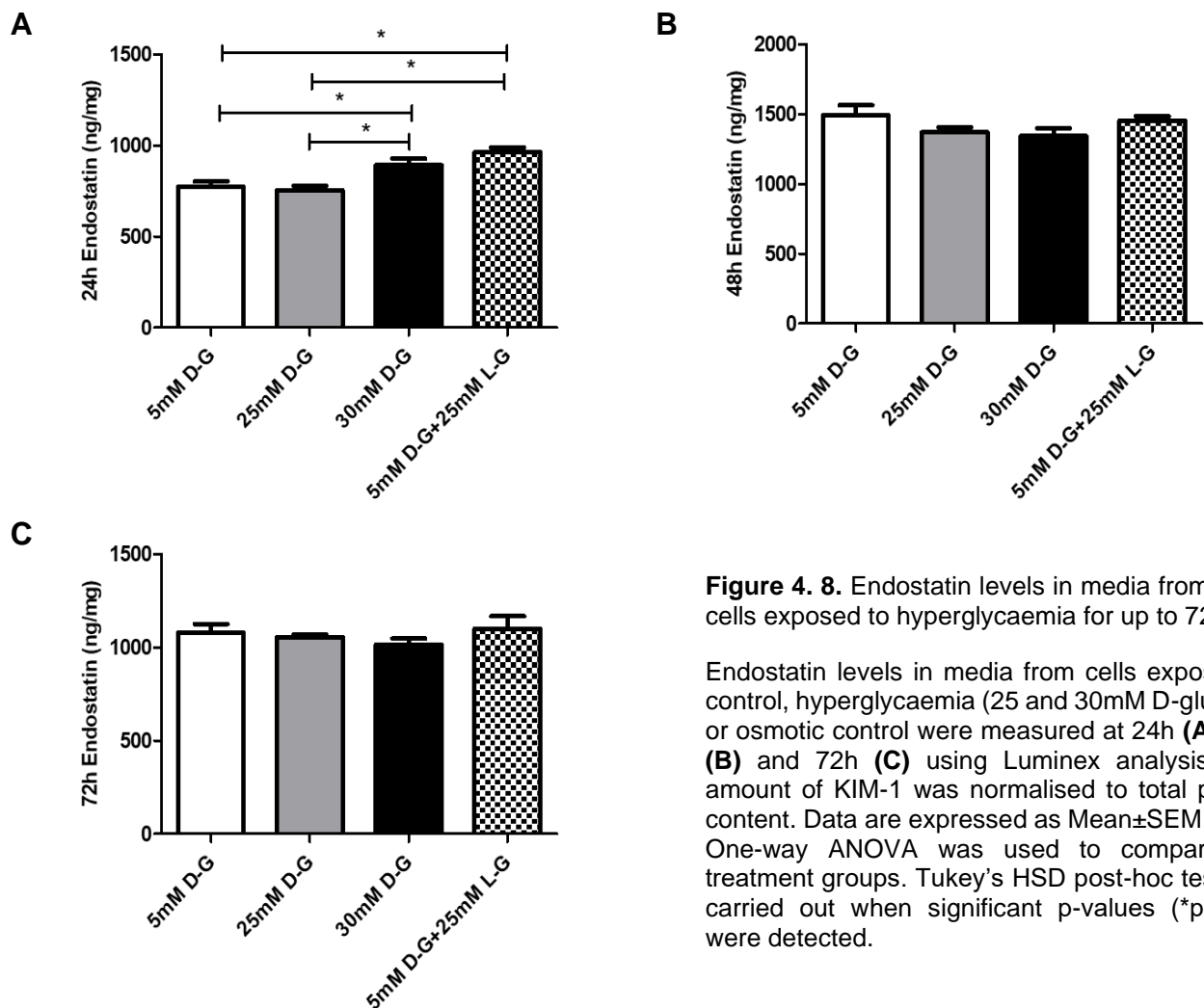
Figure 4. 8. Endostatin levels in media from HK-2 cells exposed to hyperglycaemia for up to 72h.

Endostatin levels in media from cells exposed to control, hyperglycaemia (25 and 30mM D-glucose) or osmotic control were measured at 24h **(A)**, 48h **(B)** and 72h **(C)** using Luminex analysis. The amount of KIM-1 was normalised to total protein content. Data are expressed as Mean±SEM (n=6). One-way ANOVA was used to compare the treatment groups. Tukey's HSD post-hoc test was carried out when significant p-values (*p≤0.05) were detected.

4.4 Discussion

About 10% of the world population is affected by CKD, which is linked to high mortality due to limited access to renal replacement therapy or its high cost. Although there are multiple factors leading to CKD, renal fibrosis is the final common pathway of this disease, which makes it a target for potential treatments (Duffield, 2014; Piccoli et al., 2018). Fibrosis represents the formation and accumulation of ECM as a result of a complex cross-talk between multiple cell types (e.g. epithelial, endothelial and immune cells, and mesenchymal cells such as fibroblasts, pericytes and myofibroblasts) (Duffield, 2014). Although fibrosis is a protective reaction in response to tissue injury that is linked with inflammation and tissue regeneration, even physiological wound healing rarely results in complete regeneration but leads to the formation of residual scar tissue (Rockey et al., 2015). Fibrosis may be protective in certain kidney diseases (e.g. pyelonephritis and renal infarction), where the formation of a scar may support the integrity and function of the remaining kidney. However, the excessive and prolonged accumulation of ECM as a result of persistent kidney injury caused by diabetes, hypertension, atherosclerosis, etc. can gradually lead to pathological changes to the kidney tissue and decreased kidney function over time (Jiang et al., 2003). In contrast to other organs, like the liver, which has a high regenerative potential and can recover even after severe fibrosis caused by Hepatitis C or alcohol-induced cirrhosis, the kidney, and in particular the glomerulus, has a limited regenerative potential and its threshold of irreversible fibrosis appears to be significantly lower (Koyama et al., 2016).

Renal fibrosis can affect not only the three structural compartments of the nephron (glomerulus, tubules, and vasculature), causing glomerulosclerosis,

133

tubulointerstitial fibrosis, and arteriosclerosis, but also the basement membranes of each compartment, leading to their thickening (Djudjaj and Boor, 2019). Regardless of which compartment is injured at the early stages of kidney disease, progressive TIF is the final common pathway that leads to CKD (Zeisberg and Neilson, 2010).

TIF is characterised by the excessive deposition of ECM, which disrupts the normal microarchitecture of the tubules and the connection between the tubules and the peritubular capillaries causing impaired supply of oxygen and nutrients to the tubule cells. The deposited ECM consists predominantly of collagen I and III, and fibronectin with fragments of collagen IV, which is usually part of the basement membrane that supports the tubular epithelium and the endothelial cells (Haverty et al., 1988; Eddy, 1996). It appears that TIF follows an initial tubular injury, inflammation (associated with lymphocytes and macrophage infiltration), and potentially, endothelial injury (Goligorsky, 2015; Lipphardt et al., 2017). In turn, TIF may contribute further to the injury of the tubule epithelial cells and can lead to tubular atrophy, which is irreversible (Farris and Alpers, 2014). In contrast to the glomerulus, where a direct injury to the mesangial cells can trigger glomerulosclerosis, it appears that TIF is initiated by an initial injury to the tubule epithelial and/or endothelial cells, which then leads to the abnormal response of local fibroblasts and pericytes (Djudjaj and Boor, 2019).

Diabetic nephropathy is characterised by three stages; glomerular hypertrophy with hyperfiltration; inflammation in glomeruli and tubulointerstitial cells; apoptosis (cell death) and ECM accumulation in GMBs (Makino et al., 1993; Wada and Makino, 2013). ECM proteins, such as PAI-1 and collagen I, III & IV are as markers for progression of renal fibrosis in DN in tissue biopsies and urine. A

proteomics study, for example, has demonstrated a significant reduction of collagen Iα1 and collagen IIIα1 fragments in urine from patients with type 2 diabetes, which is attributed to the reduced activity of MMPs (e.g. MMP-2, -3, and -9) (Maahs et al., 2010). Although plasma PAI-1 level is produced in trace amounts in healthy kidneys, increased expression of PAI-1, is associated with the accumulation of ECM, and thus with the manifestation of TIF, in various kidney diseases including DN, CKD and ARF (Lottermoser et al., 2001; Nicholas et al., 2005; Revelo et al., 2005; Malgorzewicz et al., 2013).

4.4.1 TGF-β1 secretion and Smad3 signalling pathway activation in response to hyperglycaemia

TGF-β1 is a powerful fibrokine which induces the production of inflammatory chemokines and cytokines (e.g. MCP-1 and IL-6), the synthesis of ECM (e.g. collagen I, III, IV, fibronectin, proteoglycans and laminin), and EMT (Phanish et al., 2006; Loboda et al., 2016). TGF-β1 is a key mediator of glomerulosclerosis and TIF in diabetes. It has been demonstrated for example, that neutralising anti-TGF-β antibodies reduces ECM mRNAs and decreases the mesangial matrix in diabetic db/db mice (Ziyadeh et al., 2000).

However, TGF-β1 has also an anti-inflammatory effect, as TGF-β1 knockout mice display a multifocal inflammatory disease in multiple tissues, with the lungs and heart being the most affected (Kulkarni et al., 1995). These pleiotropic effects are related to the balance of activation and inhibition of signalling pathways orchestrated by TGF-β1. For example, TGF-β1 can inhibit fibrosis by upregulating the expression of IkBa (an inhibitor of NF-kB) or of Smad7 (an inhibitor of the

regulatory Smads1, 2, 3, 5, and 8). It has been demonstrated, that TGF-β1 triggers renal fibrosis via the activation of the Smad2/3 signalling pathways, in particular via Smad3, suggesting that this pathway plays a major role in the TGF-β1-induced fibrosis in DN (Lan, 2012). Experiments with human PTEC have demonstrated that the activation of Smad3 in response to TGF-β1 is a key factor in EMT, whereas activation of the Smad2 pathway is involved in the up-regulation of MMP-2 (Phanish et al., 2006). Fujimoto et al. (2003) have shown that Smad3 activation mediates renal fibrosis in a model of diabetes in Smad2 and Smad3 knock-out rodents.

Several studies have reported observations on the expression of TGF-β1 and the activation of Smad3 pathway in HK-2 cells exposed to hyperglycaemia. TGF-β1 mRNA has been shown to be significantly increased in HK-2 cells exposed to 35mM D-glucose for 24h, as compared to the control (5.5mM D-glucose) (Koszegi et al., 2019). Hsieh et al. (2012) have demonstrated that exposure of HK-2 cells to 27.5mM D-glucose for 48h significantly increased the levels of TGF-β1 in the medium, alongside the increased activation of pSmad2/3 and the significant reduction of Smad7 protein levels. Similar effects on TGF-β1 and pSmad2 activation have been observed by Wong et al. (2011) after the exposure of HK-2 cells to 30mM D-glucose for 72h. pSmad2/3 levels were also significantly increased in HK-2 cells exposed to 60mM D-glucose for 48h (Zhang et al., 2019). However, apart from Koszegi et al. (2019) who have demonstrated that after 24h the osmotic control mannitol had no effect on the TGF-β1 mRNA levels, none of the other studies reported on the effect of an osmotic control. In addition, most have detected the combined activation of Smad2/3, rather than Smad3 specifically.

In contrast, the present study evaluated the levels of TGF-β1 and the activation of Smad3 in response to hyperglycaemia or the osmotic control 5mM D-glucoe+25mM L-glucose at 24h, 48h and 72h. The results demonstrated the significant effect of 30 mM D-glucose at 72h and of the osmotic control at 24h on the expression of TGF-β1. These effects were mirrored to a certain extent by the significant activation of Smad3 at 24h, 48h and 72h in response to 30mM D-glucose, and by the osmotic control at 48h and 72h. The Smad3 activation data suggest that osmotic, rather than metabolic factors, may be key in the activation of Smad3.

Interestingly, the baseline levels of TGF-β1 increased 10 fold at 72h, as compared to 24h and 48h. Based on unpublished data from our group, which demonstrate steady protein levels of αSMA in cells exposed to serum-free medium for up to 72h, it is unlikely that the TGF-β1 increase observed in this study is a result of the changing of epithelial to mesenchymal phenotype of HK-2 cells. This TGF-β1 elevation could be triggered by the increasing confluence of the HK-2 cells in the *in vitro* model of hyperglycaemia. Although the HK-2 cells reach 100% confluence after 24h in serum-free medium, they do not become quiescent in response contact inhibition. Previous experiments from our research group have demonstrated that 100% confluent HK-2 cell monolayers continue to proliferate but at lower rate in serum-free medium (doubling time of around 35h) in the presence of 5 mM D-glucose (data not shown). TGF-β1 is a powerful inhibitor of proliferation in epithelial cells and this effect is mediated by the activation of Smad3 (Zhang et al., 2017). Thus, the baseline increase of TGF-β1 at 72h may represent an adaptation mechanism to suppress proliferation and prevent the over-confluence of the cell monolayer. This is supported by results

from this study, where the highest concentration of TGF-β1 and the highest activation of Smad3 were observed in cells exposed to 30mM D-glucose, which also correlated with the lowest cell viability and migration.

4.4.2 Markers of ECM accumulation (PAI-1, Collagen I, MMP-9 and TIMP-1) in response to hyperglycaemia

The increased accumulation of ECM in renal fibrosis can be due either to increased synthesis or to decreased ECM degradation. Blood glucose fluctuation experiments in a mouse model have demonstrated that hyperglycaemia increased the expression and decreased the degradation of collagen I in the kidney, which was mediated via TGF-β/Smad and the extracellular signal-regulated kinase/mitogen-activated protein kinase (ERK/MAPK) pathways (Cheng et al., 2013). In that study, the collagen I deposition correlated with increased TIMP-1 expression and reduced MMP-1 synthesis. Cultured renal fibroblasts exposed to 25mM glucose for up to 72h responded with an increase in collagen I synthesis through the activation of TGF-β induced signalling pathways (Han et al., 1999). Evidence of the effect of hyperglycaemia on the expression of collagen I in HK-2 cells is limited to one report, where 30mM glucose significantly increased protein collagen I expression via Smad2 and Smad3 activation after 48h of exposure (Tang et al., 2015). Other studies have demonstrated that a 24h exposure of HK-2 cells to 30mM glucose had no effect on the protein expression of collagen IV (Usha Panchapakesan et al., 2005). However, longer exposure (72h) of HK-2 cells to 30 mM D-glucose induced a

significant increase in collagen IV (Wong et al., 2011). In both studies, the collagen IV upregulation was TGF-β/Smad-dependent.

Based on these findings and the activation of Smad3 discussed above, it was expected that in the present study hyperglycaemia will induce the mRNA expression of collagen I. However, no such effect was observed.

An accumulation of collagen I could be due to the inhibition of collagen I proteolysis, which is also mediated by PAI-1 and TIMPs. PAI-1 is produced in trace amounts in healthy kidneys, and increased expression of PAI-1 is associated with the accumulation of ECM in DN (Lottermoser et al., 2001; Nicholas et al., 2005; Revelo et al., 2005; Malgorzewicz et al., 2013). In rodent models, diabetes is associated with the upregulation of fibrosis markers including PAI-1, collagen I, III and IV, and fibronectin (Jeong et al., 2016; Li et al., 2018). Interestingly, PAI-1 inhibitors reduce the expression of collagen I, fibronectin, TGF-β and PAI-1 mRNA in cultured kidney tubule epithelial cells, suggesting that PAI-1 might induce the accumulation of ECM by increasing the mRNA expression of ECM components (Jeong et al., 2016). It has been demonstrated that the protein expression of PAI-1 is upregulated by TGF-β1 in HK-2 via Smad2/3 activation (Li et al., 2018). However, there is no evidence in the literature about the effect of hyperglycaemia on the expression of PAI-1 mRNA in HK-2 cells.

Based on the established link between hyperglycaemia and the activation of Smad3, in the present study it was hypothesised that hyperglycaemia will increase the mRNA and protein expression of PAI-1. However, similar to the mRNA levels of collagen I, hyperglycaemia had no effect on PAI-1 mRNA expression. Furthermore, unpublished results by our group confirm this

observation by demonstrating that the protein expression of collagen I and PAI-1 in HK-2 lysates is not affected by hyperglycaemia (Appendix 3).

Evidence has linked the progression of renal disease in patients with diabetic nephropathy with the increased expression or increased enzymatic activity of MMPs (Xu et al., 2014). The upregulation of MMPs, particularly of MMP-2 and MMP-9, appears to contribute to the progression of kidney fibrosis by inducing EMT (Zhao et al., 2013a). MMP-2 and MMP-9 disrupt the integrity of the tubule cell membrane, by cleaving laminin and collagen IV, the main components of the tubule basement membrane. Transformed mesenchymal cells then invade the interstitium and induce the deposition of ECM (Liu, 2004; Zhao et al., 2013). Peng et al. (2012) reported an increase in the protein ratio of MMP-9/TIMP-1 in HK-2 cells exposed to 30mM glucose for 48h through the overexpression of integrin-linked kinase (ILK), a downstream factor of TGF-β1. In contrast, in primary cultured rat renal tubule cells, a treatment with 30mM glucose for 24h did not increase the gelatinase activity of MMP-9 despite an increase of TGF-β1 protein levels (Chen et al., 2017). The results of the current study demonstrate that, although Smad3 was activated, the mRNA levels of TIMP-1 and MMP-9 were not affected by hyperglycaemia. In agreement with Chen et al. (2017), unpublished data from our group show that hyperglycaemia has no effect on the gelatinase activity of MMP-9 in media from HK-2 cells (Appendix 4).

4.4.3 Biomarkers of inflammation and PTC injury: IL-6, MCP-1, KIM-1 and endostatin

Animal and human studies indicate that the proinflammatory IL-6 correlates with the progression of DN (Navarro-Gonzalez and Mora-Fernandez, 2008; Feigerlová and Battaglia-Hsu, 2017; Senthilkumar et al., 2018). For example, a study involving 25 patients with DN and 30 control subjects reported a higher serum IL-6 level in patients with DN than in the controls (Taslıpınar et al., 2011). An *in vitro* study with primary human renal proximal tubule epithelial cells has shown that after 48h of exposure, 30mM D-glucose significantly increases the expression of IL-6 and TGF-β, through the activation of mitogen-activated protein kinase (MAPK) and protein kinase C (PKC) signalling pathways (Tang et al., 2009). Similar significant increases of IL-6 was observed in media from HK-2 cells exposed for 48h to 30mM glucose (Chen et al., 2018). Although Tang et al. (2009) included 30mM mannitol as an osmotic control to demonstrate its effect on the IL-6 mRNA levels, neither Tang et al. (2009) nor Chen et al. (2018), have reported on the effect of an osmotic control on IL-6 protein levels in cell supernatants.

The current study demonstrated that in HK-2 cells, both 30mM D-glucose and the osmotic control (5mM D-glucose+25mM L-glucose) significantly increased IL-6 in media after 24h, as compared to the control and 25mM D-glucose. In contrast to the results of Tang et al (2009) and Chen et al. (2018), after 48h and 72h IL-6 returned to control levels, whereas the osmotic control maintained its significantly raised levels at 48h and 72h. Such an osmotic effect of L-glucose on IL-6 levels in human PTC has not been reported previously and suggests that osmolarity may play a role in the induction of local and systemic inflammation in DN.

MCP-1 is a key chemokine, which recruits monocytes/macrophages to the renal tubulointerstitium (Morii et al., 2003; Tam et al., 2009). Upon activation, these immune cells secrete proinflammatory cytokines such as IL-1, IL-6 and IL-8, which leads to local inflammation, tubular atrophy and interstitial fibrosis (Wei et al., 2015). The expression of the MCP-1 is under the transcription regulation of NF-κB, which is activated by reactive oxygen species (Okamura and Himmelfarb, 2009). Hyperglycaemia also induces oxidative stress via mitochondrial dysfunction (Vanessa Fiorentino et al., 2013). As the mitochondrial function results in the current study indicated that hyperglycaemia and the osmotic control caused significant increase of the mitochondrial proton leak, it was expected that MCP-1 levels in media from cells exposed to hyperglycaemia will be significantly elevated. Interestingly, after 24h of exposure, the effect of hyperglycaemia on MCP-1 levels in media from HK-2 cells was similar to that for IL-6: 30mM D-glucose significantly increased MCP-1 as compared to the control and 25mM D-glucose. This result contradicts observations made by Panchapakesan et al. (2004), who demonstrated that a 24h exposure to 30mM D-glucose significantly reduced the MCP-1 levels in supernatants from HK-2 cells (Panchapakesan et al., 2004). This contradiction can be explained by the different kits used to determine the concentration of MCP-1 (e.g. ELISA vs Luminex in the current study), and the higher number of experimental repeats in the current study (n=3 vs. n=6). The osmotic controls (5mM D-glucose + 25mM L-glucose) in both studies had no significant effect on MCP-1 levels.

In the current study, hyperglycaemia (25mM D-glucose, 30mM D-glucose, and osmotic control) had no effect on the expression of MCP-1 at 48h and 72h. The

return of MCP-1 to control levels following a 24h exposure to 30mM glucose, suggests an adaptation to the increased levels of ROS.

KIM-1 (kidney injury molecule-1) is an apoptotic-cell phagocytosis and scavenger receptor, which is markedly upregulated in PTC by kidney injury, and injury can lead to tubule epithelial cell apoptosis (Han et al., 2002). KIM-1 recognises phosphatidylserine epitopes on the surface of apoptotic cells and transforms the PTC into semi-professional phagocytes by mediating phagocytosis and the clearance of luminal apoptotic cells in nephrotoxic and ischaemic acute tubular injury (Brooks and Bonventre, 2015). The levels of urinary KIM-1 may be indicative of the activity of particular kidney metalloproteinases. For example, it has been demonstrated that an increase of urinary KIM-1 correlates with its cleavage from the PTC membranes by MMPs (Guo et al., 2012; Lim et al., 2012).

There are conflicting data in the literature on the value of KIM-1 as a prognostic marker in diabetic nephropathy: a study on 15 patients with type 2 diabetes and diabetic nephropathy has shown a strong correlation with KIM-1 urinary concentrations (Ahmed and Hamed, 2015). In contrast, another study with 1,573 patients with type 1 diabetes and diabetic nephropathy has shown no prognostic benefits of KIM-1 in terms of the progression of CKD (Panduru et al., 2015). However, *in vitro* experiments have demonstrated that hyperglycaemia affects the mRNA and protein expression of KIM-1 in proximal tubule cells. For example, Gou et al. (2016) have shown that 30mM glucose significantly increases the mRNA and protein levels of KIM-1 in HK-2 cells from 8h on up to 24h, as compared to a normal glucose control (5.5mM D-glucose) and an osmotic control (5.6mM D-glucose +24.4mM mannitol) (Gou et al., 2016). However, no controls

for each time point were presented, and the authors did not state clearly exactly which time point the two controls represent.

The present study demonstrated that 30mM D-glucose and the osmotic control significantly increased the level of soluble KIM-1 in HK-2 cells after 24h as compared to the control and 25mM D-glucose. At 48h and 72h the KIM-1 level dropped to the level of the control, suggesting adaptation to hyperglycaemia.

Endostatin is a C-terminal fragment of type XVIII collagen, a component of the extracellular matrix, located in the basement membrane of the kidney. It is a potent inhibitor of angiogenesis which may be involved in the rarefaction of renal microvasculature (Futrakul and Futrakul, 2017). Endostatin inhibits tubule formation and endothelial cell proliferation and migration, and the upregulation of endostatin is associated with renal injury (Bellini et al., 2007; Cichy et al., 2009). MMP-9 cleaves and releases endostatin in the renal tissue, and a high expression of both endostatin and MMP-9 is detected in the ischaemic and reperfused mouse kidney (Bellini et al., 2007; Cichy et al., 2009).

Most studies on the effects of diabetes focus on the circulating levels of endostatin and their correlation with cardiovascular complications. Although it has been shown that endostatin is significantly increased in the renal cortex of mice with streptozotocin-induced diabetes (Ichinose et al., 2005), there is no evidence about the effect of hyperglycaemia on the release of endostatin in proximal tubule cells, and whether this may have an effect on the rarefaction of the renal microvasculature.

The present study shows that 30mM D-glucose and the osmotic control significantly increase the expression of endostatin in HK-2 cells compared to the control and 25mM D-glucose at 24h, suggesting that hyperglycaemia may inhibit

the angiogenesis of the peritubular capillaries. However, similar to the effect of hyperglycaemia on KIM-1, MCP-1 and IL-6, this effect was transient and the endostatin levels returned to those produced by cells exposed to control and 25mM D-glucose at 48h and remained there at 72h.

In the present study, specific changes in the basal levels of IL-6, MCP-1, KIM-1 and endostatin were observed over 72h. For example, the concentration of IL-6 increased slightly over 72h; the levels of MCP-1 rose at 72h, the secretion of KIM-1 steadily increased with time, and the levels of endostatin peaked at 48h and then dropped again at 72h above the respective 24h level. As these 4 parameters were measured simultaneously by Luminex technology in each sample, their different basal level patterns over 72h appear to suggest a specific reaction to the increasing stress caused by the rising confluence of the cell monolayer, rather than being a reflection of a changing HK-2 cell phenotype.

4.5 Conclusions

Markers of renal proximal tubular injury were evaluated in response to hyperglycaemia up to 72h. The present study demonstrated for the first time that osmolarity can cause the activation of phosphorylated Smad3. Although TGF-β1 was upregulated and P-Smad3 was activated by hyperglycaemia/osmolarity, they had no effect on mRNA expression of ECM components, or their protein levels up to 72h. In contrast, the increase of kidney injury and inflammation markers (e.g. IL-6, KIM-1 and endostatin) appear to be in response to the osmotic effect of hyperglycaemia.

These results suggest that by including P-Smad3, IL-6, KIM-1 and endostatin, osmolarity may play an important role in renal proximal tubular injury in DN.

In summary, in relation to the overarching aim of this study, the results in this chapter demonstrate that the metabolic and osmotic features of hyperglycaemia have differential effects on the extracellular levels of TGF-β1, markers of inflammation and proximal epithelial injury in HK-2 cells. The evidence demonstrates that the osmotic component of hyperglycaemia leads to the activation of Smad3 and increases the expression of IL-6, KIM-1 and endostatin. In contrast, the metabolic effect of hyperglycaemia induces the expression of TGF-β1.

Chapter 5: Regulation of fibrosis-related microRNAs by hyperglycaemia

5.1 Introduction

The mechanisms of renal fibrosis in diabetic nephropathy are poorly understood and the existing therapies for prevention of DN are only moderately effective. Currently, the main treatment approach is through the control of hyperglycaemia. However, targeted therapies aimed at the inhibition or reversal of renal fibrosis, in particular TIF, are almost non-existent (Nogueira et al., 2017).

It has been shown that diabetes dysregulates the expression of a number of miRNAs, and these are becoming new potential treatment targets for kidney fibrosis in DN (Slyne et al., 2015; Baker et al., 2017). Emerging evidence indicates the involvement of miRNAs in the regulation of key pathological mechanisms triggered by diabetes and hyperglycaemia. For example, several miRNAs affect the expression of the protein deacetylase Sirtuin-1, which is involved in protection against oxidative stress, apoptosis and inflammation in DN (Yang et al., 2019; Wang et al., 2019). A number of miRNAs are involved in the regulation of EMT in animal and *in vitro* models of DN. For example, miRNA 133b and 199b attenuate TGF-β1-induced EMT and renal fibrosis in DN by regulating the expression of Sirtuin-1 (Sun et al., 2018). Furthermore, miRNAs 188-5p, 302a-3p, 23a, 23b, 29, and 30c have also been implicated in EMT in DN (Zhou et al., 2015; Liu et al., 2016; Zhao et al., 2017; Tang et al., 2018; Xu et al., 2018; Xue et al., 2018). Studies on the role of miRNAs in renal fibrosis have demonstrated the involvement of miRNA 21, 23a, 29a, 192 and 455-3p in *in vivo*

or *in vitro* models of DN (Du et al., 2010; Krupa et al., 2010; McClelland et al., 2015; Wu et al., 2018; Xu et al., 2018).

Most of the research has been focused on the regulation and effect of individual miRNAs on renal fibrosis in response to hyperglycaemia.

In contrast, the aim of the present study was to investigate the metabolic and osmotic effects of hyperglycaemia on the miRNA expression of a panel of fibrosis-related miRNAs in human proximal tubule (HK-2) cells over 72h, and to identify potential diagnostic and treatment targets for DN.

5.2 Methods

5.2.1 Cell culture

HK-2 cells were maintained as described in section 2.1. The cells were exposed to different concentrations of glucose (5mM, 25mM or 30 mM D-glucose) or osmotic control (5 mM D+ 25 mM L-glucose) for 24h, 48h and 72h prior to total RNA isolation.

5.2.2 Total RNA isolation and purification

Total RNA was isolated as described in section 2.12.1.1. QIAzol lysis regent (Qiagen; #55709615) was used to generate cell lysates according to the manufacturer's recommendations. The lysates were then stored at – 80 °C prior to further analysis.

Total RNA was isolated and purified using a miRNeasy Mini Kit (Qiagen; #217004) as described in section 2.12.1.1. The RNA concentration was measured using a Nanodrop (Thermo Fisher Scientific, USA, 02611). The RNA samples were then stored at – 80 °C prior to further analysis.

5.2.3 Reverse transcriptase PCR and quantitative miRNA PCR arrays

A miScript II RT Kit (Qiagen; #218160) was used to convert total RNA to cDNA, according to the manufacturer's recommendations as described in section 2.13.1.

A miScript SYBR green PCR kit (Qiagen; # 218073) was used to measure the expression of fibrosis-related miRNA using miScript miRNA PCR Array Human

Fibrosis (Qiagen, #MIHS-117Z), according to the manufacturer's recommendations as described in section 2.13.2.

5.2.4 Quantitative real-time PCR

As described in section 2.13.3, a miScript SYBR green PCR kit from Qiagen (# 218073) was used to measure the expression of the target miRNA (miR-216) and the normalisation control snoRNA/snRNA (SNORD95) by qPCR, according to the manufacturer's recommendations.

5.2.5 Reporter plasmid-cloning of the 3'UTR of the TGF-β receptor 2 (TGFBR2)

Cloning of the 3'UTR of TGFBR2 from total RNA isolated from HK-2 cells was attempted, as described in section 2.13.4. The TGFBR2 3' UTR was cloned in the pDONR 221 vector. Fifty µl of competent *E.Coli DH5α* (#1608535, Invitrogen) were transformed with 1 µl of the reaction sample to identify putative reporter plasmids for the TGFBR2 as described in section 2.13.4.

5.2.6 Statistical analysis

Graph Pad Prism 5 software and IBM SPSS statistics version 25 software were used to analyse the data. A one-way ANOVA was used to compare the treatment groups. Tukey's HSD post-hoc test was carried out when significant p-values (*$p \leq 0.05$) were detected.

5.3 Results

5.3.1 miRNA PCR arrays

A human fibrosis miRNA PCR array was used to profile the expression of 84 fibrosis-related miRNAs (listed in Appendix 5) in HK-2 cells exposed to different concentrations of glucose: control (5mM D-glucose), hyperglycaemia (25mM D-glucose and 30mM D-glucose) and osmotic control (5mM D-glucose+25mM L-glucose) at 24h, 48h and 72h.

Sixteen miRNAs were dysregulated over the 72h of glucose exposure, and these miRNAs belonged to the following 7 groups:

1) **Pro-fibrotic:** miR-199b-5p, miR-215, miR-216a-5p, miR-382-5p, miR-5692a, miR-5011-5p;

2) **Anti-fibrotic:** miR-204-5p, miR-211-5p, miR-449b-5p;

3) **Extracellular matrix remodelling & cell adhesion:** miR-199a-5p, miR-199b-5p, miR-204-5p, miR-451a;

4) **Inflammation:** miR-204-5p, miR-122-5p, miR-199a-5p;

5) **Angiogenesis:** miR-372, miR-150-5p;

6) **Signal transduction & transcriptional regulation:** miR-122-5p, miR-204-5p, miR-372, miR-451a, miR-223-3p and

7) **Epithelial-to-mesenchymal transition:** miR-199a-5p, miR-199b-5p, miR-215, miR-382-5p, miR-325.

As compared to the control at 24h, one miRNA (miR-451a) was upregulated by both 30mM D glucose and the osmotic control, whereas 3 miRNAs (miR-199b-

5p, miR-325 and miR-5011-5p) were upregulated by the osmotic control alone, (Figure 5.1A). Three miRNAs (miR-150-5p, miR-211-5p, miR-5011-5p) were downregulated by 25mM D-glucose alone, miR-122-5p and miR-382-5p were downregulated by both 25mM and 30mM D-glucose, miR-215-5p was downregulated by 25mM D-glucose and the osmotic control, and miR-216a-5p was downregulated by 30mM D-glucose alone (Figure 5.1B).

As compared to the control at 48h, one miRNA (miR-216a-5p) was upregulated by 25mM D-glucose alone, whereas miR-150-5p was upregulated by 25mM D-glucose, 30mM D-glucose and the osmotic control (Figure 5. 1C). One miRNA (miR-204-5p) was downregulated by both 25mM D-glucose and the osmotic control, miR-211-5p was downregulated by 30mM D-glucose and the osmotic control, and two miRNAs, miR-199a-5p and miR-449b-5p, were downregulated by the osmotic control alone (Figure 5. 1D).

As compared to the control at 72h, two miRNAs (miR-204-5p and miR-372-3p) were upregulated by 25mM D-glucose alone. miR-5692a was upregulated by 25mM D-glucose and 30mM D-glucose, miR-150-5p and miR-223-3p were upregulated by both 25mM D-glucose and the osmotic control (Figure 5. 1E). In contrast, miR-122-5p was downregulated by both 25 and 30 mM D-glucose, miR-216a-5p was downregulated by 30mM D-glucose and the osmotic control, and miR-211-5p was downregulated by both 25mM D-glucose and osmotic control (Figure 5. 1F).

The list of upregulated and downregulated miRNAs at 24h, 48h and 72h and the fold-change of expression are shown in Tables 5.1A, B and C respectively.
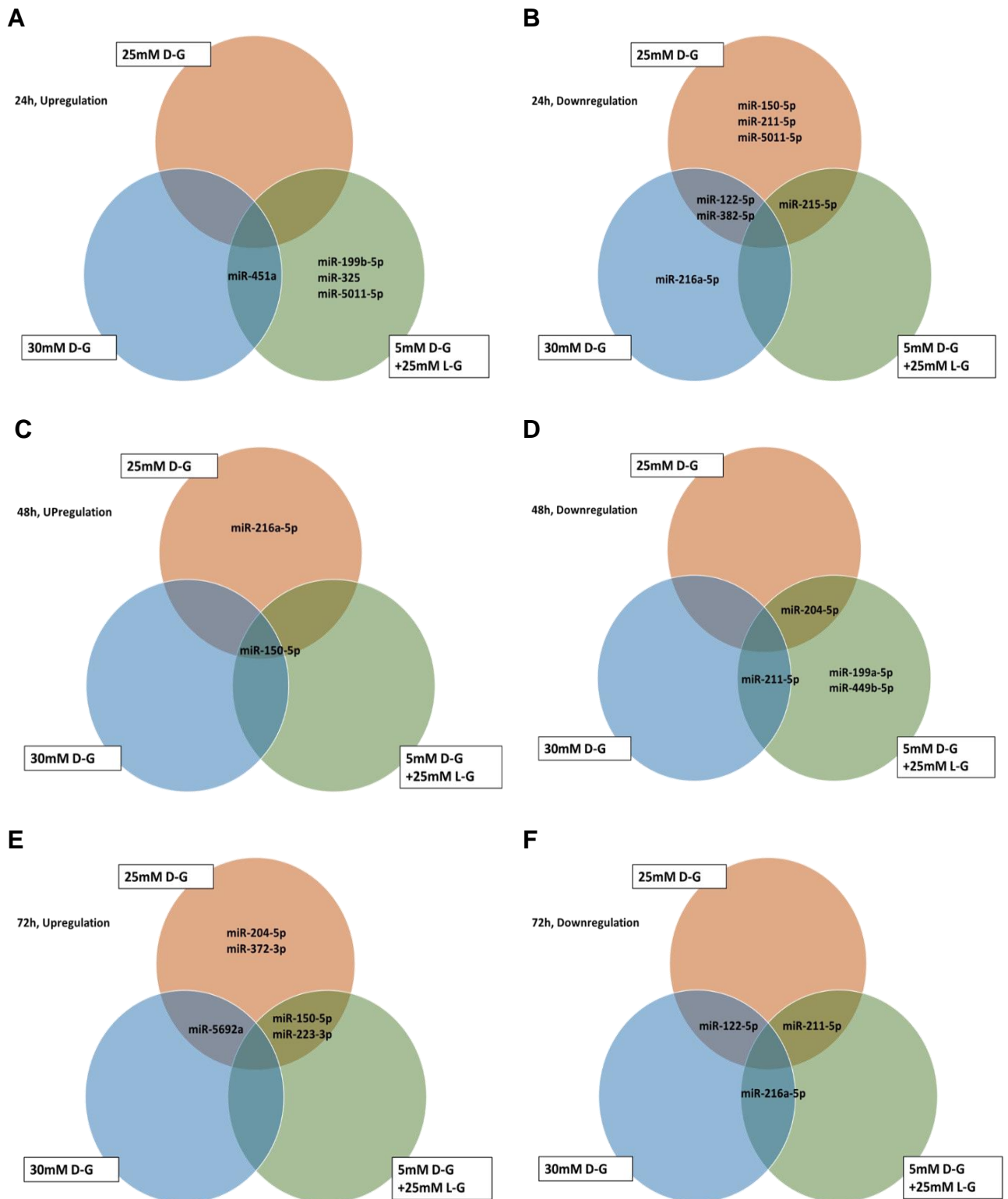
Figure 5. 1. Upregulated and downregulated fibrosis-related miRNAs in HK-2 cells exposed to different glucose concentrations. The expression of 84 fibrosis-related miRNAs was analysed in HK-2 cells exposed to control (5mM D-glucose), hyperglycaemia (25mM D-glucose and 30mM D-glucose) or osmotic control (5mM D-glucose+25mM L-glucose) for 24h, 48h and 72h. **A)** miRNAs upregulated at 24h; **B)** miRNAs downregulated at 24h; **C)** miRNAs upregulated at 48h; **D)** miRNAs downregulated at 48h; **E)** miRNAs upregulated at 72h; **F)** miRNAs downregulated at 72h. Only miRNAs upregulated or downregulated at least two-fold in comparison to the respective miRNA levels in control cell were considered to be significantly dysregulated.

Table 5. 1. Fold-change of significantly upregulated or downregulated miRNAs in HK-2 cells exposed to different concentrations of glucose.

miRNAs upregulated or downregulated by two-fold or more in response to the control (5mM D-glucose), hyperglycaemia (25mM D-glucose and 30mM D-glucose) or osmotic control (5mM D-glucose+25mM L-glucose) for 24h, 48h and 72h. **A)** miRNAs vs control at 24h; **B)** miRNAs vs control at 48h; **C)** miRNAs vs control at 72h.

A

miRNA at 24h	miRNA Upregulation			miRNA Downregulation		
	25mM D-G	30mM D-G	5mM D-G+25mM L-G	25mM D-G	30mM D-G	5mM D-G+25mM L-G
hsa-miR-122-5p	-	-	-	-7.5182	-2.5585	-
hsa-miR-150-5p	-	-	-	-2.482	-	-
hsa-miR-199b-5p	-	-	2.1987	-	-	-
hsa-miR-211-5p	-	-	-	-2.0519	-	-
hsa-miR-215-5p	-	-	-	-2.898	-	-2.1556
hsa-miR-216a-5p	-	-	-	-	-3.1349	-
hsa-miR-325	-	-	3.1188	-	-	-
hsa-miR-382-5p	-	-	-	-2.2454	-2.88	-
hsa-miR-451a	-	2.5586	3.2519	-	-	-
hsa-miR-5011-5p	-	-	4.3416	-2.0302	-	-

B

miRNA at 48h	miRNA Upregulation			miRNA Downregulation		
	25mM D-G	30mM D-G	5mM D-G+25mM L-G	25mM D-G	30mM D-G	5mM D-G+25mM L-G
hsa-miR-150-5p	3.6208	2.4343	2.6528	-	-	-
hsa-miR-199a-5p	-	-	-	-	-	-2.2978
hsa-miR-204-5p	-	-	-	-2.1477	-	-2.2577
hsa-miR-211-5p	-	-	-	-	-2.737	-2.9677
hsa-miR-216a-5p	2.1258	-	-	-	-	-
hsa-miR-449b-5p	-	-	-	-	-	-2.0321

C

miRNA at 72h	miRNA Upregulation			miRNA Downregulation		
	25mM D-G	30mM D-G	5mM D-G+25mM L-G	25mM D-G	30mM D-G	5mM D-G+25mM L-G
hsa-miR-122-5p	-	-	-	-2.2255	-2.219	-
hsa-miR-150-5p	3.6333	-	2.2287	-	-	-
hsa-miR-204-5p	2.0774	-	-	-	-	-
hsa-miR-211-5p	-	-	-	-2.0479	-	-3.0254
hsa-miR-216a-5p	-	-	-	-	-2.4451	-2.2239
hsa-miR-223-3p	2.793	-	2.8972	-	-	-
hsa-miR-372-3p	2.6881	-	-	-	-	-
hsa-miR-5692a	2.7642	2.169	-	-	-	-

5.3.2 miR-216a-5p expression

Amongst all the upregulated and downregulated miRNAs, miR-216a-5p was selected for a more detailed investigation as TGFR2 appears to be a relevant potential target regulated by miR-216a-5p.

Although miR-216a-5p was upregulated by 25mM at 48h (fold change 2.13), it was downregulated by 30mM D-glucose at 24h (fold change -3.14), and by 30mM D-glucose and the osmotic control at 72h (fold change -2.45 and -2.22, respectively). To confirm the expression pattern obtained from the human fibrosis miRNA PCR Array, the relative levels of miR-216a-5p in HK-2 cells exposed to different concentrations of glucose for 24h, 48h or 72h were evaluated using qPCR.

The results demonstrated that hyperglycaemia had no effect on the miR-216a-5p expression compared to control at 24h (Figure 5.2A). The expression of miR-216a-5p was significantly decreased by 30mM D-glucose at 48h, while the 25mM D-glucose and osmotic control had no effect as compared to the control (Figure 5.2B). At 72h, the expression of miR-216a-5p was significantly decreased by 30mM D-glucose, and moderately decreased by 25mM D-glucose as compared to the control and the osmotic control (Figure 5.2C).
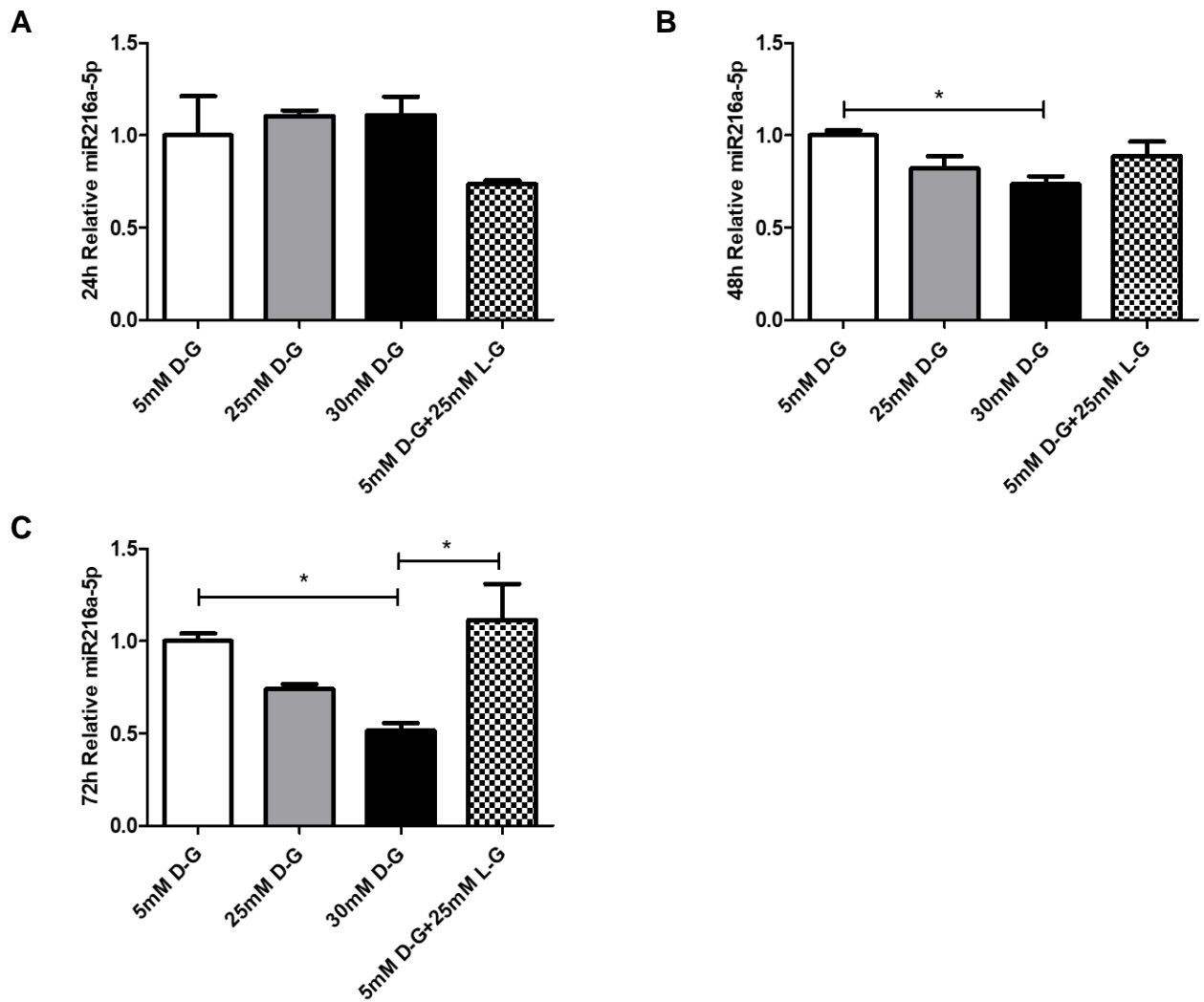
Figure 5. 2. miR-216a-5p expression in HK-2 cells exposed to different concentrations of glucose.

HK-2 cells were exposed to 5mM D-glucose, 25mM D-glucose, 30mM D-glucose, or osmotic control (5mM D-glucose+25mM L-glucose) for 24h, 48h and 72h. **A)** miR-216a-5p expression at 24h; **B)** miR-216a-5p expression at 48h; **C)** miR-216a-5p expression at 72h. The results were normalised to snoRNA/snRNA (SNORD95) expression and presented relative to the miR-216a-5p levels in control cells. Data are expressed as Mean±SEM (n=3). One-way ANOVA was used to compare the treatment groups. Tukey's HSD post-hoc test was carried out when significant p-values (*p≤0.05) were detected.

5.4 Discussion

The expression of miRNAs is tightly controlled, as they regulate the protein expression of most human protein-coding genes through RNA interference (Pratt and MacRae, 2009; Peter Boor et al., 2010). miRNAs appear to play a key role in the progression of DN and in particular in the development of fibrosis (Slyne et al., 2015). For example, reduced renal fibrosis is observed in miRNA-21 and miRNA-214 knock-out rodent models of kidney disease (Denby and Baker, 2016). Furthermore, a decrease in serum miRNA-130b correlates with TIF in patients with diabetic nephropathy (Bai et al., 2016).

Evidence from animal and *in vitro* models of DN and hyperglycaemia demonstrates that TGF-β1 is involved in the regulation of fibrosis-related miRNAs. According to Kato et al. (2007), TGF-β1 upregulates the expression of miR-192 and downregulates the Smad-interacting protein 1 (SIP1) in mouse renal glomerular mesangial cells, which in turn induces the expression of collagen. Furthermore, miR-21 is upregulated by TGF-β1 in diabetic kidneys from db/db mice, and in diabetic rat mesangial and tubule epithelial cells. miR-21 downregulates the expression of the inhibitory Smad7 and allows the activation of TGF-β/Smad3 signalling pathway, and thus the promotion of fibrosis (increase in fibrotic markers, such as collagen I, collagen IV and fibronectin) and inflammation (IL-1β, MCP-1) in diabetic kidney injury (Zhong et al., 2013; Lin et al., 2014).

miR-29 is also involved in TGF-β1-induced fibrosis. For example, the expression of miR-29a was downregulated in HK-2 cells by both hyperglycaemia and TGF-β1, resulting in the increased expression of collagen IV (Du et al., 2010). Similar

results were observed in rat tubule epithelial cells, where TGF-β1-dependent downregulation of miR-29 upregulated collagen I and III gene expression via Smad3 (Qin et al., 2011).

In the current study, from the 16 miRNAs which were up- or down-regulated, the pro-fibrotic miR216a-5p was selected for further analysis.

In the human genome, miR-216a is located on chromosome 2 in the second intron of the non-coding RNA RP23 (Kato et al., 2009) and has been associated with tumour suppression in a number of malignancies, including renal and breast cancers. Two reports from the same research group provide evidence for the role of miR-216a in glomerular fibrosis: TGF-β1 upregulates miR216a and miR217, which inhibit the expression of the phosphatase and tensin homologue (PTEN) in mouse mesangial cells (Kato et al., 2009). This then leads to a TGF-β1 mediated activation of Akt, which induces classical features of DN e.g. ECM gene expression, hypertrophy and cell survival. miR-216a also downregulates the transcription factor Y box binding protein 1 (Ybx1), which leads to Col1a2 expression and may promote glomerulosclerosis in DN (Kato et al., 2010). Based on the study by Mahimainathan et al. (2006), where rat mesangial cells exposed for 48h to 25mM glucose demonstrated hypertrophy through the downregulation of PTEN, Kato et al. (2009) speculated that hyperglycaemia will also upregulate miR-216a.

To date, there is no evidence of the effect of hyperglycaemia on the expression of miR-216a in human proximal tubule cells. The current study demonstrated by qPCR that miR-216a-5p was downregulated by 30mM D-glucose at 48h and 72h

in HK-2 cells. These data contradict the findings of Kato et al. (2009). However, there are several differences between these studies:

i) Kato et al. (2009) and Mahimainathan et al. (2006) used primary mouse mesangial or rat cells, respectively vs. the immortalised human proximal epithelial cell line used in this work;

ii) Mahimainathan et al. (2006) used 25mM glucose only, and 5mM glucose+20mM mannitol as an osmotic control vs. 5mM glucose+20mM L-glucose used in the current study;

iii) Neither Kato et al. (2009) nor Mahimainathan et al. (2006), directly demonstrated the effect of hyperglycaemia on the expression of miR-216a;

iv) Kato et al. (2009 and 2010) studied the expression of miR-216a in response to TGF-β1 treatment. However, they did not specifiy which miR-216a hairpin product, miR216a-3p or miR216-5p, mediated the observed effects. In contrast, the present study has specifically identified that miR216-5p was downregulated by hyperglycaemia.

According to the miRDB database, (http://www.mirdb.org), a potential target of miR-216a-5p is TGFBR2. TGFBR2 plays an important role in the progression of renal fibrosis through the regulation of the TGF-β/Smad3 signalling pathway. According to Meng et al. (2012), the disruption of TGFβR2 activation in rat renal tubule epithelial cells and kidney fibroblasts downregulates the TGF-β1-induced expression of collagen I, α-SMA, and fibronectin and thus it inhibits the TGF-β-induced renal fibrosis. In addition, Faherty et al. (2012) have reported that overexpression of miR-302d induced by connective tissue growth factor (CCN2/CTGF) downregulated the TGFβR2 expression in human tubule epithelial

and glomerular mesangial cells. This decreased the TGFβ-induced EMT in renal proximal tubule epithelial cells and attenuated TGFβ-induced mesangial production of fibronectin and thrombospondin.

Therefore, in the current study it was hypothesised that the downregulation of miR-216a-5p by hyperglycaemia will have a pro-fibrotic effect by upregulating the expression of TGFBR2, which upon binding to activated TGF-β could stimulate downstream signalling via Smad3.

As evidence of the ability of miR-216a-5p to regulate the expression of TGBR2 is lacking, an objective of this study was to clone the 3'UTR of TGFBR2 in a luciferase reporter vector, and to co-transfect it with a miR-216a-5p expression vector or anti-miR216-5p. Several attempts to clone the 3'UTR of TGFBR2 (6.22 kilobases) from HK-2 cells using different primer pairs were unsuccessful due to the generation of multiple products of varying sizes and poor cloning efficiency. Therefore, the 3'UTR of TGFBR2 was synthesised by Invitrogen (UK) and cloned in a pDONR 221 vector. Ongoing transfection experiments will demonstrate soon whether miR-216a-5p is a potential treatment target, by providing evidence of the ability of miR216a-5p to regulate the expression of TGFBR2.

5.5 Conclusions

Evidence for the role of hyperglycaemia on miRNA regulation in tubulointerstitial fibrosis (TIF) is limited. In the present study, 16 of 85 fibrosis-related miRNAs tested were dysregulated, with downregulation of the pro-fibrotic miR-216a-5p in response to hyperglycaemia in HK-2 cells. miRNA databases have predicted that TGFBR2 is a potential target for miR-216a-5p. Ongoing luciferase reporter

assays with the 3'UTR of TGFBR2, and miR-216a-5p or anti-miR-216a-5p will demonstrate if miR-216a-5p is a potential treatment target in DN.

In summary, the results in this chapter indicate that hyperglycaemia can modify the expression of 16 out of 85 fibrosis-related miRNAs in HK-2 cells either by its osmotic or metabolic features. In addition, a potentially important treatment target (miR-216a-5p) was identified that may regulate the expression of TGFBR2 *in vivo*. Of note, miR-216a-5pwas downregulated in response to the metabolic effect of hyperglycaemia.

Chapter 6: General discussion

Diabetic nephropathy is the most common cause of ESRD, which requires costly dialysis and transplantation. DN is characterised by the gradual decline of the GFR, albuminuria and the abnormal accumulation of ECM that ultimately leads to glomerulosclerosis and tubulointerstitial fibrosis (Kanasaki et al., 2013). There is a significant body of evidence of the key role of hyperglycaemia in DN. However, many studies do not distinguish between the metabolic and osmotic effects either due to a failure to use an osmotic control or by the use of an inappropriate osmotic control like the antioxidant mannitol.

The delineation of the metabolic and osmotic effects of hyperglycaemia may provide an insight into new pathological mechanisms and treatment targets in diabetes. Furthermore, the increasing consumption of beverages and food with artificial sweeteners that have been deemed safe by the Food and Drug Administration (USA) seem to have serious side effects on kidney health. A recent study of 3,000 female participants has demonstrated that the consumption of more than 2 servings of soda with artificial sweeteners per day correlates with a 2-fold increase in the risk of kidney function decline (Lin and Curhan, 2011). As most sweeteners seem to be of almost no caloric value, it might be useful to investigate their osmotic effect on renal cells and function.

An adequate ATP supply is key for the maintenance of electrolyte and nutrient homeostasis, and the normal function of PTCs. Several studies have demonstrated that mitochondrial dysfunction is implicated in the pathogenesis of DN (Sharma et al., 2013; Czajka and Malik, 2016). The present study shows that basal glycolysis and mitochondrial coupling efficiency are negatively affected by

30mM D-glucose and by the osmotic control, indicating an impaired ATP production mainly as a result of the osmotic effect of hyperglycaemia. It is likely that HK-2 cells exposed to 30mM D-glucose are energy depleted, as, in addition, they also display a reduction in glucose uptake after 24h and 48h of exposure, and reduced viability and wound healing properties (migration). The reduction of glucose uptake caused by 30mM D-glucose is likely to be a metabolic feature of hyperglycaemia and may be mediate either by an inhibition of glucose transporters or by downregulation/inhibition of glycolytic enzymes.

Furthermore, the significant mitochondrial proton leak (indicative of mitochondrial dysfunction) induced by 30mM D-glucose and the osmotic control suggests that the osmolarity in hyperglycaemia may contribute to an increase of mitochondrial ROS generation. In addition, cells exposed to 30mM D-glucose and the osmotic control demonstrate an impaired ability to respond to increased energy demand, as demonstrated by the decreased levels of spare respiratory capacity at 72h. This osmotic effect suggests that PTCs may be more susceptible to a secondary injury in a hyperosmotic environment, for example by albuminuria. Therefore, the impaired respiratory capacity, together with their impaired regenerative abilities provide conditions for secondary PTC damage.

Hyperglycaemia-induced upregulation of TGF-β1 may provide an additional challenge for the tubular environment in DN by stimulating EMT, promoting the deposition of ECM and upregulating pro-fibrotic miRNAs (Nandhini, 2014). In the present study, it appeared that at 48h and 72h the metabolic effect of hyperglycaemia (i.e. upregulation of by TGF-β1 25mM and 30mM D-glucose) was the predominant mechanism of TGF-β1 upregulation. Interestingly, the activation of Smad3 was very consistent at 24h, 48 and 72h: the levels of P-Smad

3 were significantly higher in cells exposed to 30mM D-glucose at these time points. This effect seemed to be driven by osmolarity, as the osmotic control significantly activated Smad3 after 48h and 72h. Surprisingly, and in contrast to the available literature, the activation of Smad3 failed to upregulate the miRNA expression of PAI-1, collagen I α1, TIMP-1 and MMP-9, and the protein expression of PAI-1 and collagen I α1. The mechanism behind this effect needs to be investigated in future but may involve the non-canonical phosphorylation of pSmad3C by cyclin-depended kinases (CDKs) in the nucleus (Tarasewicz and Jeruss, 2012). This leads to the inhibition of pSmad3C through the formation of pSmad3L/C (linker-phosphorylated Smad3C).

Hyperglycaemia seemed to have a transient osmolarity-mediated effect on the markers of PTC injury KIM-1 and endostatin, as they were upregulated only at 24h by 30mM D-glucose and the osmotic control. The mechanism of the KIM-1 and endostatin release in the medium from the cell membrane and ECM, respectively, needs to be investigated further. However, as the mRNA levels of MMP-9 and TIMP-1 remained unchanged by hyperglycaemia, either other MMPs or lysosomal enzymes are involved in this process.

The chemokine MCP-1 and the marker of inflammation IL-6 were also transiently upregulated at 24h by 30mM D-glucose, and this effect seems to be metabolic for MCP-1 and osmotic for IL-6. As these two markers are upregulated upon the activation of NF-kB and AP-1 (Tanaka et al., 2014; Haller et al., 2016), further studies are required to establish whether their upregulation is ROS-dependent (i.e. linked to the deleterious effects of hyperglycaemia on mitochondrial function) or is triggered by IL-1β, TNF-α, Angiotensin II, etc.

The metabolic and osmotic effects of hyperglycaemia on the viability, glycolysis, mitochondrial function and the expression of markers of ECM accumulation, inflammation and injury are summarised in Figure 6.1.

In terms of the effect of hyperglycaemia on the expression of fibrosis-related miRNAs in HK-2 cells, amongst the 16 dysregulated miRNAs, only 4 miRNAs were consistently up- or down-regulated at least 2 time points: miR-150-5p (regulates angiogenesis and EMT; upregulated at 48h and 72h; osmotic and metabolic effect), miR-211-5p (anti-fibrotic; downregulated at 24h, 48h, and 72h; osmotic and metabolic effect), miR-122-5p (involved in the regulation of inflammation, signal transduction and transcriptional regulation; downregulated at 24h and 72h; metabolic effect), and miR216a-5p (downregulated at 24h and 72h; metabolic effect). This is a novel observation, which outlines potential treatment targets in TIF. The data also suggest that the osmotic and metabolic components of hyperglycaemia may affect the expression of these miRNAs independently or synergistically. Further studies are required to identify potential downstream targets of miR-150-5p, miR-211-5p and miR-122-5p, and to investigate their interactions experimentally.

The present work has focused on the interaction between the antifibrotic miR216a-5p and its downstream target TGFBR2, and has corroborated the results of the fibrosis-related miRNA PCR arrays by qPCR. Figure 6.2 summarises the effect of hyperglycaemia on the expression of miR216a-5p and its potential downstream profibrotic effect. Ongoing experiments will demonstrate whether the predicted interaction of miR216a-5p and the 3'UTR of TGFBR2 is physiological.
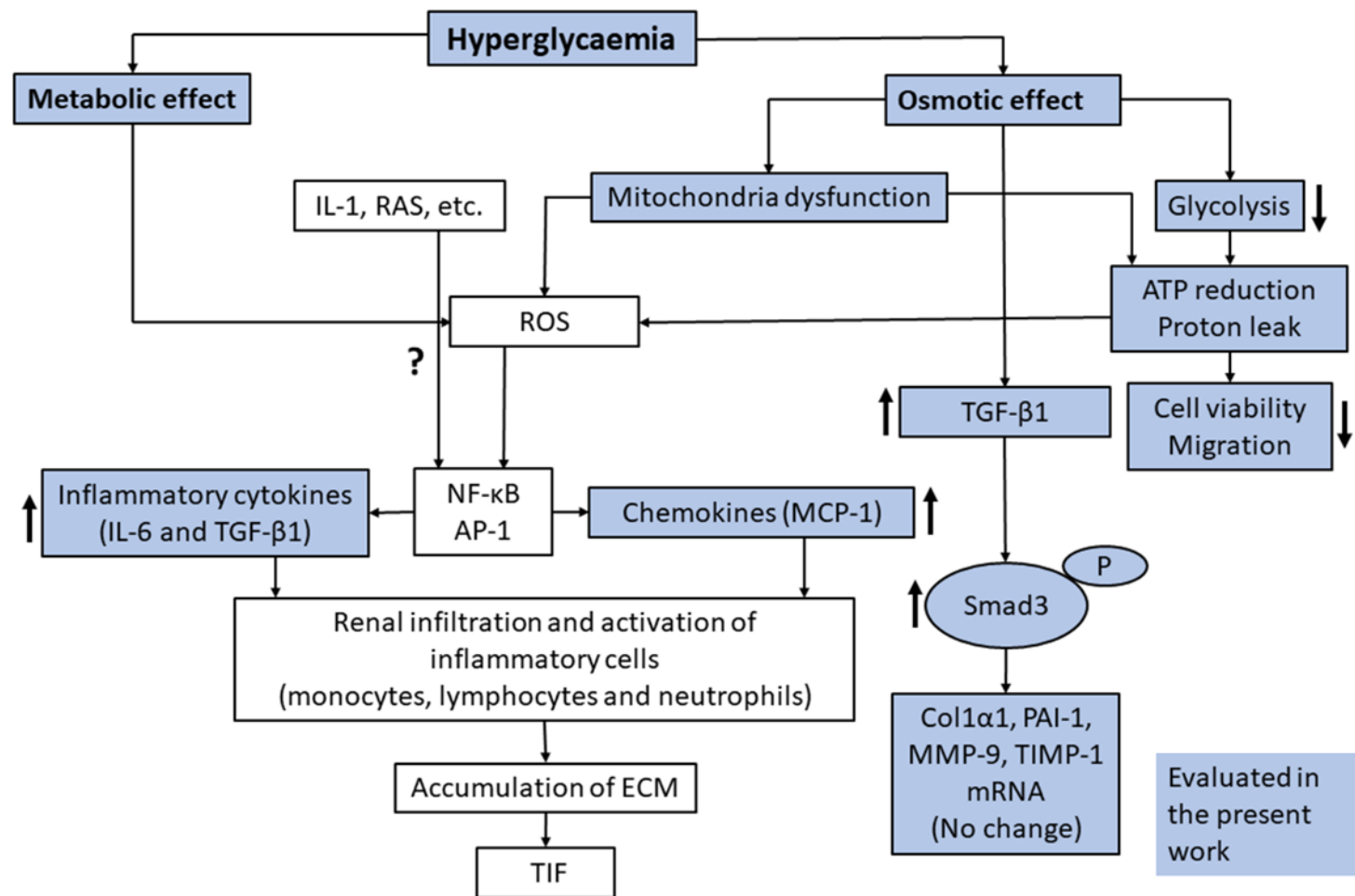
Figure 6. 2: Summary of the of metabolic and osmotic effect of hyperglycaemia on HK-2 cells. The osmotic effect of hyperglycaemia causes a reduction in mitochondrial function and glycolysis. Both metabolic and osmotic effects trigger ROS generation and activate NF-κB and AP-1. This results in the upregulation of cytokines and chemokines, which subsequently activate inflammatory cells and promote the accumulation of ECM and TIF.
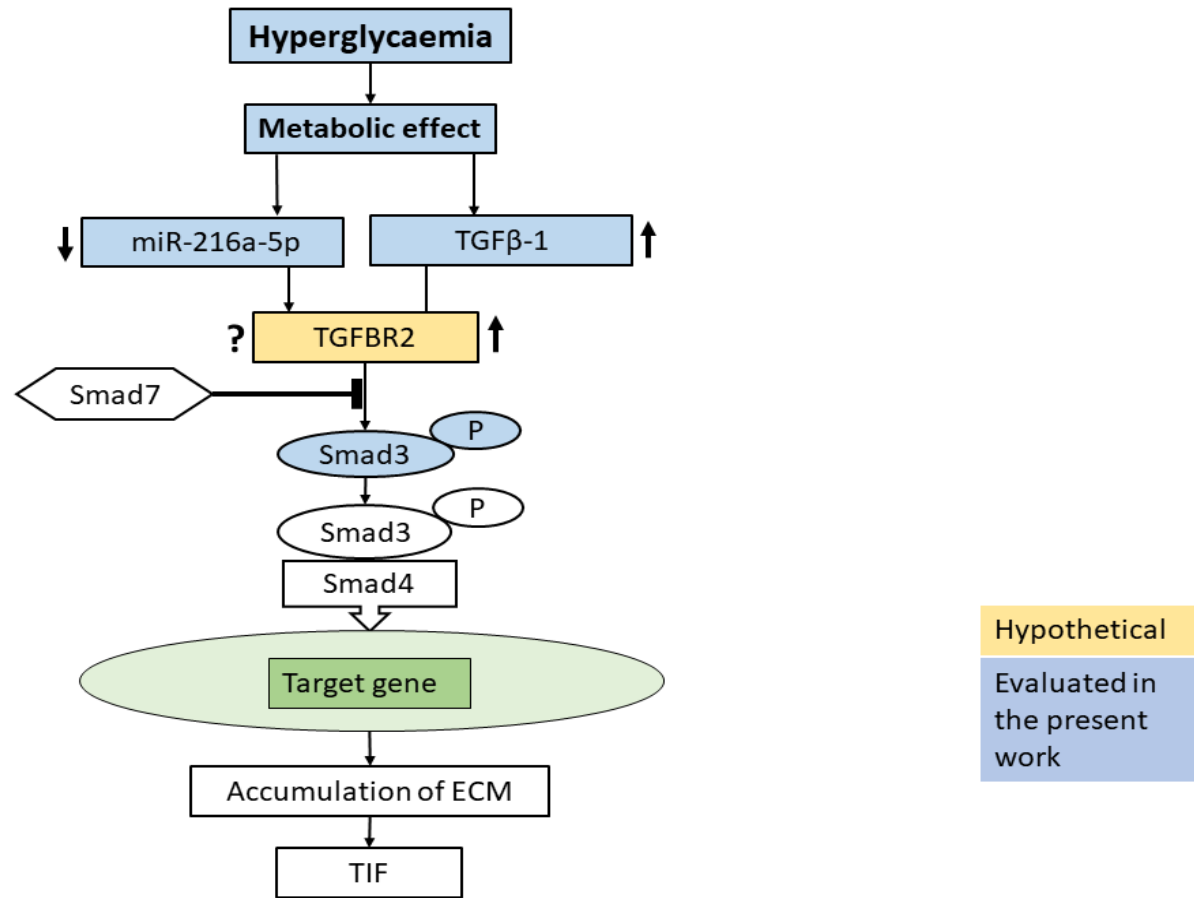
Figure 6. 3. Summary of the metabolic effect of hyperglycaemia on the expression of miR216a-5p in HK-2 cells. Hyperglycaemia downregulates miR216a-5p and increases the protein expression of TGF-β1. The downregulation of miR216a-5p may potentially upregulate the expression of TGFBR2 and activate Smad3, which would increase the ECM protein expression and lead to TIF in DN.

Chapter 7: Conclusions, limitations and future work

7.1   Conclusions

This study has evaluated the role of the metabolic and osmotic effects of hyperglycaemia on the energy production (glucose uptake, glycolysis and mitochondrial respiration), on the expression of markers of ECM accumulation, inflammation, PTC injury and chemokines, and on the expression of 84 fibrosis-related miRNAs in immortalised proximal tubule epithelial (HK-2) cells over 72h. The results have demonstrated that the osmotic and metabolic effects may induce changes independently or in synergy, as summarised in Figure 7.1. The delineation of these two effects of hyperglycaemia was only possible by the use of an appropriate osmotic control (e.g. L-glucose), which does not have a metabolic or an antioxidant effect.

The osmotic effect of hyperglycaemia appears to affect mainly the energy metabolism of the HK-2 cells by impairing the glycolysis and the mitochondrial function. This, in combination with the reduced glucose uptake in response to 30mM D-glucose, seems to have a negative effect on cell viability and migration, and may lead to a gradual renal function decline in DN. This is a novel observation, which may be relevant for future studies on the effect of artificial sweeteners on kidney function.

Both the metabolic and osmotic effect of hyperglycaemia appear to upregulate the expression of TGF-β1 and the activation of Smad3. However, these effects were not translated, as expected, into an accumulation of ECM. Furthermore, most of the markers of inflammation, PTC injury and chemokines, were

upregulated transiently at 24h, thus demonstrating the adaptation potential of HK-2 cells even to 30mM D-glucose.

A novel finding of this project was the dysregulation of 4 fibrosis-related miRNAs (miR-211-5p, miR-216a-5p, miR-150-5p, and miR122-5p) by hyperglycaemia. Future *in vitro* and *in vivo* studies will determine whether they are suitable targets in the treatment of DN.

Taken together, this study provides evidence that the metabolic and osmotic effects of hyperglycaemia may play a role in the pathogenesis of DN.
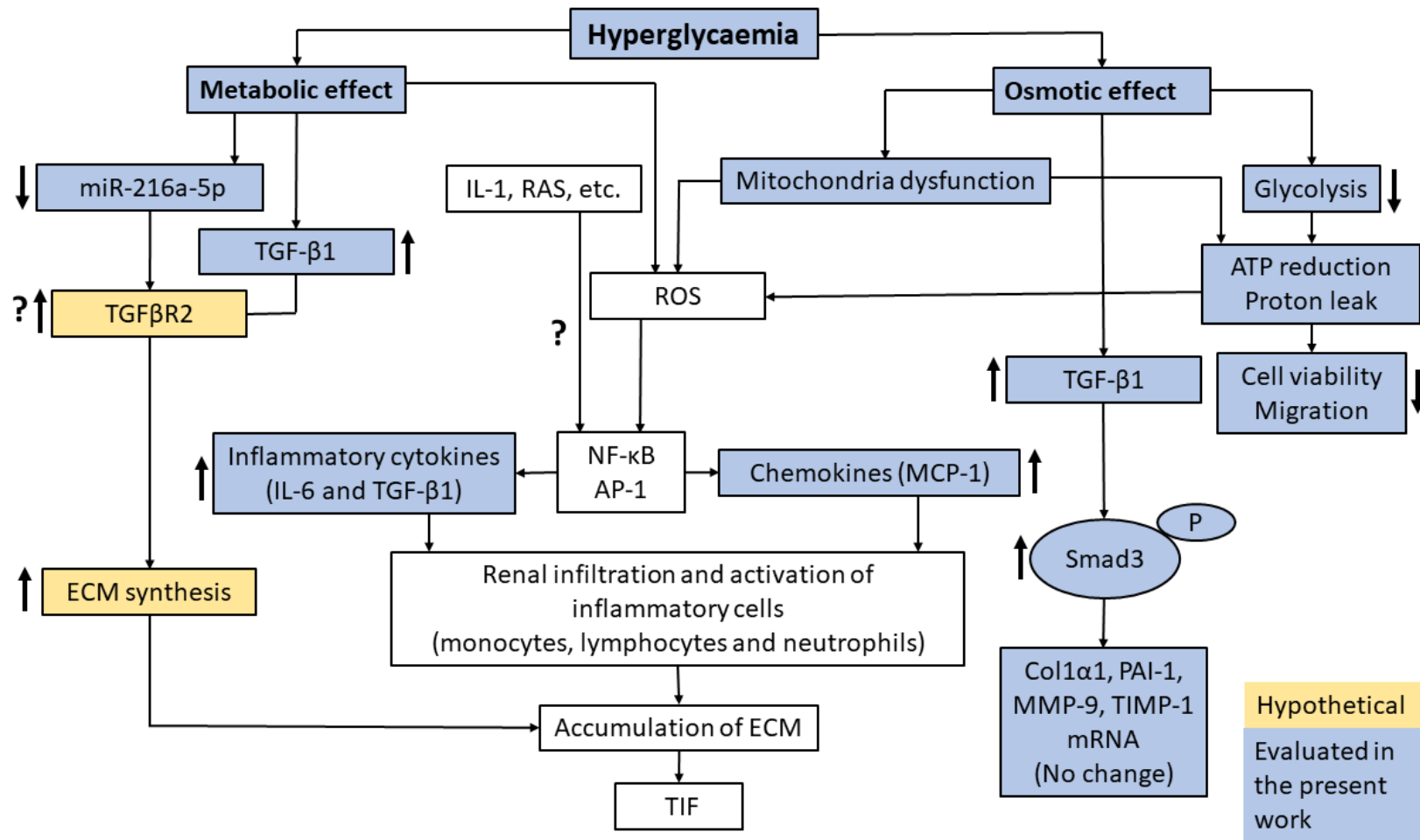
Figure 7. 2. Summary of the metabolic and osmotic effects of hyperglycaemia in HK-2 cells. The osmotic and metabolic effects may induce changes independently or in synergy, which may trigger ROS generation and activate NF-κB, AP-1 and Smad3 (via TGFBR2), resulting in upregulation of pro-fibrotic cytokines and chemokines, activation of inflammatory cells, and the accumulation of ECM and TIF.

7.2 Limitations and future work

One of the limitations of this study is the use of immortalised human renal proximal tubule cells. However, the use of primary human cells would have introduced a significant variability in the results due to the rapid loss of PTC phenotype within a couple of passages. Variability in the results could also have been introduced by the use of different donors in these experiments. The use of animal models would have been a more appropriate alternative. However, the existing obese and non-obese animal models for type 2 diabetes display varying degrees of insulin resistance and insulin deficiency. In such models, it would be difficult to administer precise amounts of the costly L-glucose, so that equimolar concentrations are achieved, that are equal to the levels of D-glucose in the diabetic animals.

Another aspect that could be considered is the exposure of the HK-2 cells to hyperglycaemia for longer than 72h to mimic diabetic conditions more closely. However, our group have observed that prolonged exposure (7 days) of HK-2 cells to hyperglycaemia results in dramatic changes to their proliferation rates and morphology, which makes the passaging of the cells and reaching cell density similar to that of control cells challenging.

A consideration should be given to the limitations of some of the methods used in this study, in particular to the CCK-8 kit, which was used to estimate cell viability. The kit is based on the reduction of the water-soluble tetrazolium salt WST-8 which is reduced by dehydrogenases to a water-soluble formazan dye. This method is convenient, as it allows the direct measurement of formazan absorbance in the cell culture 96-well plates. However, when test results are

interpreted in the context of exposure of the cells to higher glucose concentrations, the following limitation of the assay needs to be considered: although the test indicates the relative viability of cells by measuring their metabolic activity, it does not take into account the actual number of viable cells. As the test measures the metabolic activity of cells, cells exposed to higher concentrations of glucose may display increased metabolic activity or higher cell numbers, which could be misinterpreted as increased viability. An Annexin V/Propidium Iodide test using flow cytometry could provide a more accurate estimation of cell viability and the type of cell death (apoptosis or necrosis) in dying cells. However, this approach is not appropriate for adherent cells such as HK-2 cells.

An important aspect for consideration in this study is the statistical power of the experiments. The number of experimental and biological repeats in this study are in line with similar studies that report robust effects. A review of the confidence intervals and mean differences of contrasted conditions in this study (Appendices 1A, B and C) demonstrates that an increase of the sample sizes would have a marginal effect on rejecting the null hypothesis for all concerned experiments, and the observed patterns and trends of results would be maintained.

Future work should investigate the mechanism behind the lack of ECM accumulation in response to hyperglycaemia-induced Smad3 activation. The studies should include other signalling pathways and the role of CDKs.

However, the most exciting and promising future work is related to the 4 fibrosis-related miRNAs (miR-211-5p, miR-216a-5p, miR-150-5p, and miR122-5p) which were dysregulated by hyperglycaemia. Experiments will identify potential fibrosis-

related targets of these miRNAs and will test their interactions in *in vitro* experiments. Once such an interaction is confirmed, biopsies from patients with DN will be examined for miRNA expression with the aim of identifying suitable targets for the treatment of TIF.

Appendix

Appendix 1A (Chapter 3): Mean difference and 95% confidence intervals of all statistical comparisons. In bold are highlighted comparisons identified by ANOVA and Tukey's post-hoc test as statistically significant (p≤0.05). In green are highlighted cases where a larger sample size may have potentially resulted in a statistically significant mean difference

1.00: 5mM D-glucose; **2.00:** 25mM D-glucose; **3.00:** 30mM D-glucose; **4.00:** 5mM D-glucose+ 25mM L-glucose.

Cell viability test				
24h		Mean Difference	95% Confidence Interval	
(I) Conditions	(J) Conditions	(I-J)	Lower Bound	Upper Bound
1.00	2.00	12.02000	-6.3598	30.3998
	3.00	**25.28000***	**6.9002**	**43.6598**
	4.00	17.76000	-.6198	36.1398
2.00	3.00	13.26000	-5.1198	31.6398
	4.00	5.74000	-12.6398	24.1198
3.00	4.00	-7.52000	-25.8998	10.8598
48h		Mean Difference	95% Confidence Interval	
(I) Conditions	(J) Conditions	(I-J)	Lower Bound	Upper Bound
1.00	2.00	15.22000	-11.2258	41.6658
	3.00	25.88000	-.5658	52.3258
	4.00	16.06000	-10.3858	42.5058
2.00	3.00	10.66000	-15.7858	37.1058
	4.00	.84000	-25.6058	27.2858
3.00	4.00	-9.82000	-36.2658	16.6258
72h		Mean Difference	95% Confidence Interval	
(I) Conditions	(J) Conditions	(I-J)	Lower Bound	Upper Bound
1.00	2.00	19.48000	-.8594	39.8194
	3.00	**25.98000***	**5.6406**	**46.3194**
	4.00	12.98000	-7.3594	33.3194
2.00	3.00	6.50000	-13.8394	26.8394
	4.00	-6.50000	-26.8394	13.8394
3.00	4.00	-13.00000	-33.3394	7.3394

Wound healing test				
4h		Mean Difference	95% Confidence Interval	
(I) Condition	(J) Condition	(I-J)	Lower Bound	Upper Bound

(I) Condition	(J) Condition	Mean Difference (I-J)	95% Confidence Interval Lower Bound	Upper Bound
1.00	2.00	7.56667	-.4057	15.5390
	3.00	-5.46667	-13.4390	2.5057
	4.00	3.23333	-4.7390	11.2057
2.00	3.00	-13.03333*	-21.0057	-5.0610
	4.00	-4.33333	-12.3057	3.6390
3.00	4.00	8.70000*	.7276	16.6724

8h

(I) Condition	(J) Condition	Mean Difference (I-J)	95% Confidence Interval Lower Bound	Upper Bound
1.00	2.00	10.80000*	.3682	21.2318
	3.00	-9.43333	-19.8652	.9985
	4.00	4.33333	-6.0985	14.7652
2.00	3.00	-20.23333*	-30.6652	-9.8015
	4.00	-6.46667	-16.8985	3.9652
3.00	4.00	13.76667*	3.3348	24.1985

24h

(I) Condition	(J) Condition	Mean Difference (I-J)	95% Confidence Interval Lower Bound	Upper Bound
1.00	2.00	23.86667	-.7840	48.5174
	3.00	-17.80000	-42.4507	6.8507
	4.00	.86667	-23.7840	25.5174
2.00	3.00	-41.66667*	-66.3174	-17.0160
	4.00	-23.00000	-47.6507	1.6507
3.00	4.00	18.66667	-5.9840	43.3174

28h

(I) Condition	(J) Condition	Mean Difference (I-J)	95% Confidence Interval Lower Bound	Upper Bound
1.00	2.00	28.76667*	4.0439	53.4894
	3.00	-19.86667	-44.5894	4.8561
	4.00	6.33333	-18.3894	31.0561
2.00	3.00	-48.63333*	-73.3561	-23.9106
	4.00	-22.43333	-47.1561	2.2894
3.00	4.00	26.20000*	1.4773	50.9227

32h

(I) Condition	(J) Condition	Mean Difference (I-J)	95% Confidence Interval Lower Bound	Upper Bound
1.00	2.00	33.86667*	15.2841	52.4492
	3.00	-18.83333*	-37.4159	-.2508
	4.00	9.60000	-8.9825	28.1825
2.00	3.00	-52.70000*	-71.2825	-34.1175
	4.00	-24.26667*	-42.8492	-5.6841
3.00	4.00	28.43333*	9.8508	47.0159

48h

(I) Condition	(J) Condition	Mean Difference (I-J)	95% Confidence Interval Lower Bound	Upper Bound
1.00	2.00	30.23333*	7.2575	53.2092

(I) Condition	(J) Condition	Mean Difference (I-J)	Lower Bound	Upper Bound
	3.00	-16.36667	-39.3425	6.6092
	4.00	16.90000	-6.0759	39.8759
2.00	3.00	**-46.60000***	**-69.5759**	**-23.6241**
	4.00	-13.33333	-36.3092	9.6425
3.00	4.00	**33.26667***	**10.2908**	**56.2425**

Glucose intake test				
24h		Mean Difference	95% Confidence Interval	
(I) Condition	(J) Condition	(I-J)	Lower Bound	Upper Bound
1.00	2.00	-.01667	-.8346	.8013
	3.00	**1.03500***	**.2171**	**1.8529**
	4.00	-.01333	-.8313	.8046
2.00	3.00	**1.05167***	**.2337**	**1.8696**
	4.00	.00333	-.8146	.8213
3.00	4.00	**-1.04833***	**-1.8663**	**-.2304**

48h		Mean Difference	95% Confidence Interval	
(I) Condition	(J) Condition	(I-J)	Lower Bound	Upper Bound
1.00	2.00	**.86000***	**.1983**	**1.5217**
	3.00	**.91500***	**.2533**	**1.5767**
	4.00	.25667	-.4051	.9184
2.00	3.00	.05500	-.6067	.7167
	4.00	-.60333	-1.2651	.0584
3.00	4.00	-.65833	-1.3201	.0034

72h		Mean Difference	95% Confidence Interval	
(I) Condition	(J) Condition	(I-J)	Lower Bound	Upper Bound
1.00	2.00	.06667	-1.1020	1.2353
	3.00	.59833	-.5703	1.7670
	4.00	-.24167	-1.4103	.9270
2.00	3.00	.53167	-.6370	1.7003
	4.00	-.30833	-1.4770	.8603
3.00	4.00	-.84000	-2.0086	.3286

Basal Glycolysis-Glycolytic rate test				
24h		Mean Difference	95% Confidence Interval	
(I) condition	(J) condition	(I-J)	Lower Bound	Upper Bound
1.00	2.00	727.42833	-3141.9977	4596.8544
	3.00	**4620.78167***	**751.3556**	**8490.2077**
	4.00	**9776.04000***	**5906.6140**	**13645.4660**
2.00	3.00	**3893.35333***	**23.9273**	**7762.7794**
	4.00	**9048.61167***	**5179.1856**	**12918.0377**

			Mean Difference	95% Confidence Interval	
	(I) condition	(J) condition	(I-J)	Lower Bound	Upper Bound
	3.00	4.00	5155.25833*	1285.8323	9024.6844
48h			Mean Difference	95% Confidence Interval	
	(I) condition	(J) condition	(I-J)	Lower Bound	Upper Bound
	1.00	2.00	2854.82000*	601.3281	5108.3119
		3.00	3586.00667*	1332.5148	5839.4985
		4.00	7262.15833*	5008.6665	9515.6502
	2.00	3.00	731.18667	-1522.3052	2984.6785
		4.00	4407.33833*	2153.8465	6660.8302
	3.00	4.00	3676.15167*	1422.6598	5929.6435
72h			Mean Difference	95% Confidence Interval	
	(I) condition	(J) condition	(I-J)	Lower Bound	Upper Bound
	1.00	2.00	-1378.05167	-5178.1407	2422.0374
		3.00	-1824.31667	-5624.4057	1975.7724
		4.00	214.87833	-3585.2107	4014.9674
	2.00	3.00	-446.26500	-4246.3541	3353.8241
		4.00	1592.93000	-2207.1591	5393.0191
	3.00	4.00	2039.19500	-1760.8941	5839.2841

Basal Proton Efflux rate -Glycolytic rate test					
24h			Mean Difference	95% Confidence Interval	
	(I) condition	(J) condition	(I-J)	Lower Bound	Upper Bound
	1.00	2.00	299.41500	-3620.4712	4219.3012
		3.00	5174.34833*	1254.4621	9094.2345
		4.00	9943.63833*	6023.7521	13863.5245
	2.00	3.00	4874.93333*	955.0471	8794.8195
		4.00	9644.22333*	5724.3371	13564.1095
	3.00	4.00	4769.29000*	849.4038	8689.1762
48h			Mean Difference	95% Confidence Interval	
	(I) condition	(J) condition	(I-J)	Lower Bound	Upper Bound
	1.00	2.00	2901.08833*	494.5092	5307.6675
		3.00	4308.99500*	1902.4158	6715.5742
		4.00	7753.34500*	5346.7658	10159.9242
	2.00	3.00	1407.90667	-998.6725	3814.4858
		4.00	4852.25667*	2445.6775	7258.8358
	3.00	4.00	3444.35000*	1037.7708	5850.9292
72h			Mean Difference	95% Confidence Interval	
	(I) condition	(J) condition	(I-J)	Lower Bound	Upper Bound
	1.00	2.00	-1193.54167	-5457.6653	3070.5820
		3.00	-1640.10833	-5904.2320	2624.0153
		4.00	615.53333	-3648.5903	4879.6570
	2.00	3.00	-446.56667	-4710.6903	3817.5570

	4.00	1809.07500	-2455.0487	6073.1987
3.00	4.00	2255.64167	-2008.4820	6519.7653

%PER from Glycolysis-Glycolytic rate test				
24h		Mean Difference	95% Confidence Interval	
(I) condition	(J) condition	(I-J)	Lower Bound	Upper Bound
1.00	2.00	7.19833	-3.0213	17.4179
	3.00	**22.99333***	**12.7737**	**33.2129**
	4.00	**21.12500***	**10.9054**	**31.3446**
2.00	3.00	**15.79500***	**5.5754**	**26.0146**
	4.00	**13.92667***	**3.7071**	**24.1463**
3.00	4.00	-1.86833	-12.0879	8.3513
48h		Mean Difference	95% Confidence Interval	
(I) condition	(J) condition	(I-J)	Lower Bound	Upper Bound
1.00	2.00	3.25000	-4.2400	10.7400
	3.00	**15.04333***	**7.5534**	**22.5333**
	4.00	**13.65500***	**6.1650**	**21.1450**
2.00	3.00	**11.79333***	**4.3034**	**19.2833**
	4.00	**10.40500***	**2.9150**	**17.8950**
3.00	4.00	-1.38833	-8.8783	6.1016
72h		Mean Difference	95% Confidence Interval	
(I) condition	(J) condition	(I-J)	Lower Bound	Upper Bound
1.00	2.00	-3.30167	-17.3276	10.7243
	3.00	1.55833	-12.4676	15.5843
	4.00	4.12333	-9.9026	18.1493
2.00	3.00	4.86000	-9.1659	18.8859
	4.00	7.42500	-6.6009	21.4509
3.00	4.00	2.56500	-11.4609	16.5909

Compensatory Glycolysis-Glycolytic rate test				
24h		Mean Difference	95% Confidence Interval	
(I) condition	(J) condition	(I-J)	Lower Bound	Upper Bound
1.00	2.00	-156.77333	-6013.1269	5699.5802
	3.00	**6722.95333***	**866.5998**	**12579.3069**
	4.00	**12350.55000***	**6494.1964**	**18206.9036**
2.00	3.00	**6879.72667***	**1023.3731**	**12736.0802**
	4.00	**12507.32333***	**6650.9698**	**18363.6769**
3.00	4.00	5627.59667	-228.7569	11483.9502
48h		Mean Difference	95% Confidence Interval	
(I) condition	(J) condition	(I-J)	Lower Bound	Upper Bound

(I) condition	(J) condition	Mean Difference (I-J)	95% Confidence Interval Lower Bound	95% Confidence Interval Upper Bound
1.00	2.00	2445.76833	-1259.6645	6151.2012
	3.00	**6357.74000***	**2652.3072**	**10063.1728**
	4.00	**9805.77833***	**6100.3455**	**13511.2112**
2.00	3.00	**3911.97167***	**206.5388**	**7617.4045**
	4.00	**7360.01000***	**3654.5772**	**11065.4428**
3.00	4.00	3448.03833	-257.3945	7153.4712

72h

(I) condition	(J) condition	Mean Difference (I-J)	95% Confidence Interval Lower Bound	95% Confidence Interval Upper Bound
1.00	2.00	-2363.21000	-8553.7625	3827.3425
	3.00	-1726.58333	-7917.1358	4463.9691
	4.00	1686.74667	-4503.8058	7877.2991
2.00	3.00	636.62667	-5553.9258	6827.1791
	4.00	4049.95667	-2140.5958	10240.5091
3.00	4.00	3413.33000	-2777.2225	9603.8825

mitoOCR/GlycoPER (Basal)-Glycolytic rate test				

24h

(I) condition	(J) condition	Mean Difference (I-J)	95% Confidence Interval Lower Bound	95% Confidence Interval Upper Bound
1.00	2.00	-2.67500	-9.4774	4.1274
	3.00	6.40167	-.4008	13.2041
	4.00	**-6.82333***	**-13.6258**	**-.0209**
2.00	3.00	**9.07667***	**2.2742**	**15.8791**
	4.00	-4.14833	-10.9508	2.6541
3.00	4.00	**-13.22500***	**-20.0274**	**-6.4226**

48h

(I) condition	(J) condition	Mean Difference (I-J)	95% Confidence Interval Lower Bound	95% Confidence Interval Upper Bound
1.00	2.00	-4.28167	-9.6550	1.0917
	3.00	**7.17333***	**1.8000**	**12.5467**
	4.00	**-5.77167***	**-11.1450**	**-.3983**
2.00	3.00	**11.45500***	**6.0816**	**16.8284**
	4.00	-1.49000	-6.8634	3.8834
3.00	4.00	**-12.94500***	**-18.3184**	**-7.5716**

72h

(I) condition	(J) condition	Mean Difference (I-J)	95% Confidence Interval Lower Bound	95% Confidence Interval Upper Bound
1.00	2.00	6.48167	-5.7812	18.7446
	3.00	9.06000	-3.2029	21.3229
	4.00	8.51167	-3.7512	20.7746
2.00	3.00	2.57833	-9.6846	14.8412
	4.00	2.03000	-10.2329	14.2929
3.00	4.00	-.54833	-12.8112	11.7146

		Post 2-DG Acidification-Glycolytic rate test		
24h		Mean Difference	95% Confidence Interval	
	(I) condition	(J) condition	(I-J)	Lower Bound	Upper Bound
	1.00	2.00	**-5608.85667***	**-7463.4449**	**-3754.2684**
		3.00	**-5094.46833***	**-6949.0566**	**-3239.8801**
		4.00	1752.81000	-101.7783	3607.3983
	2.00	3.00	514.38833	-1340.1999	2368.9766
		4.00	**7361.66667***	**5507.0784**	**9216.2549**
	3.00	4.00	**6847.27833***	**4992.6901**	**8701.8666**
48h		Mean Difference	95% Confidence Interval	
	(I) condition	(J) condition	(I-J)	Lower Bound	Upper Bound
	1.00	2.00	**-3507.41000***	**-4856.7543**	**-2158.0657**
		3.00	**-3253.16333***	**-4602.5077**	**-1903.8190**
		4.00	**1573.36167***	**224.0173**	**2922.7060**
	2.00	3.00	254.24667	-1095.0977	1603.5910
		4.00	**5080.77167***	**3731.4273**	**6430.1160**
	3.00	4.00	**4826.52500***	**3477.1807**	**6175.8693**
72h		Mean Difference	95% Confidence Interval	
	(I) condition	(J) condition	(I-J)	Lower Bound	Upper Bound
	1.00	2.00	**-1935.92333***	**-3740.1055**	**-131.7412**
		3.00	**-2314.97500***	**-4119.1571**	**-510.7929**
		4.00	1037.93500	-766.2471	2842.1171
	2.00	3.00	-379.05167	-2183.2338	1425.1305
		4.00	**2973.85833***	**1169.6762**	**4778.0405**
	3.00	4.00	**3352.91000***	**1548.7279**	**5157.0921**

		Basal Respiration-Mitochondrial stress test		
24h		Mean Difference	95% Confidence Interval	
	(I) condition	(J) condition	(I-J)	Lower Bound	Upper Bound
	1.00	2.00	133.43310	-4643.5740	4910.4402
		3.00	391.11780	-4509.9881	5292.2237
		4.00	526.45905	-4250.5480	5303.4661
	2.00	3.00	257.68470	-4519.3224	5034.6918
		4.00	393.02595	-4256.5713	5042.6232
	3.00	4.00	135.34125	-4641.6658	4912.3483
48h		Mean Difference	95% Confidence Interval	
	(I) condition	(J) condition	(I-J)	Lower Bound	Upper Bound
	1.00	2.00	-497.79746	-3764.7834	2769.1885
		3.00	43.85382	-3308.0031	3395.7107
		4.00	-224.37258	-3491.3586	3042.6134
	2.00	3.00	541.65128	-2725.3347	3808.6373

			Mean Difference	95% Confidence Interval	
	(I) condition	(J) condition	(I-J)	Lower Bound	Upper Bound
		4.00	273.42488	-2906.4258	3453.2755
	3.00	4.00	-268.22640	-3535.2124	2998.7596

72h			Mean Difference	95% Confidence Interval	
	(I) condition	(J) condition	(I-J)	Lower Bound	Upper Bound
	1.00	2.00	540.00171	-3095.7686	4175.7720
		3.00	531.61164	-3198.6100	4261.8333
		4.00	323.32887	-3312.4415	3959.0992
	2.00	3.00	-8.39007	-3644.1604	3627.3803
		4.00	-216.67284	-3755.4718	3322.1261
	3.00	4.00	-208.28277	-3844.0531	3427.4876

	Maximal Respiration-Mitochondrial stress test				
24h			Mean Difference	95% Confidence Interval	
	(I) condition	(J) condition	(I-J)	Lower Bound	Upper Bound
	1.00	2.00	742.85241	-5307.5207	6793.2255
		3.00	252.81643	-5954.7354	6460.3683
		4.00	576.43389	-5473.9392	6626.8070
	2.00	3.00	-490.03598	-6540.4091	5560.3371
		4.00	-166.41852	-6055.4193	5722.5822
	3.00	4.00	323.61746	-5726.7557	6373.9906
48h			Mean Difference	95% Confidence Interval	
	(I) condition	(J) condition	(I-J)	Lower Bound	Upper Bound
	1.00	2.00	404.79222	-2559.5075	3369.0920
		3.00	1091.11111	-1950.1963	4132.4185
		4.00	1255.14222	-1709.1575	4219.4420
	2.00	3.00	686.31889	-2277.9809	3650.6186
		4.00	850.35000	-2034.8875	3735.5875
	3.00	4.00	164.03111	-2800.2686	3128.3309
72h			Mean Difference	95% Confidence Interval	
	(I) condition	(J) condition	(I-J)	Lower Bound	Upper Bound
	1.00	2.00	1919.18556	-3051.6644	6890.0355
		3.00	2900.66667	-2199.3178	8000.6511
		4.00	2613.11556	-2357.7344	7583.9655
	2.00	3.00	981.48111	-3989.3689	5952.3311
		4.00	693.93000	-4144.3401	5532.2001
	3.00	4.00	-287.55111	-5258.4011	4683.2989

	Spare Respiratory-Mitochondrial stress test				
24h			Mean Difference	95% Confidence Interval	
	(I) condition	(J) condition	(I-J)	Lower Bound	Upper Bound

(I) condition	(J) condition	Mean Difference (I-J)	Lower Bound	Upper Bound
1.00	2.00	2.11200	-13.3055	17.5295
	3.00	-4.46390	-20.2819	11.3541
	4.00	-6.89781	-22.3153	8.5197
2.00	3.00	-6.57590	-21.9934	8.8416
	4.00	-9.00981	-24.0161	5.9965
3.00	4.00	-2.43391	-17.8514	12.9836

48h

(I) condition	(J) condition	Mean Difference (I-J)	95% Confidence Interval Lower Bound	Upper Bound
1.00	2.00	7.51667	-25.6329	40.6662
	3.00	5.90000	-28.1107	39.9107
	4.00	12.07667	-21.0729	45.2262
2.00	3.00	-1.61667	-34.7662	31.5329
	4.00	4.56000	-27.7054	36.8254
3.00	4.00	6.17667	-26.9729	39.3262

72h

(I) condition	(J) condition	Mean Difference (I-J)	95% Confidence Interval Lower Bound	Upper Bound
1.00	2.00	11.54889	-10.7134	33.8112
	3.00	**28.54444***	**5.7038**	**51.3851**
	4.00	**23.97889***	**1.7166**	**46.2412**
2.00	3.00	16.99556	-5.2668	39.2579
	4.00	12.43000	-9.2386	34.0986
3.00	4.00	-4.56556	-26.8279	17.6968

ATP Production-Mitochondrial stress test				

24h

(I) condition	(J) condition	Mean Difference (I-J)	95% Confidence Interval Lower Bound	Upper Bound
1.00	2.00	420.25364	-3481.6544	4322.1616
	3.00	1197.31500	-2805.9582	5200.5882
	4.00	1622.70632	-2279.2017	5524.6143
2.00	3.00	777.06136	-3124.8467	4678.9694
	4.00	1202.45269	-2595.3857	5000.2911
3.00	4.00	425.39132	-3476.5167	4327.2993

48h

(I) condition	(J) condition	Mean Difference (I-J)	95% Confidence Interval Lower Bound	Upper Bound
1.00	2.00	420.25364	-3481.6544	4322.1616
	3.00	1197.31500	-2805.9582	5200.5882
	4.00	1622.70632	-2279.2017	5524.6143
2.00	3.00	777.06136	-3124.8467	4678.9694
	4.00	1202.45269	-2595.3857	5000.2911
3.00	4.00	425.39132	-3476.5167	4327.2993

72h

(I) condition	(J) condition		95% Confidence Interval	

		Mean Difference		
		(I-J)	Lower Bound	Upper Bound
1.00	2.00	1324.13444	-1982.8581	4631.1270
	3.00	2609.37778	-783.5250	6002.2806
	4.00	2227.45444	-1079.5381	5534.4470
2.00	3.00	1285.24333	-2021.7492	4592.2359
	4.00	903.32000	-2315.4702	4122.1102
3.00	4.00	-381.92333	-3688.9159	2925.0692

Proton Leak-Mitochondrial stress test				
24h		Mean Difference	95% Confidence Interval	
	(I) condition	(J) condition	(I-J)	Lower Bound	Upper Bound

24h	(I) condition	(J) condition	(I-J)	Lower Bound	Upper Bound
	1.00	2.00	-286.82054	-1460.1048	886.4637
		3.00	-806.19720	-2009.9614	397.5670
		4.00	-1096.24727	-2269.5315	77.0370
	2.00	3.00	-519.37666	-1692.6609	653.9076
		4.00	-809.42673	-1951.4178	332.5643
	3.00	4.00	-290.05007	-1463.3343	883.2342
48h			Mean Difference	95% Confidence Interval	
	(I) condition	(J) condition	(I-J)	Lower Bound	Upper Bound
	1.00	2.00	-1412.59333	-2936.3525	111.1658
		3.00	-1054.75556	-2618.0995	508.5883
		4.00	-1483.58333	-3007.3425	40.1758
	2.00	3.00	357.83778	-1165.9214	1881.5969
		4.00	-70.99000	-1554.1082	1412.1282
	3.00	4.00	-428.82778	-1952.5869	1094.9314
72h			Mean Difference	95% Confidence Interval	
	(I) condition	(J) condition	(I-J)	Lower Bound	Upper Bound
	1.00	2.00	-784.15444	-1614.0664	45.7575
		3.00	-2077.78889[*]	-2929.2605	-1226.3172
		4.00	-1904.13444[*]	-2734.0464	-1074.2225
	2.00	3.00	-1293.63444[*]	-2123.5464	-463.7225
		4.00	-1119.98000[*]	-1927.7569	-312.2031
	3.00	4.00	173.65444	-656.2575	1003.5664

Non-mitochondrial Oxygen Consumption-Mitochondrial stress test				
24h			Mean Difference	95% Confidence Interval	
	(I) condition	(J) condition	(I-J)	Lower Bound	Upper Bound
	1.00	2.00	707.36648	-928.9354	2343.6684
		3.00	1662.23200	-16.5783	3341.0423
		4.00	1934.63867[*]	298.3368	3570.9406

	(I) condition	(J) condition	Mean Difference (I-J)	95% Confidence Interval Lower Bound	95% Confidence Interval Upper Bound
	2.00	3.00	954.86551	-681.4364	2591.1674
		4.00	1227.27219	-365.3871	2819.9315
	3.00	4.00	272.40667	-1363.8952	1908.7086

48h			Mean Difference	95% Confidence Interval	
	(I) condition	(J) condition	(I-J)	Lower Bound	Upper Bound
	1.00	2.00	-575.11556	-1881.0200	730.7889
		3.00	-941.77778	-2281.6074	398.0519
		4.00	-785.72556	-2091.6300	520.1789
	2.00	3.00	-366.66222	-1672.5666	939.2422
		4.00	-210.61000	-1481.6840	1060.4640
	3.00	4.00	156.05222	-1149.8522	1461.9566

72h			Mean Difference	95% Confidence Interval	
	(I) condition	(J) condition	(I-J)	Lower Bound	Upper Bound
	1.00	2.00	480.80111	-342.1971	1303.7994
		3.00	581.11111	-263.2673	1425.4895
		4.00	721.20111	-101.7971	1544.1994
	2.00	3.00	100.31000	-722.6882	923.3082
		4.00	240.40000	-560.6477	1041.4477
	3.00	4.00	140.09000	-682.9082	963.0882

		Coupling Efficiency-Mitochondrial stress test			
24h			Mean Difference	95% Confidence Interval	
	(I) condition	(J) condition	(I-J)	Lower Bound	Upper Bound
	1.00	2.00	3.91988	-3.4820	11.3217
		3.00	**9.22118***	**1.6271**	**16.8153**
		4.00	**12.04754***	**4.6457**	**19.4494**
	2.00	3.00	5.30130	-2.1005	12.7031
		4.00	**8.12766***	**.9232**	**15.3321**
	3.00	4.00	2.82636	-4.5755	10.2282
48h			Mean Difference	95% Confidence Interval	
	(I) condition	(J) condition	(I-J)	Lower Bound	Upper Bound
	1.00	2.00	13.21667	-.6801	27.1134
		3.00	11.15556	-3.1022	25.4133
		4.00	**16.48667***	**2.5899**	**30.3834**
	2.00	3.00	-2.06111	-15.9579	11.8356
		4.00	3.27000	-10.2561	16.7961
	3.00	4.00	5.33111	-8.5656	19.2279
72h			Mean Difference	95% Confidence Interval	
	(I) condition	(J) condition	(I-J)	Lower Bound	Upper Bound
	1.00	2.00	11.82667	-5.5817	29.2351
		3.00	**33.64444***	**15.7838**	**51.5051**

		4.00	30.44667*	13.0383	47.8551
	2.00	3.00	21.81778*	4.4094	39.2262
		4.00	18.62000*	1.6759	35.5641
	3.00	4.00	-3.19778	-20.6062	14.2106

Appendix 1B (Chapter 4): Mean difference and 95% confidence intervals of all statistical comparisons. In bold are highlighted comparisons identified by ANOVA and Tukey's post-hoc test as statistically significant (p≤0.05). In green are highlighted cases where a larger sample size may have potentially resulted in a statistically significant mean difference

1.00: 5mM D-glucose; **2.00:** 25mM D-glucose; **3.00:** 30mM D-glucose; **4.00:** 5mM D-glucose+ 25mM L-glucose.

		TGF-β1 test		
24h		Mean Difference	95% Confidence Interval	
(I) condition	(J) condition	(I-J)	Lower Bound	Upper Bound
1.00	2.00	-.00763	-.1009	.0856
	3.00	-.06593	-.1592	.0273
	4.00	**-.14683***	**-.2401**	**-.0536**
2.00	3.00	-.05830	-.1515	.0349
	4.00	**-.13920***	**-.2324**	**-.0460**
3.00	4.00	-.08090	-.1741	.0123
48h		Mean Difference	95% Confidence Interval	
(I) condition	(J) condition	(I-J)	Lower Bound	Upper Bound
1.00	2.00	-.02727	-.0565	.0019
	3.00	-.00398	-.0332	.0252
	4.00	-.00933	-.0385	.0199
2.00	3.00	.02328	-.0059	.0525
	4.00	.01793	-.0113	.0471
3.00	4.00	-.00535	-.0345	.0238
72h		Mean Difference	95% Confidence Interval	
(I) condition	(J) condition	(I-J)	Lower Bound	Upper Bound
1.00	2.00	-.09000	-.2367	.0567
	3.00	**-.15997***	**-.3067**	**-.0133**
	4.00	.02795	-.1187	.1746
2.00	3.00	-.06997	-.2167	.0767
	4.00	.11795	-.0287	.2646
3.00	4.00	**.18792***	**.0412**	**.3346**

		p-SMAD test		
24h		Mean Difference	95% Confidence Interval	
(I) condition	(J) condition	(I-J)	Lower Bound	Upper Bound
1.00	2.00	-34.10000	-111.2807	43.0807
	3.00	**-77.32500***	**-154.5057**	**-.1443**

			Mean Difference	95% Confidence Interval	
		(I) condition	(J) condition	(I-J)	Lower Bound	Upper Bound

	(I) condition	(J) condition	Mean Difference (I-J)	95% Confidence Interval Lower Bound	Upper Bound
		4.00	-51.55000	-128.7307	25.6307
	2.00	3.00	-43.22500	-120.4057	33.9557
		4.00	-17.45000	-94.6307	59.7307
	3.00	4.00	25.77500	-51.4057	102.9557
48h	(I) condition	(J) condition	Mean Difference (I-J)	Lower Bound	Upper Bound
	1.00	2.00	-26.15000	-71.0511	18.7511
		3.00	**-45.50000***	**-90.4011**	**-.5989**
		4.00	**-52.57500***	**-97.4761**	**-7.6739**
	2.00	3.00	-19.35000	-64.2511	25.5511
		4.00	-26.42500	-71.3261	18.4761
	3.00	4.00	-7.07500	-51.9761	37.8261
72h	(I) condition	(J) condition	Mean Difference (I-J)	Lower Bound	Upper Bound
	1.00	2.00	-18.90000	-49.7390	11.9390
		3.00	**-45.70000***	**-76.5390**	**-14.8610**
		4.00	**-38.50000***	**-69.3390**	**-7.6610**
	2.00	3.00	-26.80000	-57.6390	4.0390
		4.00	-19.60000	-50.4390	11.2390
	3.00	4.00	7.20000	-23.6390	38.0390

Collagen1α1 test					
24h	(I) condition	(J) condition	Mean Difference (I-J)	95% Confidence Interval Lower Bound	Upper Bound
	1.00	2.00	.14214	-1.0174	1.3016
		3.00	.40871	-.7508	1.5682
		4.00	.38200	-.7775	1.5415
	2.00	3.00	.26657	-.8929	1.4261
		4.00	.23986	-.9196	1.3994
	3.00	4.00	-.02671	-1.1862	1.1328
48h	(I) condition	(J) condition	Mean Difference (I-J)	Lower Bound	Upper Bound
	1.00	2.00	.13757	-1.2248	1.5000
		3.00	.14343	-1.2190	1.5058
		4.00	-.11257	-1.4750	1.2498
	2.00	3.00	.00586	-1.3565	1.3682
		4.00	-.25014	-1.6125	1.1122
	3.00	4.00	-.25600	-1.6184	1.1064
72h	(I) condition	(J) condition	Mean Difference (I-J)	Lower Bound	Upper Bound
	1.00	2.00	.14543	-1.3056	1.5965

			Mean Difference	95% Confidence Interval	
		3.00	.21200	-1.2391	1.6631
		4.00	.01629	-1.4348	1.4673
	2.00	3.00	.06657	-1.3845	1.5176
		4.00	-.12914	-1.5802	1.3219
	3.00	4.00	-.19571	-1.6468	1.2553

PAI-1 test					
24h			Mean Difference	95% Confidence Interval	
	(I) condition	(J) condition	(I-J)	Lower Bound	Upper Bound
	1.00	2.00	.03029	-.6282	.6888
		3.00	.13586	-.5226	.7943
		4.00	.11643	-.5420	.7749
	2.00	3.00	.10557	-.5529	.7640
		4.00	.08614	-.5723	.7446
	3.00	4.00	-.01943	-.6779	.6390
48h			Mean Difference	95% Confidence Interval	
	(I) condition	(J) condition	(I-J)	Lower Bound	Upper Bound
	1.00	2.00	.40614	-.4914	1.3037
		3.00	.39286	-.5047	1.2904
		4.00	.32386	-.5737	1.2214
	2.00	3.00	-.01329	-.9108	.8842
		4.00	-.08229	-.9798	.8152
	3.00	4.00	-.06900	-.9665	.8285
72h			Mean Difference	95% Confidence Interval	
	(I) condition	(J) condition	(I-J)	Lower Bound	Upper Bound
	1.00	2.00	-.05814	-.8646	.7484
		3.00	.01143	-.7951	.8179
		4.00	.08629	-.7202	.8928
	2.00	3.00	.06957	-.7369	.8761
		4.00	.14443	-.6621	.9509
	3.00	4.00	.07486	-.7316	.8814

MMP-9 test					
24h			Mean Difference	95% Confidence Interval	
	(I) condition	(J) condition	(I-J)	Lower Bound	Upper Bound
	1.00	2.00	-.02014	-.4024	.3621
		3.00	-.02029	-.4026	.3620
		4.00	.00957	-.3727	.3919
	2.00	3.00	-.00014	-.3824	.3821
		4.00	.02971	-.3526	.4120

		Mean Difference	95% Confidence Interval	
(I) condition	(J) condition	(I-J)	Lower Bound	Upper Bound
3.00	4.00	.02986	-.3524	.4121

48h

		Mean Difference	95% Confidence Interval	
(I) condition	(J) condition	(I-J)	Lower Bound	Upper Bound
1.00	2.00	.05271	-.5428	.6482
	3.00	-.32014	-.9157	.2754
	4.00	-.00471	-.6002	.5908
2.00	3.00	-.37286	-.9684	.2227
	4.00	-.05743	-.6529	.5381
3.00	4.00	.31543	-.2801	.9109

72h

		Mean Difference	95% Confidence Interval	
(I) condition	(J) condition	(I-J)	Lower Bound	Upper Bound
1.00	2.00	-.09529	-1.5998	1.4092
	3.00	-.24571	-1.7502	1.2588
	4.00	-.69886	-2.2033	.8056
2.00	3.00	-.15043	-1.6549	1.3541
	4.00	-.60357	-2.1081	.9009
3.00	4.00	-.45314	-1.9576	1.0513

TIMP-1 test				

24h

		Mean Difference	95% Confidence Interval	
(I) condition	(J) condition	(I-J)	Lower Bound	Upper Bound
1.00	2.00	.06229	-.3889	.5134
	3.00	.17443	-.2767	.6256
	4.00	.15386	-.2973	.6050
2.00	3.00	.11214	-.3390	.5633
	4.00	.09157	-.3596	.5427
3.00	4.00	-.02057	-.4717	.4306

48h

		Mean Difference	95% Confidence Interval	
(I) condition	(J) condition	(I-J)	Lower Bound	Upper Bound
1.00	2.00	.15214	-.2514	.5557
	3.00	.04671	-.3569	.4503
	4.00	.07171	-.3319	.4753
2.00	3.00	-.10543	-.5090	.2982
	4.00	-.08043	-.4840	.3232
3.00	4.00	.02500	-.3786	.4286

72h

		Mean Difference	95% Confidence Interval	
(I) condition	(J) condition	(I-J)	Lower Bound	Upper Bound
1.00	2.00	.00843	-1.4029	1.4198
	3.00	.08400	-1.3274	1.4954
	4.00	-.59929	-2.0107	.8121
2.00	3.00	.07557	-1.3358	1.4869

	4.00	-.60771	-2.0191	.8037
3.00	4.00	-.68329	-2.0947	.7281

IL-6 test				
24h				
		Mean Difference	95% Confidence Interval	
(I) condition	(J) condition	(I-J)	Lower Bound	Upper Bound
1.00	2.00	9188.39810	-1359.4271	19736.2233
	3.00	**-21829.36366***	**-32377.1888**	**-11281.5385**
	4.00	**-29431.32566***	**-39979.1508**	**-18883.5005**
2.00	3.00	**-31017.76175***	**-41565.5869**	**-20469.9366**
	4.00	**-38619.72376***	**-49167.5489**	**-28071.8986**
3.00	4.00	-7601.96200	-18149.7872	2945.8632
48h				
		Mean Difference	95% Confidence Interval	
(I) condition	(J) condition	(I-J)	Lower Bound	Upper Bound
1.00	2.00	2893.24846	-4678.2774	10464.7743
	3.00	3774.10726	-3797.4186	11345.6331
	4.00	**-14633.34744***	**-22204.8733**	**-7061.8216**
2.00	3.00	880.85880	-6690.6671	8452.3847
	4.00	**-17526.59590***	**-25098.1218**	**-9955.0700**
3.00	4.00	**-18407.45470***	**-25978.9806**	**-10835.9288**
72h				
		Mean Difference	95% Confidence Interval	
(I) condition	(J) condition	(I-J)	Lower Bound	Upper Bound
1.00	2.00	-3782.40936	-21173.0090	13608.1903
	3.00	734.13111	-16656.4686	18124.7308
	4.00	**-31429.15992***	**-48819.7596**	**-14038.5603**
2.00	3.00	4516.54047	-12874.0592	21907.1401
	4.00	**-27646.75056***	**-45037.3502**	**-10256.1509**
3.00	4.00	**-32163.29103***	**-49553.8907**	**-14772.6914**

MCP-1 test				
24h				
		Mean Difference	95% Confidence Interval	
(I) condition	(J) condition	(I-J)	Lower Bound	Upper Bound
1.00	2.00	616.26714	-452.2579	1684.7922
	3.00	**-1514.17213***	**-2582.6972**	**-445.6471**
	4.00	-841.02549	-1909.5505	227.4995
2.00	3.00	**-2130.43927***	**-3198.9643**	**-1061.9143**
	4.00	**-1457.29262***	**-2525.8176**	**-388.7676**
3.00	4.00	673.14665	-395.3784	1741.6717
48h				
		Mean Difference	95% Confidence Interval	
(I) condition	(J) condition	(I-J)	Lower Bound	Upper Bound

(I) condition	(J) condition	Mean Difference (I-J)	95% Confidence Interval Lower Bound	95% Confidence Interval Upper Bound
1.00	2.00	-718.77010	-2728.0239	1290.4837
	3.00	-230.03704	-2239.2909	1779.2168
	4.00	-1692.00146	-3701.2553	317.2524
2.00	3.00	488.73306	-1520.5208	2497.9869
	4.00	-973.23135	-2982.4852	1036.0225
3.00	4.00	-1461.96441	-3471.2183	547.2894

72h		Mean Difference	95% Confidence Interval	
(I) condition	(J) condition	(I-J)	Lower Bound	Upper Bound
1.00	2.00	-2309.34163	-6159.8016	1541.1183
	3.00	-312.69933	-4163.1593	3537.7606
	4.00	-3624.16190	-7474.6219	226.2981
2.00	3.00	1996.64230	-1853.8177	5847.1023
	4.00	-1314.82027	-5165.2802	2535.6397
3.00	4.00	-3311.46257	-7161.9225	538.9974

		KIM-1 test		
24h		Mean Difference	95% Confidence Interval	
(I) condition	(J) condition	(I-J)	Lower Bound	Upper Bound
1.00	2.00	67403.77780	-32137.9927	166945.5483
	3.00	**-236811.39282***	**-336353.1633**	**-137269.6223**
	4.00	**-227605.51217***	**-327147.2827**	**-128063.7417**
2.00	3.00	**-304215.17062***	**-403756.9411**	**-204673.4001**
	4.00	**-295009.28997***	**-394551.0605**	**-195467.5195**
3.00	4.00	9205.88065	-90335.8899	108747.6512
48h		Mean Difference	95% Confidence Interval	
(I) condition	(J) condition	(I-J)	Lower Bound	Upper Bound
1.00	2.00	27457.88487	-57802.8218	112718.5915
	3.00	13958.66327	-71302.0434	99219.3699
	4.00	-29333.75385	-114594.4605	55926.9528
2.00	3.00	-13499.22160	-98759.9282	71761.4850
	4.00	-56791.63872	-142052.3453	28469.0679
3.00	4.00	-43292.41712	-128553.1237	41968.2895
72h		Mean Difference	95% Confidence Interval	
(I) condition	(J) condition	(I-J)	Lower Bound	Upper Bound
1.00	2.00	-19089.24083	-99049.4443	60870.9626
	3.00	43256.52822	-36703.6753	123216.7317
	4.00	-23788.57195	-103748.7754	56171.6315
2.00	3.00	62345.76905	-17614.4344	142305.9725
	4.00	-4699.33112	-84659.5346	75260.8724
3.00	4.00	-67045.10017	-147005.3036	12915.1033

			Endostatin test		
24h			Mean Difference	95% Confidence Interval	
	(I) condition	(J) condition	(I-J)	Lower Bound	Upper Bound
	1.00	2.00	19617.00430	-94320.1801	133554.1887
		3.00	**-119021.25518***	**-232958.4396**	**-5084.0708**
		4.00	**-189370.67873***	**-303307.8631**	**-75433.4944**
	2.00	3.00	**-138638.25948***	**-252575.4439**	**-24701.0751**
		4.00	**-208987.68303***	**-322924.8674**	**-95050.4987**
	3.00	4.00	-70349.42355	-184286.6079	43587.7608
48h			Mean Difference	95% Confidence Interval	
	(I) condition	(J) condition	(I-J)	Lower Bound	Upper Bound
	1.00	2.00	121799.22700	-81108.7027	324707.1567
		3.00	149210.76783	-53697.1619	352118.6975
		4.00	39498.49100	-163409.4387	242406.4207
	2.00	3.00	27411.54083	-175496.3889	230319.4705
		4.00	-82300.73600	-285208.6657	120607.1937
	3.00	4.00	-109712.27683	-312620.2065	93195.6529
72h			Mean Difference	95% Confidence Interval	
	(I) condition	(J) condition	(I-J)	Lower Bound	Upper Bound
	1.00	2.00	20594.77162	-158345.7453	199535.2885
		3.00	62546.60272	-116393.9142	241487.1196
		4.00	-23485.91318	-202426.4301	155454.6037
	2.00	3.00	41951.83110	-136988.6858	220892.3480
		4.00	-44080.68480	-223021.2017	134859.8321
	3.00	4.00	-86032.51590	-264973.0328	92908.0010

Appendix 1C (Chapter 5): Mean difference and 95% confidence intervals of all statistical comparisons. In bold are highlighted comparisons identified by ANOVA and Tukey's post-hoc test as statistically significant (p≤0.05). In green are highlighted cases where a larger sample size may have potentially resulted in a statistically significant mean difference

1.00: 5mM D-glucose; **2.00:** 25mM D-glucose; **3.00:** 30mM D-glucose; **4.00:** 5mM D-glucose+ 25mM L-glucose.

		miR-216a-5p test		
24h		Mean Difference	95% Confidence Interval	
(I) condition	(J) condition	(I-J)	Lower Bound	Upper Bound
1.00	2.00	-.10467	-.6434	.4340
	3.00	-.10967	-.6484	.4290
	4.00	.26400	-.2747	.8027
2.00	3.00	-.00500	-.5437	.5337
	4.00	.36867	-.1700	.9074
3.00	4.00	.37367	-.1650	.9124
48h		Mean Difference	95% Confidence Interval	
(I) condition	(J) condition	(I-J)	Lower Bound	Upper Bound
1.00	2.00	.17933	-.0829	.4415
	3.00	**.26433***	**.0021**	**.5265**
	4.00	.11300	-.1492	.3752
2.00	3.00	.08500	-.1772	.3472
	4.00	-.06633	-.3285	.1959
3.00	4.00	-.15133	-.4135	.1109
72h		Mean Difference	95% Confidence Interval	
(I) condition	(J) condition	(I-J)	Lower Bound	Upper Bound
1.00	2.00	.25933	-.2037	.7223
	3.00	**.48567***	**.0227**	**.9487**
	4.00	-.11600	-.5790	.3470
2.00	3.00	.22633	-.2367	.6893
	4.00	-.37533	-.8383	.0877
3.00	4.00	**-.60167***	**-1.0647**	**-.1387**

Appendix 2: Average Ct values of triplicate qPCR samples for Col1a1, PAI-1, TIMP-1, MMP-9 and GAPDH

	Ct values	Samples	Col1a1	PAI-1	MMP-9	TIMP-1	GAPDH
24h	5mM D-Glu	1	24.33	21.83	28.27	19.25	15.79
		2	24.36	21.73	28.18	19.18	15.64
		3	23.82	21.74	28.18	19.40	15.97
		4	23.92	21.42	27.71	19.15	15.51
		5	32.87	22.62	28.07	19.81	15.21
		6	33.26	22.41	28.07	19.71	14.93
		7	33.74	22.64	28.27	19.70	15.20
	25mM D-Glu	8	24.24	21.74	27.95	19.26	15.58
		9	24.08	21.51	27.69	19.07	15.44
		10	23.95	21.47	27.77	19.04	15.40
		11	24.10	21.44	28.07	19.34	15.67
		12	32.42	22.47	27.92	19.70	15.05
		13	32.61	22.40	27.98	19.55	14.97
		14	32.40	22.52	28.03	19.61	15.06
	30mM D-Gluc	15	23.89	21.35	27.49	18.87	15.31
		16	24.43	20.73	27.28	18.85	14.43
		17	23.97	21.31	27.41	18.94	15.21
		18	24.46	21.37	27.29	19.00	14.96
		19	33.18	22.63	27.97	19.66	15.09
		20	32.85	22.54	27.92	19.56	15.03
		21	32.27	22.38	27.85	19.71	14.94
	30mM L-Gluc	22	24.59	20.79	27.85	19.16	14.84
		23	23.66	21.32	27.45	18.92	15.21
		24	25.22	21.99	27.90	19.50	15.61
		25	24.05	21.35	27.43	18.95	15.29
		26	32.67	22.92	27.97	19.66	14.94
		27	32.81	22.86	28.26	19.71	15.23
		28	32.70	22.53	28.01	19.60	15.06
48h	5mM D-Glu	29	23.98	21.70	27.47	19.02	15.68
		30	24.41	20.56	27.91	19.08	15.98
		31	24.28	21.90	27.61	18.85	15.57
		32	24.32	22.08	28.24	18.97	15.77
		33	32.99	23.29	28.09	19.24	15.22
		34	32.70	23.60	28.33	19.19	15.40
		35	32.57	23.53	28.13	19.26	15.30
	25mM D-Glu	36	24.10	22.00	27.44	18.87	15.49
		37	24.25	21.72	27.70	18.99	15.41
		38	24.04	21.90	27.58	18.88	15.51
		39	24.48	22.13	27.95	19.08	15.61
		40	32.26	23.49	27.93	19.44	15.27
		41	32.57	23.89	28.29	19.48	15.33
		42	33.04	23.68	28.11	19.39	15.11
	30mM D-Gluc	43	25.04	22.32	27.90	19.31	15.92
		44	23.98	21.97	27.05	18.73	15.60
		45	24.47	22.08	26.78	18.86	15.64
		46	24.18	21.96	27.27	18.73	15.56
		47	32.55	23.71	28.00	19.63	15.35
		48	32.51	23.51	27.96	19.05	15.20
		49	32.52	23.67	28.00	19.59	15.20
	30mM L-Gluc	50	23.66	21.89	27.49	18.77	15.70
		51	23.72	21.68	27.64	18.65	15.48
		52	24.37	22.19	27.72	19.31	15.84
		53	24.47	21.92	28.26	19.35	15.76
		54	32.73	23.50	27.87	19.26	15.18
		55	33.03	23.61	28.22	19.40	15.36
		56	32.88	24.05	28.43	19.74	15.60
72h	5mM D-Glu	57	25.37	23.41	28.54	19.48	16.21
		58	25.04	22.75	28.01	19.02	15.78
		59	24.94	22.93	28.13	18.99	15.81
		60	24.76	22.48	27.58	18.72	15.57
		61	32.84	24.09	28.26	19.46	15.79
		62	33.80	24.33	28.56	19.40	15.82

		63	32.55	24.07	28.33	19.18	15.57
	25mM D-Glu	64	25.13	23.11	27.95	18.79	15.72
		65	25.19	22.07	27.66	18.87	15.53
		66	25.62	23.60	28.21	19.50	16.59
		67	25.44	22.51	28.01	19.23	15.81
		68	33.75	24.40	28.24	19.54	15.63
		69	33.11	24.16	28.26	19.21	15.56
		70	33.37	24.30	28.16	19.18	15.54
	30mM D-Gluc	71	25.28	21.99	27.29	18.98	15.42
		72	25.23	22.97	27.42	18.77	15.55
		73	25.05	22.63	27.29	18.96	15.70
		74	24.79	22.74	27.49	18.74	15.48
		75	34.47	24.04	27.86	19.16	15.38
		76	33.61	24.28	28.22	19.48	15.63
		77	33.62	24.54	28.24	19.59	15.88
	30mM L-Gluc	78	25.10	21.88	27.71	18.73	15.12
		79	25.25	23.37	27.58	18.99	15.96
		80	29.68	28.52	31.33	22.38	21.56
		81	25.10	22.06	27.89	18.16	14.36
		82	32.83	24.01	27.90	19.02	15.36
		83	33.02	23.97	27.86	19.15	15.46
		84	33.39	24.33	28.31	19.29	15.71

Appendix 3: Effect of hyperglycaemia on the protein expression of PAI-1 and collagen-1

The time-course effects of different concentrations of glucose on the expression of ECM proteins was evaluated by Western blot as shown below in Figures 1A (24h), Figure 2A (48h) and 3A (72h).

Although there was a decrease in the expression of PAI-1 in cell exposed to 30 mM D-glucose, there were no significant difference in PAI-1 expression between the control (5 mM D-glucose), 25 mM D-glucose, 30 mM D-glucose and 5 mM D-glucose + 25 mM L-glucose samples after 24 hours (Figure 1B). At 48 h 30 mM D-glucose and 5 mM D-glucose+25 mM L-glucose samples showed similar levels of PAI-1 expression to the control (Figure 2B). A decrease of PAI-1 expression was observed in cells exposed to 25 mM D-glucose, however the difference was not statistically significant. Although at 72 hours the expression of PAI-1 in response to 30 mM D-glucose showed an increase of 19%, there were no statistically significant difference in PAI-1 expression between the control and any of the treatments (Figure 3B).

There was no significant difference in the expression of collagen-1 between the control (5 mM D-glucose), 25mM D-glucose and 5 mM D-glucose + 25 mM L-glucose (Figure 1B). The expression of collagen-1 in cells exposed to 30mM D-glucose was similar to that of the control cells, with a decrease of approximately 20%. There was no change in collagen-1 expression at 48 h in any of the treatment conditions (Figure 2B). Similarly, at 72h 30mM D-glucose and 5 mM D-glucose+25 mM L-glucose had no effect on the expression of collagen-1. However, there was a slightly increse of collagen-1 expression in response to 25mM D-glucose (Figure 3B).
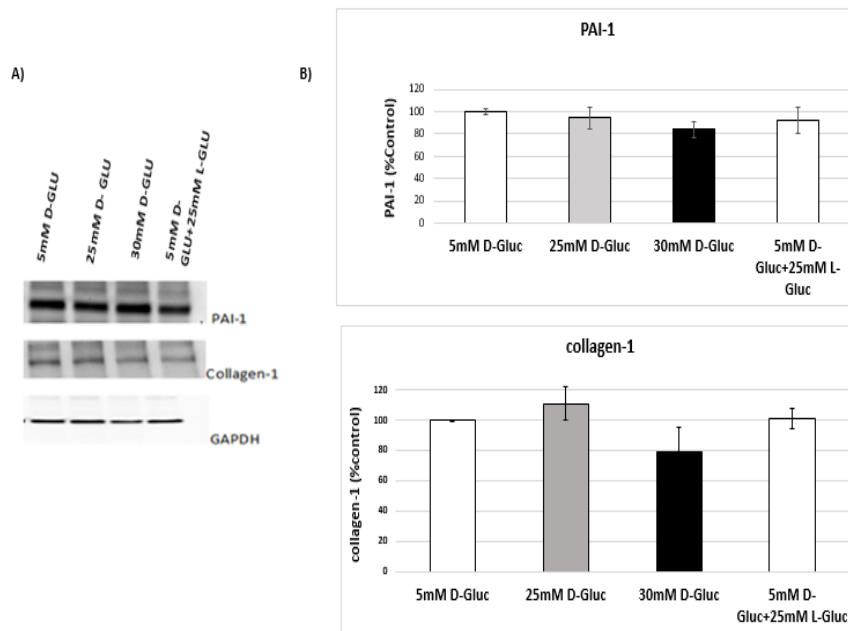
Figure 1: Effect of hyperglycaemia on the expression of PAI-1 and Collagen-1 at 24 hours. A) Representative Western blot images of PAI-1 and Collagen-1 protein expression in lysates from cell exposed to hyperglycemia for 24h. B) Densitometric analysis of Collagen-1 and PAI-1 bands, normalised to GAPDH; (n=6).
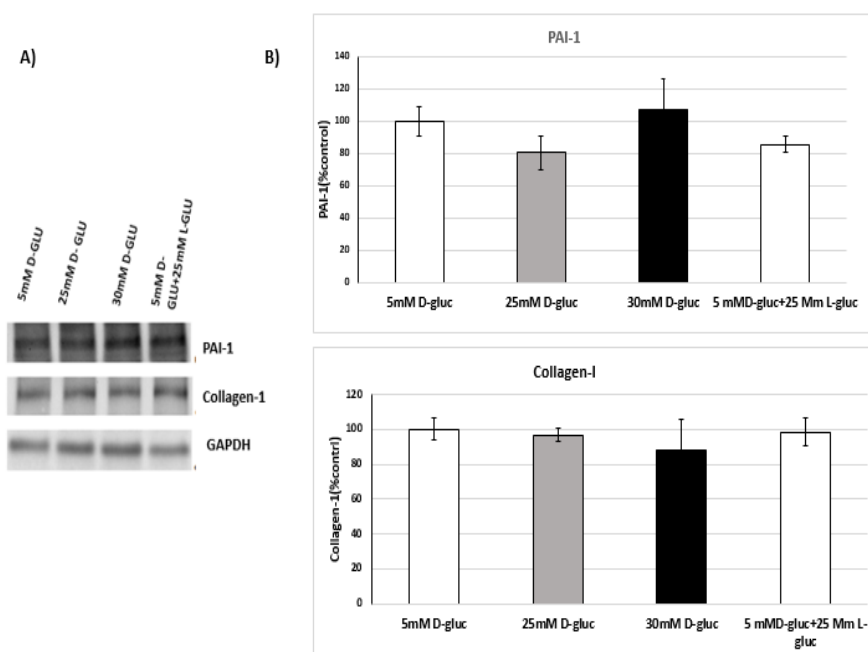

Figure 2: Effect of hyperglycaemia on the expression of PAI-1 and Collagen-1 at 48 hours. A) Representative Western blot images of PAI-1 and Collagen-1 protein expression in lysates from cell exposed to hyperglycemia for 48h. B) Densitometric analysis of Collagen-1 and PAI-1 bands, normalised to GAPDH; (n=6).
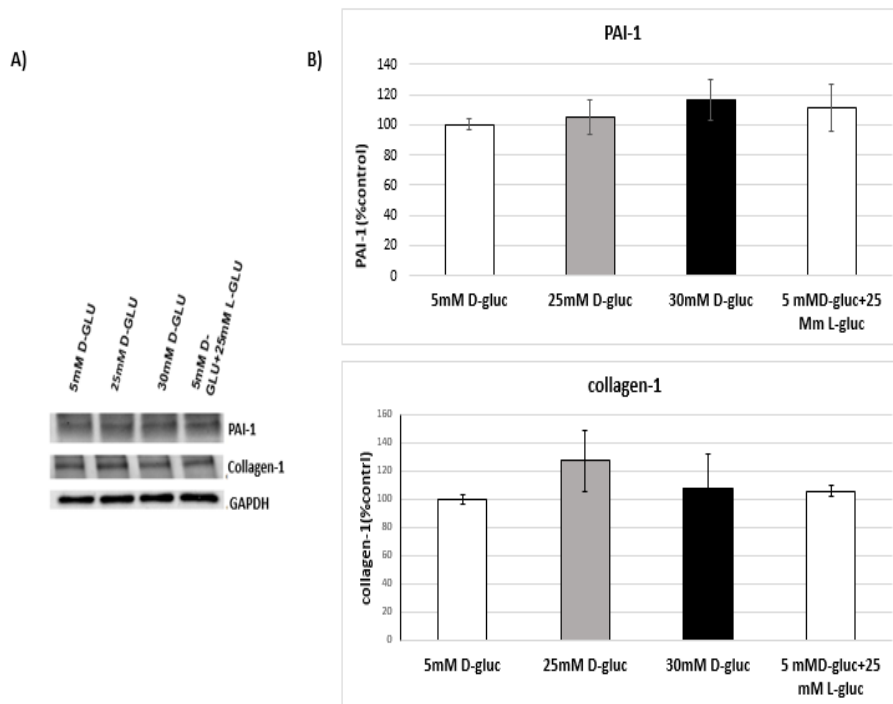
Figure 3: Effect of hyperglycaemia on the expression of PAI-1 and Collagen-1 at 72 hours. A) Representative Western blot images of PAI-1 and Collagen-1 protein expression in lysates from cell exposed to hyperglycemia for 24h. B) Densitometric analysis of Collagen-1 and PAI-1 bands, normalised to GAPDH; (n=6).

Appendix 4: MMP-9 gelatinase activity in response to hyperglycaemia

MMP-9 gelatinase activity was evaluated by gelatine zymography gels in media from cells exposed to varying concentrations of glucose for 72h (Figure 4A). Scanning electron densitometry analysis demonstrated that there was a significant difference in the expression of gelatinases in cell media between the control and 25mM D-glucose samples (Figure 4B). In contrast to 30 mM D-glucose, 25 mM D-glucose induced a significant 20% increase in gelatinase activity.
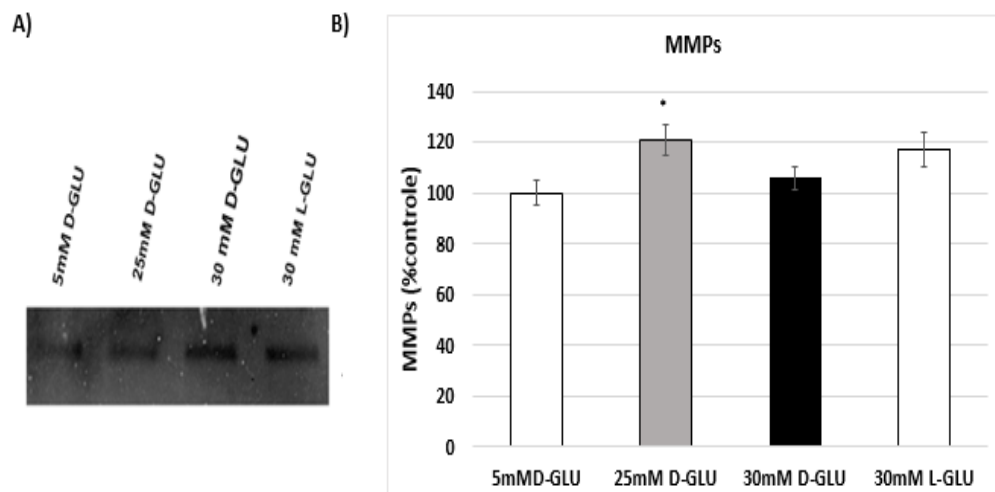

Figure 4: Gelatine zymography of media from cells exposed to varying concentrations of glucose
A) Representative image of inverted gelatine zymography gel MMP-9 bands. B) Densitometric analysis of MMP-9 bands (*p<0.05; n=4).

Appendix 5: Human Fibrosis miRNome miScript miRNA PCR Array layout

(Qiagen, # MIHS-117Z)

Wells A1 to G12 (**1–84**) each contain a miScript Primer Assay for a human fibrosis related mature miRNA:

cel-miR-39-3p, hsa-let-7d-5p, hsa-miR-1-3p, hsa-miR-101-3p, hsa-miR-107, hsa-miR-10a-5p, hsa-miR-10b-5p, hsa-miR-122-5p, hsa-miR-125b-5p, hsa-miR-126-3p, hsa-miR-129-5p, hsa-miR-132-3p, hsa-miR-133a-3p, hsa-miR-141-3p, hsa-miR-142-3p, hsa-miR-143-3p, hsa-miR-145-5p, hsa-miR-146a-5p, hsa-miR-146b-5p, hsa-miR-150-5p, hsa-miR-155-5p, hsa-miR-15b-5p, hsa-miR-16-5p, hsa-miR-17-5p, hsa-miR-18a-5p, hsa-miR-192-5p, hsa-miR-194-5p, hsa-miR-195-5p, hsa-miR-196a-5p, hsa-miR-199a-5p, hsa-miR-199b-5p, hsa-miR-19a-3p, hsa-miR-19b-3p, hsa-miR-200a-3p, hsa-miR-200b-3p, hsa-miR-203a-3p, hsa-miR-204-5p, hsa-miR-208a-3p, hsa-miR-20a-5p, hsa-miR-21-5p, hsa-miR-211-5p, hsa-miR-215-5p, hsa-miR-216a-5p, hsa-miR-217, hsa-miR-223-3p, hsa-miR-23a-3p, hsa-miR-25-3p, hsa-miR-26a-5p, hsa-miR-26b-5p, hsa-miR-27a-3p, hsa-miR-27b-3p, hsa-miR-29a-3p, hsa-miR-29b-3p, hsa-miR-29c-3p, hsa-miR-302b-3p, hsa-miR-30a-5p, hsa-miR-31-5p, hsa-miR-32-5p, hsa-miR-324-5p, hsa-miR-324-3p, hsa-miR-325, hsa-miR-328-3p, hsa-miR-335-5p, hsa-miR-338-5p, hsa-miR-34a-5p, hsa-miR-372-3p, hsa-miR-375, hsa-miR-377-3p, hsa-miR-378a-3p, hsa-miR-382-5p, hsa-miR-449a, hsa-miR-449b-5p, hsa-miR-451a, hsa-miR-491-5p, hsa-miR-5011-5p, hsa-miR-503-5p, hsa-miR-5692a, hsa-miR-590-5p, hsa-miR-661, hsa-miR-663a, hsa-miR-7-5p, hsa-miR-744-5p, hsa-miR-874-3p, hsa-miR-92a-3phsa-miR-148a-3p

Wells H1 and H2 contain replicate *C. elegans* miR-39 miScript Primer Assays that can be used as an alternative normalizer for array data (**Ce**).

Wells H3 to H8 each contain an assay for a different snoRNA/snRNA that can be used as a normalization control for the array data (**SN1**=SNORD61 assay, **SN2**=SNORD68 assay, **SN3**=SNORD72 assay, **SN4**=SNORD95 assay, **SN5**=SNORD96A assay, **SN6**=RNU6B/RNU6-2 assay).

Wells H9 and H10 contain replicate reverse transcription controls (**miRTC**). Wells H11 and H12 contain replicate positive PCR controls (**PPC**).

References

Abou Dagher, G., Harmouche, E., Jabbour, E., Bachir, R., Zebian, D. and Bou Chebl, R. (2015) 'Sepsis in hemodialysis patients.' *BMC emergency medicine*, 15 pp. 30-30.

Ahmed, N. (2005) 'Advanced glycation endproducts—role in pathology of diabetic complications.' *Diabetes Research and Clinical Practice*, 67(1) pp. 3-21.

Ahmed, S. A. and Hamed, M. A. (2015) 'Kidney injury molecule-1 as a predicting factor for inflamed kidney, diabetic and diabetic nephropathy Egyptian patients.' *Journal of Diabetes and Metabolic Disorders*, 14, 02/25

Alberts, B., Johnson, A., Lewis, J., Raff, M., Roberts, K. and Walter, P. (2002) 'The extracellular matrix of animals.' *In Molecular Biology of the Cell. 4th edition*. Garland Science,

Alelign, T. and Petros, B. (2018) 'Kidney Stone Disease: An Update on Current Concepts.' *Advances in urology*, 2018 pp. 3068365-3068365.

Alicic, R. Z., Rooney, M. T. and Tuttle, K. R. (2017) 'Diabetic kidney disease: challenges, progress, and possibilities.' *Clinical Journal of the American Society of Nephrology*, 12(12) pp. 2032-2045.

André, P. and Villain, F. (2017) 'Free radical scavenging properties of mannitol and its role as a constituent of hyaluronic acid fillers: a literature review.' *International journal of cosmetic science*, 39(4) pp. 355-360.

Aronson, D. and Rayfield, E. J. (2002) 'How hyperglycemia promotes atherosclerosis: molecular mechanisms.' *Cardiovascular diabetology*, 1 pp. 1-1.

Bai, X., Geng, J., Zhou, Z., Tian, J. and Li, X. (2016) 'MicroRNA-130b improves renal tubulointerstitial fibrosis via repression of Snail-induced epithelial-mesenchymal transition in diabetic nephropathy.' *Scientific Reports*, 6, 02/03

Baker, M. A., Davis, S. J., Liu, P., Pan, X., Williams, A. M., Iczkowski, K. A., Gallagher, S. T., Bishop, K., Regner, K. R. and Liu, Y. (2017) 'Tissue-specific microRNA expression patterns in four types of kidney disease.' *Journal of the American Society of Nephrology*, 28(10) pp. 2985-2992.

Bakris, G. L., Fonseca, V. A., Sharma, K. and Wright, E. M. (2009) 'Renal sodium–glucose transport: role in diabetes mellitus and potential clinical implications.' *Kidney international*, 75(12) pp. 1272-1277.

Bao, Y., Ao, Y., Yi, B. and Batubayier, J. (2019) 'High levels of glucose induce epithelial-mesenchymal transition in renal proximal tubular cells through PERK-eIF2α pathway.' *Chinese medical journal*, 132(7) pp. 868-872.

Baron, A. D. (2001) 'Impaired glucose tolerance as a disease.' *The American Journal of Cardiology*, 88(6, Supplement 1), 7/26/, pp. 16-19.

Barutta, F., Bruno, G., Grimaldi, S. and Gruden, G. (2015) 'Inflammation in diabetic nephropathy: moving toward clinical biomarkers and targets for treatment.' *Endocrine*, 48(3) pp. 730-742.

Batzios, S. P., Zafeiriou, D. I. and Papakonstantinou, E. (2013) 'Extracellular matrix components: An intricate network of possible biomarkers for lysosomal storage disorders?' *FEBS Letters*, 587(8), 4/17/, pp. 1258-1267.

Beckman, J. A. and Creager, M. A. (2016) 'Vascular complications of diabetes.' *Circulation research*, 118(11) pp. 1771-1785.

Bellini, M. H., Coutinho, E. L., Filgueiras, T. C., Maciel, T. T. and Schor, N. (2007) 'Endostatin expression in the murine model of ischaemia/reperfusion-induced acute renal failure.' *Nephrology*, 12(5) pp. 459-465.

Berg, J. M., Tymoczko, J. L. and Stryer, L. (2002) 'Each organ has a unique metabolic profile.' *Biochemistry*, pp. 851-854.

Bergmann, C., Guay-Woodford, L. M., Harris, P. C., Horie, S., Peters, D. J. M. and Torres, V. E. (2018) 'Polycystic kidney disease.' *Nature reviews. Disease primers*, 4(1) pp. 50-50.

Bermudez, O. I. (2004) 'Diabetes Mellitus, Diagnosis and Treatment in the Elderly.' *In* Editor-in-Chief: Luciano, M. (ed.) *Encyclopedia of Endocrine Diseases*. New York: Elsevier, pp. 661-665.

Beto, J. A. and Bansal, V. K. (2004) 'Medical nutrition therapy in chronic kidney failure: integrating clinical practice guidelines.' *Journal of American Dietetic Association*, 104(3), Mar, pp. 404-409.

Bhargava, P. and Schnellmann, R. G. (2017) 'Mitochondrial energetics in the kidney.' *Nature Reviews Nephrology*, 13(10) p. 629.

Bhattacharyya, A., Chattopadhyay, R., Mitra, S. and Crowe, S. E. (2014) 'Oxidative stress: an essential factor in the pathogenesis of gastrointestinal mucosal diseases.' *Physiological reviews*, 94(2) pp. 329-354.

Bonventre, J. V. (2012) 'Can We Target Tubular Damage to Prevent Renal Function Decline in Diabetes?' *Seminars in nephrology*, 32(5) pp. 452-462.

Bonventre, J. V. (2014) 'Kidney Injury Molecule-1: A Translational Journey.' *Transactions of the American Clinical and Climatological Association*, 125 pp. 293-299.

Boor, P., Ostendorf, T. and Floege, J. (2010) 'Renal fibrosis: novel insights into mechanisms and therapeutic targets.' *Nat Rev Nephrol*, 6(11) pp. 643-656.

Boor, P., Sebekova, K., Ostendorf, T. and Floege, J. (2007) 'Treatment targets in renal fibrosis.' *Nephrol Dial Transplant*, 22(12) pp. 3391-3407.

Borghese, M. F. A., Majowicz, M. P., Ortiz, M. C., del Rosario Passalacqua, M., Speziale, N. B. S. and Vidal, N. A. (2009) 'Expression and activity of SGLT2 in diabetes induced by streptozotocin: relationship with the lipid environment.' *Nephron Physiology*, 112(3) pp. p45-p52.

Brand, M. D., Affourtit, C., Esteves, T. C., Green, K., Lambert, A. J., Miwa, S., Pakay, J. L. and Parker, N. (2004) 'Mitochondrial superoxide: production, biological effects, and activation of uncoupling proteins.' *Free Radical Biology and Medicine*, 37(6) pp. 755-767.

Briasoulis, A. and Bakris, G. L. (2013) 'Chronic kidney disease as a coronary artery disease risk equivalent.' *Current cardiology reports*, 15(3) p. 340.

Brooks, C. R. and Bonventre, J. V. (2015) 'KIM-1/TIM-1 in proximal tubular cell immune response.' *Oncotarget*, 6(42), 12/15

Cantley, J. and Ashcroft, F. M. (2015) 'Q&A: insulin secretion and type 2 diabetes: why do β-cells fail?' *BMC biology*, 13 pp. 33-33.

Carroll, R. G. (2007) '11 - Renal System and Urinary Tract.' *In* Carroll, R. G. (ed.) *Elsevier's Integrated Physiology*. Philadelphia: Mosby, pp. 117-137.

Chacko, B. K., Benavides, G. A., Reily, C., Johnson, M. S. and Darley-Usmar, V. (2010) 'Chronic Hyperglycemia Induced Attenuation of Mitochondrial Reserve Capacity Mediates Mesangial Cell Dysfunction in Diabetes.' *Free Radical Biology and Medicine*, (49) p. S36.

Chang, A. S., Hathaway, C. K., Smithies, O. and Kakoki, M. (2016) 'Transforming growth factor-β1 and diabetic nephropathy.' *American journal of physiology. Renal physiology*, 310(8) pp. F689-F696.

Chawla, A., Chawla, R. and Jaggi, S. (2016) 'Microvasular and macrovascular complications in diabetes mellitus: Distinct or continuum?' *Indian journal of endocrinology and metabolism*, 20(4) pp. 546-551.

Che, R., Yuan, Y., Huang, S. and Zhang, A. (2013) 'Mitochondrial dysfunction in the pathophysiology of renal diseases.' *American Journal of Physiology-Renal Physiology*, 306(4) pp. F367-F378.

Chen, P., Yuan, Y., Zhang, T., Xu, B., Gao, Q. and Guan, T. (2018) 'Pentosan polysulfate ameliorates apoptosis and inflammation by suppressing activation of the p38 MAPK pathway in high glucose-treated HK-2 cells.' *International journal of molecular medicine*, 41(2) pp. 908-914.

Chen, X., Cobbs, A., George, J., Chima, A., Tuyishime, F. and Zhao, X. (2017) 'Endocytosis of albumin induces matrix metalloproteinase-9 by activating the ERK signaling pathway in renal tubule epithelial cells.' *International journal of molecular sciences*, 18(8) p. 1758.

Cheng, X., Gao, W., Dang, Y., Liu, X., Li, Y., Peng, X. and Ye, X. (2013) 'Both ERK/MAPK and TGF-Beta/Smad signaling pathways play a role in the kidney fibrosis of diabetic mice accelerated by blood glucose fluctuation.' *Journal of diabetes research*, 2013

Chow, Ozols, E., Nikolic-Paterson, D. J., Atkins, R. C. and Tesch, G. H. (2004) 'Macrophages in mouse type 2 diabetic nephropathy: correlation with diabetic state and progressive renal injury.' *Kidney international*, 65(1) pp. 116-128.

Chow, Nikolic-Paterson, D. J., Ozols, E., Atkins, R. C., Rollin, B. J. and Tesch, G. H. (2006) 'Monocyte chemoattractant protein-1 promotes the development of diabetic renal injury in streptozotocin-treated mice.' *Kidney international*, 69(1) pp. 73-80.

Chow, F. Y., Nikolic-Paterson, D. J., Ozols, E., Atkins, R. C. and Tesch, G. H. (2005) 'Intercellular adhesion molecule-1 deficiency is protective against nephropathy in type 2 diabetic db/db mice.' *Journal of the American Society of Nephrology*, 16(6) pp. 1711-1722.

Chung, A. C.-K. and Lan, H. Y. (2015) 'MicroRNAs in renal fibrosis.' *Frontiers in physiology*, 6 p. 50.

Chung, A. C. K., Zhang, H., Kong, Y.-Z., Tan, J.-J., Huang, X. R., Kopp, J. B. and Lan, H. Y. (2010) 'Advanced glycation end-products induce tubular CTGF via TGF-beta-independent Smad3 signaling.' *Journal of the American Society of Nephrology : JASN*, 21(2) pp. 249-260.

Cichy, M. C., Paiva, M. B. S., Dagli, M. L. Z., Sanches, D. S., Schor, N. and Bellini, M. (2015) 'Endostatin co-localises with MMP9-in the renal tubular cells in an experimental model ischemia/reperfusion.' *Jacobs Journal of Nephrology and Urology*, 2(2) pp. 1-7.

Cichy, M. C., Rocha, F. G. G., Tristão, V. R., Pessoa, E. A., Cenedeze, M. A., Nürmberg Junior, R., Schor, N. and Bellini, M. H. (2009) 'Collagen XVIII/endostatin expression in experimental endotoxemic acute renal failure.' *Brazilian Journal of Medical and Biological Research*, 42 pp. 1150-1155.

Conserva, F., Pontrelli, P., Accetturo, M. and Gesualdo, L. (2013) 'The pathogenesis of diabetic nephropathy: focus on microRNAs and proteomics.' *J nephrol*, 26(5) pp. 811-820.

Cooper, G. M. and Hausman, R. E. (2000) *The cell: a molecular approach.* Vol. 10. ASM press Washington, DC.

Coughlan, M. T., Nguyen, T.-V., Penfold, S. A., Higgins, G. C., Thallas-Bonke, V., Tan, S. M., Van Bergen, N. J., Sourris, K. C., Harcourt, B. E. and Thorburn, D. R. (2016) 'Mapping time-course

mitochondrial adaptations in the kidney in experimental diabetes.' *Clinical science*, 130(9) pp. 711-720.

Czajka, A. and Malik, A. N. (2016) 'Hyperglycemia induced damage to mitochondrial respiration in renal mesangial and tubular cells: implications for diabetic nephropathy.' *Redox biology*, 10 pp. 100-107.

Czajka, A., Ajaz, S., Gnudi, L., Parsade, C. K., Jones, P., Reid, F. and Malik, A. N. (2015) 'Altered Mitochondrial Function, Mitochondrial DNA and Reduced Metabolic Flexibility in Patients With Diabetic Nephropathy.' *EBioMedicine*, 2(6) pp. 499-512.

Dalal, P., Sangha, H. and Chaudhary, K. (2011) 'In peritoneal dialysis, is there sufficient evidence to make "PD first" therapy?' *International journal of nephrology*, 2011

Dasari, S. R., Oza-Frank, R. and Venkat Narayan, K. M. (2008) 'Diabetes Mellitus Prevention.' *In* Editor-in-Chief: Kris, H. (ed.) *International Encyclopedia of Public Health*. Oxford: Academic Press, pp. 146-152.

Davies, J. A. (2001) 'Extracellular Matrix.' *ENCYCLOPEDIA OF LIFE SCIENCES*, pp. 1-7.

Davis, G. E. and Senger, D. R. (2005) 'Endothelial Extracellular Matrix.' *Journal of American Heart Association*, 97 pp. 1093-1107.

Dedkova, E. N. (2015) Some Like it Hot: Cardioprotective Effect of Curcumin in Chronic Kidney Disease. Springer, 29 (2), pp 101-103.

Denby, L. and Baker, A. H. (2016) 'Targeting non-coding RNA for the therapy of renal disease.' *Current Opinion in Pharmacology*, 27, 4//, pp. 70-77.

Deshmane, S. L., Kremlev, S., Amini, S. and Sawaya, B. E. (2009) 'Monocyte chemoattractant protein-1 (MCP-1): an overview.' *Journal of interferon & cytokine research*, 29(6) pp. 313-326.

Dewanjee, S. and Bhattacharjee, N. (2018) 'MicroRNA: a new generation therapeutic target in diabetic nephropathy.' *Biochemical Pharmacology*,

Diabetes-UK. (2018) *Diabetes Prevalence 2018*. UK: Diabetes UK. [Online] [Accessed on 11 Jun 2019] https://www.diabetes.org.uk/professionals/position-statements-reports/statistics/diabetes-prevalence-2018

Dijke, P. and Heldin, C.-H. (2007) *Smad signal transduction: Smads in proliferation, differentiation and disease.* Vol. 5. Springer.

Djudjaj, S. and Boor, P. (2019) 'Cellular and molecular mechanisms of kidney fibrosis.' *Molecular Aspects of Medicine*, 65 pp. 16-36.

Docherty, N. G., O'Sullivan, O. E., Healy, D. A., Fitzpatrick, J. M. and Watson, R. W. G. (2006) 'Evidence that inhibition of tubular cell apoptosis protects against renal damage and development of fibrosis following ureteric obstruction.' *American Journal of Physiology-Renal Physiology*, 290(1) pp. F4-F13.

Du, B., Ma, L.-M., Huang, M.-B., Zhou, H., Huang, H.-L., Shao, P., Chen, Y.-Q. and Qu, L.-H. (2010) 'High glucose down-regulates miR-29a to increase collagen IV production in HK-2 cells.' *FEBS letters*, 584(4) pp. 811-816.

Duffield, J. S. (2014) 'Cellular and molecular mechanisms in kidney fibrosis.' *The Journal of clinical investigation*, 124(6) pp. 2299-2306.

Eddy, A. A. (1996) 'Molecular insights into renal interstitial fibrosis.' *Journal of the American Society of Nephrology*, 7(12) pp. 2495-2508.

Eddy, A. A. (2002) 'Plasminogen activator inhibitor-1 and the kidney.' *American Journal of Physiology-Renal Physiology*, 283(2) pp. F209-F220.

Eddy, A. A., Kim, H., López-Guisa, J., Oda, T., Soloway, P. D., McCulloch, L., Liu, E. and Wing, D. (2000) 'Interstitial fibrosis in mice with overload proteinuria: deficiency of TIMP-1 is not protective.' *Kidney international*, 58(2) pp. 618-628.

Efstratiadis, G., Divani, M., Katsioulis, E. and Vergoulas, G. (2009a) 'Renal fibrosis.' *Hippokratia*, 13(4) pp. 224-229.

Efstratiadis, G., Divani, M., Katsioulis, E. and Vergoulas, G. (2009b) 'Renal fibrosis.' *Hippokratia*, 13(4) p. 224.

Eirin, A., Lerman, A. and Lerman, L. O. (2017) 'The Emerging Role of Mitochondrial Targeting in Kidney Disease.' *Handbook of experimental pharmacology*, 240 pp. 229-250.

Eknoyan, G. and Nagy, J. (2005) 'A history of diabetes mellitus or how a disease of the kidneys evolved into a kidney disease.' *Advances in Chronic Kidney Disease*, 12(2), 4//, pp. 223-229.

Elmarakby, A. A. and Sullivan, J. C. (2012) 'Relationship between oxidative stress and inflammatory cytokines in diabetic nephropathy.' *Cardiovascular Therapeutics*, 30(1) pp. 49-59.

Evcimen, N. D. and King, G. L. (2007) 'The role of protein kinase C activation and the vascular complications of diabetes.' *Pharmacological research*, 55(6) pp. 498-510.

Farris, A. B. and Alpers, C. E. (2014) 'What is the best way to measure renal fibrosis?: A pathologist's perspective.' *Kidney international supplements*, 4(1) pp. 9-15.

Feigerlová, E. and Battaglia-Hsu, S.-F. (2017) 'IL-6 signaling in diabetic nephropathy: From pathophysiology to therapeutic perspectives.' *Cytokine & Growth Factor Reviews*, 37 pp. 57-65.

Foris, L. A. and Bashir, K. (2019) *Uremia.* Treasure Island (FL): StatPearls [Internet].

Frantz, C., Stewart, K. M. and Weaver, V. M. (2010) 'The extracellular matrix at a glance.' *Journal of Cell Science*, 123(24) p. 4195.

Fujimoto, M., Maezawa, Y., Yokote, K., Joh, K., Kobayashi, K., Kawamura, H., Nishimura, M., Roberts, A. B., Saito, Y. and Mori, S. (2003) 'Mice lacking Smad3 are protected against streptozotocin-induced diabetic glomerulopathy.' *Biochemical and biophysical research communications*, 305(4) pp. 1002-1007.

Futrakul, N. and Futrakul, P. (2017) 'Biomarker for early renal microvascular and diabetic kidney diseases.' *Renal failure*, 39(1) pp. 505-511.

García-García, P. M., Getino-Melián, M. A., Domínguez-Pimentel, V. and Navarro-González, J. F. (2014) 'Inflammation in diabetic kidney disease.' *World journal of diabetes*, 5(4) p. 431.

Gerich, J. E. (2010) 'Role of the kidney in normal glucose homeostasis and in the hyperglycaemia of diabetes mellitus: therapeutic implications.' *Diabetic Medicine*, 27(2), Feb, 2010/06/16, pp. 136-142.

Ghezzi, C., Loo, D. D. F. and Wright, E. M. (2018) 'Physiology of renal glucose handling via SGLT1, SGLT2 and GLUT2.' *Diabetologia*, 61(10) pp. 2087-2097.

Ghosh, A. K. and Vaughan, D. E. (2012) 'PAI-1 in tissue fibrosis.' *Journal of cellular physiology*, 227(2) pp. 493-507.

Goh, S.-Y. and Cooper, M. E. (2008) 'The role of advanced glycation end products in progression and complications of diabetes.' *The Journal of Clinical Endocrinology & Metabolism*, 93(4) pp. 1143-1152.

Goldin, A., Beckman, J. A., Schmidt, A. M. and Creager, M. A. (2006) 'Advanced Glycation End Products.' *American Heart Association*, 114 pp. 597-605.

Goligorsky, M. S. (2015) 'Pathogenesis of endothelial cell dysfunction in chronic kidney disease: a retrospective and what the future may hold.' *Kidney research and clinical practice*, 34(2) pp. 76-82.

Gonzalez-Avila, G., Iturria, C., Vadillo-Ortega, F., Ovalle, C. and Montano, M. (1998) 'Changes in matrix metalloproteinases during the evolution of interstitial renal fibrosis in a rat experimental model.' *Pathobiology*, 66(5) p. 196.

Gou, R., Chen, J., Sheng, S., Wang, R., Fang, Y., Yang, Z., Wang, L. and Tang, L. (2016) 'KIM-1 mediates high glucose-induced autophagy and apoptosis in renal tubular epithelial cells.' *Cellular Physiology and Biochemistry*, 38(6) pp. 2479-2488.

Grahammer, F., Schell, C. and Huber, T. B. (2013) 'The podocyte slit diaphragm—from a thin grey line to a complex signalling hub.' *Nature Reviews Nephrology*, 9(10) p. 587.

Granata, S., Dalla Gassa, A., Tomei, P., Lupo, A. and Zaza, G. (2015) 'Mitochondria: a new therapeutic target in chronic kidney disease.' *Nutrition & Metabolism*, 12 p. 49.

Green, D., Roberts, P. R., New, D. I. and Kalra, P. A. (2011) 'Sudden cardiac death in hemodialysis patients: an in-depth review.' *American Journal of Kidney Diseases*, 57(6) pp. 921-929.

Guo, L., Takino, T., Endo, Y., Domoto, T. and Sato, H. (2012) 'Shedding of kidney injury molecule-1 by membrane-type 1 matrix metalloproteinase.' *The Journal of Biochemistry*, 152(5) pp. 425-432.

Gupta, M., Chaturvedi, R. and Jain, A. (2013) 'Role of monocyte chemoattractant protein-1 (MCP-1) as an immune-diagnostic biomarker in the pathogenesis of chronic periodontal disease.' *Cytokine*, 61(3) pp. 892-897.

Ha, H. and Lee, H. B. (2005) 'Reactive oxygen species amplify glucose signalling in renal cells cultured under high glucose and in diabetic kidney.' *Nephrology*, 10 pp. S7-S10.

Haase, V. H. (2006) 'Hypoxia-inducible factors in the kidney.' *American journal of physiology. Renal physiology*, 291(2) pp. F271-F281.

Hagiwara, H., Kaizu, K., Uriu, K., Noguchi, T., Takagi, I., Qie, Y. L., Seki, T. and Ariga, T. (2003) 'Expression of type-1 plasminogen activator inhibitor in the kidney of diabetic rat models.' *Thrombosis Research*, 111(4-5) pp. 301-309.

Haller, H., Bertram, A., Nadrowitz, F. and Menne, J. (2016) 'Monocyte chemoattractant protein-1 and the kidney.' *Current opinion in nephrology and hypertension*, 25(1) pp. 42-49.

Hamm, L. L., Nakhoul, N. and Hering-Smith, K. S. (2015) 'Acid-Base Homeostasis.' *Clinical journal of the American Society of Nephrology : CJASN*, 10(12) pp. 2232-2242.

Han, D. C., Isono, M., Hoffman, B. B. and Ziyadeh, F. N. (1999) 'High glucose stimulates proliferation and collagen type I synthesis in renal cortical fibroblasts: mediation by autocrine activation of TGF-β.' *Journal of the American Society of Nephrology*, 10(9) pp. 1891-1899.

Han, W. K., Bailly, V., Abichandani, R., Thadhani, R. and Bonventre, J. V. (2002) 'Kidney Injury Molecule-1 (KIM-1): a novel biomarker for human renal proximal tubule injury.' *Kidney international*, 62(1) pp. 237-244.

Haverty, T. P., Kelly, C. J., Hines, W. H., Amenta, P. S., Watanabe, M., Harper, R. A., Kefalides, N. A. and Neilson, E. G. (1988) 'Characterization of a renal tubular epithelial cell line which secretes the autologous target antigen of autoimmune experimental interstitial nephritis.' *The Journal of Cell Biology*, 107(4) pp. 1359-1368.

Haynes, R. J. and Winearls, C. G. (2010) 'Chronic kidney disease.' *Surgery (Oxford)*, 28(11) pp. 525-529.

He, F., Peng, F., Xia, X., Zhao, C., Luo, Q., Guan, W., Li, Z., Yu, X. and Huang, F. (2014) 'MiR-135a promotes renal fibrosis in diabetic nephropathy by regulating TRPC1.' *Diabetologia*, 57(8) pp. 1726-1736.

Heldin, C.-H., Landström, M. and Moustakas, A. (2009) 'Mechanism of TGF-β signaling to growth arrest, apoptosis, and epithelial–mesenchymal transition.' *Current Opinion in Cell Biology*, 21(2) pp. 166-176.

Hertig, A., Berrou, J., Allory, Y., Breton, L., Commo, F., De Beauregard, M.-A. C., Carmeliet, P. and Rondeau, E. (2003) 'Type 1 plasminogen activator inhibitor deficiency aggravates the course of experimental glomerulonephritis through overactivation of transforming growth factor beta.' *The FASEB journal*, 17(13) pp. 1904-1906.

Hewitson, T. D., Holt, S. G. and Smith, E. R. (2017) 'Progression of tubulointerstitial fibrosis and the chronic kidney disease phenotype–role of risk factors and epigenetics.' *Frontiers in pharmacology*, 8 p. 520.

Higgins, D. F., Kimura, K., Iwano, M. and Haase, V. H. (2008) 'Hypoxia-inducible factor signaling in the development of tissue fibrosis.' *Cell cycle (Georgetown, Tex.)*, 7(9) pp. 1128-1132.

Higgins, D. F., Kimura, K., Bernhardt, W. M., Shrimanker, N., Akai, Y., Hohenstein, B., Saito, Y., Johnson, R. S., Kretzler, M. and Cohen, C. D. (2007) 'Hypoxia promotes fibrogenesis in vivo via HIF-1 stimulation of epithelial-to-mesenchymal transition.' *The Journal of clinical investigation*, 117(12) pp. 3810-3820.

Higgins, G. C. and Coughlan, M. T. (2014) 'Mitochondrial dysfunction and mitophagy: the beginning and end to diabetic nephropathy?' *British Journal of Pharmacology*, 171(8), 03/28

Hill, N. R., Fatoba, S. T., Oke, J. L., Hirst, J. A., O'Callaghan, C. A., Lasserson, D. S. and Hobbs, F. D. R. (2016) 'Global prevalence of chronic kidney disease–a systematic review and meta-analysis.' *PloS one*, 11(7) p. e0158765.

Hills, C. E. and Squires, P. E. (2010) 'TGF-β1-Induced Epithelial-to-Mesenchymal Transition and Therapeutic Intervention in Diabetic Nephropathy.' *American Journal of Nephrology*, 31(1) pp. 68-74.

Hills, C., Price, G. W., Wall, M. J., Kaufmann, T. J., Tang, S. C.-w., Yiu, W. H. and Squires, P. E. (2018) 'Transforming growth factor beta 1 drives a switch in connexin mediated cell-to-cell

communication in tubular cells of the diabetic kidney.' *Cellular Physiology and Biochemistry*, 45(6) pp. 2369-2388.

Hoffman, M. (2009) *Picture of the Kidneys*. US: WebMD. [Online] [Accessed on 02 Jul 2019] https://www.webmd.com/kidney-stones/picture-of-the-kidneys#1

Hou, X., Tian, J., Geng, J., Li, X., Tang, X., Zhang, J. and Bai, X. (2016) 'MicroRNA-27a promotes renal tubulointerstitial fibrosis via suppressing PPARγ pathway in diabetic nephropathy.' *Oncotarget*, 7(30) pp. 47760-47776.

Hsieh, P.-f., Liu, S.-F., Lee, T.-C., Huang, J.-S., Yin, L.-T., Chang, W.-T., Chuang, L.-Y., Guh, J.-Y., Hung, M.-Y. and Yang, Y.-L. (2012) 'The role of IL-7 in renal proximal tubule epithelial cells fibrosis.' *Molecular immunology*, 50(1-2) pp. 74-82.

Huang, S. S. and Huang, J. S. (2005) 'TGF-β control of cell proliferation.' *Journal of Cellular Biochemistry*, 96(3) pp. 447-462.

Ichii, O. and Horino, T. (2018) 'MicroRNAs associated with the development of kidney diseases in humans and animals.' *Journal of toxicologic pathology*, 31(1) pp. 23-34.

Ichimura, T., Brooks, C. R. and Bonventre, J. V. (2012) 'Kim-1/Tim-1 and Immune cells: Shifting Sands.' *Kidney international*, 81(9) pp. 809-811.

Ichimura, T., Asseldonk, E. J., Humphreys, B. D., Gunaratnam, L., Duffield, J. S. and Bonventre, J. V. (2008) 'Kidney injury molecule–1 is a phosphatidylserine receptor that confers a phagocytic phenotype on epithelial cells.' *The Journal of Clinical Investigation*, 118(5), 04/15

Ichinose, K., Maeshima, Y., Yamamoto, Y., Kitayama, H., Takazawa, Y., Hirokoshi, K., Sugiyama, H., Yamasaki, Y., Eguchi, K. and Makino, H. (2005) 'Antiangiogenic endostatin peptide ameliorates renal alterations in the early stage of a type 1 diabetic nephropathy model.' *Diabetes*, 54(10) pp. 2891-2903.

Ito, Y., Goldschmeding, R., Kasuga, H., Claessen, N., Nakayama, M., Yuzawa, Y., Sawai, A., Matsuo, S., Weening, J. J. and Aten, J. (2010) 'Expression patterns of connective tissue growth factor and of TGF-β isoforms during glomerular injury recapitulate glomerulogenesis.' *American Journal of Physiology-Renal Physiology*, 299(3) pp. F545-F558.

ivyrose. (2018) *The Structure of a Kidney nephron*. UK: ivyRose. [Online] [Accessed on 02 Jul 2019] https://www.ivyroses.com/TermsofUse.php

Iwano, M., Plieth, D., Danoff, T. M., Xue, C., Okada, H. and Neilson, E. G. (2002) 'Evidence that fibroblasts derive from epithelium during tissue fibrosis.' *The Journal of clinical investigation*, 110(3) pp. 341-350.

Jeong, B. Y., Uddin, M. J., Park, J. H., Lee, J. H., Lee, H. B., Miyata, T. and Ha, H. (2016) 'Novel plasminogen activator inhibitor-1 inhibitors prevent diabetic kidney injury in a mouse model.' *PLoS One*, 11(6) p. e0157012.

Jha, J. C., Banal, C., Chow, B. S. M., Cooper, M. E. and Jandeleit-Dahm, K. (2016) 'Diabetes and Kidney Disease: Role of Oxidative Stress.' *Antioxidants & redox signaling*, 25(12) pp. 657-684.

Jiang, X., Tsitsiou, E., Herrick, S. E. and Lindsay, M. A. (2010) 'MicroRNAs and the regulation of fibrosis.' *The FEBS journal*, 277(9) pp. 2015-2021.

Jiang, Z., Seo, J. Y., Ha, H., Lee, E. A., Kim, Y. S., Han, D. C., Uh, S. T., Park, C. S. and Lee, H. B. (2003) 'Reactive oxygen species mediate TGF-beta1-induced plasminogen activator inhibitor-1 upregulation in mesangial cells.' *Biochemical and Biophysical Research Communications*, 309(4), Oct 3, 2003/09/19, pp. 961-966.

Jung, G.-S., Kim, M.-K., Choe, M. S., Lee, K.-M., Kim, H.-S., Park, Y. J., Choi, H.-S., Lee, K.-U., Park, K.-G. and Lee, I.-K. (2009) 'The orphan nuclear receptor SHP attenuates renal fibrosis.' *Journal of the American Society of Nephrology*, 20(10) pp. 2162-2170.

Kamesaki, H., Nishizawa, K., Michaud, G. Y., Cossman, J. and Kiyono, T. (1998) 'TGF-β1 induces the cyclin-dependent kinase inhibitor p27Kip1 mRNA and protein in murine B cells.' *The Journal of Immunology*, 160(2) pp. 770-777.

Kanasaki, K., Taduri, G. and Koya, D. (2013) 'Diabetic nephropathy: the role of inflammation in fibroblast activation and kidney fibrosis.' *Frontiers in Endocrinology*, 4, 02/06

Kanwar, Y. S., Wada, J., Sun, L., Xie, P., Wallner, E. I., Chen, S., Chugh, S. and Danesh, F. R. (2008) 'Diabetic nephropathy: mechanisms of renal disease progression.' *Experimental Biolog and Medicine (Maywood)*, 233(1) pp. 4-11.

Kato, M. and Natarajan, R. (2015) 'MicroRNAs in diabetic nephropathy: functions, biomarkers, and therapeutic targets.' *Annals of the New York Academy of Sciences*, 1353(1) pp. 72-88.

Kato, M., Zhang, J., Wang, M., Lanting, L., Yuan, H., Rossi, J. J. and Natarajan, R. (2007) 'MicroRNA-192 in diabetic kidney glomeruli and its function in TGF-beta-induced collagen expression via inhibition of E-box repressors.' *Proceedings of the National Academy of Sciences of the United States of America*, 104(9) pp. 3432-3437.

Kato, M., Wang, L., Putta, S., Wang, M., Yuan, H., Sun, G., Lanting, L., Todorov, I., Rossi, J. J. and Natarajan, R. (2010) 'Post-transcriptional up-regulation of Tsc-22 by Ybx1, a target of miR-216a, mediates TGF-{beta}-induced collagen expression in kidney cells.' *The Journal of biological chemistry*, 285(44) pp. 34004-34015.

Kato, M., Putta, S., Wang, M., Yuan, H., Lanting, L., Nair, I., Gunn, A., Nakagawa, Y., Shimano, H., Todorov, I., Rossi, J. J. and Natarajan, R. (2009) 'TGF-beta activates Akt kinase through a microRNA-dependent amplifying circuit targeting PTEN.' *Nature cell biology*, 11(7) pp. 881-889.

Kerr, M., Bray, B., Medcalf, J., O'Donoghue, D. J. and Matthews, B. (2012) 'Estimating the financial cost of chronic kidney disease to the NHS in England.' *Nephrology Dialysis Transplantation*, 27(suppl 3) pp. iii73-iii80.

Khoshjou, F. and Dadras, F. (2014) 'Mitochondrion and its role in diabetic nephropathy.' *Iranian journal of kidney diseases*, 8(5) p. 355.

Kim, C.-S., Park, S. and Kim, J. (2017) 'The role of glycation in the pathogenesis of aging and its prevention through herbal products and physical exercise.' *Journal of exercise nutrition & biochemistry*, 21(3) pp. 55-61.

Kinnunen, A. I., Sormunen, R., Elamaa, H., Seppinen, L., Miller, R. T., Ninomiya, Y., Janmey, P. A. and Pihlajaniemi, T. (2011) 'Lack of Collagen XVIII Long Isoforms Affects Kidney Podocytes, whereas the Short Form Is Needed in the Proximal Tubular Basement Membrane.' *The Journal of Biological Chemistry*, 286(10), 12/30

Klein, T. and Bischoff, R. (2011) 'Physiology and pathophysiology of matrix metalloproteases.' *Amino acids*, 41(2) pp. 271-290.

Koesters, R., Kaissling, B., Lehir, M., Picard, N., Theilig, F., Gebhardt, R., Glick, A. B., Hähnel, B., Hosser, H., Gröne, H.-J. and Kriz, W. (2010) 'Tubular overexpression of transforming growth factor-beta1 induces autophagy and fibrosis but not mesenchymal transition of renal epithelial cells.' *The American journal of pathology*, 177(2) pp. 632-643.

Komala, M. G., Panchapakesan, U., Pollock, C. and Mather, A. (2013) 'Sodium glucose cotransporter 2 and the diabetic kidney.' *Current opinion in nephrology and hypertension*, 22(1) pp. 113-119.

Koszegi, S., Molnar, A., Lenart, L., Hodrea, J., Balogh, D. B., Lakat, T., Szkibinszkij, E., Hosszu, A., Sparding, N. and Genovese, F. (2019) 'RAAS inhibitors directly reduce diabetes-induced renal fibrosis via growth factor inhibition.' *The Journal of physiology*, 597(1) pp. 193-209.

Koyama, Y., Xu, J., Liu, X. and Brenner, D. A. (2016) 'New developments on the treatment of liver fibrosis.' *Digestive diseases*, 34(5) pp. 589-596.

Krag, S., Danielsen, C. C., Carmeliet, P., Nyengaard, J. and Wogensen, L. (2005) 'Plasminogen activator inhibitor-1 gene deficiency attenuates TGF-β1-induced kidney disease.' *Kidney International*, 68(6) pp. 2651-2666.

Krupa, A., Jenkins, R., Luo, D. D., Lewis, A., Phillips, A. and Fraser, D. (2010a) 'Loss of MicroRNA-192 promotes fibrogenesis in diabetic nephropathy.' *Journal of the American Society of Nephrology : JASN*, 21(3) pp. 438-447.

Krupa, A., Jenkins, R., Luo, D. D., Lewis, A., Phillips, A. and Fraser, D. (2010b) 'Loss of MicroRNA-192 promotes fibrogenesis in diabetic nephropathy.' *Journal of the American Society of Nephrology*, 21(3) pp. 438-447.

Kulkarni, A. B., Ward, J. M., Yaswen, L., Mackall, C. L., Bauer, S. R., Huh, C.-G., Gress, R. E. and Karlsson, S. (1995) 'Transforming growth factor-beta 1 null mice. An animal model for inflammatory disorders.' *The American journal of pathology*, 146(1) p. 264.

Kuzuya, T., Nakagawa, S., Satoh, J., Kanazawa, Y., Iwamoto, Y., Kobayashi, M., Nanjo, K., Sasaki, A., Seino, Y., Ito, C., Shima, K., Nonaka, K. and Kadowaki, T. (2002) 'Report of the Committee on the classification and diagnostic criteria of diabetes mellitus.' *Diabetes Research and Clinical Practice*, 55(1), 1//, pp. 65-85.

Lackie, P. M. (2008) 'Molecular portfolios: cells interacting with matrix in repairing airway epithelium: This editorial discusses the findings of the paper in this issue by Stevens et al.[3] pp. 1901-10.' *Clinical & Experimental Allergy*, 38(12) pp. 1840-1843.

Lameire, N., Van Biesen, W. and Vanholder, R. (2005) 'Acute renal failure.' *Lancet*, 365(9457), Jan 29-Feb 4, 2005/02/01, pp. 417-430.

Lan, H. Y. (2012) 'Transforming growth factor-β/S mad signalling in diabetic nephropathy.' *Clinical and Experimental Pharmacology and Physiology*, 39(8) pp. 731-738.

Lee, C.-C. and Huang, T.-S. (2005) 'Plasminogen activator inhibitor-1: the expression, biological functions, and effects on tumorigenesis and tumor cell adhesion and migration.' *J Cancer Mol*, 1(1) pp. 25-36.

Levey, A. S. and Coresh, J. (2012) 'Chronic kidney disease.' *Lancet*, 379(9811), Jan 14, 2011/08/16, pp. 165-180.

Levey, A. S., De Jong, P. E., Coresh, J., Nahas, M. E., Astor, B. C., Matsushita, K., Gansevoort, R. T., Kasiske, B. L., et al. (2011) 'The definition, classification, and prognosis of chronic kidney disease: a KDIGO Controversies Conference report.' *Kidney international*, 80(1) pp. 17-28.

Li, Wang, W., Huang, X. R., Oldfield, M., Schmidt, A. M., Cooper, M. E. and Lan, H. Y. (2004) 'Advanced glycation end products induce tubular epithelial-myofibroblast transition through the RAGE-ERK1/2 MAP kinase signaling pathway.' *The American journal of pathology*, 164(4) pp. 1389-1397.

Li, J. H., Huang, X. R., Zhu, H.-J., Johnson, R. and Lan, H. Y. (2003) 'Role of TGF-β signaling in extracellular matrix production under high glucose conditions.' *Kidney international*, 63(6) pp. 2010-2019.

Li, P. K., Szeto, C. C., Piraino, B., de Arteaga, J., Fan, S., Figueiredo, A. E., Fish, D. N., Goffin, E., Kim, Y.-L. and Salzer, W. (2016) 'ISPD peritonitis recommendations: 2016 update on prevention and treatment.' *Peritoneal Dialysis International*, 36(5) pp. 481-508.

Li, P. K., Szeto, C. C., Piraino, B., Bernardini, J., Figueiredo, A. E., Gupta, A., Johnson, D. W., Kuijper, E. J., Lye, W. C., Salzer, W., Schaefer, F. and Struijk, D. G. (2010) 'Peritoneal dialysis-related infections recommendations: 2010 update.' *Peritoneal Dialysis International*, 30(4), Jul-Aug, 2010/07/16, pp. 393-423.

Li, Y., Dai, C., Wu, C. and Liu, Y. (2007a) 'PINCH-1 promotes tubular epithelial-to-mesenchymal transition by interacting with integrin-linked kinase.' *Journal of the American Society of Nephrology*, 18(9) pp. 2534-2543.

Li, Y., Yang, J., Dai, C., Wu, C. and Liu, Y. (2003) 'Role for integrin-linked kinase in mediating tubular epithelial to mesenchymal transition and renal interstitial fibrogenesis.' *The Journal of clinical investigation*, 112(4) pp. 503-516.

Li, Y., Yang, J., Luo, J.-H., Dedhar, S. and Liu, Y. (2007b) 'Tubular epithelial cell dedifferentiation is driven by the helix-loop-helix transcriptional inhibitor Id1.' *Journal of the American Society of Nephrology*, 18(2) pp. 449-460.

Li, Z., Hong, Z., Peng, Z., Zhao, Y. and Shao, R. (2018) 'Acetylshikonin from Zicao ameliorates renal dysfunction and fibrosis in diabetic mice by inhibiting TGF-β1/Smad pathway.' *Human cell*, 31(3) pp. 199-209.

Liang, C.-C., Park, A. Y. and Guan, J.-L. (2007) 'In vitro scratch assay: a convenient and inexpensive method for analysis of cell migration in vitro.' *Nat. Protocols*, 2(2), 02//print, pp. 329-333.

Lim, A. I., Chan, L. Y. Y., Lai, K. N., Tang, S. C. W., Chow, C. W., Lam, M. F. and Leung, J. C. K. (2012) 'Distinct role of matrix metalloproteinase-3 in kidney injury molecule-1 shedding by kidney proximal tubular epithelial cells.' *The international journal of biochemistry & cell biology*, 44(6) pp. 1040-1050.

Lim, C. T. S., Nordin, N. Z., Fadhlina, N. Z., Anim, M. S., Kalaiselvam, T., Haikal, W. Z. and Goh, B. L. (2019) 'Rapid decline of renal function in patients with type 2 diabetes with heavy proteinuria: a report of three cases.' *BMC nephrology*, 20(1) p. 22.

Lin, J. and Curhan, G. C. (2011) 'Associations of sugar and artificially sweetened soda with albuminuria and kidney function decline in women.' *Clinical Journal of the American Society of Nephrology*, 6(1) pp. 160-166.

Lin, L., Gan, H., Zhang, H., Tang, W., Sun, Y., Tang, X., Kong, D., Zhou, J., Wang, Y. and Zhu, Y. (2014) 'MicroRNA-21 inhibits SMAD7 expression through a target sequence in the 3'untranslated region and inhibits proliferation of renal tubular epithelial cells.' *Molecular medicine reports*, 10(2) pp. 707-712.

Lipphardt, M., Song, J. W., Matsumoto, K., Dadafarin, S., Dihazi, H., Müller, G. and Goligorsky, M. S. (2017) 'The third path of tubulointerstitial fibrosis: aberrant endothelial secretome.' *Kidney international*, 92(3) pp. 558-568.

Liu, Tran, S., Sachetelli, S., Filep, J. G., Ingelfinger, J. R. and Chan, J. S. D. (2007) 'Catalase overexpression attenuates angiotensinogen expression and apoptosis in diabetic mice.' *Kidney international*, 71(9) pp. 912-923.

Liu, B., Li, C., Liu, Z., Dai, Z. and Tao, Y. (2012) 'Increasing extracellular matrix collagen level and MMP activity induces cyst development in polycystic kidney disease.' *BMC Nephrology*, 13(119) pp. 1-8.

Liu, H., Wang, X., Liu, S., Li, H., Yuan, X., Feng, B., Bai, H., Zhao, B., Chu, Y. and Li, H. (2016) 'Effects and mechanism of miR-23b on glucose-mediated epithelial-to-mesenchymal transition in diabetic nephropathy.' *The international journal of biochemistry & cell biology*, 70 pp. 149-160.

Liu, J.-H., Chen, M.-M., Huang, J.-W., Wann, H., Ho, L.-K., Pan, W. H. T., Chen, Y.-C., Liu, C.-M., Yeh, M.-Y. and Tsai, S.-K. (2010) 'Therapeutic effects and mechanisms of action of mannitol during H2O2-induced oxidative stress in human retinal pigment epithelium cells.' *Journal of Ocular Pharmacology and Therapeutics*, 26(3) pp. 249-257.

Liu, Y. (2004) 'Epithelial to mesenchymal transition in renal fibrogenesis: pathologic significance, molecular mechanism, and therapeutic intervention.' *Journal of the American Society of Nephrology*, 15(1) pp. 1-12.

Liu , Y. (2006) 'Renal fibrosis: New insights into the pathogenesis and therapeutics.' *Kidney International*, 69(2) pp. 213-217.

Liu, Y. (2010) 'New insights into epithelial-mesenchymal transition in kidney fibrosis.' *Journal of the American Society of Nephrology : JASN*, 21(2) pp. 212-222.

Liu, Y. (2011) 'Cellular and molecular mechanisms of renal fibrosis.' *Nature Reviews Nephrology*, 7(12) p. 684.

Loboda, A., Sobczak, M., Jozkowicz, A. and Dulak, J. (2016) 'TGF-β1/Smads and miR-21 in renal fibrosis and inflammation.' *Mediators of inflammation*, 2016

Lottermoser, K., Petras, S., Pöge, U., Fimmers, R., Hertfelder, H. J., Schiermeyer, B., Vetter, H. and Düsing, R. (2001) 'The fibrinolytic system in chronic renal failure.' *European journal of medical research*, 6(9) pp. 372-376.

Lovisa, S., LeBleu, V. S., Tampe, B., Sugimoto, H., Vadnagara, K., Carstens, J. L., Wu, C.-C., Hagos, Y., et al. (2015) 'Epithelial-to-mesenchymal transition induces cell cycle arrest and parenchymal damage in renal fibrosis.' *Nature medicine*, 21(9) p. 998.

Lyons, R. M., Gentry, L. E., Purchio, A. F. and Moses, H. L. (1990) 'Mechanism of activation of latent recombinant transforming growth factor beta 1 by plasmin.' *The Journal of cell biology*, 110(4) pp. 1361-1367.

López-Novoa, J. M., Martínez-Salgado, C., Rodríguez-Peña, A. B. and Hernández, F. J. L. (2010) 'Common pathophysiological mechanisms of chronic kidney disease: Therapeutic perspectives.' *Pharmacology & Therapeutics*, 128(1) pp. 61-81.

Maahs, D. M., Siwy, J., Argilés, À., Cerna, M., Delles, C., Dominiczak, A. F., Gayrard, N., Iphöfer, A., Jänsch, L. and Jerums, G. (2010) 'Urinary collagen fragments are significantly altered in diabetes: a link to pathophysiology.' *PLoS One*, 5(9) p. e13051.

Mahimainathan, L., Das, F., Venkatesan, B. and Choudhury, G. G. (2006) 'Mesangial cell hypertrophy by high glucose is mediated by downregulation of the tumor suppressor PTEN.' *Diabetes*, 55(7) pp. 2115-2125.

Makino, H., Yamasaki, Y., Haramoto, T., Shikata, K., Hironaka, K., Ota, Z. and Kanwar, Y. S. (1993) 'Ultrastructural changes of extracellular matrices in diabetic nephropathy revealed by high resolution scanning and immunoelectron microscopy.' *Laboratory investigation; a journal of technical methods and pathology*, 68(1) pp. 45-55.

Makris, K. and Spanou, L. (2016) 'Acute Kidney Injury: Definition, Pathophysiology and Clinical Phenotypes.' *The Clinical biochemist. Reviews*, 37(2) pp. 85-98.

Malgorzewicz, S., Skrzypczak-Jankun, E. and Jankun, J. (2013) 'Plasminogen activator inhibitor-1 in kidney pathology (Review).' *International Journal of Molecular Medicine*, 31(3) pp. 503-510.

Marks, J., Carvou, N. J. C., Debnam, E. S., Srai, S. K. and Unwin, R. J. (2003) 'Diabetes increases facilitative glucose uptake and GLUT2 expression at the rat proximal tubule brush border membrane.' *The Journal of physiology*, 553(1) pp. 137-145.

Masola, V., Gambaro, G., Tibaldi, E., Onisto, M., Abaterusso, C. and Lupo, A. (2011) 'Regulation of heparanase by albumin and advanced glycation end products in proximal tubular cells.' *Biochimica et Biophysica Acta (BBA) - Molecular Cell Research*, 1813(8) pp. 1475-1482.Mather, A. and Pollock, C. (2010) 'Renal glucose transporters: novel targets for hyperglycemia management.' *Nature reviews Nephrology*, 6(5) p. 307.

Mather, A. J., Pollock, C. A. and Panchapakesan, U. (2011) 'Renoprotection with sodium glucose cotransporter 2 inhibition.' *ASN Kidney Week*,

Mather, A. and Pollock, C. (2011) 'Glucose handling by the kidney.' *Kidney International*, 79 pp. S1-S6.

Matheus, A. S. d. M., Tannus, L. R. M., Cobas, R. A., Palma, C. C. S., Negrato, C. A. and Gomes, M. d. B. (2013) 'Impact of diabetes on cardiovascular disease: an update.' *International journal of hypertension*, 2013 pp. 653789-653789.

Mauer, S. M., Steffes, M. W., Ellis, E. N., Sutherland, D. E., Brown, D. M. and Goetz, F. C. (1984) 'Structural-functional relationships in diabetic nephropathy.' *The Journal of clinical investigation*, 74(4) pp. 1143-1155.

Małgorzewicz, S., Skrzypczak-Jankun, E. and Jankun, J. (2013) 'Plasminogen activator inhibitor-1 in kidney pathology.' *International journal of molecular medicine*, 31(3) pp. 503-510.

McBride, H. M., Neuspiel, M. and Wasiak, S. (2006) 'Mitochondria: More Than Just a Powerhouse.' *Current Biology*, 16(14) pp. R551-R560.

McClelland, A. D., Herman-Edelstein, M., Komers, R., Jha, J. C., Winbanks, C. E., Hagiwara, S., Gregorevic, P., Kantharidis, P. and Cooper, M. E. (2015) 'miR-21 promotes renal fibrosis in diabetic nephropathy by targeting PTEN and SMAD7.' *Clinical Science*, 129(12) pp. 1237-1249.

McFarlane, P., Gilbert, R. E., MacCallum, L. and Senior, P. (2013) 'Chronic Kidney Disease in Diabetes.' *Canadian Journal of Diabetes*, 37(Supplement 1), 2013,

McMahon, A. P. (2016) 'Development of the mammalian kidney.' *In Current topics in developmental biology*. Vol. 117. Elsevier, pp. 31-64.

Meng, X.-M., Chung, A. C. K. and Lan, H. Y. (2013) 'Role of the TGF-β/BMP-7/Smad pathways in renal diseases.' *Clinical science*, 124(4) pp. 243-254.

Meng, X.-M., Tang, P. M.-K., Li, J. and Lan, H. Y. (2015) 'TGF-β/Smad signaling in renal fibrosis.' *Frontiers in physiology*, 6 p. 82.

Meng, X. M., Huang, X. R., Xiao, J., Chen, H. y., Zhong, X., Chung, A. C. K. and Lan, H. Y. (2012) 'Diverse roles of TGF-β receptor II in renal fibrosis and inflammation in vivo and in vitro.' *The Journal of pathology*, 227(2) pp. 175-188.

Mezzano, S., Droguett, A., Burgos, M. E., Ardiles, L. G., Flores, C. A., Aros, C. A., Caorsi, I., Vío, C. P., Ruiz-Ortega, M. and Egido, J. (2003) 'Renin-angiotensin system activation and interstitial inflammation in human diabetic nephropathy.' *Kidney International*, 64 pp. S64-S70.

Morais, C., Westhuyzen, J., Pat, B., Gobe, G. and Healy, H. (2005) 'High ambient glucose is effect neutral on cell death and proliferation in human proximal tubular epithelial cells.' *American Journal of Physiology-Renal Physiology*, 289(2) pp. F401-F409.

Morcos, M., Sayed, A. A. R., Bierhaus, A., Yard, B., Waldherr, R., Merz, W., Kloeting, I., Schleicher, E., Mentz, S. and el Baki, R. F. A. (2002) 'Activation of tubular epithelial cells in diabetic nephropathy.' *Diabetes*, 51(12) pp. 3532-3544.

Morii, T., Fujita, H., Narita, T., Shimotomai, T., Fujishima, H., Yoshioka, N., Imai, H., Kakei, M. and Ito, S. (2003) 'Association of monocyte chemoattractant protein-1 with renal tubular damage in diabetic nephropathy.' *Journal of diabetes and its complications*, 17(1) pp. 11-15.

Morrisey, K., Steadman, R., Williams, J. D. and Phillips, A. O. (1999) 'Renal proximal tubular cell fibronectin accumulation in response to glucose is polyol pathway dependent.' *Kidney international*, 55(1) pp. 160-167.

Munger, J. S., Huang, X., Kawakatsu, H., Griffiths, M. J. D., Dalton, S. L., Wu, J., Pittet, J.-F., Kaminski, N., Garat, C. and Matthay, M. A. (1999) 'A mechanism for regulating pulmonary inflammation and fibrosis: the integrin αvβ6 binds and activates latent TGF β1.' *Cell*, 96(3) pp. 319-328.

Munusamy, S. and MacMillan-Crow, L. A. (2009) 'Mitochondrial superoxide plays a crucial role in the development of mitochondrial dysfunction during high glucose exposure in rat renal proximal tubular cells.' *Free Radical Biology and Medicine*, 46(8), 2009/04/15/, pp. 1149-1157.

Musiał, K. and Zwolińska, D. (2011) 'Matrix metalloproteinases (MMP-2,9) and their tissue inhibitors (TIMP-1,2) as novel markers of stress response and atherogenesis in children with chronic kidney disease (CKD) on conservative treatment.' *Cell stress & chaperones*, 16(1) pp. 97-103.

Nandhini, T. (2014) 'Molecular Mechanism in Renal Fibrosis-A Review.' *Journal of Pharmaceutical Sciences and Research*, 6(10) p. 334.

Nath, K. A. (1992) 'Tubulointerstitial changes as a major determinant in the progression of renal damage.' *American Journal of Kidney Diseases*, 20(1) pp. 1-17.

Navarro-Gonzalez, J. F. and Mora-Fernandez, C. (2008) 'The role of inflammatory cytokines in diabetic nephropathy.' *Journal of the American Society of Nephrology*, 19(3) pp. 433-442.

Navarro-González, J. F., Mora-Fernández, C., De Fuentes, M. M. and García-Pérez, J. (2011) 'Inflammatory molecules and pathways in the pathogenesis of diabetic nephropathy.' *Nature Reviews Nephrology*, 7(6) p. 327.

Nazar, C. M. J. (2014) 'Mechanism of hypertension in diabetic nephropathy.' *Journal of nephropharmacology*, 3(2) pp. 49-55.

NHS. (2018) *Statistics about organ donation*. UK: NHS blood and transplant. [Online] [Accessed on 07 Jun 2019] https://www.organdonation.nhs.uk/helping-you-to-decide/about-organ-donation/statistics-about-organ-donation/

NHS-England. (2013) *Renal Transplantation*. UK: NHS-England. [Online] [Accessed on 07 Jun 2019] https://www.england.nhs.uk/wp-content/uploads/2014/.../a07-renal-transpl-ad-0414.pdf

Nicholas, S. B., Aguiniga, E., Ren, Y., Kim, J., Wong, J., Govindarajan, N., Noda, M., Wang, W., Kawano, Y. and Collins, A. (2005) 'Plasminogen activator inhibitor-1 deficiency retards diabetic nephropathy.' *Kidney international*, 67(4) pp. 1297-1307.

NIDDK. (2018) *The Kidney Precision Medicine Project*. United States: National Institute of Diabetes and Digestive and Kidney Diseases. [Online] [Accessed on 02 Jul 2019] https://kpmp.org/Glossary/nephron/

Nogueira, A., Pires, M. J. and Oliveira, P. A. (2017) 'Pathophysiological mechanisms of renal fibrosis: a review of animal models and therapeutic strategies.' *In vivo*, 31(1) pp. 1-22.

Okamura, D. M. and Himmelfarb, J. (2009) 'Tipping the redox balance of oxidative stress in fibrogenic pathways in chronic kidney disease.' *Pediatric nephrology*, 24(12) p. 2309.

Okura, T. (2010) 'Efonidipine improves renal function and decreases proteinuria in elderly hypertensive patients in the JATOS study.' *Hypertension Research*, 33(11) p. 1112.

Orasanu, G. and Plutzky, J. (2009) 'The Pathologic Continuum of Diabetic Vascular Disease.' *Journal of the American College of Cardiology*, 53(5) pp. S35-S42.

Palatini, P. (2012) 'Glomerular hyperfiltration: a marker of early renal damage in pre-diabetes and pre-hypertension.' *Nephrol Dial Transplant*, 27(5) pp. 1708-1714.

Panchapakesan, U., Pollock, C. A. and Chen, X. M. (2004) 'The effect of high glucose and PPAR-γ agonists on PPAR-γ expression and function in HK-2 cells.' *American Journal of Physiology-Renal Physiology*, 287(3) pp. F528-F534.

Panchapakesan, U., Sumual, S., Pollock, C. A. and Chen, X. (2005) 'PPARγ agonists exert antifibrotic effects in renal tubular cells exposed to high glucose.' *American Journal of Physiology-Renal Physiology*, 289(5) pp. F1153-F1158.

Panduru, N. M., Sandholm, N., Forsblom, C., Saraheimo, M., Dahlström, E. H., Thorn, L. M., Gordin, D., Tolonen, N., Wadén, J., Harjutsalo, V., Bierhaus, A., Humpert, P. M. and Groop, P.-H. (2015) 'Kidney Injury Molecule-1 and the Loss of Kidney Function in Diabetic Nephropathy: A Likely Causal Link in Patients With Type 1 Diabetes.' *Diabetes Care*, 38(6) p. 1130.

Park, S.-H., Choi, H.-J., Lee, J.-H., Woo, C.-H., Kim, J.-H. and Han, H.-J. (2001) 'High glucose inhibits renal proximal tubule cell proliferation and involves PKC, oxidative stress, and TGF-β1.' *Kidney international*, 59(5) pp. 1695-1705.

Patel, V., Chowdhury, R. and Igarashi, P. (2009) 'Advances in the pathogenesis and treatment of polycystic kidney disease.' *Curr Opin Nephrol Hypertens*, 18(2) pp. 99-106.

Pecoits-Filho, R., Abensur, H., Betônico, C. C. R., Machado, A. D., Parente, E. B., Queiroz, M., Salles, J. E. N., Titan, S. and Vencio, S. (2016) 'Interactions between kidney disease and diabetes: dangerous liaisons.' *Diabetology & Metabolic Syndrome*, 8, 07/28

Peng, J., Zheng, H., Wang, X. and Cheng, Z. (2017) 'Upregulation of TLR4 via PKC activation contributes to impaired wound healing in high-glucose-treated kidney proximal tubular cells.' *PloS one*, 12(5) pp. e0178147-e0178147.

Perico, L., Morigi, M. and Benigni, A. (2016) 'Mitochondrial Sirtuin 3 and Renal Diseases.' *Nephron*, 134(1) pp. 14-19.

Peter, W. L., Schoolwerth, A. C., McGowan, T. and McClellan, W. M. (2003) 'Chronic kidney disease: issues and establishing programs and clinics for improved patient outcomes.' *American Journal of Kidney Diseases*, 41(5) pp. 903-924.

Phanish, M. K., Wahab, N. A., Colville-Nash, P., Hendry, B. M. and Dockrell, M. E. C. (2006) 'The differential role of Smad2 and Smad3 in the regulation of pro-fibrotic TGFβ1 responses in human proximal-tubule epithelial cells.' *Biochemical Journal*, 393(2) pp. 601-607.

Phillips, A. O. and Steadman, R. (2002) 'Diabetic nephropathy: the central role of renal proximal tubular cells in tubulointerstitial injury.' *Histology and Histopathollogy*, 17(1) pp. 247-252.

Piccoli, G. B., Alrukhaimi, M., Liu, Z.-H., Zakharova, E., Levin, A. and World Kidney Day Steering, C. (2018) 'What we do and do not know about women and kidney diseases; questions unanswered and answers unquestioned: reflection on World Kidney Day and International Woman's Day.' *BMC nephrology*, 19(1) pp. 66-66.

Pietilä, I. and Vainio, S. J. (2014) 'Kidney development: an overview.' *Nephron Experimental Nephrology*, 126(2) pp. 40-44.

Pollak, M. R., Quaggin, S. E., Hoenig, M. P. and Dworkin, L. D. (2014) 'The glomerulus: the sphere of influence.' *Clinical Journal of the American Society of Nephrology*, 9(8) pp. 1461-1469.

Pratt, A. J. and MacRae, I. J. (2009) 'The RNA-induced silencing complex: a versatile gene-silencing machine.' *Journal of Biological Chemistry*, 284(27) pp. 17897-17901.

Prodjosudjadi, W., Gerritsma, J. S. J., Klar-Mohamad, N., Gerritsen, A. F., Bruijn, J. A. and Daha, M. R. (1995) 'Production and cytokine-mediated regulation of monocyte chemoattractant protein-1 by human proximal tubular epithelial cells.' *Kidney international*, 48(5) pp. 1477-1486.

PublicHealthEngland. (2015) *Estimates of the number of people aged 16 and over with chronic kidney disease (CKD) in local and regional areas across England*. GOV.UK. [Online] [Accessed on 04th Jun 2019] https://www.gov.uk/government/publications/ckd-prevalence-estimates-for-local-and-regional-populations

Pyram, R., Kansara, A., Banerji, M. A. and Loney-Hutchinson, L. (2012) 'Chronic kidney disease and diabetes.' *Maturitas*, 71(2) pp. 94-103.

Pérez-Morales, R. E., del Pino, M. D., Valdivielso, J. M., Ortiz, A., Mora-Fernández, C. and Navarro-González, J. F. (2018) 'Inflammation in Diabetic Kidney Disease.' *Nephron*, pp. 1-5.

Qin, W., Chung, A. C. K., Huang, X. R., Meng, X.-M., Hui, D. S. C., Yu, C.-M., Sung, J. J. Y. and Lan, H. Y. (2011) 'TGF-β/Smad3 signaling promotes renal fibrosis by inhibiting miR-29.' *Journal of the American Society of Nephrology*, 22(8) pp. 1462-1474.

Quent, V. M. C., Loessner, D., Friis, T., Reichert, J. C. and Hutmacher, D. W. (2010) 'Discrepancies between metabolic activity and DNA content as tool to assess cell proliferation in cancer research.' *Journal of cellular and molecular medicine*, 14(4) pp. 1003-1013.

Rahman, M. and Smith, M. C. (1998) 'Chronic renal insufficiency: a diagnostic and therapeutic approach.' *Archives of internal Medicine*, 158(16) pp. 1743-1752.

Rahman, M., Shad, F. and Smith, M. C. (2012) 'Acute kidney injury: a guide to diagnosis and management.' *American family physician*, 86(7 pp. 631-639)

Ramasamy, R., Vannucci, S. J., Yan, S. S., Herold, K., Yan, S. F. and Schmidt, A. M. (2005) 'Advanced glycation end products and RAGE: a common thread in aging, diabetes, neurodegeneration, and inflammation.' *Glycobiology*, 15(7) pp. 16R-28R.

Rahmoune, H., Thompson, P. W., Ward, J. M., Smith, C. D., Hong, G. and Brown, J. (2005) 'Glucose transporters in human renal proximal tubular cells isolated from the urine of patients with non–insulin-dependent diabetes.' *Diabetes*, 54(12) pp. 3427-3434.

R&DSystem. (2019) *Luminex Assay Principle*. UK: R&D System. [Online] [Accessed on 08 Dec 2019] https://www.rndsystems.com/resources/technical/luminex-assay-principle

Revelo, M. P., Federspiel, C., Helderman, H. and Fogo, A. B. (2005) 'Chronic allograft nephropathy: expression and localization of PAI-1 and PPAR-γ.' *Nephrology Dialysis Transplantation*, 20(12) pp. 2812-2819.

Rhyu, D. Y., Park, J., Sharma, B. R. and Ha, H. (2012) 'Role of reactive oxygen species in transforming growth factor-beta1-induced extracellular matrix accumulation in renal tubular epithelial cells.' *Transplantation Proceedings*, 44(3) pp. 625-628.

Riegersperger, M. and Sunder-Plassmann, G. (2007) 'How to prevent progression to end stage renal disease.' *Journal of renal care*, 33(3) pp. 105-107.

Rockey, D. C., Bell, P. D. and Hill, J. A. (2015) 'Fibrosis—a common pathway to organ injury and failure.' *New England Journal of Medicine*, 372(12) pp. 1138-1149.

Romagnani, P., Remuzzi, G., Glassock, R., Levin, A., Jager, K. J., Tonelli, M., Massy, Z., Wanner, C. and Anders, H.-J. (2017) 'Chronic kidney disease.' *Nature Reviews Disease Primers*, 3 p. 17088.

Rowe, P. A., Campbell-Thompson, M. L., Schatz, D. A. and Atkinson, M. A. (2011) 'The pancreas in human type 1 diabetes.' *Seminars in immunopathology*, 33(1) pp. 29-43.

Said, S. and Hernandez, G. T. (2014) 'The link between chronic kidney disease and cardiovascular disease.' *Journal of nephropathology*, 3(3) p. 99.

Santer, R. and Calado, J. (2010) 'Familial Renal Glucosuria and SGLT2: From a Mendelian Trait to a Therapeutic Target.' *Clinical Journal of the American Society of Nephrology*, 5(1) p. 133.

Schena, F. P. and Gesualdo, L. (2005) 'Pathogenetic mechanisms of diabetic nephropathy.' *Journal of the American Society of Nephrology*, 16(3 suppl 1) pp. S30-S33.

Schena, F. P., Serino, G. and Sallustio, F. (2013) 'MicroRNAs in kidney diseases: new promising biomarkers for diagnosis and monitoring.' *Nephrology Dialysis Transplantation*, 29(4) pp. 755-763.

Schrier, R. W., Wang, W., Poole, B. and Mitra, A. (2004) 'Acute renal failure: definitions, diagnosis, pathogenesis, and therapy.' *the Journal of Clinical Investigation*, 114(1), Jul, 2004/07/03, pp. 5-14.

Scott, R. P. and Quaggin, S. E. (2015) 'The cell biology of renal filtration.' *J Cell Biol*, 209(2) pp. 199-210.

Senthilkumar, G. P., Anithalekshmi, M. S., Yasir, M., Parameswaran, S., Packirisamy, R. m. and Bobby, Z. (2018) 'Role of omentin 1 and IL-6 in type 2 diabetes mellitus patients with diabetic nephropathy.' *Diabetes & Metabolic Syndrome: Clinical Research & Reviews*, 12(1) pp. 23-26.

Sharaf El Din, U. A. A., Salem, M. M. and Abdulazim, D. O. (2016) 'Stop chronic kidney disease progression: Time is approaching.' *World journal of nephrology*, 5(3) pp. 258-273.

Sharma and Sharma, P. L. (2013) 'Role of different molecular pathways in the development of diabetes-induced nephropathy.' *J. Diabetes Metab. S*, 9 p. 004.

Sharma, K., Karl, B., Mathew, A. V., Gangoiti, J. A., Wassel, C. L., Saito, R., Pu, M., Sharma, S., You, Y.-H., Wang, L., Diamond-Stanic, M., Lindenmeyer, M. T., Forsblom, C., Wu, W., Ix, J. H., Ideker, T., Kopp, J. B., Nigam, S. K., Cohen, C. D., Groop, P.-H., Barshop, B. A., Natarajan, L., Nyhan, W. L. and Naviaux, R. K. (2013) 'Metabolomics Reveals Signature of Mitochondrial Dysfunction in Diabetic Kidney Disease.' *Journal of the American Society of Nephrology : JASN*, 24(11), 08/15

Shenouda, S. M., Widlansky, M. E., Chen, K., Xu, G., Holbrook, M., Tabit, C. E., Hamburg, N. M., Frame, A. A., Caiano, T. L. and Kluge, M. A. (2011) 'Altered mitochondrial dynamics contributes to endothelial dysfunction in diabetes mellitus.' *Circulation*, 124(4) pp. 444-453.

Shin, J. H., Kim, K. M., Jeong, J. U., Shin, J. M., Kang, J. H., Bang, K. and Kim, J.-H. (2019) 'Nrf2-Heme Oxygenase-1 Attenuates High-Glucose-Induced Epithelial-to-Mesenchymal Transition of Renal Tubule Cells by Inhibiting ROS-Mediated PI3K/Akt/GSK-3β Signaling.' *Journal of diabetes research*, 2019

Sifuentes-Franco, S., Padilla-Tejeda, D. E., Carrillo-Ibarra, S. and Miranda-Díaz, A. G. (2018) 'Oxidative stress, apoptosis, and mitochondrial function in diabetic nephropathy.' *International journal of endocrinology*, 2018

Slyne, J., Slattery, C., McMorrow, T. and Ryan, M. P. (2015a) 'New developments concerning the proximal tubule in diabetic nephropathy: in vitro models and mechanisms.' *Nephrology Dialysis Transplantation*, 30(suppl_4) pp. iv60-iv67.

Slyne, J., Slattery, C., McMorrow, T. and Ryan, M. P. (2015b) 'New developments concerning the proximal tubule in diabetic nephropathy: in vitro models and mechanisms.' *Nephrology Dialysis Transplantation*, 30(4) pp. iv60-iv67.

Soetikno, V., Watanabe, K., Lakshamanan, A. P., Arumugam, S., Sari, F. R., Sukumaran, V., Thandavarayan, R. A., Harima, M., Suzuki, K. and Kawachi, H. (2012) 'Role of Protein Kinase c-MAPK, oxidative stress and inflammation pathways in diabetic nephropathy.' *J Nephrol Therapeutic S*, 2 p. 001.

Soltoff, S. P. (1986) 'ATP and the regulation of renal cell function.' *Annual review of physiology*, 48(1) pp. 9-31.

Steigerwalt, S. (2008) 'Management of Hypertension in Diabetic Patients With Chronic Kidney Disease.' *Diabetes Spectrum*, 21(1) p. 30.

Stieger, N., Worthmann, K., Teng, B., Engeli, S., Das, A. M., Haller, H. and Schiffer, M. (2012) 'Impact of high glucose and transforming growth factor–β on bioenergetic profiles in podocytes.' *Metabolism*, 61(8) pp. 1073-1086.

Strutz, F. M. (2009) 'EMT and proteinuria as progression factors.' *Kidney international*, 75(5) pp. 475-481.

Su, H., Lei, C.-T. and Zhang, C. (2017a) 'Interleukin-6 signaling pathway and its role in kidney disease: an update.' *Frontiers in immunology*, 8 pp. 405-415.

Su, H., Lei, C.-T. and Zhang, C. (2017b) 'Interleukin-6 signaling pathway and its role in kidney disease: an update.' *Frontiers in immunology*, 8 p. 405.

Subramanya, A. R. and Ellison, D. H. (2014) 'Distal convoluted tubule.' *Clinical journal of the American Society of Nephrology : CJASN*, 9(12) pp. 2147-2163.

Suh, J. H. and Miner, J. H. (2013) 'The glomerular basement membrane as a barrier to albumin.' *Nature Reviews Nephrology*, 9(8) p. 470.

Sun, L., Xiao, L., Nie, J., Liu, F.-Y., Ling, G.-H., Zhu, X.-J., Tang, W.-B., Chen, W.-C., Xia, Y.-C., Zhan, M., Ma, M.-M., Peng, Y.-M., Liu, H., Liu, Y.-H. and Kanwar, Y. S. (2010) 'p66Shc mediates high-glucose and angiotensin II-induced oxidative stress renal tubular injury via mitochondrial-dependent apoptotic pathway.' *American journal of physiology. Renal physiology*, 299(5) pp. F1014-F1025.

Sun, Z., Ma, Y., Chen, F., Wang, S., Chen, B. and Shi, J. (2018) 'miR-133b and miR-199b knockdown attenuate TGF-β1-induced epithelial to mesenchymal transition and renal fibrosis by targeting SIRT1 in diabetic nephropathy.' *European journal of pharmacology*, 837 pp. 96-104.

Sureshbabu, A., Muhsin, S. A. and Choi, M. E. (2016) 'TGF-β signaling in the kidney: profibrotic and protective effects.' *American Journal of Physiology-Renal Physiology*, 310(7) pp. F596-F606.

Suzuki, D., Miyazaki, M., Naka, R., Koji, T., Yagame, M., Jinde, K., Endoh, M., Nomoto, Y. and Sakai, H. (1995) 'In situ hybridization of interleukin 6 in diabetic nephropathy.' *Diabetes*, 44(10) pp. 1233-1238.

Szablewski, L. (2017) 'Distribution of glucose transporters in renal diseases.' *Journal of biomedical science*, 24(1) p. 64.

Tabatabai, N. M., Sharma, M., Blumenthal, S. S. and Petering, D. H. (2009) 'Enhanced expressions of sodium–glucose cotransporters in the kidneys of diabetic Zucker rats.' *Diabetes research and clinical practice*, 83(1) pp. e27-e30.

Tam, F. W. K., Riser, B. L., Meeran, K., Rambow, J., Pusey, C. D. and Frankel, A. H. (2009) 'Urinary monocyte chemoattractant protein-1 (MCP-1) and connective tissue growth factor (CCN2) as prognostic markers for progression of diabetic nephropathy.' *Cytokine*, 47(1) pp. 37-42.

Tan, A. L. Y., Sourris, K. C., Harcourt, B. E., Thallas-Bonke, V., Penfold, S., Andrikopoulos, S., Thomas, M. C., O'Brien, R. C., Bierhaus, A., Cooper, M. E., Forbes, J. M. and Coughlan, M. T. (2009) 'Disparate effects on renal and oxidative parameters following RAGE deletion, AGE accumulation inhibition, or dietary AGE control in experimental diabetic nephropathy.' *American Journal of Physiology-Renal Physiology*, 298(3) pp. F763-F770.

Tanaka, T., Narazaki, M. and Kishimoto, T. (2014) 'IL-6 in inflammation, immunity, and disease.' *Cold Spring Harbor perspectives in biology*, 6(10) p. a016295.

Tanaka, Y., Kume, S., Kitada, M., Kanasaki, K., Uzu, T., Maegawa, H. and Koya, D. (2011) 'Autophagy as a therapeutic target in diabetic nephropathy.' *Experimental diabetes research*, 2012

Tang, S. C. W., Chan, L. Y. Y., Leung, J. C. K., Cheng, A. S., Chan, K. W., Lan, H. Y. and Lai, K. N. (2009) 'Bradykinin and high glucose promote renal tubular inflammation.' *Nephrology Dialysis Transplantation*, 25(3) pp. 698-710.

Tang, W.-b., Ling, G.-h., Sun, L., Zhang, K., Zhu, X., Zhou, X. and Liu, F.-y. (2015) 'Smad anchor for receptor activation regulates high glucose-induced EMT via modulation of Smad2 and Smad3 activities in renal tubular epithelial cells.' *Nephron*, 130(3) pp. 213-220.

Tang, W.-b., Zheng, L., Yan, R., Yang, J., Ning, J., Peng, L., Zhou, Q. and Chen, L. (2018) 'miR302a-3p May Modulate Renal Epithelial-Mesenchymal Transition in Diabetic Kidney Disease by Targeting ZEB1.' *Nephron*, 138(3) pp. 231-242.

Tarasewicz, E. and Jeruss, J. S. (2012) 'Phospho-specific Smad3 signaling: impact on breast oncogenesis.' *Cell Cycle*, 11(13) pp. 2443-2451.

Taslıpınar, A., Yaman, H., Yılmaz, M. I., Demırbas, S., Saglam, M., Taslıpınar, M. Y., Agıllı, M., Kurt, Y. G., Sonmez, A. and Azal, O. (2011) 'The relationship between inflammation, endothelial dysfunction and proteinuria in patients with diabetic nephropathy.' *Scandinavian journal of clinical and laboratory investigation*, 71(7) pp. 606-612.

TeSlaa, T. and Teitell, M. A. (2014) 'Techniques to monitor glycolysis.' *In Methods in enzymology*. Vol. 542. Elsevier, pp. 91-114.

Thomas, R., Kanso, A. and Sedor, J. R. (2008) 'Chronic kidney disease and its complications.' *Primary care: Clinics in office practice*, 35(2) pp. 329-344.

Tran, M. and Parikh, S. M. (2014) 'Mitochondrial biogenesis in the acutely injured kidney.' *Nephron Clinical practice*, 127(1-4) pp. 42-45.

Triplitt, C. L. (2012) 'Understanding the kidneys' role in blood glucose regulation.' *American Journal of Managed Care*, 18(1) p. S11.

Vallon, V. (2010) 'The proximal tubule in the pathophysiology of the diabetic kidney.' *American Journal of Physiology-Regulatory, Integrative and Comparative Physiology*, 300(5) pp. R1009-R1022.

Vallon, V. (2011) 'Molecular determinants of renal glucose reabsorption. Focus on "Glucose transport by human renal Na+/D-glucose cotransporters SGLT1 and SGLT2".' *American journal of physiology. Cell physiology*, 300(1) pp. C6-C8.

Van Buren, P. N. and Toto, R. (2011) 'Hypertension in diabetic nephropathy: epidemiology, mechanisms, and management.' *Advances in chronic kidney disease*, 18(1) pp. 28-41.

Vanessa Fiorentino, T., Prioletta, A., Zuo, P. and Folli, F. (2013) 'Hyperglycemia-induced oxidative stress and its role in diabetes mellitus related cardiovascular diseases.' *Current pharmaceutical design*, 19(32) pp. 5695-5703.

Verzola, D., Bertolotto, M. B., Villaggio, B., Ottonello, L., Dallegri, F., Frumento, G., Berruti, V., Gandolfo, M. T., Garibotto, G. and Deferrari, G. (2002) 'Taurine prevents apoptosis induced by high ambient glucose in human tubule renal cells.' *Journal of investigative medicine*, 50(6) pp. 443-451.

Vestra, D., Michele, Mussap, M., Gallina, P., Bruseghin, M., Cernigoi, A. M., Saller, A., Plebani, M. and Fioretto, P. (2005) 'Acute-phase markers of inflammation and glomerular structure in patients with type 2 diabetes.' *Journal of the American Society of Nephrology*, 16(3 suppl 1) pp. S78-S82.

Viedt, C. and Orth, S. R. (2002) 'Monocyte chemoattractant protein-1 (MCP-1) in the kidney: does it more than simply attract monocytes?' *Nephrology Dialysis Transplantation*, 17(12) pp. 2043-2047.

Wada, Furuichi, K., Sakai, N., Iwata, Y., Yoshimoto, K., Shimizu, M., Takeda, S.-I., Takasawa, K., Yoshimura, M. and Kida, H. (2000) 'Up-regulation of monocyte chemoattractant protein-1 in tubulointerstitial lesions of human diabetic nephropathy.' *Kidney international*, 58(4) pp. 1492-1499.

Wada, J. and Makino, H. (2013) 'Inflammation and the pathogenesis of diabetic nephropathy.' *Clinical science*, 124(3) pp. 139-152.

Wang, Rangan, G. K., Tay, Y.-C., Wang, Y. A. O. and Harris, D. C. (1999) 'Induction of monocyte chemoattractant protein-1 by albumin is mediated by nuclear factor κB in proximal tubule cells.' *Journal of the American Society of Nephrology*, 10(6) pp. 1204-1213.

Wang, Wang, Y., Minto, A. W., Wang, J., Shi, Q., Li, X. and Quigg, R. J. (2008) 'MicroRNA-377 is up-regulated and can lead to increased fibronectin production in diabetic nephropathy.' *The FASEB Journal*, 22(12) pp. 4126-4135.

Wang, Komers, R., Carew, R., Winbanks, C. E., Xu, B., Herman-Edelstein, M., Koh, P., Thomas, M., Jandeleit-Dahm, K. and Gregorevic, P. (2012) 'Suppression of microRNA-29 expression by TGF-β1 promotes collagen expression and renal fibrosis.' *Journal of the American Society of Nephrology*, 23(2) pp. 252-265.

Wang, B., Koh, P., Winbanks, C., Coughlan, M. T., McClelland, A., Watson, A., Jandeleit-Dahm, K., Burns, W. C., Thomas, M. C. and Cooper, M. E. (2011) 'miR-200a prevents renal fibrogenesis through repression of TGF-β2 expression.' *diabetes*, 60(1) pp. 280-287.

Wang, B., Herman-Edelstein, M., Koh, P., Burns, W., Jandeleit-Dahm, K., Watson, A., Saleem, M., Goodall, G. J., Twigg, S. M., Cooper, M. E. and Kantharidis, P. (2010) 'E-cadherin expression is

regulated by miR-192/215 by a mechanism that is independent of the profibrotic effects of transforming growth factor-beta.' *Diabetes*, 59(7) pp. 1794-1802.

Wang, W., Sun, W., Cheng, Y., Xu, Z. and Cai, L. (2019) 'Role of sirtuin-1 in diabetic nephropathy.' *Journal of Molecular Medicine*, 97(3) pp. 291-309.

Webster, A. C., Nagler, E. V., Morton, R. L. and Masson, P. (2017) 'Chronic kidney disease.' *The Lancet*, 389(10075) pp. 1238-1252.

Wei, M., Li, Z., Xiao, L. and Yang, Z. (2015) 'Effects of ROS-relative NF-κB signaling on high glucose-induced TLR4 and MCP-1 expression in podocyte injury.' *Molecular immunology*, 68(2) pp. 261-271.

Wolf, G. (2004) 'New insights into the pathophysiology of diabetic nephropathy: from haemodynamics to molecular pathology.' *European Journal of Clinical Investigation*, 34(12) pp. 785-796.

Wong, M. G., Panchapakesan, U., Qi, W., Silva, D. G., Chen, X.-M. and Pollock, C. A. (2011) 'Cation-independent mannose 6-phosphate receptor inhibitor (PXS25) inhibits fibrosis in human proximal tubular cells by inhibiting conversion of latent to active TGF-β1.' *American Journal of Physiology-Renal Physiology*, 301(1) pp. F84-F93.

Wu, J., Liu, J., Ding, Y., Zhu, M., Lu, K., Zhou, J., Xie, X., Xu, Y., Shen, X. and Chen, Y. (2018) 'MiR-455-3p suppresses renal fibrosis through repression of ROCK2 expression in diabetic nephropathy.' *Biochemical and biophysical research communications*, 503(2) pp. 977-983.

Xu, H., Sun, F., Li, X. and Sun, L. (2018) 'Down-regulation of miR-23a inhibits high glucose-induced EMT and renal fibrogenesis by up-regulation of SnoN.' *Human cell*, 31(1) pp. 22-32.

Xu, X., Xiao, L., Xiao, P., Yang, S., Chen, G., Liu, F., Kanwar, Y. S. and Sun, L. (2014) 'A glimpse of matrix metalloproteinases in diabetic nephropathy.' *Current medicinal chemistry*, 21(28) pp. 3244-3260.

Xue, M., Cheng, Y., Han, F., Chang, Y., Yang, Y., Li, X., Chen, L., Lu, Y., Sun, B. and Chen, L. (2018) 'Triptolide attenuates renal tubular epithelial-mesenchymal transition via the MiR-188-5p-mediated PI3K/AKT pathway in diabetic kidney disease.' *International journal of biological sciences*, 14(11) p. 1545.

Yan, L. j. (2018) 'Redox imbalance stress in diabetes mellitus: Role of the polyol pathway.' *Animal models and experimental medicine*, 1(1) pp. 7-13.

Yang, L., Besschetnova, T. Y., Brooks, C. R., Shah, J. V. and Bonventre, J. V. (2010) 'Epithelial cell cycle arrest in G2/M mediates kidney fibrosis after injury.' *Nature medicine*, 16(5) p. 535.

Yang, S., Fei, X., Lu, Y., Xu, B., Ma, Y. and Wan, H. (2019) 'miRNA-214 suppresses oxidative stress in diabetic nephropathy via the ROS/Akt/mTOR signaling pathway and uncoupling protein 2.' *Experimental and therapeutic medicine*, 17(5) pp. 3530-3538.

Yasar, Y., Songul, Kuru, P., Toksoy Oner, E. and Agirbasli, M. (2014) 'Functional stability of plasminogen activator inhibitor-1.' *The scientific world journal*, 2014, p. 11

Yu, Border, W. A., Huang, Y. and Noble, N. A. (2003) 'TGF-β isoforms in renal fibrogenesis.' *Kidney international*, 64(3) pp. 844-856.

Yu, Sheu, S.-S., Robotham, J. L. and Yoon, Y. (2008) 'Mitochondrial fission mediates high glucose-induced cell death through elevated production of reactive oxygen species.' *Cardiovascular research*, 79(2) pp. 341-351.

Zanchi, C., Macconi, D., Trionfini, P., Tomasoni, S., Rottoli, D., Locatelli, M., Rudnicki, M., Vandesompele, J., Mestdagh, P. and Remuzzi, G. (2017) 'MicroRNA-184 is a downstream effector of albuminuria driving renal fibrosis in rats with diabetic nephropathy.' *Diabetologia*, 60(6) pp. 1114-1125.

Zazzeroni, L., Pasquinelli, G., Nanni, E., Cremonini, V. and Rubbi, I. (2017) 'Comparison of quality of life in patients undergoing hemodialysis and peritoneal dialysis: a systematic review and meta-analysis.' *Kidney and Blood Pressure Research*, 42(4) pp. 717-727.

Zeisberg, M. and Neilson, E. G. (2010) 'Mechanisms of tubulointerstitial fibrosis.' *Journal of American Society of Nephrology*, 21(11), Nov, 2010/09/25, pp. 1819-1834.

Zhan, M., Usman, I. M., Sun, L. and Kanwar, Y. S. (2015) 'Disruption of renal tubular mitochondrial quality control by Myo-inositol oxygenase in diabetic kidney disease.' *Journal of the American Society of Nephrology : JASN*, 26(6) pp. 1304-1321.

Zhang, H., Wei, X., Lu, S., Lin, X., Huang, J., Chen, L., Huang, X., Jiang, L., Li, Y. and Qin, L. (2019) 'Protective effect of DMDD, isolated from the root of Averrhoa carambola L., on high glucose induced EMT in HK-2 cells by inhibiting the TLR4-BAMBI-Smad2/3 signaling pathway.' *Biomedicine & Pharmacotherapy*, 113 p. 108705.

Zhang, J., Liu, J. and Qin, X. (2018) 'Advances in early biomarkers of diabetic nephropathy.' *Revista da Associação Médica Brasileira*, 64(1) pp. 85-92.

Zhang, S., Ntasis, E., Kabtni, S., van den Born, J., Navis, G., Bakker, S. J. L., Krämer, B. K., Yard, B. A. and Hauske, S. J. (2016) 'Hyperglycemia does not affect iron mediated toxicity of cultured endothelial and renal tubular epithelial cells: influence of L-carnosine.' *Journal of diabetes research*, 2016

Zhang, Y., Alexander, P. B. and Wang, X.-F. (2017) 'TGF-β family signaling in the control of cell proliferation and survival.' *Cold Spring Harbor perspectives in biology*, 9(4) p. a022145.

Zhao, H., Dong, Y., Tian, X., Tan, T. K., Liu, Z., Zhao, Y., Zhang, Y., Harris, D. C. H. and Zheng, G. (2013a) 'Matrix metalloproteinases contribute to kidney fibrosis in chronic kidney diseases.' *World journal of nephrology*, 2(3) p. 84.

Zhao, H., Dong, Y., Tian, X., Tan, T. K., Liu, Z., Zhao, Y., Zhang, Y., Harris, D. C. H. and Zheng, G. (2013b) 'Matrix metalloproteinases contribute to kidney fibrosis in chronic kidney diseases.' *World journal of nephrology*, 2(3) pp. 84-89.

Zhao, Y., Yin, Z., Li, H., Fan, J., Yang, S., Chen, C. and Wang, D. W. (2017) 'MiR-30c protects diabetic nephropathy by suppressing epithelial-to-mesenchymal transition in db/db mice.' *Aging cell*, 16(2) pp. 387-400.

Zhong, X., Chung, A. C. K., Chen, H.-Y., Dong, Y., Meng, X. M., Li, R., Yang, W., Hou, F. F. and Lan, H. Y. (2013) 'miR-21 is a key therapeutic target for renal injury in a mouse model of type 2 diabetes.' *Diabetologia*, 56(3) pp. 663-674.

Zhou, L., Xu, D.-y., Sha, W.-g., Shen, L., Lu, G.-y., Yin, X. and Wang, M.-j. (2015) 'High glucose induces renal tubular epithelial injury via Sirt1/NF-kappaB/microR-29/Keap1 signal pathway.' *Journal of translational medicine*, 13(1) p. 352.

Ziyadeh, F. N., Hoffman, B. B., Han, D. C., Iglesias-De la Cruz, M. C., Hong, S. W., Isono, M., Chen, S., McGowan, T. A. and Sharma, K. (2000) 'Long-term prevention of renal insufficiency, excess matrix gene expression, and glomerular mesangial matrix expansion by treatment with monoclonal antitransforming growth factor-β antibody in db/db diabetic mice.' *Proceedings of the National Academy of Sciences*, 97(14) pp. 8015-8020.